The School of Engineering

ENG 337-(EQC 2001/465)
Bracing capacity of partially grouted concrete masonry walls with openings
Kok Choon Voon, Associate Professor, Jason Ingham, School of Engineering, University of Auckland

THE UNIVERSITY OF AUCKLAND
NEW ZEALAND

Department of Civil and Environmental Engineering

Bracing Capacity of Partially Grouted Concrete Masonry Walls with Openings

by

Kok Choon Voon
Associate Professor Jason Ingham

April 2006

School of Engineering
Report No. 629

Whakapukahatanga Taiao
New Zealand Maori for
Strengthening the environment - built and natural

For further information contact:
Department of Civil and Environmental Engineering, School of Engineering
The University of Auckland, Private Bag 92019, Auckland, New Zealand
Telephone 64-9-3737599 ext.88166 or ext. 85715 Facsimile 64-9-3737462
Web www.cee.auckland.ac.nz Email cee-enquiries@auckland.ac.nz

Bracing Capacity of Partially Grouted Concrete Masonry Walls with Openings

by

Kok Choon Voon

Associate Professor Jason Ingham

School of Engineering Report No. 629

Department of Civil and Environmental Engineering

The University of Auckland

New Zealand

April 2006

Abstract

Masonry shear walls have attracted the attention of many researchers because of their role as lateral force resisting elements. However, most of this research was carried out in order to study the behaviour of solid masonry shear walls, despite the fact that masonry walls are commonly constructed with openings. Consequently, eight partially grout-filled nominally reinforced concrete masonry walls with openings were tested under cyclic lateral loading at the University of Auckland. These walls had variations in trimming reinforcement, and a range of opening geometries. The objectives of this research were to study the performance of concrete masonry walls with openings under seismic loading conditions and to validate the adequacy of NZS 4229:1999 in addressing the bracing capacity of these types of masonry walls.

Test results indicated that the size of openings and the length of trimming reinforcement significantly affected the lateral strength of the tested walls. The observation of diagonal cracking patterns that aligned well with the load paths by which shear force was assumed to be transferred to the foundation in the strut mechanism supported the use of strut-and-tie analysis as a viable tool to evaluate the flexural strength of walls of this type. Strength prediction using the improved strut-and-tie method and the modified plastic collapse analysis were found to closely match the experimental results of the perforated walls tested in this study. Strength prediction by the simplified strut-and-tie method was found to closely match the test results of masonry walls with a single opening, but significant underestimation of strength by this method was found for walls with double openings. The full plastic collapse analysis was found to significantly over-predict the strength of all perforated walls included in this study.

Finally, the NZS 4229:1999 detail for shrinkage control joints was shown to result in adequate structural performance. In addition, shrinkage control joints constructed in accordance with the NZS 4229:1999 prescription resulted in masonry bracing capacity substantially in excess of the tabulated values in the standard, with gradual strength and stiffness degradation. This increase in strength is due to pier double bending that is not considered by the standard.

Disclaimer

This report was prepared for EQC Project No. 01/465. The opinions and conclusions presented herein are those of the authors, and do not necessarily reflect those of the University of Auckland or any of the sponsoring parties to this project.

Acknowledgement

The authors greatly appreciate the financial support provided by the Earthquake Commission Research Foundation (EQC). Thanks also go to Firth Industries Ltd., W. Stevenson and Sons Ltd., and Ready Mix Concrete Ltd. for donating the necessary masonry block units, grout and labour for construction of the masonry walls. Their contributions are gratefully appreciated. The authors wish to acknowledge the contribution by Pacific Steel in providing the necessary reinforcing steel for this project. Thanks also go to Hank Mooy and Tony Daligan for providing assistance in setting up the test specimens.

Table of Contents

Abstract i

Disclaimer ii

Acknowledgement iii

Table of Contents iv

List of Figures viii

List of Tables xiii

List of Symbols xiv

Chapter 1

Introduction 1

1.1 General 1

1.2 Scope of Study 4

Chapter 2

Literature Review 5

2.1 Introduction 5

2.2 Research Conducted in New Zealand 5

2.3 Research Conducted Overseas 9

2.4 NZS 4229:1999 Codification of Wall Capacity 10

2.5 Shrinkage Control Joint 12

Chapter 3

Test Programme 14

3.1 Introduction 14

3.2 Test Set-up 14

3.3 Construction Materials 16

3.3.1 Concrete Masonry Block 16

3.3.2 Mortar and Grout 17

3.3.3 Reinforcing Steel 17

3.4 Specimen Construction Details 17

3.5 Instrumentation 19

3.5.1 Installation of Instrumentation 20

3.6 Material Properties 22

3.6.1 Reinforcing Steel 22
3.6.2 Mortar and Grout 23
3.6.3 Prisms 23
Chapter 4
Wall Strength Prediction 26
4.1 Flexural Strength of Perforated Walls 26
4.1.1 NZS 4229:1999 Procedure 26
4.1.2 Simple Strut-and-Tie Models 26
4.1.3 Improved Strut-and-Tie Models 30
4.1.4 Full Plastic Collapse Analysis 33
4.1.5 Modified Plastic Collapse Analysis 35
4.2 Flexural strength of wall without opening 38
4.3 Masonry Shear Strength 39
4.4 Predicted Strength Summary 40
4.5 Testing Procedure 42
4.6 Miscellaneous 44
4.7 Data Reduction 45
Chapter 5
Experimental Results 48
5.1 Wall 1 48
5.2 Wall 2 51
5.3 Wall 3 53
5.4 Wall 4 55
5.5 Wall 5 57
5.6 Wall 6 59
5.7 Wall 7 61
5.8 Wall 8 63
5.9 Wall 9 65
5.10 Wall 10 67
Chapter 6
Discussion of Test Results 69
6.1 Introduction 69
6.2 Result Summary 69
6.3 Depth of Openings 71

6.3 Effect of Trimming Reinforcement 75
6.4 Effect of Shrinkage Control Joint 78
6.5 Wall Strength Prediction 79
6.6 Possible Amendment to NZS 4229:1999 84
6.6.1 Extended Trimming Reinforcement 85
6.6.2 Amendment to NZS 4229:1999 bracing capacity 86
6.6.2 No Amendment to NZS 4229:1999 88
Chapter 7
Conclusion 94
Chapter 8
Reference 96
Appendix A
Experimental Results – Series A "Walls with Openings" 99
A.1 Wall 1 99
A.1.1 Pre-test 99
A.1.2 Testing 100
A.1.3 Summary Behaviour 108
A.1.4 Panel Displacement Components 110
A.2 Wall 2 111
A.2.1 Pre-test 111
A.2.2 Testing 111
A.2.3 Summary Behaviour 119
A.2.4 Panel Displacement Components 120
A.3 Wall 3 122
A.3.1 Pre-test 122
A.3.2 Testing 122
A.3.3 Summary Behaviour 128
A.3.4 Panel Displacement Components 129
A.4 Wall 4 131
A.4.1 Pre-test 131
A.4.2 Testing 131
A.4.3 Summary Behaviour 137
A.4.4 Panel Displacement Components 138

A.5 Wall 5 ... 140
A.5.1 Pre-test ... 140
A.5.2 Testing ... 140
A.5.3 Summary Behaviour ... 147
A.5.4 Panel Displacement Components ... 148
A.6 Wall 6 ... 150
A.6.1 Pre-test ... 150
A.6.2 Testing ... 150
A.6.3 Summary Behaviour ... 156
A.6.4 Panel Displacement Components ... 158
A.7 Wall 7 ... 160
A.7.1 Pre-test ... 160
A.7.2 Testing ... 160
A.7.3 Summary Behaviour ... 167
A.7.4 Panel Displacement Components ... 169
A.8 Wall 8 ... 170
A.8.1 Pre-test ... 170
A.8.2 Testing ... 170
A.8.3 Summary Behaviour ... 177
A.8.4 Panel Displacement Components ... 178
Appendix B
Experimental Results – Series B "Walls with Control Joints" ... 180
B.1 Wall 9 ... 181
B.1.1 Pre-test ... 181
B.1.2 Testing ... 182
B.1.3 Summary Behaviour ... 191
B.1.4 Panel Displacement Components ... 192
B.2 Wall 10 ... 194
B.2.1 Pre-test ... 195
B.2.2 Testing ... 195
B.2.3 Summary Behaviour ... 202
B.2.4 Panel Displacement Components ... 203
Appendix C- Shear Displacement Component ... 205
Appendix D – Bending Moment Capacity ... 212

List of Figures

Figure 1.1 Strut-and-tie modelling of nominally reinforced concrete masonry walls. 2
Figure 2.1 Typical reinforcement details of nominally reinforced concrete masonry wall. 6
Figure 2.2 Force-displacement histories of partially grout-filled concrete masonry walls....... 7
Figure 2.3 Force-displacement history of partially grout-filled concrete masonry wall with openings. 8
Figure 2.4 Failure mechanisms for wall with opening........ 9
Figure 3.1 Typical test set-up........ 15
Figure 3.2 Details of concrete footing........ 15
Figure 3.3 15-Series concrete masonry units. 16
Figure 3.4 Series A, wall geometries and reinforcing details. 18
Figure 3.5 Series B, wall geometries and reinforcing details. 19
Figure 3.6 Portal displacement transducer. 20
Figure 3.7 Instrumentation for test wall. 21
Figure 3.8 Instrumentation mounted on wall before testing. 21
Figure 3.9 Reinforcing steel subjected to tensile test........ 22
Figure 3.10 Stress-strain curve for D12 reinforcing bars........ 23
Figure 3.11 Masonry prisms grouting. 24
Figure 3.12 Masonry prism subjected to compression test. 24
Figure 4.1 Identification of bracing panels 27
Figure 4.2 Simplified strut-and-tie models in push direction (forces in kN). 29
Figure 4.3 Simplified strut-and-tie models in pull direction (forces in kN). 30
Figure 4.4 Strut-and-tie models in push direction (forces in kN). 32
Figure 4.5 Strut-and-tie models in pull direction (forces in kN). 33
Figure 4.6 Full plastic collapse analyses in push direction (moments in kNm). 35
Figure 4.7 Full plastic analyses in pull direction (moments in kNm). 36
Figure 4.8 Modified plastic collapse analysis in push direction (moments in kNm)........ 38
Figure 4.9 Modified plastic collapse analysis in pull direction (moments in kNm). 39
Figure 4.10 Strut-and-tie models for masonry walls without opening. 40
Figure 4.11 Effective areas for shear. 41
Figure 4.12 Definition of yield displacement. 44
Figure 4.13 Imposed displacement history in terms of ductility........ 44

Figure 4.14 Rocking displacement....46
Figure 4.15 Flexural displacement....47
Figure 5.1 Force-displacement history for Wall 1....50
Figure 5.2 Wall 1 cracking pattern at end of testing....50
Figure 5.3 Force-displacement history for Wall 2....52
Figure 5.4 Wall 2 cracking pattern at end of testing....52
Figure 5.5 Force-displacement history for Wall 3....54
Figure 5.6 Wall 3 cracking pattern at end of testing....54
Figure 5.7 Force-displacement history for Wall 4....56
Figure 5.8 Wall 4 cracking pattern at end of testing....56
Figure 5.9 Force-displacement history for Wall 5....58
Figure 5.10 Wall 5 cracking pattern at end of testing....58
Figure 5.11 Force-displacement history for Wall 6....60
Figure 5.12 Wall 6 cracking pattern at end of testing....60
Figure 5.13 Force-displacement history for Wall 7....62
Figure 5.14 Wall 7 cracking pattern at end of testing....62
Figure 5.15 Force-displacement history of Wall 8....64
Figure 5.16 Wall 8 cracking pattern at end of testing....64
Figure 5.17 Force-displacement history for Wall 9....66
Figure 5.18 Wall 9 cracking pattern at end of testing....66
Figure 5.19 Force-displacement history for Wall 10....68
Figure 5.20 Wall 10 cracking pattern at end of testing....68
Figure 6.1 Effect of opening for walls constructed according to NZS 4229:1999 specifications....73
Figure 6.2 Effect of opening on the 2600 mm long walls....73
Figure 6.3 Strut-and-tie models in push direction....74
Figure 6.4 Effect of openings on the 4200 mm perforated masonry walls....75
Figure 6.5 Effect of trimming reinforcement on the 2600 mm long perforated masonry walls 77
Figure 6.6 Effect of trimming reinforcement on the 4200 mm long perforated masonry walls 77
Figure 6.7 Effect of shrinkage control joint on partially grout-filled masonry walls....78
Figure 6.8 Effect of double bending of central pier on wall strength....81
Figure 6.9 Accuracy of strength predictions....83

Figure 6.10 Proposed amendment to trimming reinforcement. 85
Figure 6.11 Extension to trimming reinforcement. 86
Figure 6.12 Masonry wall with varying pier lengths and opening depth. 87
Figure 6.13 Comparison of predicted strengths. 88
Figure 6.14 Bracing panel for design example. 92
Figure A.1.1 Wall 1 geometry and reinforcing details. 100
Figure A.1.2 Condition of test wall at end of first ductility 2 push cycle. 104
Figure A.1.3 Condition of test wall at end of first ductility 8 pull cycle. 104
Figure A.1.4 Condition of test wall after cycling to displacement ductility 12. 106
Figure A.1.5 Condition of test wall after first push cycle to ductility 14. 106
Figure A.1.6 Force-displacement behaviour for Wall 1. 109
Figure A.1.7 Components of displacement. 110
Figure A.2.1 Wall 2 geometry and reinforcing details. 111
Figure A.2.2 Condition of test wall at end of first ductility 4 pull cycle. 115
Figure A.2.3 Condition of test wall at end of first ductility 10 push cycle. 115
Figure A.2.4 Condition of test wall after cycling to displacement ductility 12. 118
Figure A.2.5 Condition of test wall after cycling to displacement ductility 16. 118
Figure A.2.6 Force-displacement behaviour of Wall 2. 120
Figure A.2.7 Components of displacement. 121
Figure A.3.1 Wall 3 geometry and reinforcing details. 122
Figure A.3.2 Condition of test wall at end of first ductility 6 pull cycle. 125
Figure A.3.3 Condition of test wall at end of second ductility 8 push cycle. 127
Figure A.3.4 Condition of test wall at end of second ductility 10 push cycle. 127
Figure A.3.5 Force-displacement behaviour of Wall 3. 129
Figure A.3.6 Components of displacement. 130
Figure A.4.1 Wall 4 geometry and reinforcing details. 131
Figure A.4.2 Condition of test wall at end of first ductility 4 pull cycle. 135
Figure A.4.3 Condition of test wall at end of second ductility 8 push cycle 135
Figure A.4.4 Condition of test wall at end of first ductility 12 push cycle. 137
Figure A.4.5 Force-displacement behaviour of Wall 4. 138
Figure A.4.6 Components of displacement. 139
Figure A.5.1 Wall 5 geometry and reinforcing details. 140
Figure A.5.2 Condition of test wall at end of first ductility 4 pull cycle. 143
Figure A.5.3 Condition of test wall at end of second ductility 14 push cycle. 146

Figure A.5.4 Force-displacement behaviour of Wall 5....................148
Figure A.5.5 Components of displacement....................149
Figure A.6.1 Wall 6 geometry and reinforcing details....................150
Figure A.6.2 Condition of test wall at end of second ductility 4 push cycle....................153
Figure A.6.3 Condition of test wall at end of first ductility 6 push cycle....................153
Figure A.6.4 Condition of test wall at end of first ductility 8 push cycle....................155
Figure A.6.5 Condition of test wall at end of first ductility 12 pull cycle....................155
Figure A.6.6 Force-displacement behaviour of Wall 6....................158
Figure A.6.7 Components of displacement....................159
Figure A.7.1 Wall 7 geometry and reinforcing details....................160
Figure A.7.2 Condition of test wall at end of first ductility 2 push cycle....................162
Figure A.7.3 Condition of test wall at end of first ductility 4 pull cycle....................162
Figure A.7.4 Condition of test wall at end of second ductility 8 push cycle....................166
Figure A.7.5 Condition of test wall at end of first ductility 14 push cycle....................166
Figure A.7.6 Force-displacement behaviour of Wall 7....................168
Figure A.7.7 Components of displacement....................169
Figure A.8.1 Wall 8 geometry and reinforcing details....................170
Figure A.8.2 Condition of test wall at end of first ductility 4 push cycle....................173
Figure A.8.3 Condition of test wall at end of first ductility 4 pull cycle....................173
Figure A.8.4 Condition of test wall at end of second ductility 8 push cycle....................176
Figure A.8.5 Condition of test wall at end of second ductility 8 pull cycle....................176
Figure A.8.6 Force-displacement behaviour for Wall 8....................178
Figure A.8.7 Components of displacement....................179
Figure B.1.1 Wall 9 geometry and reinforcing details....................181
Figure B.1.2 Condition of test wall after first ductility 6 pull cycle....................186
Figure B.1.3 Condition of test wall after first ductility 10 pull cycle....................186
Figure B.1.4 Condition of test wall after first ductility 22 push cycle....................190
Figure B.1.5 Condition of test wall after first ductility 30 push cycle....................190
Figure B.1.6 Force-displacement behaviour for Wall 9....................192
Figure B.1.7 Components of displacement....................193
Figure B.2.1 Wall 10 geometry and reinforcing details....................194
Figure B.2.2 Condition of test wall after first ductility 4 pull cycle....................198
Figure B.2.3 Condition of test wall after second ductility 6 push cycle....................198
Figure B.2.4 Condition of test wall after first ductility 8 push cycle....................201

Figure B.2.5 Condition of test wall after second ductility 10 push cycle. 201
Figure B.2.6 Force-displacement behaviour for Wall 10...203
Figure B.2.7 Components of displacement. 204
Figure C.1 Wall panel section. 205
Figure C.2 Nodal displacement of a panel section. 206
Figure C.3 Components of panel deformation. 207
Figure D.1 Reinforcement details for concrete masonry pier and lintel. 212

List of Tables

Table 2.1 Bracing Capacities* for 15 Series Partially Grouted Concrete Masonry.................11
Table 4.1 Prediction of wall strengths, based upon measured material properties..................41
Table 6.1 Summary of test results for the 2600 mm long masonry walls................................71
Table 6.2 Summary of test results and wall strength predictions 82
Table 6.3 Strength predictions for walls with 800 mm deep single opening...........................89
Table 6.4 Strength predictions for walls with 1000 mm deep single opening.........................90
Table 6.5 Strength predictions for walls with 1200 mm deep single opening.........................91
Table 6.6 Bracing capacity for design example a 92
Table 6.7 Bracing capacity for design example b 93

List of Symbols

A_s	=	area of tension longitudinal reinforcing steel
b_f	=	maximum width of ungrouted flue
b_w	=	effective wed width
C_1	=	shear strength coefficient
C_2	=	shear strength coefficient
d	=	distance from extreme compression fibre to centroid of longitudinal tension reinforcement
f_{cb}	=	mean strength of concrete masonry unit
f_g	=	mean grout strength
f_m	=	mean masonry compressive strength
f'_m	=	characteristic masonry compressive strength
f_y	=	characteristic yield strength of reinforcement
F_{code}	=	code specified wall nominal strength
$F_{code,amd}$	=	wall bracing capacity according to proposed amended procedure
$F_{code,no\text{-}op}$	=	code specified nominal strength for wall without opening
$F_{n,fr}$	=	nominal wall strength according to plastic hinge model
$F_{n,no\text{-}op}$	=	nominal strength of wall without opening
$F_{n,st}$		nominal wall strength according to simplified strut-and-tie model
$F_{n,ST}$		nominal wall strength according to strut-and-tie model
h_e	=	effective wall height in the plane of applied loading
jd	=	level arm
M_{bc}	=	flexural strength for the coupling element section at compression pier end
M_{bt}	=	flexural strength for the coupling element section at tension pier end
M_c	=	flexural strength for the compression pier end sections
M_n	=	nominal bending strength for structural member
M_t	=	flexural strength for the tension pier end sections
P_{ovt}	=	axial force due to overturning
p_w	=	$A_s/b_w d$
T	=	tension force from longitudinal reinforcement
U_b	=	flexural component of displacement

U_r	=	rocking component of displacement
U_s	=	shear component of displacement
v_{bm}	=	basic type-dependent shear strength of masonry
v_m	=	maximum permitted type-dependent shear stress provided by masonry
V_c	=	ultimate lateral load capacity of compression pier
V_t	=	ultimate lateral load capacity of tension pier
W_t	=	wall self weight
x_{cb}	=	standard deviation of strength of concrete masonry unit
x_g	=	standard deviation of strength of grout
x_m		standard deviation of strength of masonry strength
Δ_y	=	nominal yield displacement
α	=	parameter for compressive stress block
ω	=	wall section curvature
ϕ	=	strength reduction factor
υ	=	wall section rotation

Chapter 1

Introduction

1.1 General

For many decades masonry has been used as a common structural material in a large proportion of New Zealand building projects. However, the poor performance of unreinforced masonry in the magnitude 7.8 1931 Hawke's Bay Earthquake (Dowrick, 1998; Scott, 1999) subsequently led to the development of conservative concrete masonry design provisions based on the principle of capacity design (Priestley, 1980), which requires the dependable shear strength to exceed the maximum lateral loading necessary to develop the wall flexural overstrength. Consequently, a typical detail was the use of ϕ 12 mm grade 300 MPa reinforcement at 400 mm centres, both vertically and horizontally, in fully-grouted concrete masonry walls.

The recent promulgation of alternative construction forms has resulted in the perception within New Zealand that reinforced concrete masonry is an expensive form of construction when compared with competing products and systems. Consequently, a decision was made by the New Zealand concrete masonry industry to develop a non-specific design standard NZS 4229:1999 which, whilst retaining suitable conservatism, was more realistic in its treatment of measured experimental response. In particular, attention was given to permitting the use of partially grout-filled nominally reinforced concrete masonry in the most seismically active regions of New Zealand. Furthermore, efforts were made to simplify use of the standard so that the design of single and double storey masonry structures, not containing crowds and not dedicated to the preservation of human life (such as hospitals), could be effectively conducted by architects and architectural draftspersons with limited, if any, input from consulting structural engineers.

The in-plane lateral strength of a concrete masonry wall panel is specified in NZS 4229:1999 through determination of its "bracing capacity", with the bracing capacity values being derived from wall tests conducted at the University of Auckland by Brammer (1995) and Davidson

(1996), of which only two considered the performance of walls with openings. However, it was subsequently identified that an important trimming reinforcement detail adopted in testing of these two walls differed from that specified in NZS 4229:1999. Hence, a third wall, having an opening and with reinforcement detailing complying with NZS 4229:1999 was tested (Ingham et al., 2001). The experimental result indicated that this wall did not achieve the bracing capacity prescribed in NZS 4229:1999 and subsequent assessment showed that the existing design standard may be non-conservative in its treatment of walls with openings.

In seeking to understand why the third wall did not achieve its predicted strength, it was established that a strut-and-tie analysis of the structure demonstrated that the Standard incorrectly defined the geometry of a "bracing panel", whose geometry is used to establish lateral wall strength. This analysis is shown diagrammatically in Figure 1.1. Figure 1.1a shows the reinforcement detailing for the test conducted by Davidson (1996). The resultant strut-and-tie analysis is shown in Figure 1.1b, with struts indicated by a broader element thickness. The resultant bracing panels based on the geometry of the diagonal struts of Figure 1.1b is shown in Figure 1.1c. As validated through the discussed analysis procedure, NZS 4229:1999 currently defines the geometry of bracing panels based upon the vertical dimensions of the smallest adjacent openings (see also Figure 4.1 for more details).

In Figure 1.1d it is shown that when the trimming reinforcement is shortened to comply with the current NZS 4229:1999 specification, the geometry of the right-most diagonal strut is modified. The corresponding modification to the bracing panel is shown in Figure 1.1e. This effectively shows that the current Standard-defined bracing panel geometry is non-conservative as taller bracing panels have less capacity than shorter bracing panels of the same length. Furthermore, when the wall is instead loaded to the left (see Figure 1.1f), the geometry of the struts is further changed, and an alternative bracing panel distribution is developed as shown in Figure 1.1g.

Possible amendments to the process would be to either adopt bracing panel dimensions based upon the geometry of the largest adjacent wall opening, or to separately analyse the wall for the two direction of loading. Another solution would be to prescribe an extended trimming reinforcement detail as per Figure 1.1a. However, before such actions are taken it was deemed necessary to validate the strut-and-tie analysis through the testing of partially grouted concrete masonry walls with openings. These walls required variations in trimming reinforcement detailing, including that complying to NZS 4229:1999, and also required a range of opening geometries.

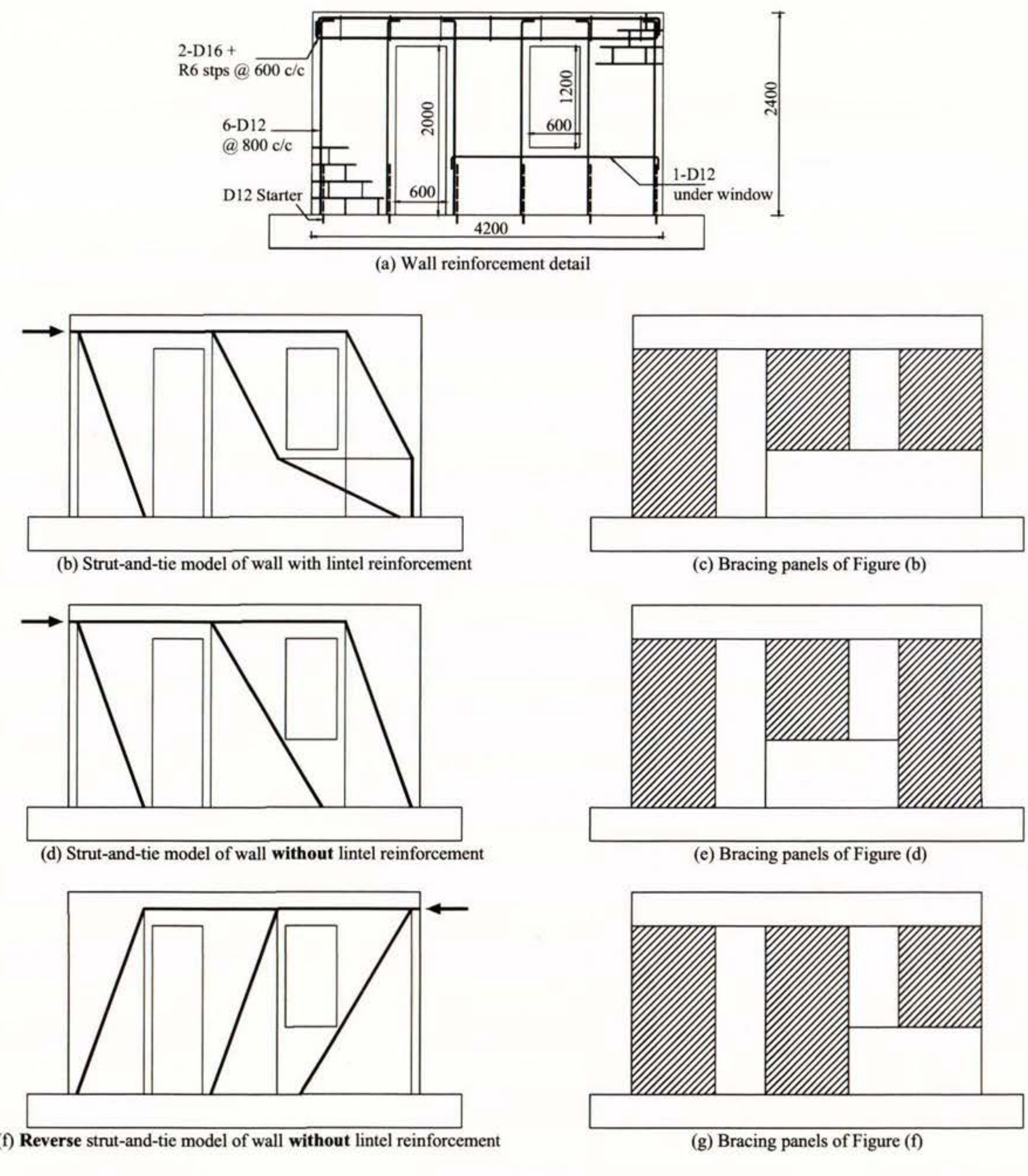

(a) Wall reinforcement detail

(b) Strut-and-tie model of wall with lintel reinforcement

(c) Bracing panels of Figure (b)

(d) Strut-and-tie model of wall **without** lintel reinforcement

(e) Bracing panels of Figure (d)

(f) **Reverse** strut-and-tie model of wall **without** lintel reinforcement

(g) Bracing panels of Figure (f)

Figure 1.1 Strut-and-tie modelling of nominally reinforced concrete masonry walls.

1.2 Scope of Study

This report describes the results from structural testing of eight perforated single storey-height partially grout-filled concrete masonry walls that were constructed and assembled using New Zealand masonry units utilizing pumice aggregate, and assembled using common local construction techniques. The primary objective of this study was to validate the adequacy of NZS 4229:1999 in addressing the bracing capacity of masonry walls containing openings. These eight partially grouted concrete masonry walls had variations in trimming reinforcement detailing, including those complying to NZS 4229:1999, and a range of penetration geometries. A parallel issue was to investigate the influence which shrinkage control joints has on the bracing capacity of partially grouted concrete masonry walls. NZS 4229:1999 prescribed a procedure to account for shrinkage control joints, but this detail had never been verified through structural testing. Consequently, experimental testing on two partially grout-filled concrete masonry walls was conducted to validate the structural adequacy of the shrinkage control joint detail published in NZS 4229:1999.

Chapter 2 of this report provides a brief review of previous studies that attempted to establish the lateral strength of masonry walls containing openings. Chapter 3 describes the construction and loading procedure used in the testing of the ten partially grout-filled concrete masonry walls mentioned above. Chapter 4 presents experimental results and Chapter 5 investigates the effect of design parameters on these experimental results. Chapter 6 of this report determines the adequacy of NZS 4229:1999 in addressing the lateral strength of masonry walls containing openings. This was achieved by comparing the results derived using the NZS 4229:1999 prescribed bracing capacities with those predicted using the modified plastic collapse analysis for perforated masonry walls.

Chapter 2

Literature Review

2.1 Introduction

Because of their role as lateral load resisting elements, masonry shear walls have attracted the attention of many researchers. However, most of this research was carried out to study the behaviour of solid masonry shear walls, despite the fact that masonry walls are commonly constructed with openings. Introducing openings in a wall alters its behaviour and adds complexity and difficulties in analysis and design. An extensive literature review by Voon and Ingham (2003) verified the earlier finding by Brammer (1995) that there exists little data from outside New Zealand that is directly relevant to the performance of nominally reinforced masonry walls that were constructed according to the specifications contained in NZS 4229:1999. This section of the report provides a brief review of those studies that have direct relevance to the issues discussed in Section 1.1.

2.2 Research Conducted in New Zealand

Brammer (1995) performed quasi-static in-plane cyclic load tests on twelve nominally reinforced concrete masonry walls. Nine of these walls were partially grout-filled, where only those cells containing vertical reinforcement were grouted, and the remaining three walls were solid grout-filled. All walls were constructed to a common height of 2400 mm with horizontal reinforcement placed in a bond beam within the top two courses, but varied in wall length and thickness (see Figure 2.1 for typical reinforcement of a nominally reinforced concrete masonry wall). None of the walls had applied axial load. The main objective of this study was to compare the attained test behaviour with that assumed and predicted by the New Zealand design standards NZS 4229 and NZS 4230, and to examine the response of nominally reinforced masonry walls when subjected to cyclic loading. Attention was given to maximum strength, stiffness, ductility, modes of failure, force-displacement characteristics, base course slip, and also the shear and flexural components of displacement.

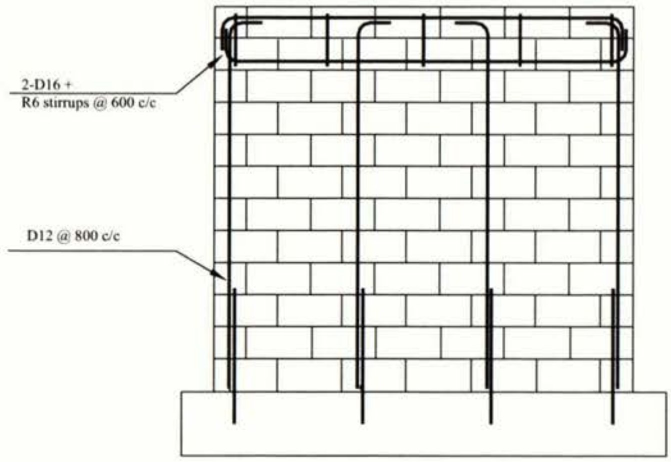

Figure 2.1 Typical reinforcement details of nominally reinforced concrete masonry wall.

Due to the lack of horizontal shear reinforcement in the walls of Brammer's study, it was observed that most walls failed in diagonal tension with failure characterized by the development of early flexural cracking which was later exaggerated by diagonal cracking that extended throughout the whole masonry wall. Figure 2.2 shows the force-displacement response derived from two typical wall tests, for partially grout-filled walls with lengths of 2600 mm and 4200 mm respectively. In both cases, the walls were constructed of 15 series concrete masonry precast units, with a corresponding wall thickness of 140 mm. From Figure 2.2 a number of general characteristics of partially grout-filled concrete masonry walls can be identified:

1. The maximum strength was typically developed during the first excursion to $\mu = 4$. Following this, cracking became significant and strength degraded.
2. Less hysteretic energy was expended during the second cycle to any displacement level, when compared with the first displacement cycle. This is illustrated by the more pinched hysteresis loops on the second cycle.
3. None of the tests exhibited a sudden failure, as is typical for conventional shear failure. Instead, strength degraded in a gradual manner.
4. Lateral displacements mostly arose from both flexure and shear modes of deformation. The presence of shear deformation is implied in Figure 2.2 through the pinched nature of the inelastic hysteresis loops.
5. The absence of damage in the solid grout-filled bond beam and the general geometry of the deformed walls supported the notion of frame-type action being developed at later stages of testing.

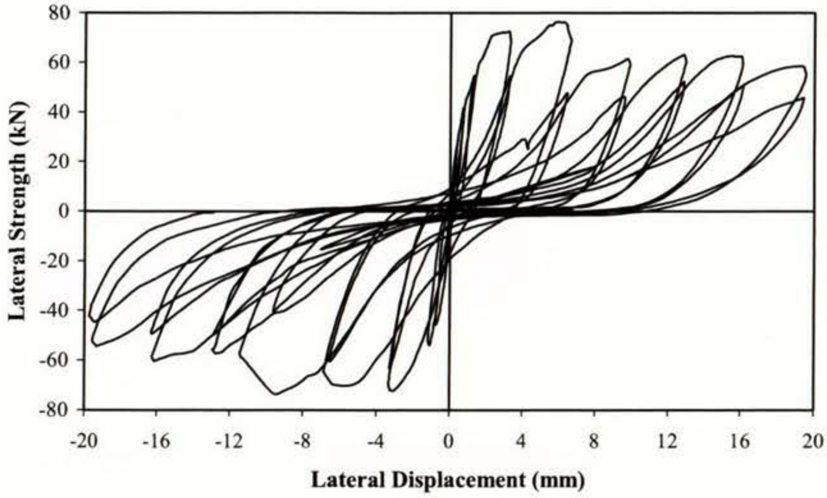

(a) 2600 x 2400 x 140

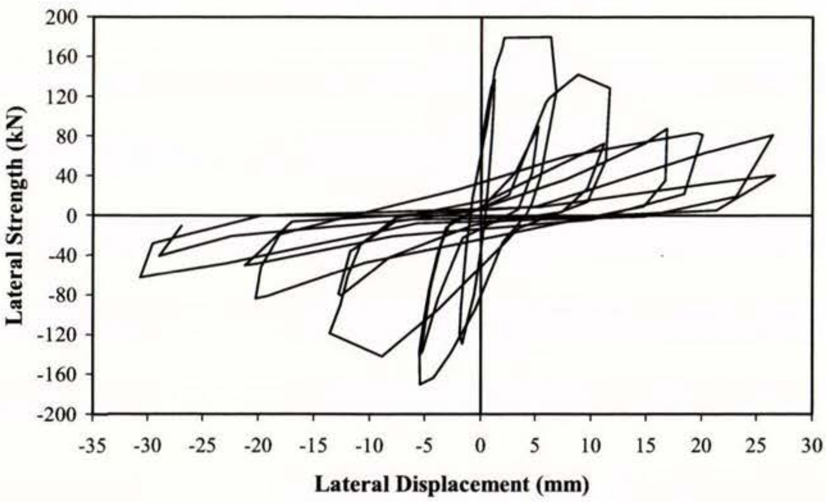

(b) 4200 x 2400 x 140

Figure 2.2 Force-displacement histories of partially grout-filled concrete masonry walls.

An important finding concluded from this study was that the ductile diagonal tension mode developed even in the case when the dependable shear strength predicted using NZS 4230:1990 shear expressions was less than the wall nominal flexural strength. This indicated that the predicted shear strength using NZS 4230:1990 was of limited relevance for concrete masonry structures having a reinforcement distribution as indicated by Figure 2.1 and supporting little axial compressive load. It was concluded that this was partially because NZS 4230:1990 was conservative in shear prediction, but more importantly due to the frame action generated by the use of a bond beam and the shear friction generated between blocks during lateral deformation. The information collected from Brammer's study was then used to develop the bracing capacity tables presented in NZS 4229:1999.

Davidson (1996) extended Brammer's research to investigate the behaviour of walls with openings and applied axial compression stress. Two nominally reinforced concrete masonry walls having the same geometry (4200 mm long x 2400 mm high x 190 mm wide) were constructed so that they had an identical arrangement of a 2000 mm x 600 mm 'doorway' and a 1200 mm x 600 mm 'window' (see Figure 1.1a), with the only difference being the magnitude of the applied axial compressive load. The 'doorway' and 'window' were arranged in a manner enabling the vertical reinforcement to be placed at 800 mm centres. Please note that the reinforcement used in this study was of $f_y = 275$ MPa.

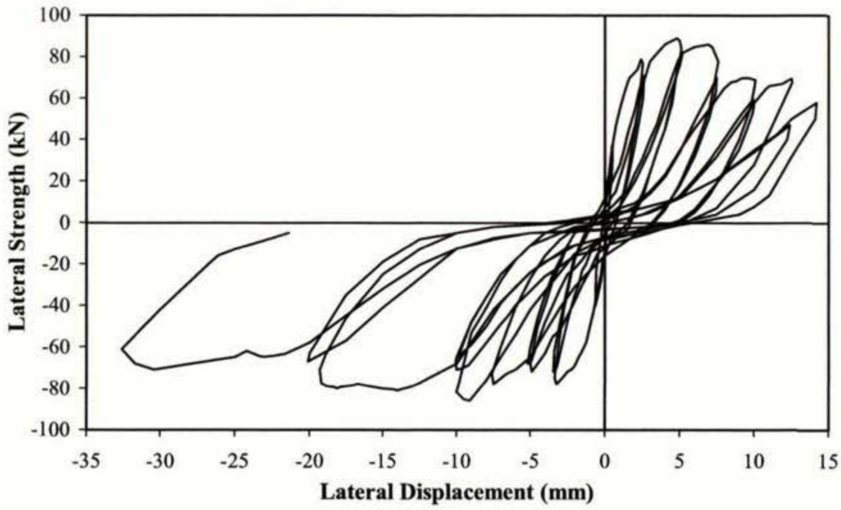

Figure 2.3 Force-displacement history of partially grout-filled concrete masonry wall with openings.

The force-displacement response of the 4200 mm long perforated concrete masonry wall with axial compressive load is shown in Figure 2.3. A comparison of this test result with those obtained by Brammer (1995) illustrated that the capacity of the masonry wall with openings, tested by Davidson, was approximately half that of the complete wall. Furthermore, the test results successfully showed that compression stress was effective in increasing the lateral strength of the perforated masonry wall. Consequently, it was concluded from this study that openings have a detrimental effect on the lateral strength of masonry walls while axial compression stress is beneficial. Furthermore, it was successfully illustrated that a plastic hinge model which assumed flexural hinges forming at the bases of all piers, at the top of the central pier and in the lintels was able to represent the bracing capacity of the partially grout-filled masonry walls included in this study.

In addition to the experimental studies conducted by Brammer and Davidson at the University of Auckland, two research projects were conducted at the University of

Canterbury as part of the development of NZS4229:1999. The first of these was conducted by Singh et al. (1999). The study established that ductile response could be achieved for long walls loaded out-of-plane. This study was further extended (Zhang, 1998) to investigate the performance of two walls that had door and window openings at structurally inappropriate locations. The information gathered at the University of Canterbury was used in the development of the bond beam criteria in NZS4229:1999.

2.3 Research Conducted Overseas

Elshafie et al. (2002) conducted experimental testing on thirteen single storey-height $^1/_3$-scale solid grout-filled masonry walls with openings. The primary objective of this study was to develop a simple analysis approach employing plastic hinge failure mechanisms to predict failure mechanism and lateral load carrying capacity. The test specimens in this study were designed to behave mainly in a flexural mode by forming plastic hinges at the member ends (i.e. enough shear reinforcement was provided to suppress shear failure in different wall elements). Experimental results from this study showed that the plastic hinge model developed by Leiva at al. (1990a, 1990b and 1994) provided a good estimate for the lateral load capacity of masonry shear walls containing openings. Consequently, the following failure mechanisms may develop, depending on the relative strength of the wall sections:

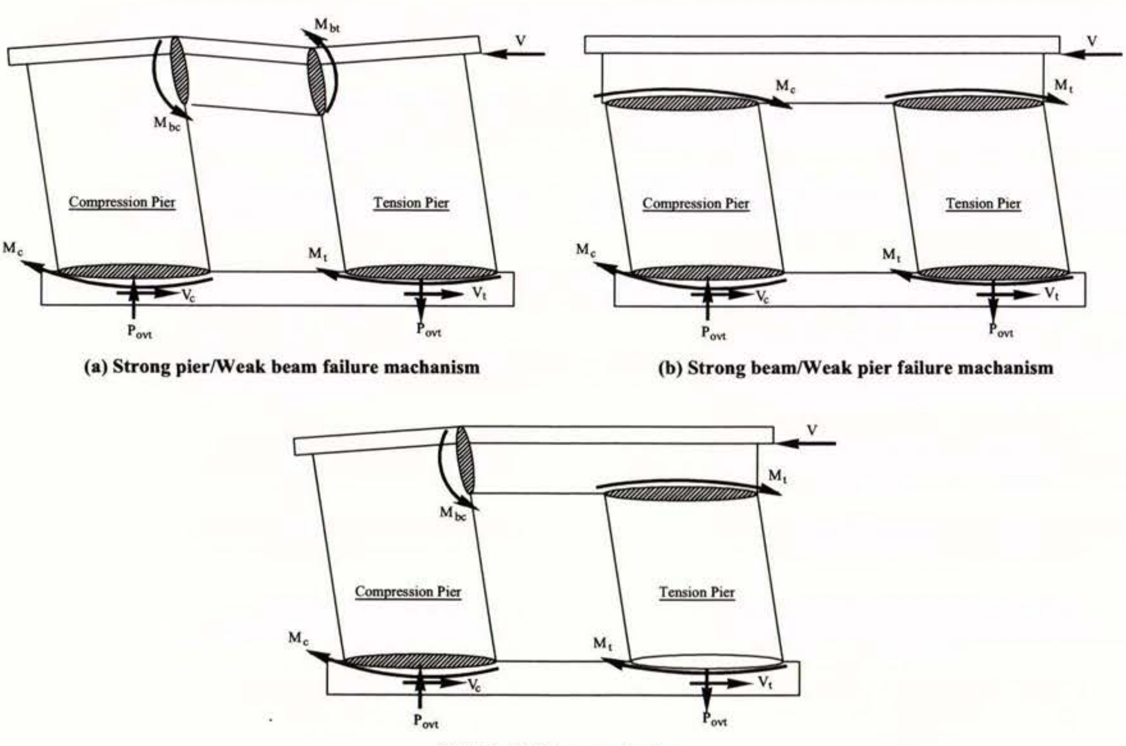

Figure 2.4 Failure mechanisms for wall with opening.

a) Strong pier/weak beam mechanism in which the wall fails by forming plastic hinges (shaded areas) at both ends of the coupling beam(s), then plastic hinges at the pier bases as shown in Figure 2.4a;
b) Strong beam/weak pier mechanism in which the wall fails by forming plastic hinges at both ends of all piers as shown in Figure 2.4b;
c) Mixed mechanism in which a combination of mechanisms (a) and (b) develops as shown in Figure 2.4c;

The experimental results of Elshafie et al. (2002) indicated that a simple model proposed by Hart et al. (1988) provided a good estimate for the post-cracking stiffness of the test specimens. Also, it was observed in this study that for shear walls with similar overall dimensions and flexural reinforcement arrangements, the effects of openings on the reduction of the wall strength and stiffness were proportional, i.e. the ratio of reduction in stiffness due to openings is equal to the ratio of reduction in strength.

2.4 NZS 4229:1999 Codification of Wall Capacity

Wall bracing capacities were calculated considering the masonry performance once the nominal shear strength had been exceeded. As demonstrated by Brammer (1995), it was established that nominal lateral strength was satisfactorily evaluated based on a rectangular masonry compression stress block using Equation 2-1, assuming $f_y = 300$ MPa and $f'_m = 8$ MPa, and treating the walls as vertical flexural cantilevers with a height measured to the centre of the fully grouted bond beam. Bracing capacities are reported in NZS 4229:1999 in tabular form for various wall thickness and grout-fill options, as illustrated in Table 2.1 for partially grouted 15 Series (140 mm thick) concrete masonry, where 100 bracing units corresponds to 5 kN. It is necessary to point out that conservatism of the NZS 4229:1999 evaluated bracing capacities with respect to the experimental results (Brammer, 1995 and Davidson, 1996) was primarily attributed to the actual material strengths being significantly greater than specified, the adoption of a flexural strength reduction factor of $\phi = 0.8$, and a further reduction to 80% of the evaluated capacity for walls having a length greater than 3.0 m. Also, in all cases the calculation assumed the vertical reinforcement of $\varnothing$ 12 mm to be distributed at a maximum spacing of 800 mm (where possible) or for bars to be spaced in the least favourable positions, resulting in the most conservative flexural strength.

$$F_n = \frac{\frac{W_t}{2}\left(L - \frac{W_t + \sum_i^n A_{si} f_{yi}}{0.85 f'_m b}\right) + \sum_i^n A_{si} f_{yi} j d_i}{H} \quad (2\text{-}1)$$

Table 2.1 Bracing Capacities* for 15 Series Partially Grouted Concrete Masonry

Panel height (m)	Panel length (m)										
	0.8	**1.2**	**1.6**	**2.0**	**2.4**	**2.8**	**3.2**	**3.6**	**4.4**	**5.2**	**6.0**
0.8	385	650	1005	1425	1935	2505	2525	3110	4455	6040	7870
1.0	330	560	865	1230	1670	2165	2185	2690	3855	5225	6810
1.2	275	470	730	1035	1405	1825	1840	2265	3250	4415	5750
1.4	245	420	650	930	1260	1635	1650	2030	2920	3960	5160
1.6	215	370	575	820	1115	1445	1460	1800	2580	3505	4575
1.8	195	335	525	750	1020	1325	1340	1650	2370	3220	4200
2.0	180	305	480	680	925	1205	1220	1500	2155	2930	3825
2.2	165	280	445	635	860	1120	1335	1400	2005	2730	3565
2.4	155	260	410	585	800	1040	1050	1295	1860	2530	3305
2.6	145	245	385	550	750	980	985	1220	1755	2385	3115
2.8	130	230	360	515	705	915	925	1140	1645	2240	2920
3.0	125	215	340	490	665	870	880	1085	1560	2125	2780

* 100 Bracing Units corresponds to 5 kN

Recalling that NZS 4229:1999 is primarily intended for use by architects and draftspersons, rather than structural engineers, a simplified procedure was adopted for the assessment of bracing capacity. The strategy employed in NZS 4229:1999 for proportioning bracing capacity is primarily dependent on wall geometry. The assumption was that the bracing capacity of a masonry wall having penetrations could be determined based on the geometry of individual bracing panels, as demonstrated by the shaded areas shown in Figure 4.1, where the geometry of each bracing panel is based upon the vertical dimension of the smallest adjacent opening. The total bracing capacity is then assumed to be the sum of the capacities provided by the individual bracing panels of the wall. From Table 2.1 it is evident that the wall bracing capacity increases as the panel length increases, but diminishes as the panel height increases. This prompted some observers to comment on the influence which a small wall opening would have, as this would effectively generate two bracing panels with a small height, rather than a single panel that is taller and longer, such that it is conceivable that the addition of a small wall opening might result in the evaluated capacity of the wall to increase.

2.5 Shrinkage Control Joint

Differential movement creates cracking in masonry construction when excessive stress is allowed to develop. Control joints are one method used to relieve horizontal tensile stresses due to shrinkage of the concrete masonry units, mortar, and when used, grout. They are essentially vertical separations built into the wall at locations where stress concentrations may occur. Control joints are typically only required in exposed concrete masonry walls, where shrinkage cracking may detract from the appearance of the wall. Shrinkage cracks in concrete masonry are an aesthetic, rather than a structural concern (Beck at al., 1988). In many cases, horizontal reinforcement is used to control shrinkage cracking, but strategically located control joints will further assist in the elimination of random cracks, and prevent moisture penetration which might otherwise occur.

The placing of control joints in walls is a matter of judgement by the designers with consideration being given to the type of construction, shape of walls (accounting for features such as openings) and the amount of reinforcement in the walls and exposure to weather. In the case of nominally reinforced concrete masonry walls, NZS 4229:1999 requires shrinkage control joints to be provided at no more than 6 m centres. In addition, NZS 4229:1999 requires that vertical control joints be located:

a) Within 600 mm of return angles in T and U-shape structures;
b) Within 600 mm of L shaped corners or by restricting the spacing to the next control joint to 3.2 m maximum;
c) At changes in wall height exceeding 600 mm;
d) At changes in wall thickness.

NZS 4229:1999 requires that the non-structural reinforcement, such as the horizontal reinforcement that is used for crack control only, should be discontinuous through a control joint, since this will otherwise restrict horizontal movement. However, structural reinforcement, such as bond beam and lintel reinforcement at the floor and roof diaphragms that resists diaphragm cord tension, must be continuous through the control joint.

Chapter 3

Test Programme

3.1 Introduction

In order to compare the standard predicted and the actual wall behaviour, and to ascertain the force-displacement and other behavioural characteristics of partially grout-filled nominally reinforced concrete masonry walls, two series (A and B) of masonry walls were tested in the Civil Engineering Test Hall at the University of Auckland, consisting of a total of ten masonry walls. The eight specimens tested in Series A were concrete masonry walls containing openings. These walls had a range of opening geometries and variations in the trimming reinforcement detailing below window openings. The objectives for this part of the research were to study the performance of concrete masonry walls with openings under seismic loading and to validate the adequacy of NZS 4229:1999 in addressing the bracing capacity of these types of masonry walls. The remaining two test specimens of Series B were solid built concrete masonry walls (i.e. no opening within the wall) that incorporated a vertical shrinkage control joint at the centre of each wall. These two walls were tested to validate the structural adequacy of the shrinkage control joint detail published in NZS 4229:1999.

3.2 Test Set-up

The testing of specimens (except the second wall test of Series B, see Appendix B.2 for detailed description) reported herein was conducted according to the set-up shown in Figure 3.1. The test set-up and method of loading adopted in this experimental programme were designed to simulate the response that a masonry shear wall would experience during seismic excitation. Although a single-storey wall does not have the complexity of a multi-storey structure, it is advantageous to consider due to the ease of data interpretation. Horizontal cyclic loading was applied to the top of the wall via a 150 x 75 steel channel as shown in Figure 3.1, which was fastened to the top of the bond beam by cast-in bolts. The jack was fastened to the strong wall and the tested wall was stabilised from moving in its out-of-plane direction by two parallel horizontal struts which were positioned perpendicular to the wall and hinged to the channel and a reaction frame. It is recognised that this type of horizontal force transfer is of a cantilevered wall type and therefore may not be representative of all structures.

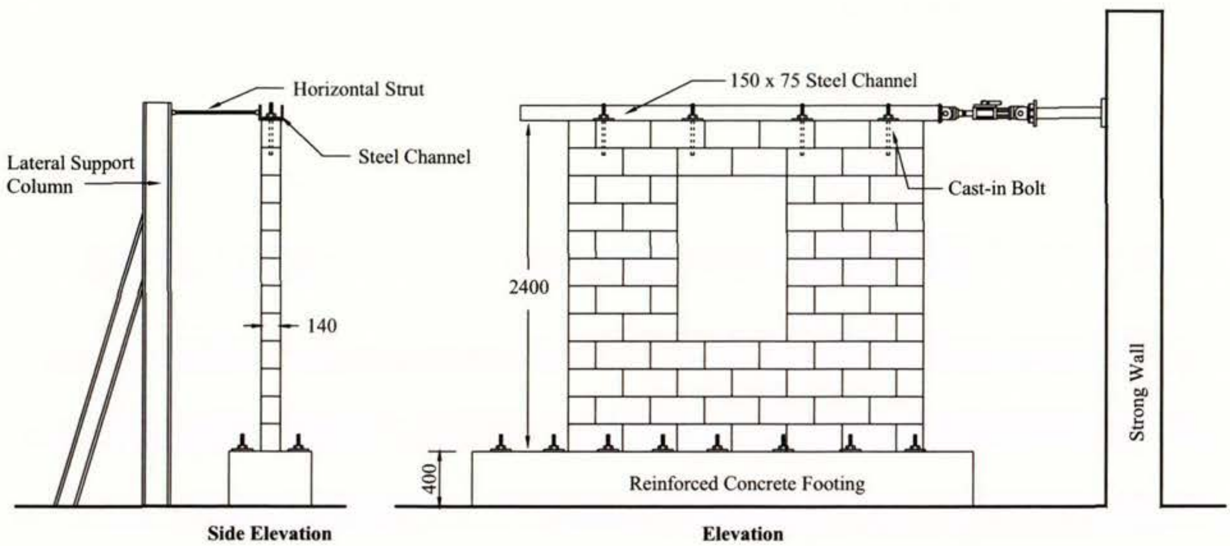

Figure 3.1 Typical test set-up.

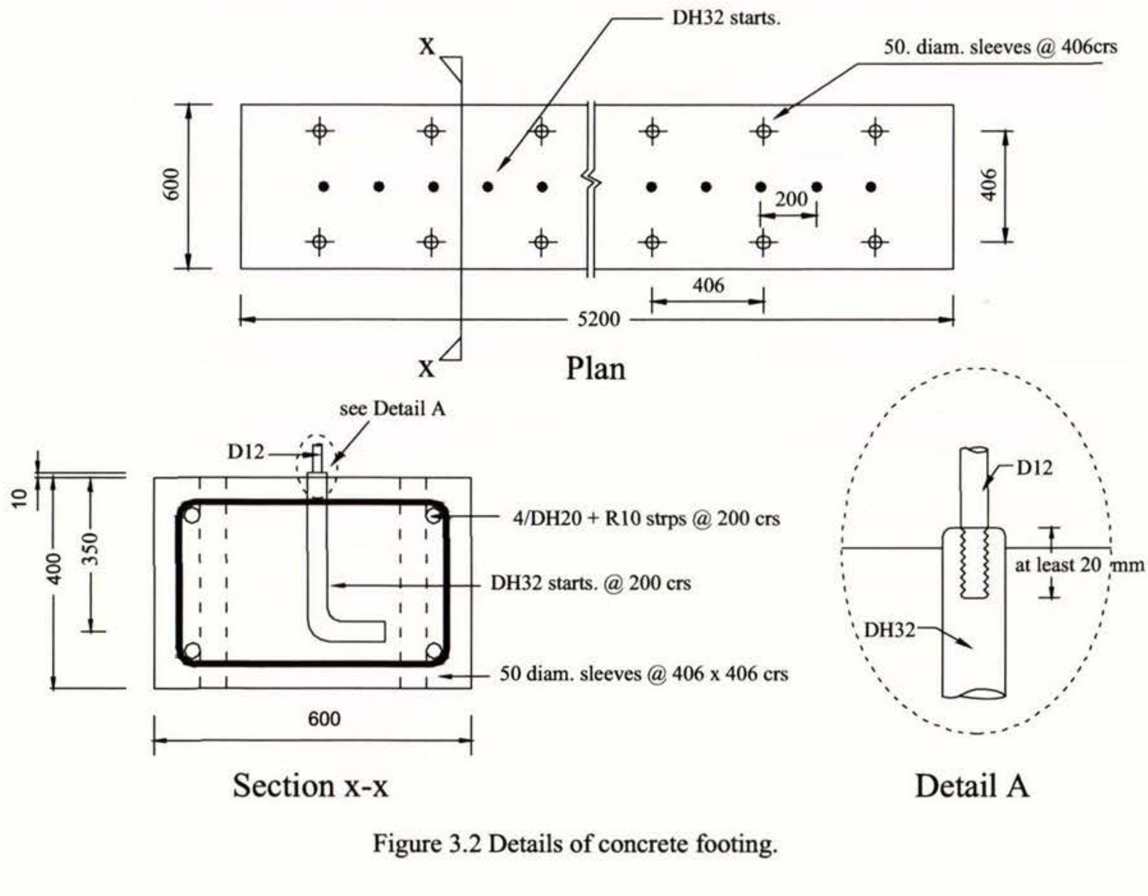

Figure 3.2 Details of concrete footing.

All walls were constructed on a 5.2 m long re-usable reinforced concrete footing. As shown in Figure 3.2, the re-usable concrete footing had DH32 starter bars spaced at 200 mm centres that were drilled and tapped to accommodate D12 vertical reinforcement. The concrete footing was stressed down to the laboratory floor with eight high strength steel rods, each loaded to approximately 300 kN so that sufficient shear friction was provided to eliminate any slip between the footings and the floor. Each of the wall D12 starters was first tapped at one end, then threaded into the DH32 starters that protruded from the reinforced concrete base. The wall vertical reinforcement was lap-spliced immediately above the foundation, imitating typical construction practice as indicated in Figure 8.1 of NZS 4229:1999.

3.3 Construction Materials

The walls were constructed by experienced blocklayers under supervision, and consisted of a running bond pattern of standard grey precast concrete masonry block units using DRICON™ trade mortar. Prior to wall construction, the 650 mm long D12 starter bars were threaded into the DH32 starters that protruded from the concrete footing, allowing the D12 starter reinforcement to penetrate the wall to a distance of not less than 600 mm.

3.3.1 Concrete Masonry Block

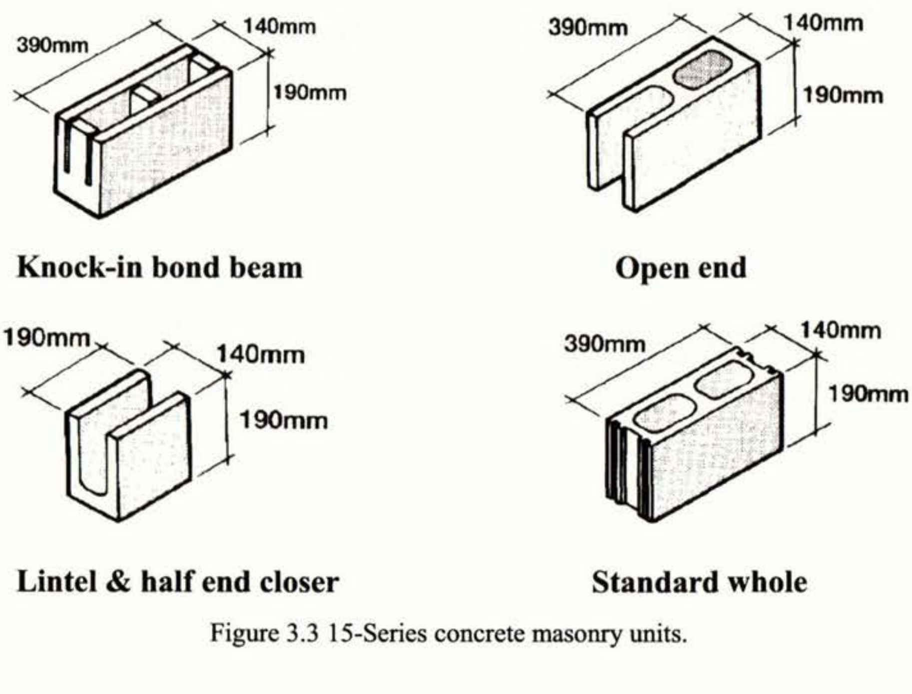

Figure 3.3 15-Series concrete masonry units.

The masonry blocks used in this study were standard production 15 series concrete masonry precast units (CMUs). Open-end bond beam CMUs were used at the bond beam layer to allow the placement of D16 horizontal reinforcing steel. Half end-closer blocks were used at the edge and lintel positions. See Figure 3.3 for block geometries.

3.3.2 Mortar and Grout

DRICON^{TM} mortarmix – a mortar that is commonly used in masonry construction throughout New Zealand, was used as mortar for construction of the test walls. High slump ready-mix grout using small aggregate was employed to partially fill the concrete masonry walls. An expansive chemical additive (SIKA Cavex) was also added to the grout to avoid formation of voids caused by high shrinkage of the grout.

3.3.3 Reinforcing Steel

All reinforcing steel used in this study was grade 300 MPa, consisting of D12 for the vertical reinforcement, D16 for the bond beam reinforcement and R6 for stirrups. The vertical reinforcement was erected as discussed in section 3.2, and the D16 had standard 90^{o} hooks at both ends.

3.4 Specimen Construction Details

The geometries and reinforcement details of the ten single-storey masonry walls are shown in Figures 3.4 and 3.5. All ten walls were partially grout-filled, where only those cells containing reinforcement were grouted, and were constructed to a common height of 2400 mm. None of the ten masonry walls had applied axial compression load. The eight test specimens in Series A had variations in trimming reinforcement detailing (see Figure 3.4), including those complying to NZS 4229:1999, and a range of penetration geometries. As described in Section 3.2, the wall vertical reinforcement was lap-spliced immediately above the foundation, and was generally spaced at 800 mm centres as shown in Figure 3.4, with the exception being the two 3600 mm long walls in Series B where vertical bars were located at 100 mm away from the control joints as shown in Figure 3.5. The horizontal reinforcement in all walls consisted of two D16 reinforcing bars placed in a solid grout-filled bond beam within the top two block courses and a D16 trimming reinforcing bar placed below a window opening.

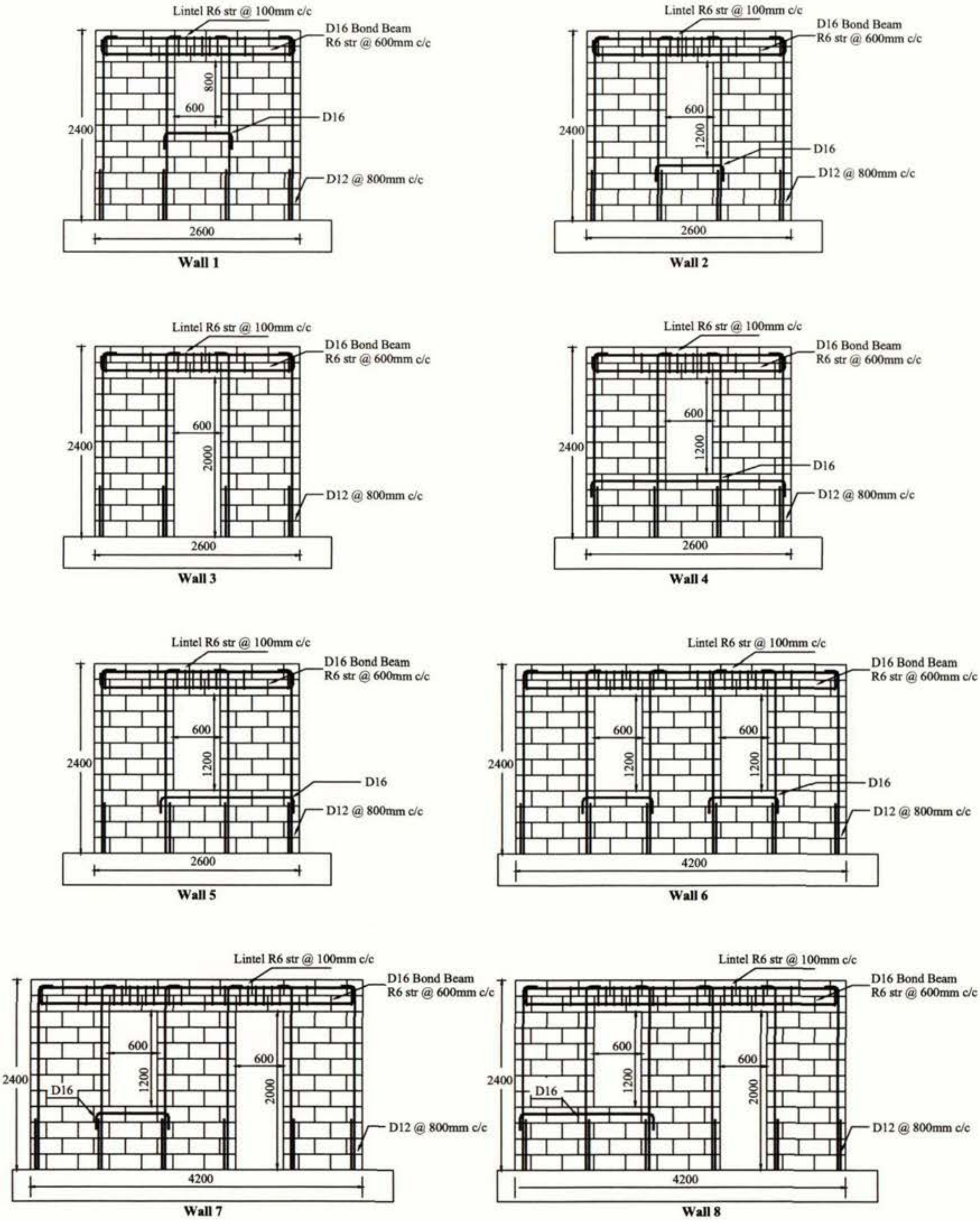

Figure 3.4 Series A, wall geometries and reinforcing details.

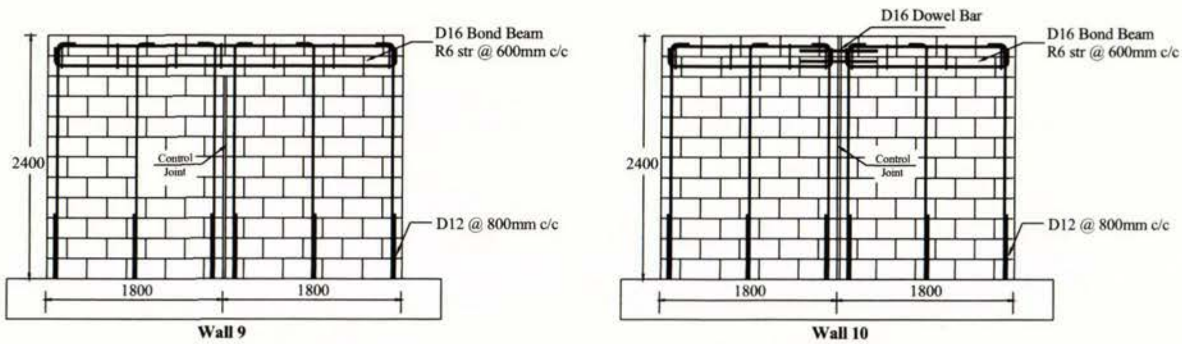

Figure 3.5 Series B, wall geometries and reinforcing details.

Unlike the eight masonry walls shown in Figure 3.4, the two specimens in Series B were solid built (i.e. no penetration) and had a vertical control joint at the centre of each wall. These two walls shared similar constructional details, with the only difference being the detailing of bond beam reinforcement at the control joint position. As shown in Figure 3.5, the control joint of Wall 9 was constructed in accordance with the specification of NZS 4229:1999, where the joint was terminated below the bond beam and the horizontal bond beam reinforcement was continuous through the joint. In the case of Wall 10, the control joint penetrated the full height of the wall and the horizontal bond beam reinforcing bars were terminated at 100 mm away from the joint. Two 800 mm long D16 dowel bars were placed across the control joint to transfer shear. In order to prevent the flow of grout across the control joint at the bond beam layer, a thin polystyrene strip was inserted to form a gap between the two piers, and the D16 dowel bars were then punched through the polystyrene strip. The dowels were greased and placed in a plastic sleeve on one side to avoid bonding to the grout.

3.5 Instrumentation

The wall instrumentation included two types of instruments: load cells and portal displacement transducers. Both types of devices were calibrated on a regular basis. At various stages of testing, all displacement transducers and the load cell were scanned by a data logger and the measured displacements from the transducers and force magnitudes from the load cell were recorded by a computer.

Portal displacement transducer

Portal displacement transducers consisted of a strain gauge attached to a spring steel strip between two rigid portal legs as shown in Figure 3.6. This type of instrument is capable of measuring relative movement between the legs. Any axial movement causes the steel strip to be subjected to flexure, and the transducer is calibrated so that the resulting strain in the strain gauge correlates to the axial displacement. This type of device is capable of measuring displacements of about ± 50 mm with acceptable accuracy.

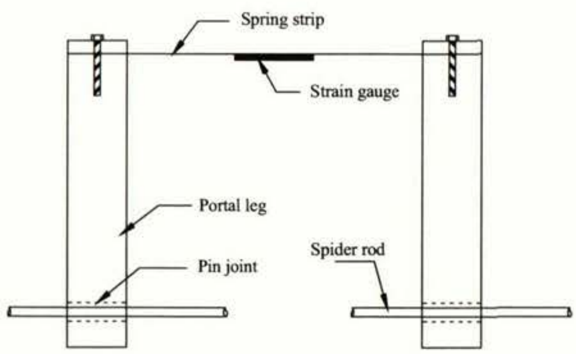

Figure 3.6 Portal displacement transducer.

Load cell

This device measured the magnitude of applied force from the hydraulic actuator. It consisted of a steel cylinder with strain gauges attached to the outer surface. Any deformation of the cylinder due to applied force caused a change in voltage output in the strain gauges.

3.5.1 Installation of Instrumentation

The arrangement for the measuring instrumentation is shown in Figures 3.7 and 3.8. A load cell to measure the magnitude of the lateral force was placed between the actuator and the steel channel, denoted as [0] in Figure 3.7. Portal displacement transducers, denoted as [1] and [2], measured lateral displacement at the top of the wall while displacements at the window levels were measured by instruments [3] and [4]. Portal displacement transducers [47] – [49] were used to measure sliding of the wall relative to the concrete footing, and transducers [45] and [46] measured the uplift at wall toe positions. Any slip in the steel channel and the concrete footing were measured by transducers [50] and [51] respectively. Further transducers were placed according to the configuration shown in Figure 3.7 to attain the shear and flexural components of deformation.

Measuring points were formed by drilling into the masonry and epoxy grouting 10 mm diameter mild steel studs that were threaded to accept aluminium rosettes. Steel rods of 4 mm diameter were fixed to the rosettes in a formation of 'spider webs' that triangulated the wall between the measuring points, as shown Figure 3.7.

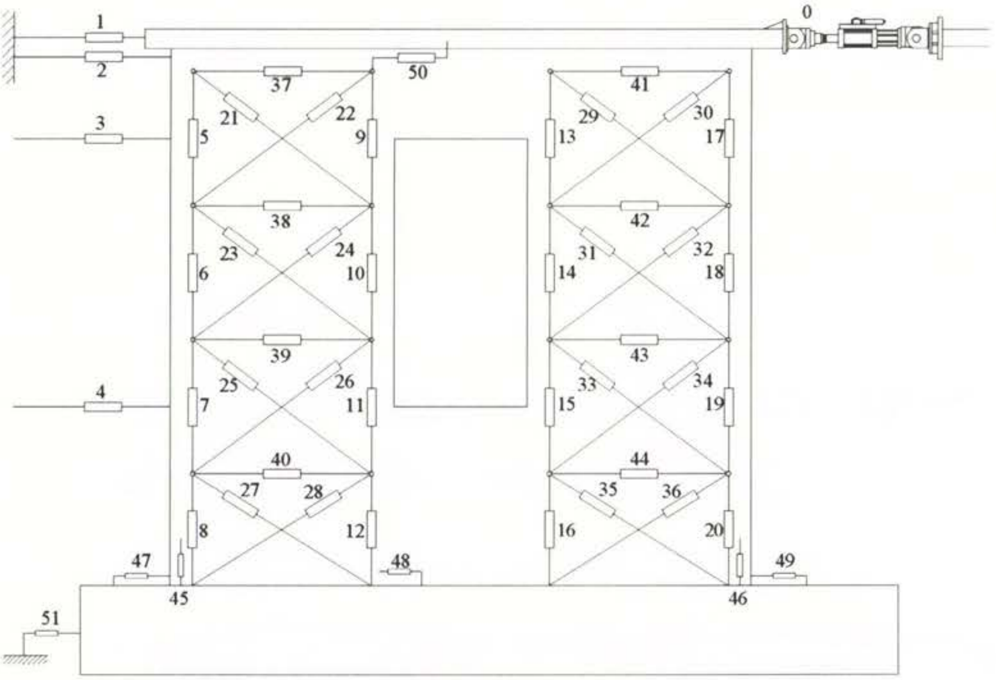

Figure 3.7 Instrumentation for test wall.

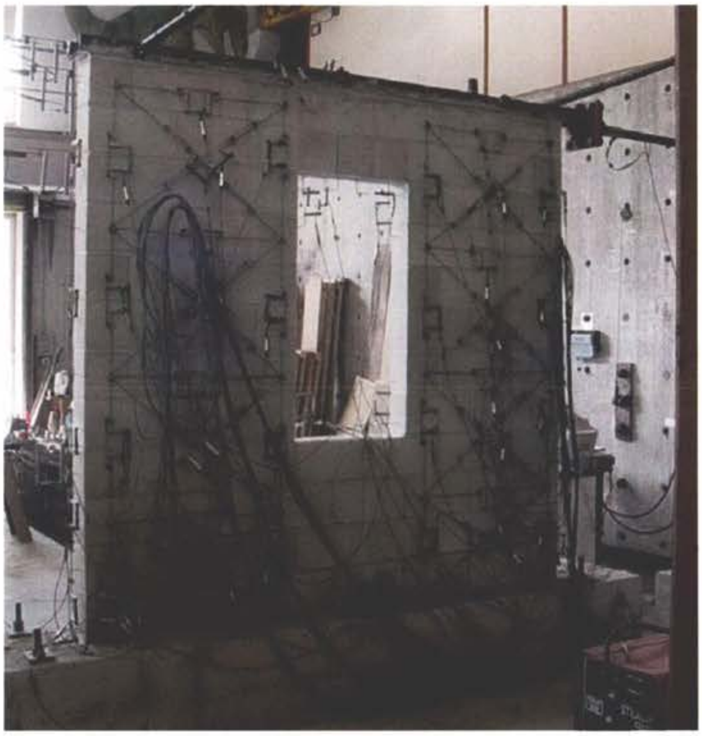

Figure 3.8 Instrumentation mounted on wall before testing.

3.6 Material Properties

Material testing was carried out to evaluate the key material properties: concrete masonry crushing strength (f'_m), compressive strength of mortar (f'_j) and grout (f'_g) used in wall construction, and the yield strength (f_y) of the reinforcing steel. Facilities for the compressive and tensile tests were both available at the University of Auckland.

3.6.1 Reinforcing Steel

Samples were taken from steel reinforcement used as flexural reinforcement in the wall panels. The samples were subjected to tensile testing using the Avery Universal Testing Machine at the University, see Figure 3.9. Each type of reinforcing steel used in the walls was from the same batch. Consequently, the average strengths of 305 MPa and 315 MPa were applied as the yield strength for the D12 and D16 reinforcing bars used in this experimental programme. An illustration of the tensile test results is presented in Figure 3.10.

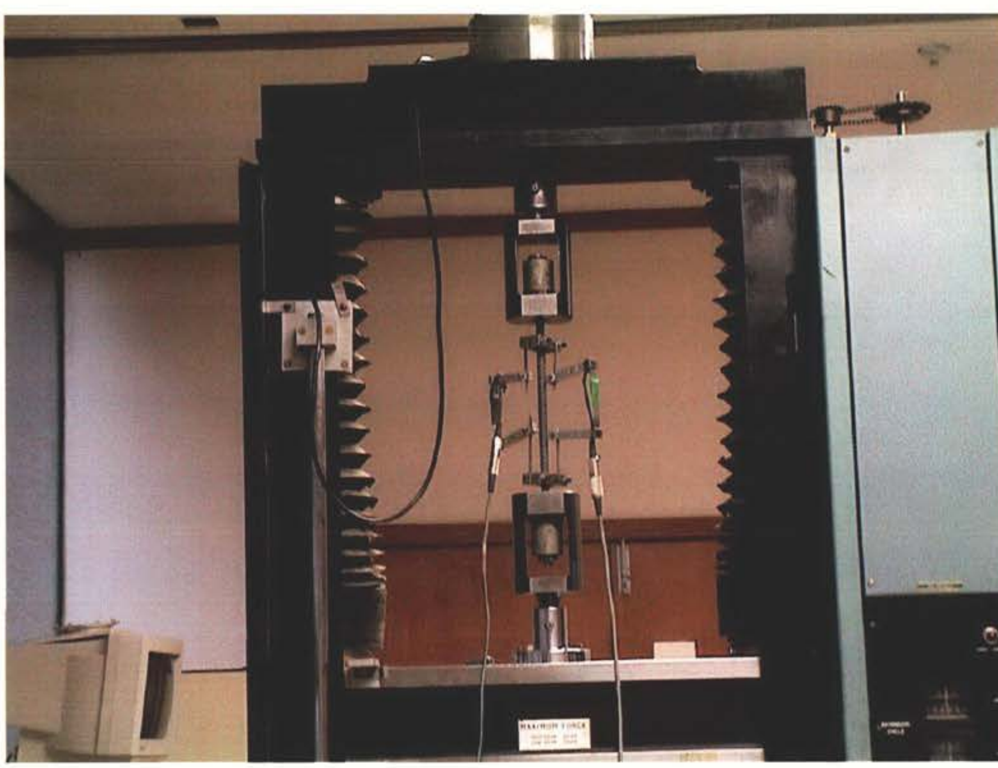

Figure 3.9 Reinforcing steel subjected to tensile test.

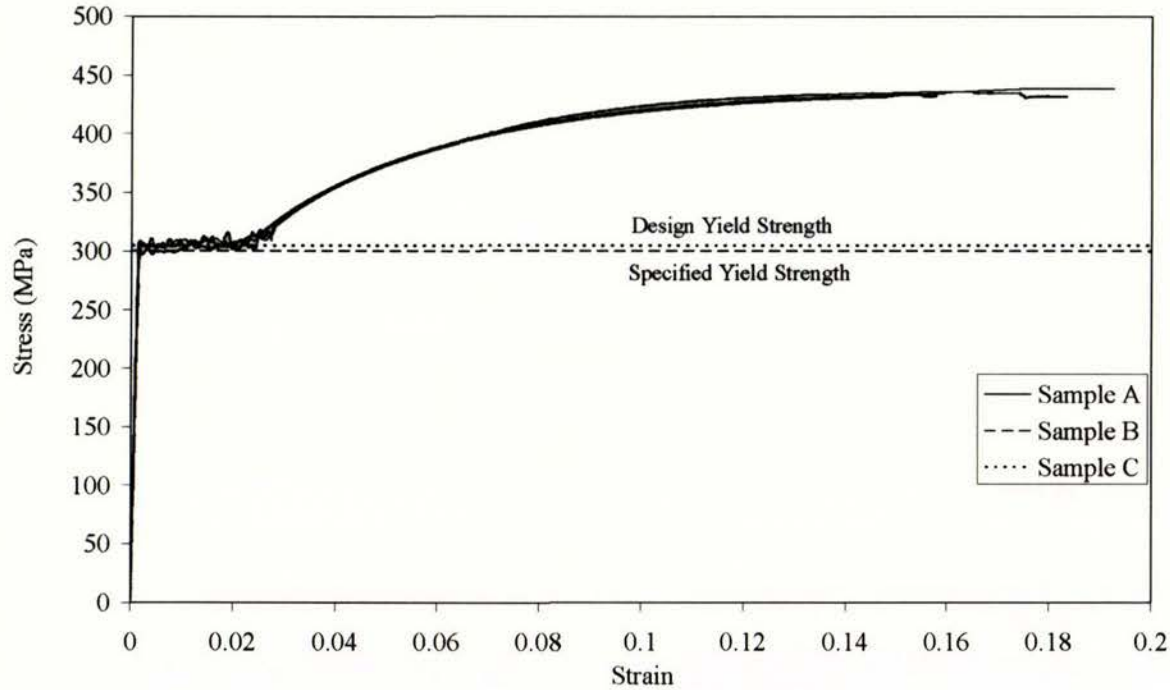

Figure 3.10 Stress-strain curve for D12 reinforcing bars.

3.6.2 Mortar and Grout

Standard test cylinders (100 mm diameter x 200 mm high) were taken from each batch of mortar and grout mixes.

3.6.3 Prisms

Masonry prisms were built at the completion of laying each wall (see Figure 3.11), using the same mortar and CMUs used in the wall. These prisms were built of three CMUs stacked on top of each other using the same construction technique as was used for the wall. The prisms were then filled at the same time as the walls, using the same grout. The prisms were tested using an Avery Testing Machine as shown in Figure 3.12. This type of test specimen provided the most accurate estimate of masonry compressive strength, f'_m . It is noted that f'_m for concrete masonry walls constructed of regular materials, found by prism testing at the University of Auckland, has consistently been above the $f'_m = 12$ MPa specified by NZS 4230:2004 for Type B Observation masonry.

Figure 3.11 Masonry prisms grouting.

Figure 3.12 Masonry prism subjected to compression test.

In the absence of machine testing, NZS 4230:2004 presents the following equations to estimate the characteristic masonry compressive strength f'_m :

$$f_m = 0.59\alpha f_{cb} + 0.90(1-\alpha)f_g \tag{3-1}$$

$$x_m = \sqrt{0.35\alpha^2 x_{cb}^2 + 0.81(1-\alpha)^2 x_g^2} \tag{3-2}$$

$$f'_m = f_m - 1.65x_m \tag{3-3}$$

where α represents the fraction of the gross cross-sectional area occupied by the masonry unit. In these equations, the terms f_{cb}, f_g and f_m represent the mean strength of CMU, grout and masonry respectively. Finally, x_{cb}, x_g and x_m represent the standard deviation of strength of CMU, grout and masonry respectively.

Chapter 4

Wall Strength Prediction

4.1 Flexural Strength of Perforated Walls

Prior to testing, the flexural strengths of the masonry walls were evaluated using the bracing capacity values (see Table 2.1) specified by NZS 4229:1999. Furthermore, two analytical methods were also employed to evaluate the wall strengths: strut-and-tie model (Yanez et al., 1991; Wu and Li, 2003) and plastic hinge model (Leiva et al., 1990; Davidson, 1996; Elshafie et al., 2002).

4.1.1 NZS 4229:1999 Procedure

The procedure employed in NZS 4229:1999 for proportioning bracing capacity was described in Section 2.4. The assumption was that the bracing capacity of a masonry wall having penetrations and/or shrinkage control joints could be determined based on the geometry of individual bracing panels, as demonstrated by the shaded areas shown in Figure 4.1, where the bracing capacity geometry of each bracing panel is based upon the vertical dimension of the smallest adjacent opening. The total bracing capacity is then assumed to be the sum of the capacities provided by the individual bracing panels of the wall. The evaluated wall strengths using the NZS 4229:1999 specified procedure are identified as F_{code} in Table 4.1. From Table 4.1 it is clearly illustrated that the wall strength decreases as the depth of opening increases. This is because taller bracing panels have less capacity than shorter bracing panels of the same length.

4.1.2 Simple Strut-and-Tie Models

Due to the presence of openings in Walls 1 to 8, Equation 2-1 was deemed to be inappropriate for evaluating the nominal flexural strength of these test specimens. Consequently, two types of strut-and-tie models were employed to evaluate wall strengths. The first type was a simplified strut-and-tie model, which assumed that all panels were pinned at the bond beam centre and lateral force was applied to the bracing panels from the

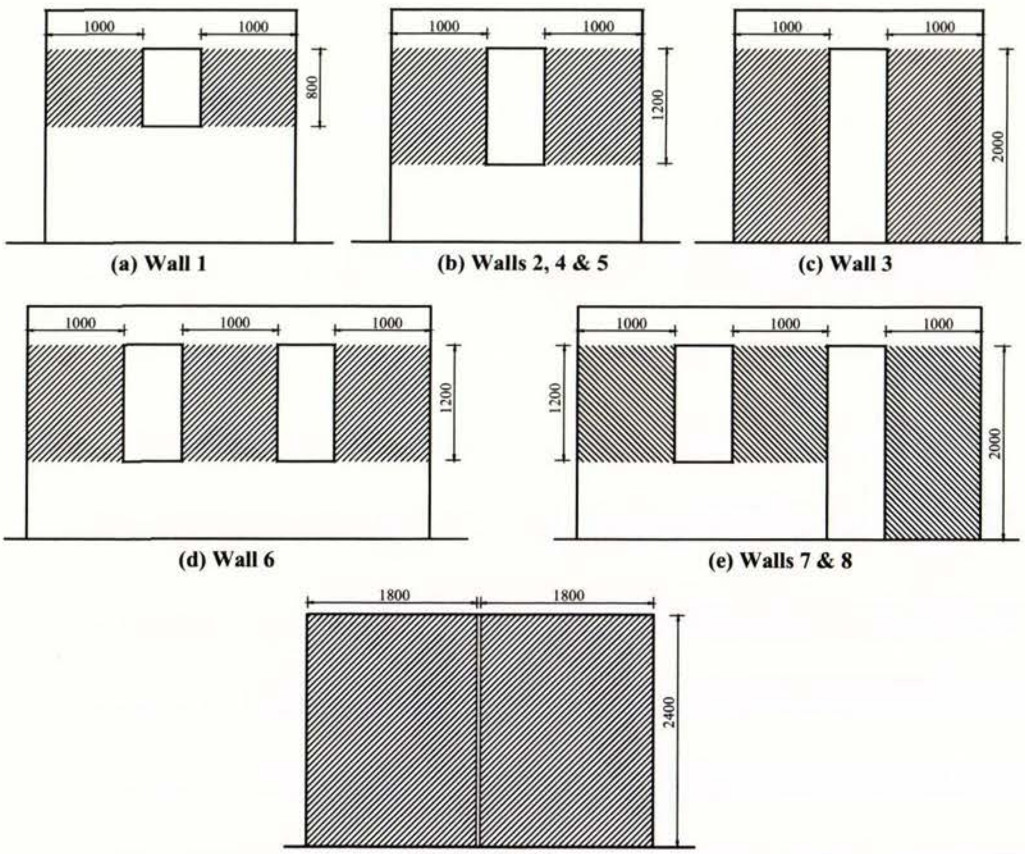

Figure 4.1 Identification of bracing panels

centre of the bond beam. In addition, the effect of wall self-weights was not considered in this simplified strut-and-tie model in order to ease the analysis process. The resultant strut-and-tie analyses using this simplified procedure are diagrammatically shown in Figures 4.2 and 4.3 for the push and pull directions respectively, where the strut are components indicated by a broader element thickness. It is also illustrated in Figure 4.2 that the introduction of extended trimming reinforcement beneath the window in Walls 4 and 5 would result in an increase in wall strength when compared to that predicted for Wall 2. This was due to a change of slope of the strut components in the right hand side panels of Walls 4 and 5. Similarly, the effect of extended trimming reinforcement in the pull direction can be observed by comparing the geometries of the left-most diagonal struts in Walls 4 and 8 with those predicted for Walls 2 and 7. The evaluated lateral wall strengths using the simplified strut-and-tie analysis is identified as $F_{n,st}$ in Table 4.1.

For Walls 9 and 10, regardless of the detailing of bond beam horizontal reinforcement, the wall flexural strengths were evaluated (according to the simplified strut-and-tie model) as the sum of strength provided by the individual 1.8 m long cantilever piers. The predicted lateral wall strengths for these two walls are presented in Figures 4.2 and 4.3 for the push and pull directions respectively.

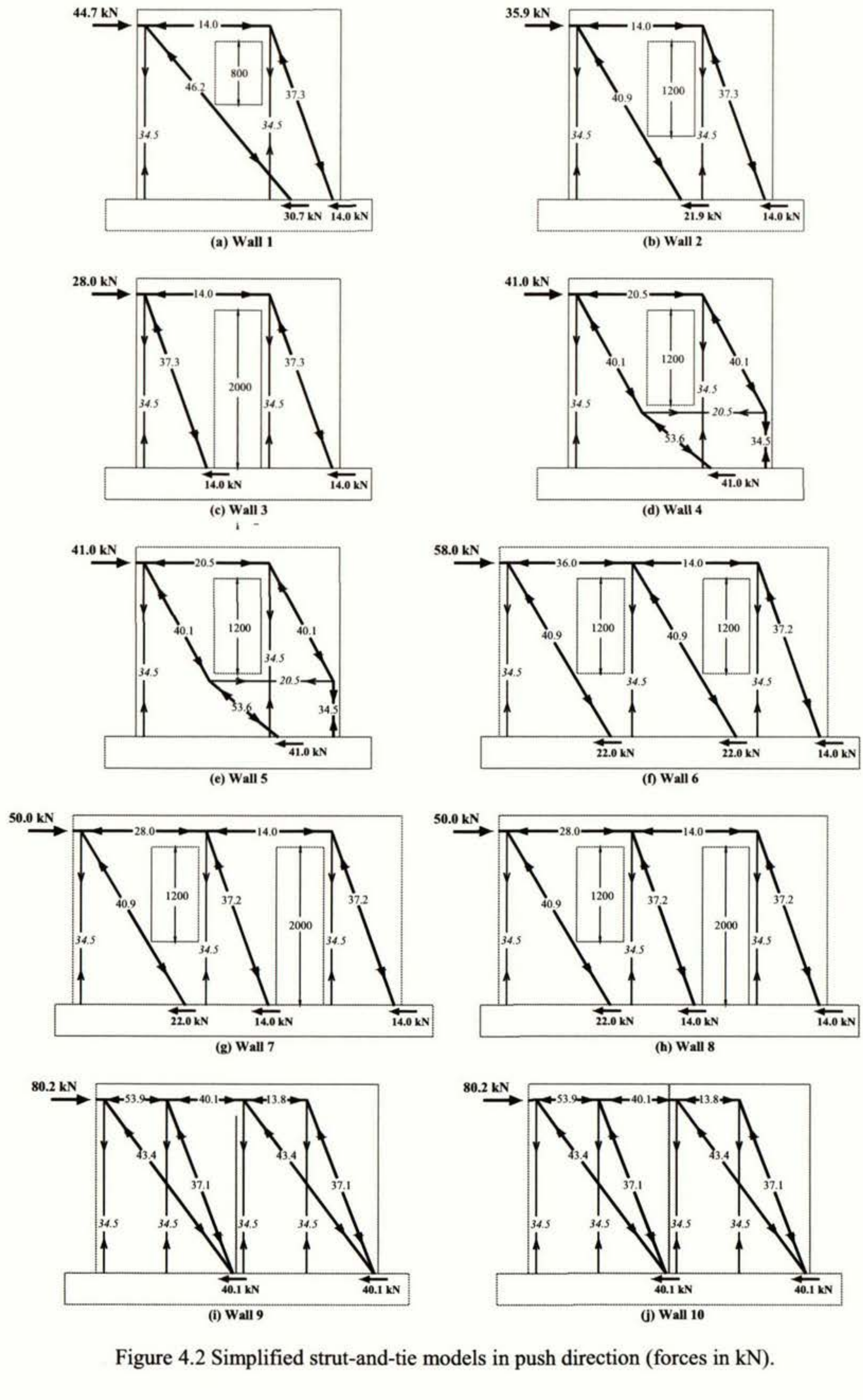

Figure 4.2 Simplified strut-and-tie models in push direction (forces in kN).

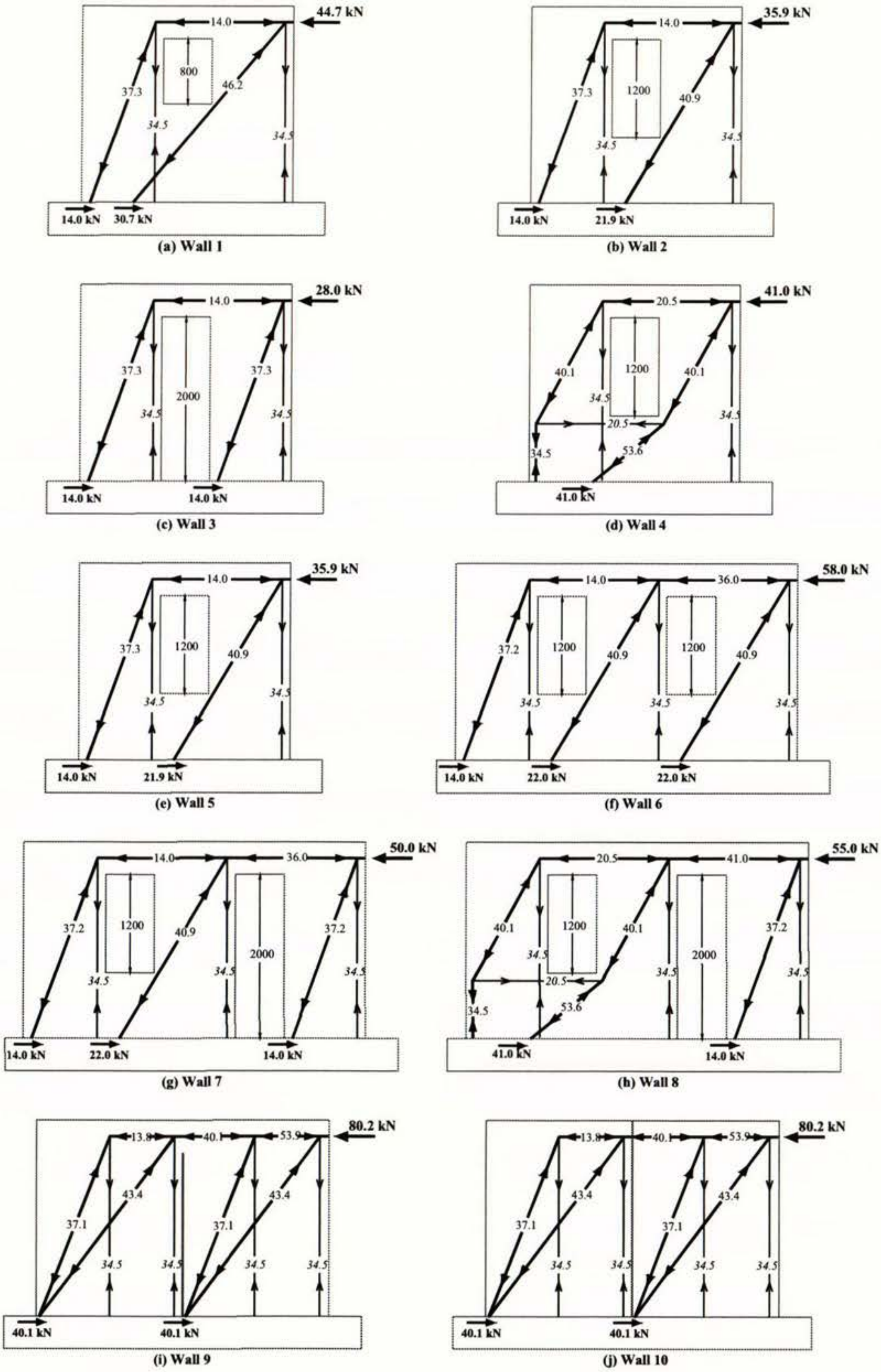

Figure 4.3 Simplified strut-and-tie models in pull direction (forces in kN).

4.1.3 Improved Strut-and-Tie Models

A second set of strut-and-tie models considered lateral force that was applied as a single point load at the centre of the wall top. These models are referred to here as "improved" to clearly delineate them from the "simple" models previously discussed. The lateral force was then transferred from the wall top to the bond beam centre through a triangular truss, which was subsequently applied to the bracing panels. Unlike the simplified models presented in Figures 4.2 and 4.3, the wall self-weight of 1.6 kN/m^2 was considered to act along the bond beam centre in the second strut-and-tie model. The resultant strut-and-tie analyses using the above mentioned procedure are diagrammatically shown in Figures 4.4 and 4.5 for the push and pull directions respectively, where the strut components are indicated by a broader element thickness. Similar to the simplified strut-and-tie analysis procedure discussed earlier, increase in predicted strengths are illustrated in Figures 4.4 and 4.5 when extended trimming reinforcement are included in walls having the same dimensions and identical penetration geometries. By comparing the strut-and-tie analyses presented in Figures 4.2-4.5, it is clearly shown that the addition of wall self-weight in the strut-and-tie analysis resulted in predicted strength increases of 4% to 10% for the 2.6 m long perforated concrete masonry included in this study. For the 4.2 m long masonry walls with two openings, the inclusion of wall self-weight and double bending of the central pier (see Figures 4.4 and 4.5) resulted in significant increase in the predicted strengths by 23% to 52% when compared to those predicted using the simplified strut-and-tie models. The predicted lateral wall strengths using the strut-and-tie models illustrated in Figures 4.4 and 4.5 are identified as $F_{n,ST}$ in Table 4.1.

For Wall 9 that had a control joint constructed in accordance with the NZS 4229:1999 specification, the strut-and-tie models presented in Figures 4.4 and 4.5 show that the double bending at bond beam centre was capable of generating some strength and led to the yielding of both D12 reinforcing bars positioned adjacent to the control joint. Consequently, the lateral strength of Wall 9 evaluated using the improved strut-and-tie model was about 32% higher than that predicted using the simplified strut-and-tie method. For Wall 10, the strength predicted using the model presented in Figure 4.4 was similar to that predicted using the simplified strut-and-tie model. Predicted strengths of similar magnitude were generated for this wall because both models considered the 10 mm control joint sufficient to prevent the proper transfer of shear across the bond beams.

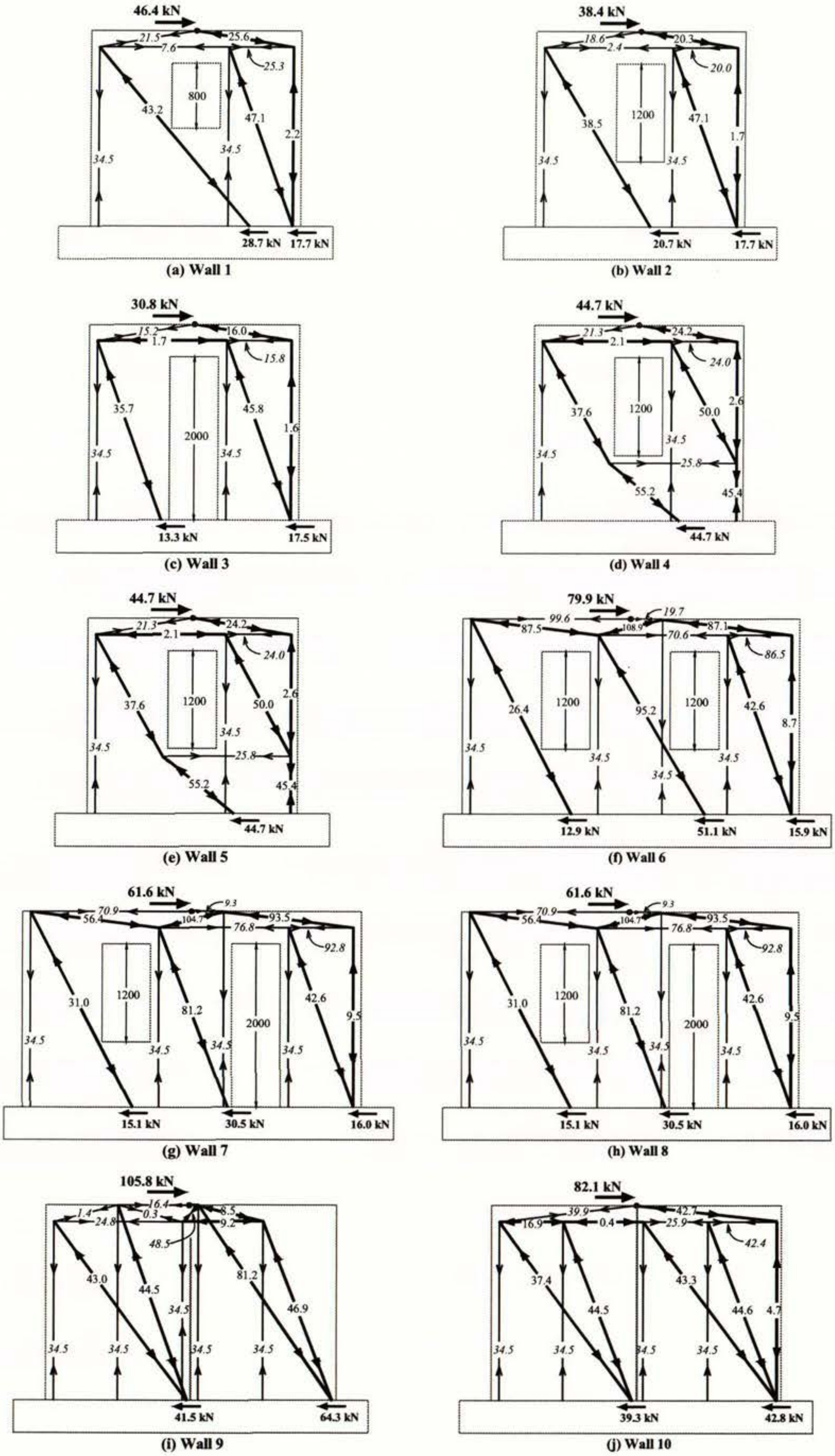

Figure 4.4 Strut-and-tie models in push direction (forces in kN).

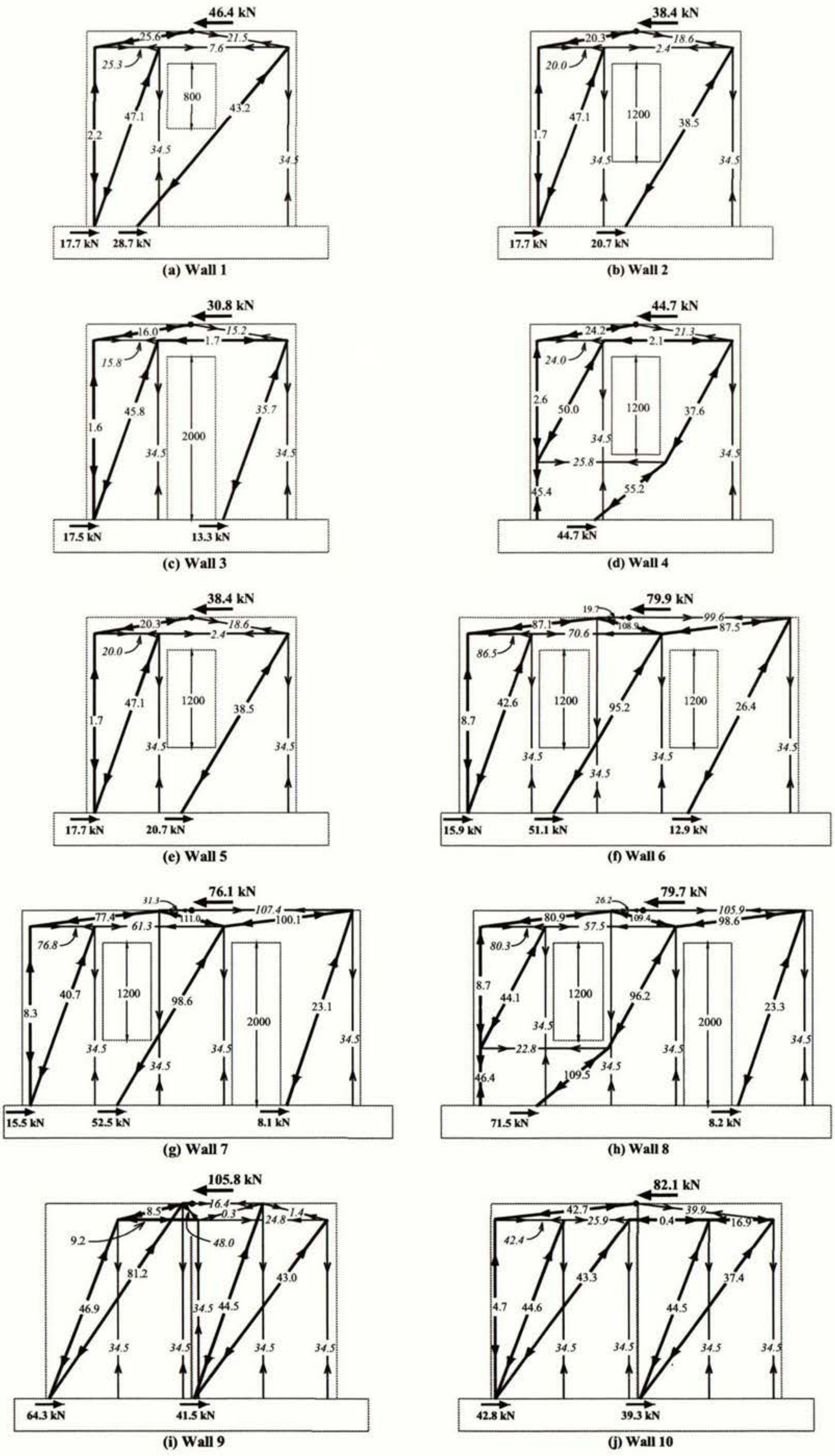

Figure 4.5 Strut-and-tie models in pull direction (forces in kN).

4.1.4 Full Plastic Collapse Analysis

The method used here was to assume that a flexural collapse mechanism could form and then calculate the lateral force required to cause this collapse. A number of collapse mechanisms are possible, with that which required the least work being the most likely. Similar to the procedure employed by Davidson (1998), the walls were treated as frames comprising of vertical piers in order to develop the plastic bending moment diagrams shown in Figures 4.6 and 4.7. The pier and lintel strengths evaluated according to the procedures presented in Appendix D were established to be 30.7 kNm and 17.5 kNm respectively. By conducting a push-over or plastic collapse analysis, it was found that the flexural strength at the base of each pier was developed, but that the moments at the top of the piers were mostly, but not completely governed by the pier strength. These strength critical member joint interfaces are identified by the thickened lines shown in Figures 4.6 and 4.7.

An illustration of the wall strength calculation is presented here for Wall 2. For the wall pushed to the right (away from the strong wall) as shown in Figure 4.6, the critical member height of the left pier was that of the window opening (1.2 m) and the height of the right pier was that of the door opening (2.0 m). Hence, the base shears of the two piers were as follows:

The left pier	(30.7 + 30.7)/1.2 = 51.2 kN
The right pier	(28.1 + 30.7)/2.0 = 29.4 kN
	Sum = 80.6 kN

Hence, the predicted strength in the push direction was 80.6 kN. However, this lateral strength was calculated neglecting the influence of axial force in each pier. The shear force in the lintel, resulted from the rotational moment, gave rise to axial forces in the outer piers. These shear forces were calculated based upon the slope of the lintel bending moments shown in Figure 4.6 and assuming that these shears acted through the centreline of the piers. Therefore, the axial force in each pier was established to be (42.2 + 36.8)/1.6 = 49.4 kN. This axial force in turn increased or decreased the moment capacity of the two piers by approximately 49.4 x 0.5 = 24.7 kNm (please note that the 0.5 m was the approximate length of lever arm between the pier centre and masonry compression edge). For the mechanism chosen and the wall displaced to the right, the increase or decrease in wall strength was calculated as follow:

The left pier $\quad -24.7/1.2 = -20.6$ kN

The right pier $\quad 24.7/2.0 = 12.4$ kN

Consequently, this resulted in a reduction of approximately 8.2 kN. However, this value was not considered in order to ease the analysis process. The evaluated wall strengths using the plastic collapse analysis are identified as $F_{n,fr}$ in Table 4.1.

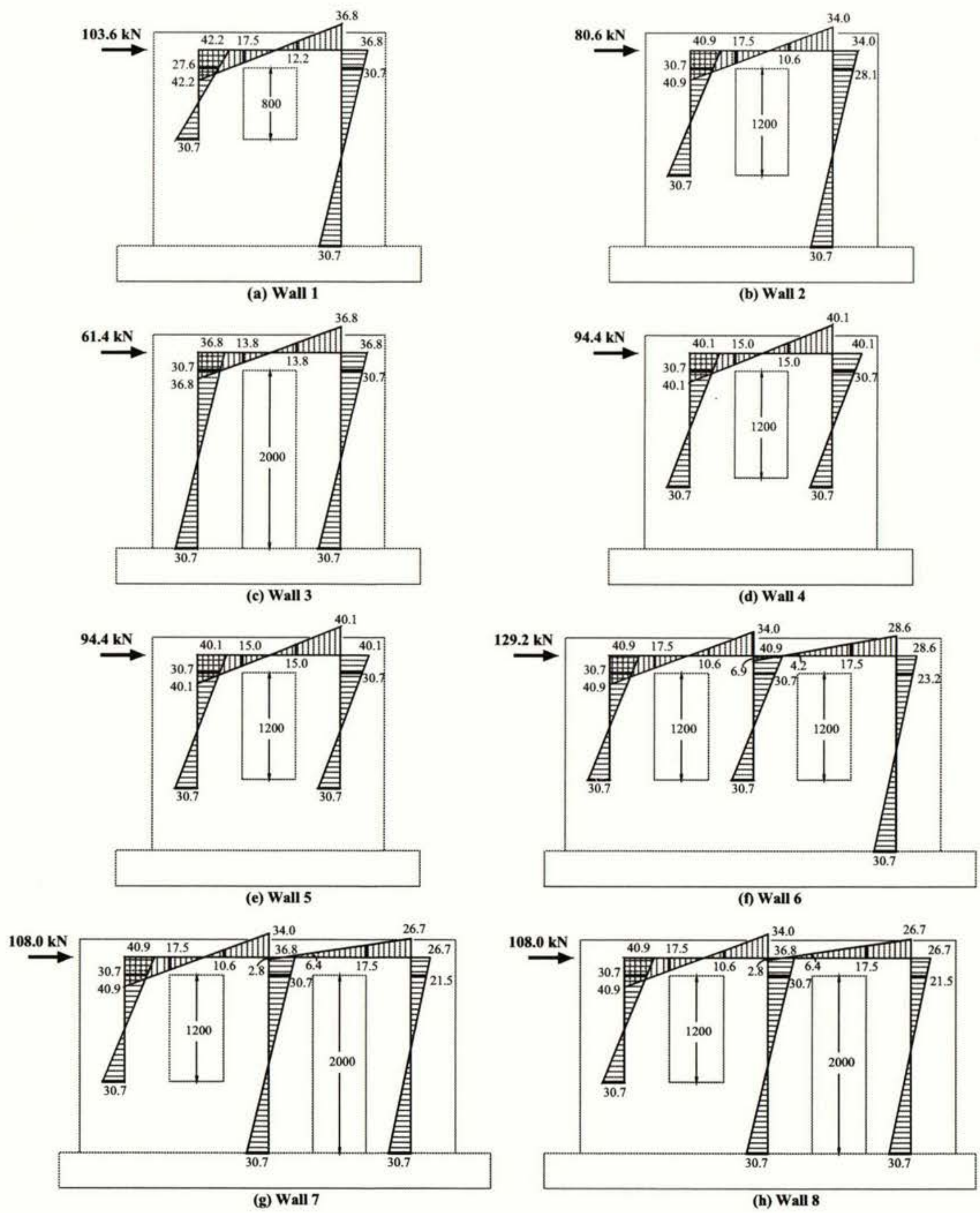

Figure 4.6 Full plastic collapse analyses in push direction (moments in kNm).

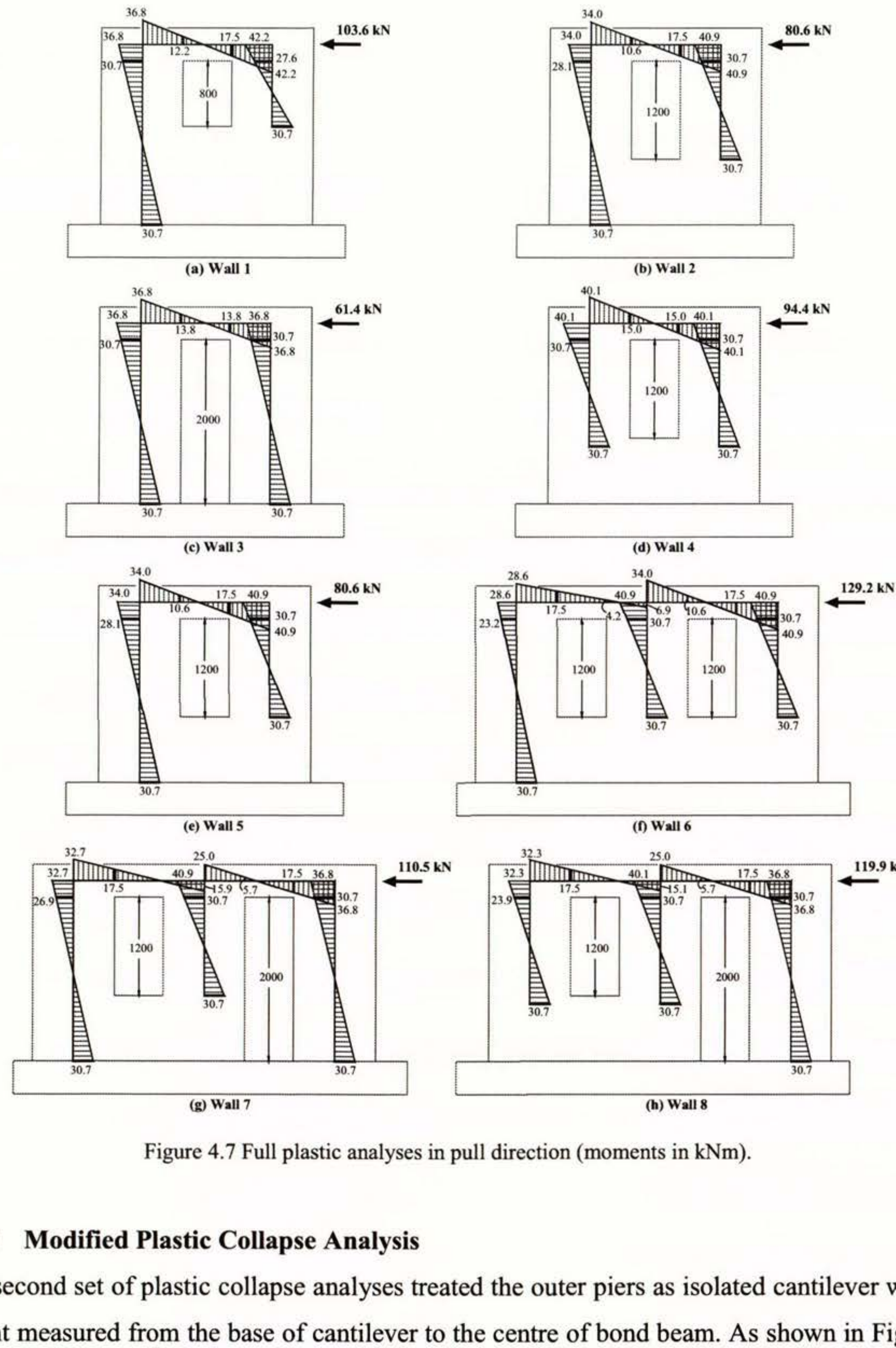

Figure 4.7 Full plastic analyses in pull direction (moments in kNm).

4.1.5 Modified Plastic Collapse Analysis

The second set of plastic collapse analyses treated the outer piers as isolated cantilever with a height measured from the base of cantilever to the centre of bond beam. As shown in Figures 4.8 and 4.9, this modified analysis method only considered the double bending to occur in the central pier of the 4.2 m long perforated masonry walls. The strength critical member joint interfaces are identified by the thickened lines shown in Figures 4.8 and 4.9. Similar to the full plastic collapse analyses presented in Figures 4.6 and 4.7, the influence of axial force (resulted from wall self weight and rotational moment in the lintel) was not considered in this modified analysis method. The predicted lateral wall strength using this modified analysis methods are identified as $F_{n,FR}$ in Table 4.1.

An illustration of the wall strength calculation is presented here for Wall 6. For the wall pushed to the right (away from the strong wall) as shown in Figure 4.6, the critical member height of the left and central piers were from the bond beam centre to the underside of the window (1.4 m) and the height of the right pier was taken from the bond beam centre to the foundation face (2.2 m). Hence, the base shears of the three piers were as follows:

The left pier	30.7/1.4 = 21.9 kN
The central pier	(40.9 + 30.7)/1.4 = 51.1 kN
The right pier	30.7/2.2 = 14.0 kN
	Sum = 87.0 kN

Hence, the predicted strength in the push direction was 87.0 kN. As anticipated, the $F_{n,FR}$ values are significantly less than those evaluated according to $F_{n,fr}$. This is primarily because the outer piers were considered as isolated cantilever in the $F_{n,FR}$ method, which resulted in significantly less strength than if the piers were allowed to develop their full flexural strength at both ends.

Similar to other analysis methods discussed earlier, increases in $F_{n,FR}$ are evaluated when extended trimming reinforcement is included in walls having the same dimensions and identical penetration geometries. In addition, comparison of $F_{n,FR}$ with the wall strength predictions shown in Figures 4.2-4.5 indicated that the predicted $F_{n,FR}$ values for the 2.6 m long perforated concrete masonry walls were identical to those predicted according to the simplified strut-and-tie models (i.e. $F_{n,st}$). For the 4.2 m long concrete masonry walls with two openings, the inclusion of double bending of the central pier resulted in $F_{n,FR}$ values that were about 33% to 58% more than those predicted according to $F_{n,st}$. Despite the significantly simplified approach adopted by the modified plastic collapse analysis, the wall strengths predicted according to $F_{n,FR}$ approximately matched those of the $F_{n,ST}$, with $F_{n,FR}/F_{n,ST}$ ranges from 0.91 to 1.09 for the perforated concrete masonry walls included in this study.

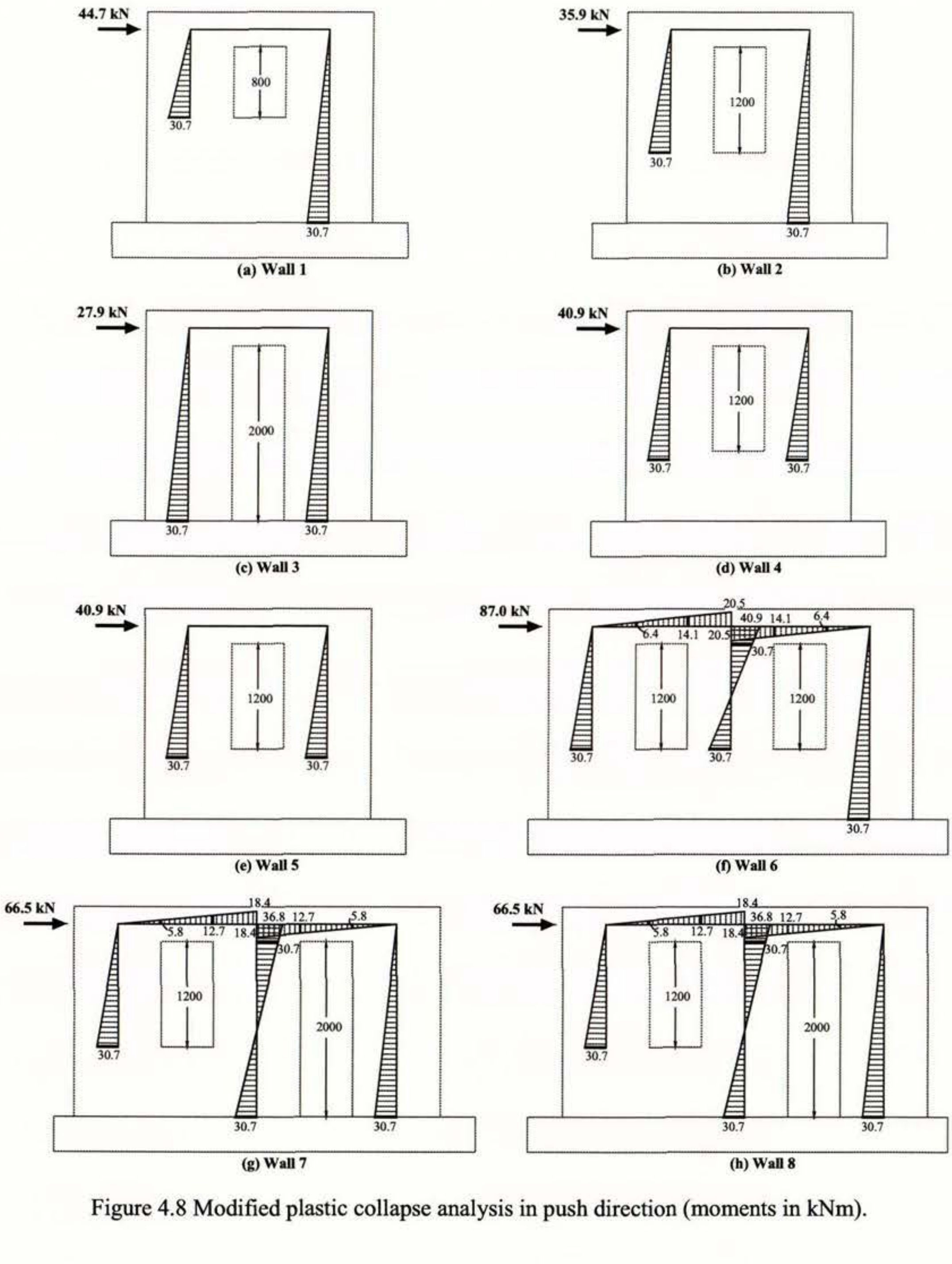

Figure 4.8 Modified plastic collapse analysis in push direction (moments in kNm).

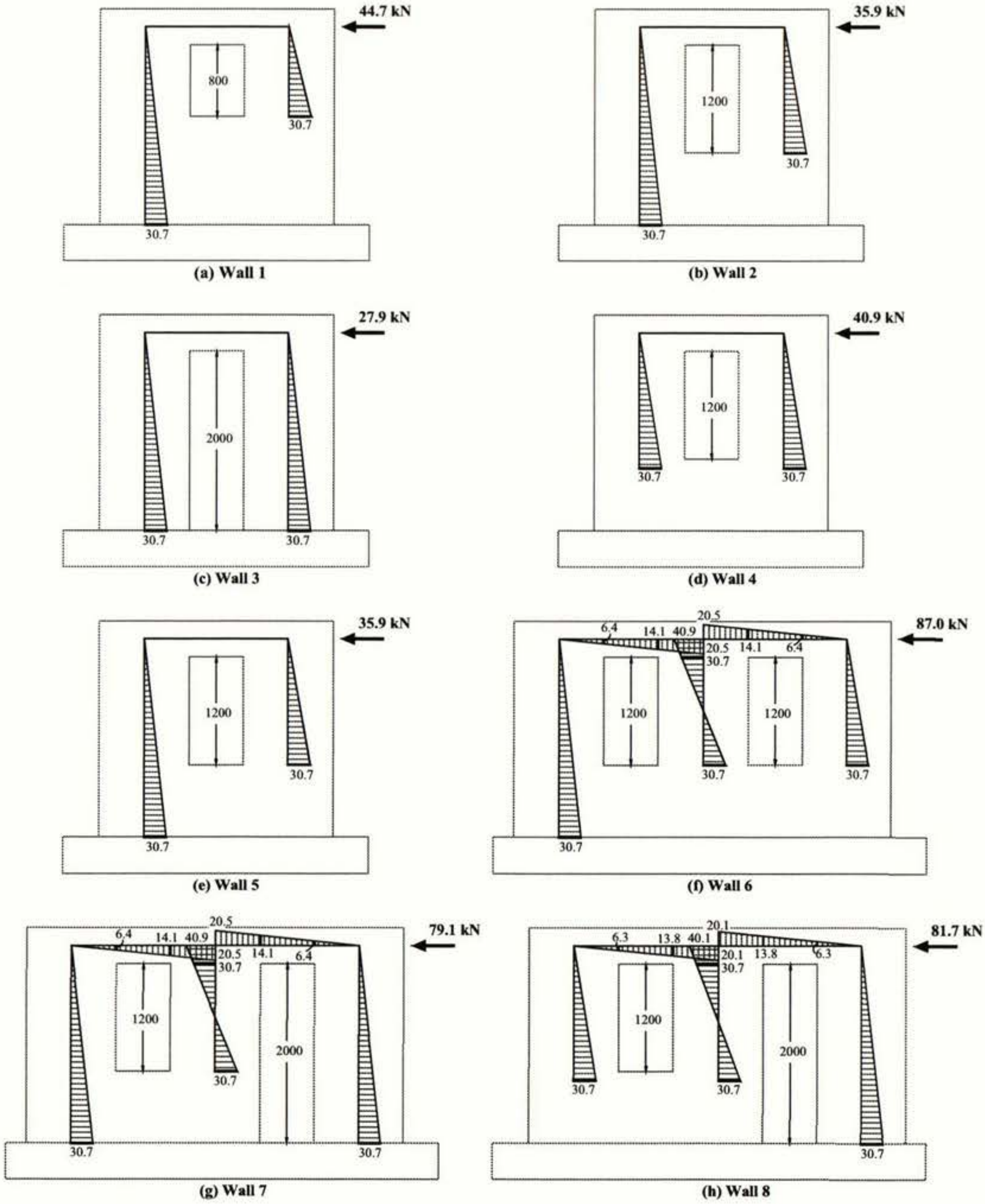

Figure 4.9 Modified plastic collapse analysis in pull direction (moments in kNm).

4.2 Flexural strength of wall without opening

For the purpose of strength comparison presented in Chapter 6, the flexural strengths of Walls 1-8 were re-evaluated to provide lateral strengths for the corresponding solid built walls (i.e. no opening). Figure 4.10 presents illustration of the strut-and-tie models for one of the 2.6 m and 4.2 m long walls. In both cases, wall density of 1.6 kN/m^2 was considered. The evaluated wall strengths using the discussed method are identified in Table 4.1 as $F_{n,no\text{-}op}$.

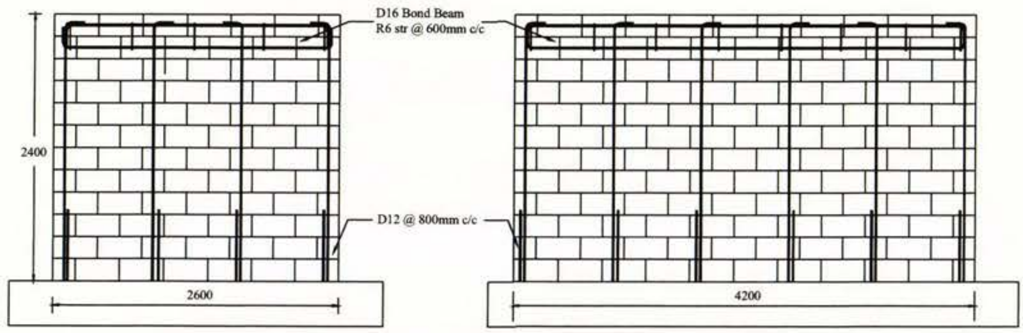

(a) Wall reinforcement details

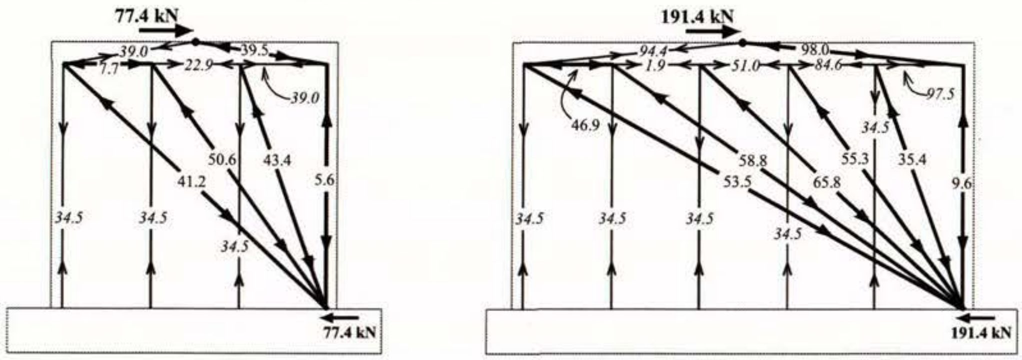

(b) Strut-and-tie models (forces in kN)

Figure 4.10 Strut-and-tie models for masonry walls without opening.

4.3 Masonry Shear Strength

Table 4.1 also includes the nominal shear strength values, V_n, calculated using Equations 4-1 and 4-2 provided by NZS 4230:2004, where v_{bm} is equal to $0.2\sqrt{f'_m}$. Equation 4-2 is a shear expression recently adopted by the New Zealand masonry design standard, NZS 4230:2004, which takes into account the beneficial influence of the dowel action of tension longitudinal reinforcement and the influence of wall aspect ratio on v_m. These conditions are represented by the C_1 and C_2 terms. As shown in Equation 4-2, for masonry walls that have aspect ratios of $h_e/\ell_w < 1.0$ and/or p_w greater than 0.07%, v_{bm} may be amplified by the C_1 and C_2 terms to give v_m.

$$V_n = v_m b_w d \tag{4-1}$$

and

$$v_m = (C_1 + C_2)v_{bm} \tag{4-2}$$

where

(a) $C_1 = 33p_w \dfrac{f_y}{300}$, where $p_w = A_s/b_w d$

(b) for walls:

(i) for $h_e/\ell_w < 0.25$, $C_2 = 1.5$;

(ii) for $0.25 \le h_e/\ell_w \le 1.0$, $C_2 = 0.42[4 - 1.75(h_e/\ell_w)]$;

(iii) for $h_e/\ell_w > 1.0$, $C_2 = 1.0$.

For masonry walls there is frequently some difficulty in determining the effective section area, $b_w d$, to be used in Equation 4-1. NZS 4230:2004 recommends the use of guidelines illustrated in Figure 4.11. For partially grouted walls the effective section width for shear will be the net thickness of the face-shells. This limitation is necessary to satisfy requirements of continuity of shear flow and to avoid the possibility of vertical shear failure up a continuous ungrouted flue. For concrete masonry units with ungrouted flues, typically $b_w = 60$ mm.

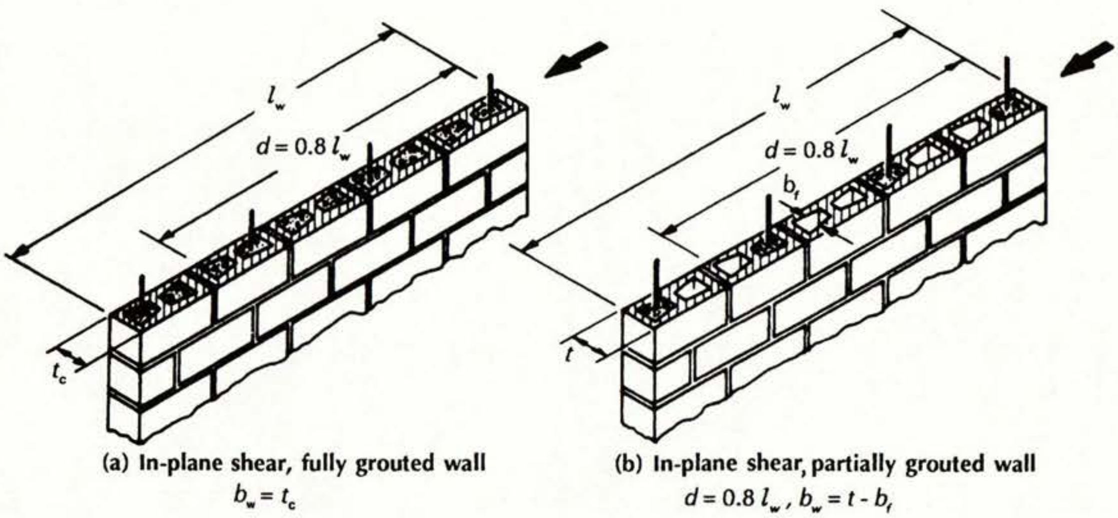

Figure 4.11 Effective areas for shear.

4.4 Predicted Strength Summary

The predicted wall strengths described in sections 4.1-4.3 are summarised in Table 4.1. Although the masonry shear strengths were higher than the predicted flexural strengths, it was anticipated that all walls would fail in diagonal tension due to partial grouting and the lack of distributed horizontal shear reinforcement. This was preferable to the hinge-sliding

Table 4.1 Prediction of wall strengths, based upon measured material properties

Wall	f'_m	$F_{n,st}$	$F_{n,ST}$	$F_{n,fr}$	$F_{n,FR}$	$F_{n,no\text{-}op}$	F_{code}	V_n
1	16.2	44.7	46.4	103.6	44.7	77.3	51.8	81.0
2	12.9	35.9	38.4	80.6	35.9	77.0	37.3	69.1
3	14.4	28.0	30.8	61.4	27.9	77.1	24.3	73.0
4	16.5	41.0	44.7	94.4	40.9	77.3	37.3	78.1
5	18.9	41.0 (push) 35.9 (pull)	44.7 (push) 38.4 (pull)	94.4 (push) 80.6 (pull)	40.9 (push) 35.9 (pull)	77.5	37.3	83.5
6	16.5	58.0	79.9	129.2	87.0	191.4	55.9	117.2
7	18.0	50.0	61.6 (push) 76.1 (pull)	108.0 (push) 110.5 (pull)	66.5 (push) 79.1 (pull)	191.6	49.4	122.4
8	18.0	50.0 (push) 55.0 (pull)	61.6 (push) 79.7 (pull)	108.0 (push) 119.9 (pull)	66.5 (push) 81.7 (pull)	191.6	49.4	122.4
9	23.8	80.2	105.8	---	---	---	49.8	169.0
10	23.8	80.2	82.1	---	---	---	49.8	169.0
Units	**MPa**	**kN**	**kN**	**kN**	**kN**	**kN**	**kN**	**kN**

Note:

1. $F_{n,st}$ is the nominal wall strength predicted according to the simplified strut-and-tie model discussed in section 4.1.2.
2. $F_{n,ST}$ is the nominal wall strength predicted according to the improved strut-and-tie model discussed in section 4.1.3.
3. $F_{n,fr}$ is the nominal wall strength predicted according to the full plastic collapse analysis discussed in section 4.1.4.
4. $F_{n,FR}$ is the nominal wall strength predicted according to the modified plastic collapse analysis discussed in section 4.1.5.
5. $F_{n,no\text{-}op}$ is the nominal wall strength predicted for the corresponding solid built walls discussed in section 4.2.
6. F_{code} is the code specified wall nominal strength.

mode, where lateral force was resisted only by dowel action of the vertical reinforcement once a crack opened up along the entire length of the wall/foundation interface (Priestley, 1976). While four procedures were used to evaluate the wall predicted strengths, only values within the shaded columns in Table 4.1 were chosen as the assumed nominal lateral wall strengths on the day of testing (see Appendices A and B). For the 2.6 m long perforated masonry walls and the walls with control joint, the $F_{n,st}$ values were used instead of the $F_{n,ST}$ since $F_{n,st}$ had the advantage of being easier to evaluate and they were only 2% to 10% less than $F_{n,ST}$. In addition, it was expected that a full plastic mechanism would not develop in the nominally reinforced perforated masonry walls. Davidson (1998) successfully observed from his study that the response of individual piers was effectively independent, therefore supporting the assumption of pin formation in the outer piers at the bond beam centre. For the masonry walls with double openings, $F_{n,ST}$ was used as the predicted flexural strengths for the 4.2 m long walls. It was expected that double bending of the central pier would significantly increase the lateral strength of the 4.2 m long walls. The $F_{n,fr}$ and $F_{n,FR}$ values are useful when compared to the experimentally measured wall strengths presented in Chapters 5 and 6. Although the wall strengths predicted according to the modified plastic collapse analysis were successfully shown to closely match those predicted using the strut-and-tie models, only values predicted using the strut-and-tie methods were used as the assumed nominal wall strengths (on the day of testing) because they had the advantage of providing a comparison between the cracking patterns on the tested walls and the load paths by which the shear forces were shown to transfer to the foundation in the strut mechanisms. However, on any other occasions, it is deemed appropriate to employ the modified plastic collapse analysis as an alternative to strut-and-tie method when analysing the lateral strength capacities of partially grout-filled perforated concrete masonry walls that were constructed according to NZS 4229:1999 specifications.

4.5 Testing Procedure

The testing procedure adopted was that described by Park (1989), which for more than a decade has been the standard test procedure used in New Zealand to establish available ductility capacity in a manner consistent with New Zealand design standards. The advantage of this method is that the test can proceed without prior knowledge of the actual strength and ductility capacity of the test specimen. Also, Liddell et al. (2000) have found, when testing reinforced concrete beams, that this loading history results in less damage than when using alternative loading histories considering a larger number of cycles at each displacement interval. In addition, Liddell et al. determined that the New Zealand loading history resulted in hysteretic response most similar to that obtained for structures that were subjected to cyclic loading corresponding to earthquake records. The steps in Park's procedure are:

1. Calculate the nominal lateral force (F_n) required to develop the wall flexural strength.
2. Apply a lateral force equal to ¾ of F_n in one direction and record displacement of the wall Δ_a.

3. Unload the wall and repeat step (2) in the reverse direction to obtain Δ_b. Extrapolate straight lines from the origin of the force/displacement plot through the points (¾ F_n, Δ_a) and (-¾ F_n, Δ_b) and find their intersection with the nominal lateral force. This step is illustrated in Figure 4.12. The yield displacement is Δ_y as shown in the figure. The displacement Δ at a ductility value of μ is defined as $\mu * \Delta_y$.
4. Apply lateral force slowly in a sequence so that the top of the wall is displaced to the ductility levels shown in Figure 4.13.

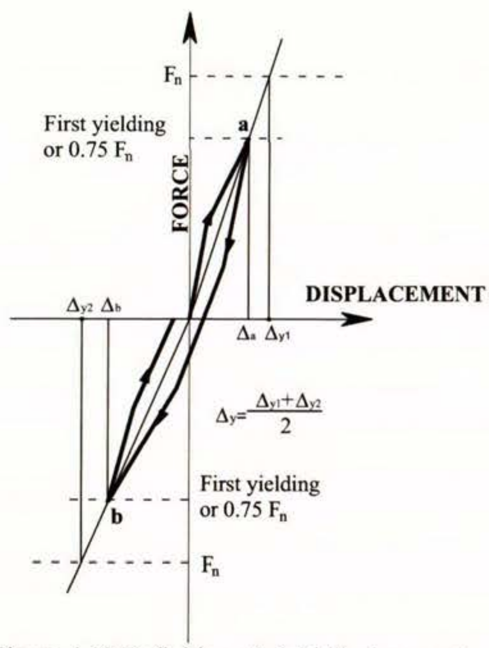

Figure 4.12 Definition of yield displacement.

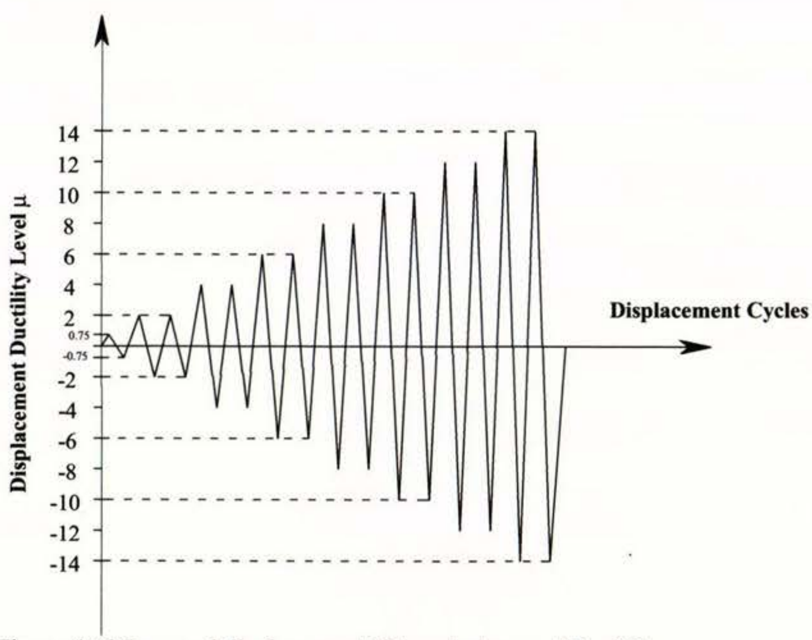

Figure 4.13 Imposed displacement history in terms of ductility.

In New Zealand a practice has evolved over time whereby the available displacement ductility, μ_{av}, of a structural element may be established from laboratory testing. The method has been reported by Park (1989), and is based on the notion that performance is satisfactory if a tested element can sustain four complete (bi-directional) loading cycles to μ_{av}, with less than 20% loss in peak strength. However, as μ_{av} is unknown prior to the test, it is assumed that μ_{av} may adequately be determined from the expression:

$$\mu_{av} = \frac{\sum|\mu_i|}{8} \tag{4-3}$$

where $|\mu_i|$ is the absolute magnitude of each ductility semi-cycle during the loading history. As an illustration, two complete cycles in both directions to $\mu = 2$ results in $\sum|\mu_i| = 8$ and a further two complete cycles to $\mu = 4$ results in $\sum|\mu_i| = 24$. Finally, it is noted that NZS 4203:1992 stipulates $\mu \leq 4$ for reinforced concrete masonry, such that accurate determination of ductility capacity above this level was of little relevance.

4.6 Miscellaneous

Precondition

Prior to initiation of the loading procedure, each test wall was inspected for any pre-test cracking or damage in order to avoid confusion with damage attributed to the applied loading.

Crack marking

During testing, visual observations were carefully noted along with key force and displacement readings at the extreme of each load excursion. Cracks due to applied loading in the push directions were marked in red and cracks due to pull excursions were marked in black. Also, photos were taken of any significant structural event during testing. In reporting, the term “compression toe” was used to describe the end of the wall by the base in compression due to flexural action, and the term “heel” described the opposite end of the wall that was experiencing decompression/uplift. The position of “compression toe” and “heel” depended on loading direction; the two terms reversed in position when the loading direction was reversed.

4.7 Data Reduction

It was determined that the wall displacement consisted of four components: rocking and sliding deformation, flexural deformation, and shear deformation. As described earlier in section 3.5, instrumentation was attached to the wall as shown in Figure 3.7 to allow the deformation components to be isolated.

Rocking deformation:

The rocking (uplift) deformation was recorded by the two portal displacement transducers placed at the two ends of the wall-foundation base interface. At a given wall state, the rocking displacement component was calculated by extrapolating the rotation measured between the wall ends. This is demonstrated in Figure 4.14. Hence, the rotation, θ_r of the wall due to rocking on its base was:

$$\theta_r = \frac{d_{r1} - d_{r2}}{\ell_w + 2\ell_s} \qquad (4\text{-}4)$$

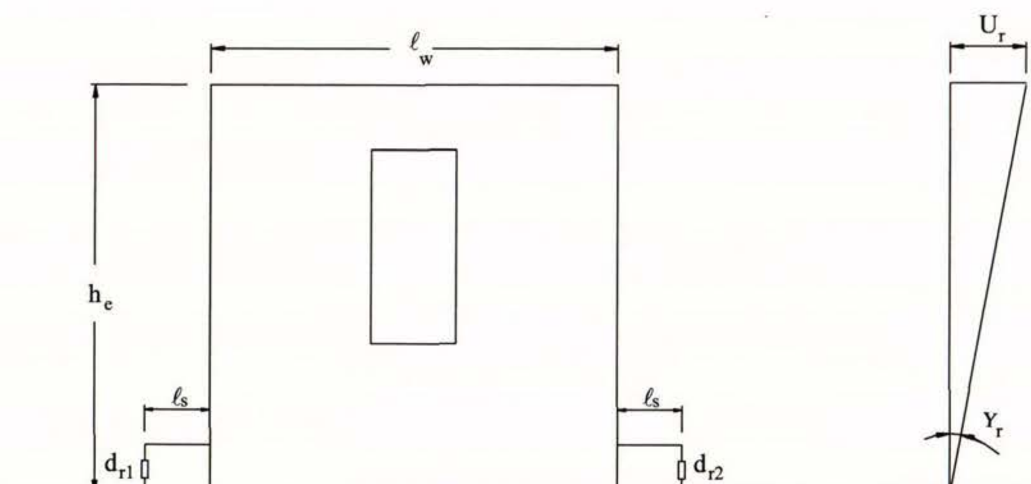

Figure 4.14 Rocking displacement.

where d_{r1} and d_{r2} are the deformations measured by the portal displacement transducer, noting that elongation is represented by positive displacement, and ℓ_s is the distance between the wall end and the transducer. Therefore, the resulting rocking displacement recorded was evaluated as:

$$U_r = \theta_r h_e \qquad (4\text{-}5)$$

Flexural deformation

Instrumentation mounted on the wall allowed the calculation of flexural deformation. Assuming that plane sections remain plane, the wall rotation, θ_i at height (x_i) above the base could be evaluated by Equation 4-6.

$$\theta_i = \frac{d_{b1} - d_{b2}}{L} \tag{4-6}$$

where d_{b1} and d_{b2} were the displacement measured by the pair of instruments shown in Figure 4.15. The resulting displacement u_{bi} at the top of the wall due to θ_i could be evaluated as:

$$u_{bi} = \theta_i (h_e - x_i) \tag{4-7}$$

and

$$U_b = \sum_i u_b$$

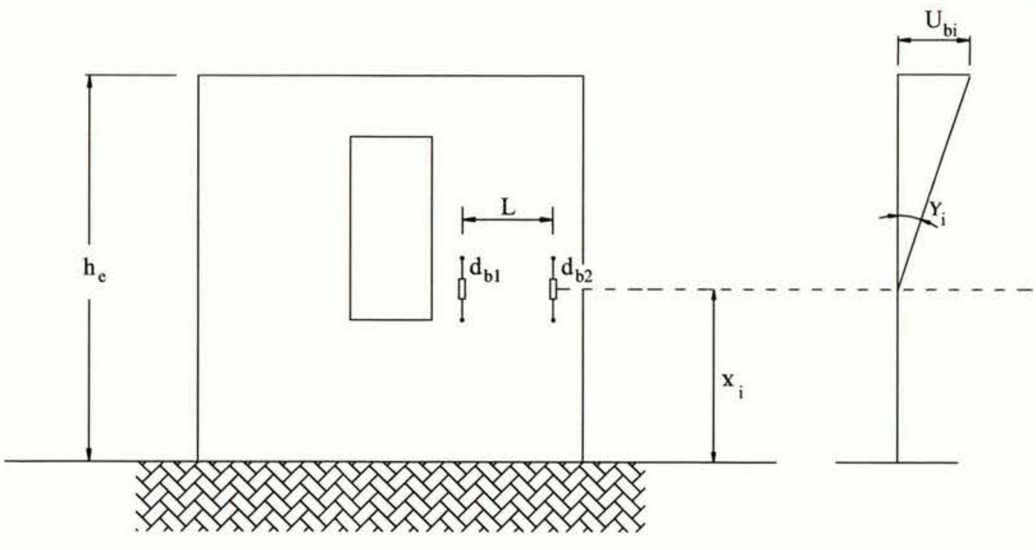

Figure 4.15 Flexural displacement.

Shear deformation

The method used in this report for calculating the shear deformation component was based on Hiraishi (1984) and Brammer (1995), with more detailed description provided in Appendix C. The mentioned method utilised the measured relative displacements between points on the wall face (transducers mounted diagonally on the wall, as shown in Figure 3.7) to evaluate the shear component of deformation.

All walls tested at the University of Auckland had numerous panel sections attached to the wall face. The dimensions of each panel section were defined by the length, L, the height, h, and the diagonal length, d (see Figure C.1 in Appendix C for clarification). The following formula was used to calculate the shear deformation component (u_s) for each panel:

$$u_s = \frac{d(\delta_{d2} - \delta_{d1})}{2L} - \frac{h^2}{6(2d_u + h)}(\delta_{v1} - \delta_{v2}) \tag{4-8}$$

and

$$U_s = \sum u_s$$

where δ's were the measured relative deformation within each panel section, and d_u was the distance between the two upper points of each panel section and the top of the wall. The sum of u_s from one column of the panel section was necessary to evaluate U_s. If more than one column of panel sections were considered, then the results were averaged.

Sliding deformation

This component was used to measure slip between the wall and the base. Sliding may become significant when there is a low friction coefficient, such as when using a friction breaker or water proof membrane, or when the wall is positioned on a smooth finished slab. All walls reported here were built on a purposely roughened concrete surface in order to reduce the magnitude of sliding.

Chapter 5

Experimental Results

This chapter summarizes the behaviour of the ten walls tested in Series A and B. For detailed descriptions of the experimental results, please refer to Appendices A and B. This chapter reports the overall force-displacement response of the ten tests and the maximum strength developed in each test specimen. The nominal strengths shown on the force-displacement (F-D) curves are without a strength reduction factor (i.e. $\phi = 1.0$). This report defines loading in the push direction as positive and loading in the pull direction as negative.

5.1 Wall 1

The measured force-displacement curve for Wall 1 is presented in Figure 5.1, depicting the lateral displacement at the top of the wall as a function of the applied lateral shear force. The maximum push direction strength of 50.2 kN was measured during the first push cycle to displacement ductility six, and the maximum pull direction strength of -49.0 kN was measured during the first pull cycle to displacement ductility four. The average yield displacement (Δ_y) for this partially grouted wall was evaluated to be 0.82 mm. The test wall was defined as failing during the first pull cycle to displacement ductility 10, giving it a ductility capacity of $\mu_{av} > 6.0$.

Due to the lack of distributed horizontal shear reinforcement and the fact that the wall was partially grout-filled, the test wall was observed to fail in a diagonal tension mode. This type of failure is characterised by the development of early horizontal flexural cracking, which is later exaggerated by diagonal cracking that extends throughout the wall panel. It was observed during experimental testing that the (diagonal) cracking patterns of this wall aligned well with the load paths by which shear force was transferred to the foundation in the strut mechanism. The cracking pattern for this wall is depicted in Figure 5.2, with the shaded areas indicating masonry crushing.

The nominal lateral wall strength derived using the strut-and-tie analysis, along with the strength value derived from NZS 4229:1999 (denoted NZS-4229) are included in Figure 5.1. Also shown in this plot is the theoretical failure point, corresponding to the cycle in which the peak strength failed to exceed 80% of the maximum previously attained strength. From Figure 5.1, it was observed that Wall 1 did not achieve the bracing capacity prescribed by NZS 4229:1999. NZS 4229:1999 over-predicted the lateral strength of this perforated wall by about 3.3% and 5.4% in the respective push and pull directions. Consequently, this test result indicates that the existing standard may be non-conservative in its treatment of walls containing small opening. Furthermore, Figure 5.1 shows that the experimentally measured wall strength was at least 5% higher than the predicted $F_{n,ST}$.

As shown in Figure 5.1, Wall 1 exhibited gradual strength degradation despite significant stiffness degradation. This desirable behaviour of the nominally reinforced partially grout-filled concrete masonry wall with opening was created by the solid filled bond beam on top of the piers, which caused frame-type action at latter stage of testing. This notion was supported by the absence of significant structural damage in the bond beam. Furthermore, the force-displacement plot in Figure 5.1 consistently illustrated a pinched shape. This was primarily due to the presence of significant shear deformation in this type of masonry construction (see section A.1.4). It was also observed that less hysteretic energy was expended during the second cycle to any displacement level, when compared with the first displacement cycle. This is illustrated in Figure 5.1 by the more pinched hysteresis loops of the second cycle.

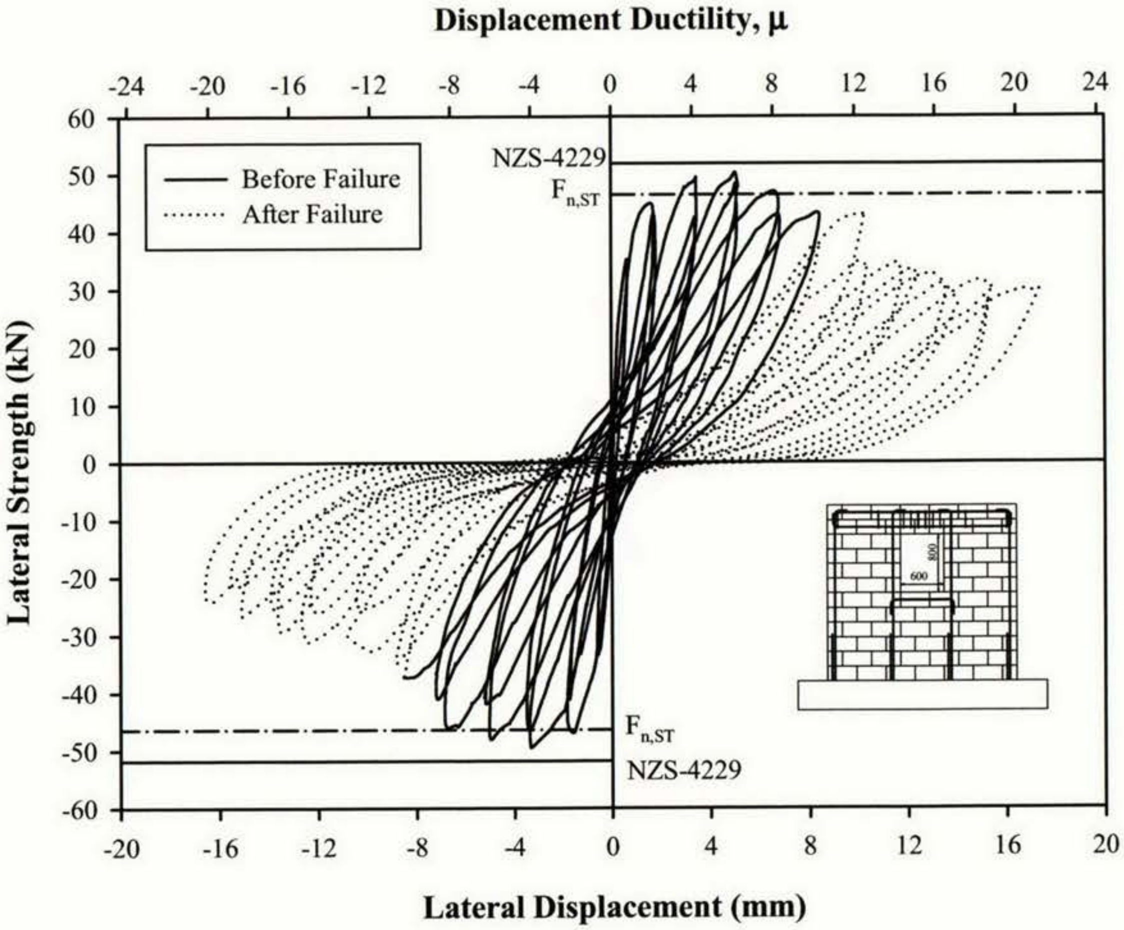

Figure 5.1 Force-displacement history for Wall 1.

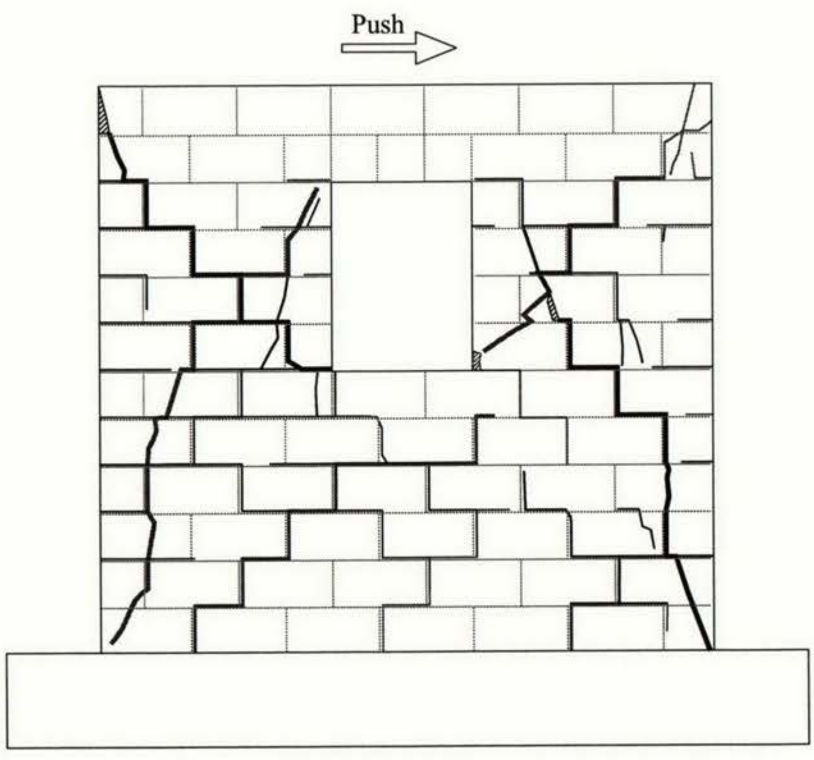

Figure 5.2 Wall 1 cracking pattern at end of testing.

5.2 Wall 2

The measured force-displacement curve for Wall 2 is presented in Figure 5.3, depicting the lateral displacement at the top of the wall as a function of the applied lateral force. The maximum push and pull direction strengths of 41.2 kN and -38.7 kN were measured during the first cycle to displacement ductility 4. Despite the presence of wide open diagonal cracks, the wall exhibited a gradual and fairly symmetrical strength degradation in both directions of loading. Consequently, it was possible to classify Wall 2 as having a diagonal tension failure mode. The desirable behaviour of this nominally reinforced partially grout-filled concrete masonry wall with window opening was created by the solid filled bond beam that caused frame-type action at latter stage of testing.

As shown in Figure 5.3, it was established that the maximum strength developed by Wall 2 was at least 4% higher (pull direction) than the bracing capacity prescribed by NZS 4229:1999, therefore suggesting that the conservatism of NZS 4229:1999 increases as the depth of penetration increases (the window in this wall had a depth of 1200 mm as compared to that of 800 mm in Wall 1). The wall nominal strength predicted according to $F_{n,ST}$ was about 4% less than the maximum strength achieved by the wall.

As shown in Figure 5.4, the diagonal cracking patterns of this wall aligned well with the load paths by which shear force was transferred to the foundation in the strut mechanism. This observation supports the use of strut-and-tie analysis as the tool to evaluate the strength of walls with reinforcement details complying with the specifications of NZS 4229:1999.

Similar to Figure 5.1, the force-displacement plot in Figure 5.3 consistently illustrated a pinched shape. This was primarily due to the presence of significant shear deformation in this type of masonry construction. It was also observed that less hysteretic energy was expended during the second cycle to any displacement level, when compared with the first displacement cycle. This is shown by the more pinched hysteresis loops of the second cycle.

The average yield displacement (Δ_y) for this partially grouted wall was evaluated to be 0.57 mm. The test wall was defined as failing during the second push cycle to displacement ductility 10, giving it a ductility capacity of $\mu_{av} > 6.0$.

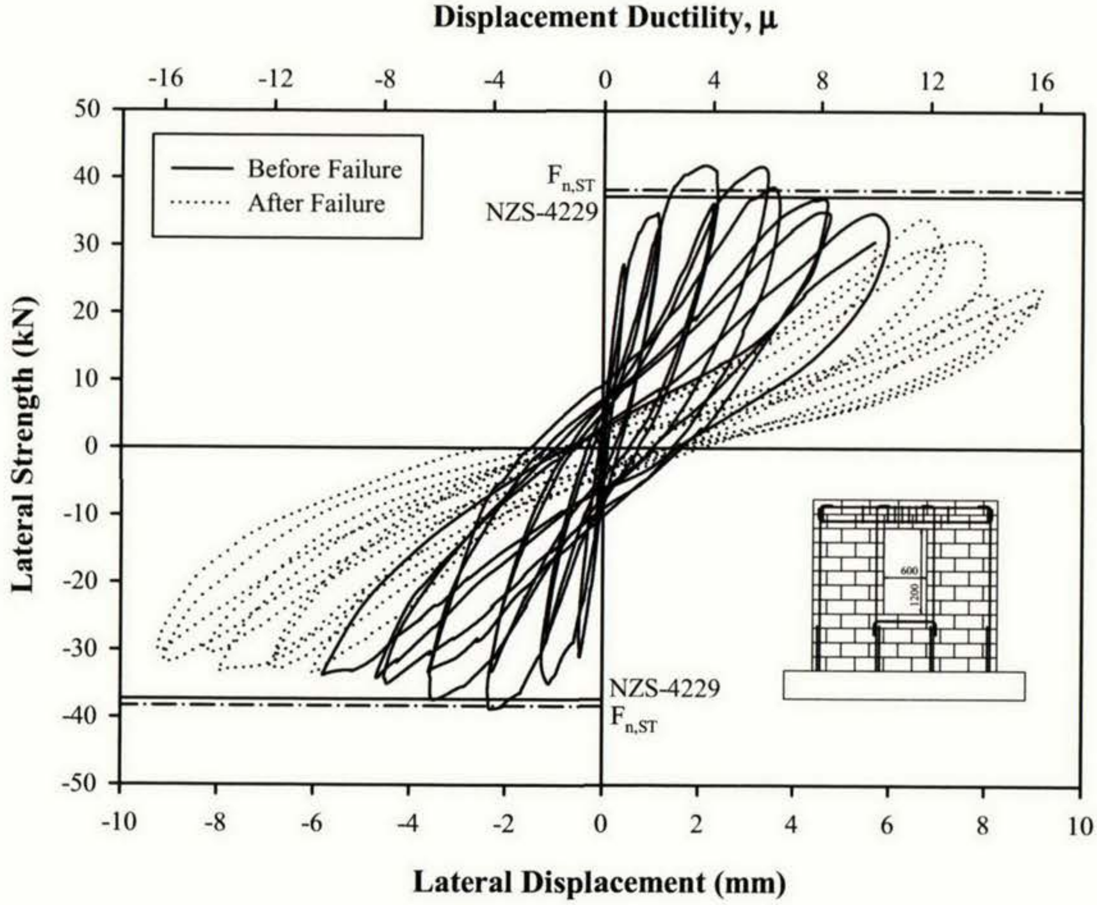

Figure 5.3 Force-displacement history for Wall 2.

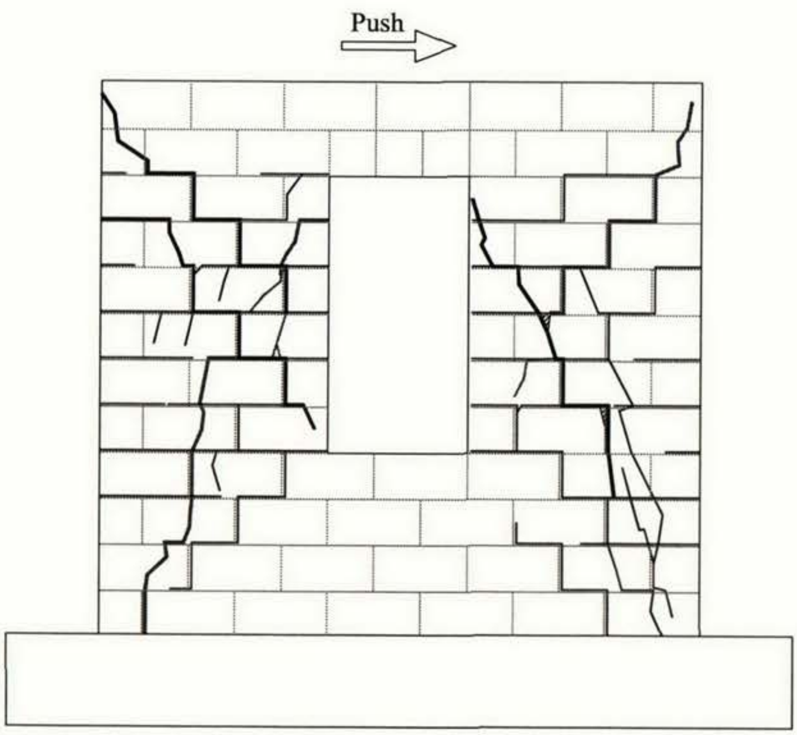

Figure 5.4 Wall 2 cracking pattern at end of testing.

5.3 Wall 3

The measured force-displacement curve for Wall 3 is presented in Figure 5.5, depicting the lateral displacement at the top of the wall as a function of the applied lateral force. The maximum push and pull direction strengths of 33.3 kN and -34.4 kN were measured during the first cycle to displacement ductility 4. This wall was classified as failing in a diagonal tension mode. This failure mode was characterised by the gradual and fairly symmetrical degradation of strength in both direction of loading and the presence of widely open diagonal cracks on both piers. The desirable behaviour of this nominally reinforced partially grout-filled concrete masonry wall was created by the solid filled bond beam on top of the piers, which caused a frame-type action at latter stage of testing.

As shown in Figure 5.5, it was established that the maximum strength achieved by Wall 3 was at least 37% higher than the bracing capacity prescribed by NZS 4229:1999, therefore further suggesting that the conservatism of NZS 4229:1999 increases as the depth of penetration increases (this wall had an opening of 2000 mm deep, as compared to the depth of window openings of 800 mm and 1200 mm in Walls 1 and 2 respectively). The maximum strength recorded during experimental testing was about 10% higher than the nominal strength predicted according to $F_{n,ST}$.

As shown in Figure 5.6, the diagonal cracking patterns on this wall aligned well with the load paths by which shear force was transferred to the foundation in the strut mechanism. This observation supports the use of strut-and-tie analysis as the tool to evaluate the strength of walls with reinforcement details complying with the specifications of NZS 4229:1999.

The average yield displacement (Δ_y) for this partially grouted wall was evaluated to be 1.07 mm. The test wall was defined as failing during the second pull cycle to displacement ductility 8, giving it a ductility capacity of $\mu_{av} > 6.0$.

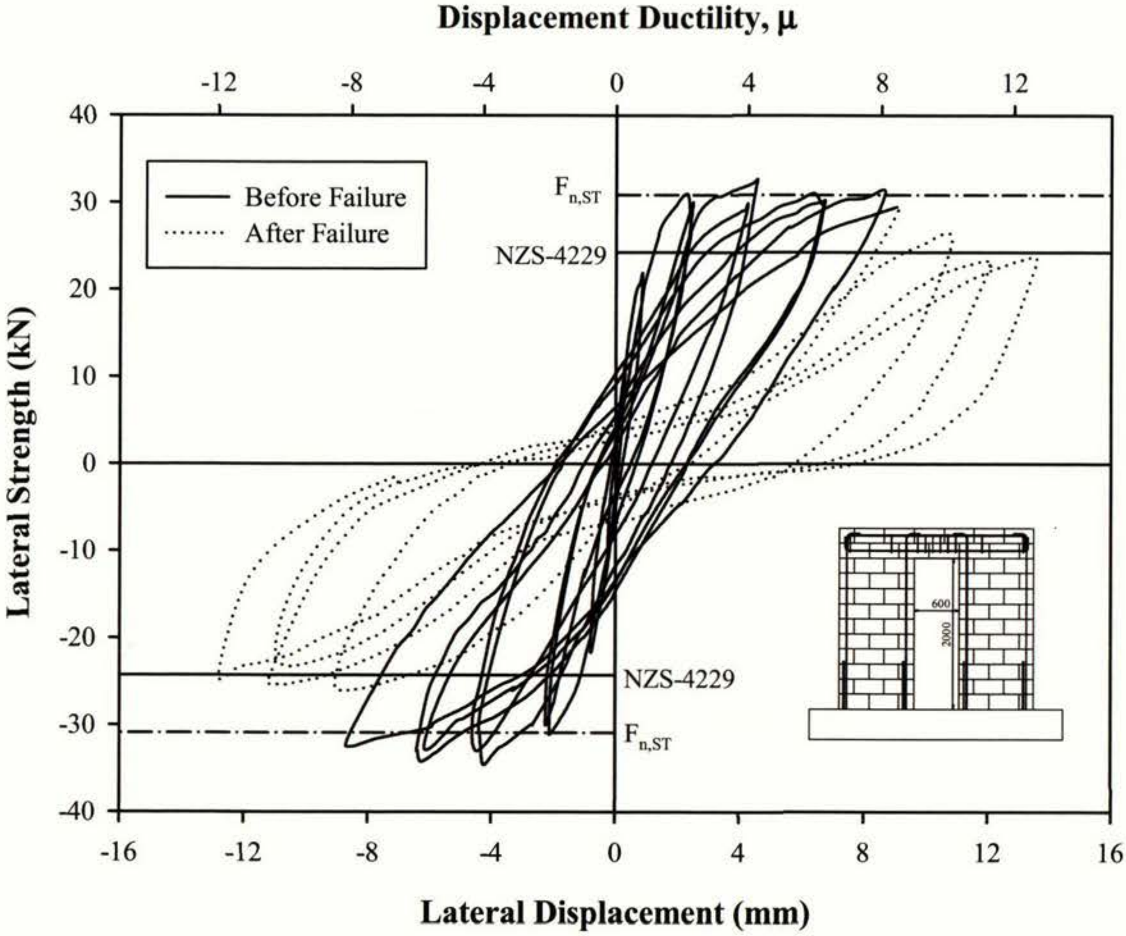

Figure 5.5 Force-displacement history for Wall 3.

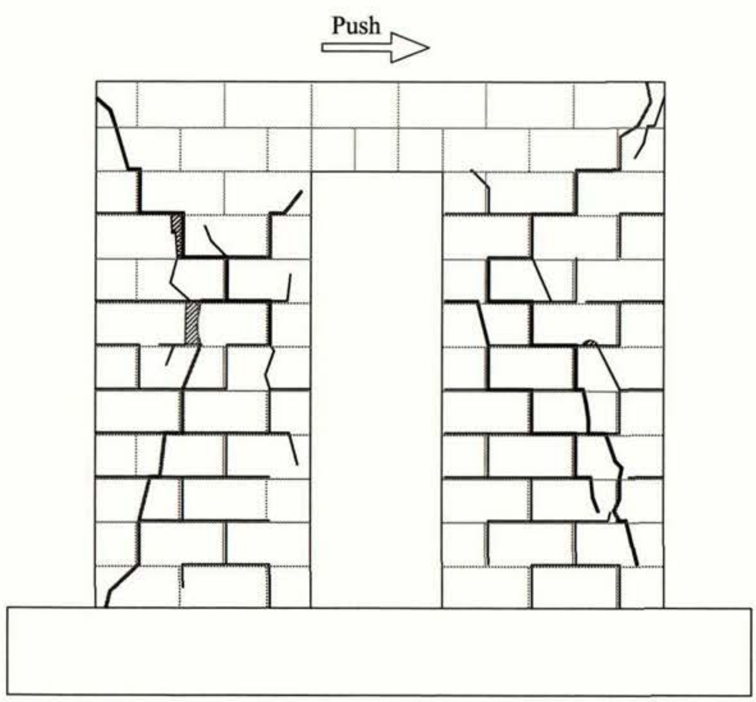

Figure 5.6 Wall 3 cracking pattern at end of testing.

5.4 Wall 4

The measured force-displacement curve for Wall 4 is presented in Figure 5.7, depicting the lateral displacement at the top of the wall as a function of the applied lateral force. The maximum push and pull direction strengths of 47.7 kN and -47.1 kN were measured during the first cycle to displacement ductility 2 and 4 respectively. This wall was classified as having a diagonal tension failure mode. This failure mode was characterised by the gradual and fairly symmetrical degradation of strength in both direction of loading, despite the presence of widely open diagonal cracks on both the left and right piers. The desirable behaviour of this nominally reinforced partially grout-filled concrete masonry wall was created by the solid filled bond beam at the top of the wall, which caused a frame-type action at latter stage of testing.

As shown in Figure 5.7, it was established that the maximum strength achieved by Wall 4 was about 28% higher than the bracing capacity prescribed by NZS 4229:1999, therefore suggesting that the conservatism of NZS 4229:1999 increases when the trimming reinforcement is extended below an opening (as compare to the F_{max}/F_{code} of 1.13 in Wall 2). The wall nominal strength predicted according to $F_{n,ST}$ was about 6% less than the maximum strength achieved by the wall.

As shown in Figures 5.8, the diagonal cracking patterns on this wall aligned well with the load paths by which shear force was transferred to the foundation in the strut mechanism. Consequently, this observation further supports the use of strut-and-tie analysis as the tool to evaluate the strength of perforated concrete masonry walls that are nominally reinforced and of partially grout-filled construction.

The average yield displacement (Δ_y) for this partially grouted wall was evaluated to be 1.15 mm. The test wall was defined as failing during the first push cycle to displacement ductility 6, giving it a ductility capacity μ_{av} of 4.5.

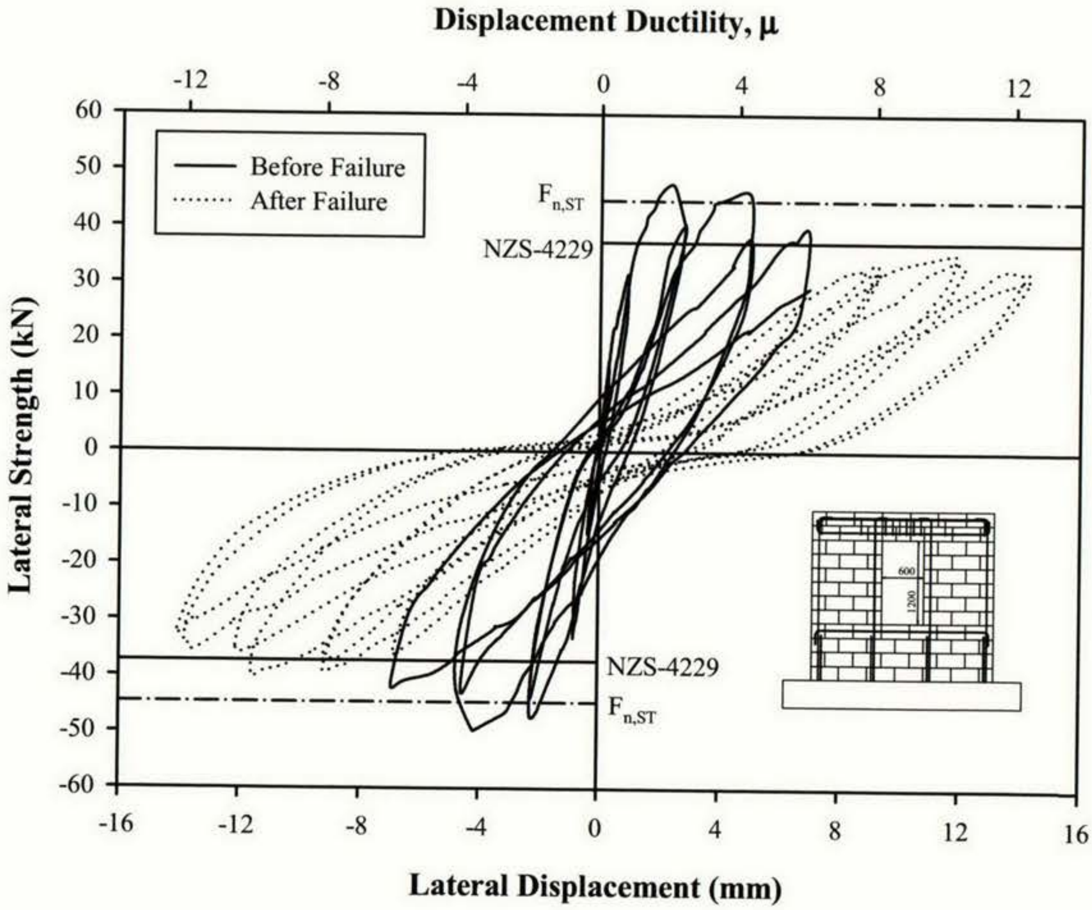

Figure 5.7 Force-displacement history for Wall 4.

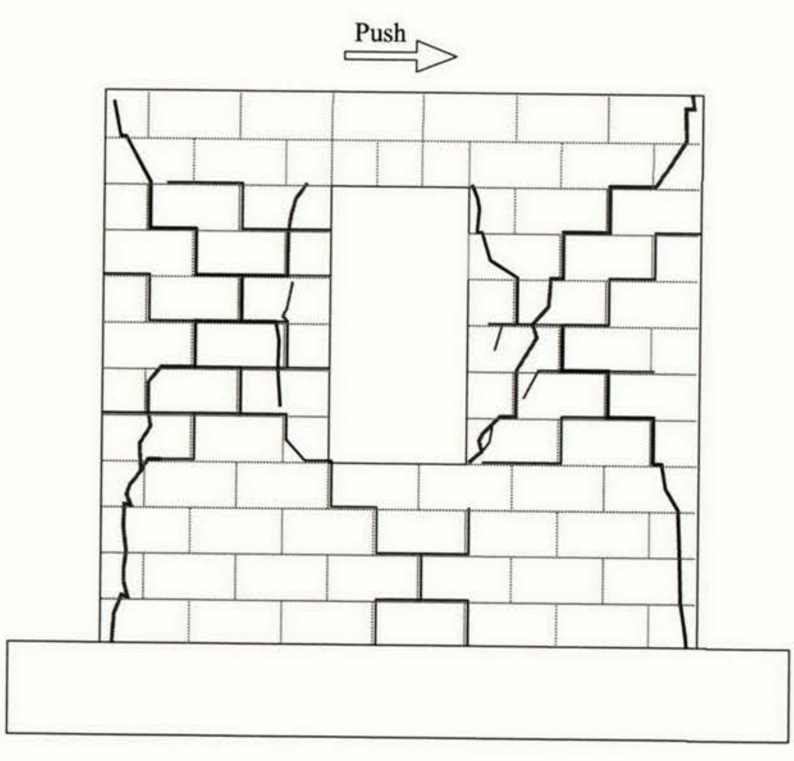

Figure 5.8 Wall 4 cracking pattern at end of testing.

5.5 Wall 5

The measured force-displacement curve for Wall 5 is presented in Figure 5.9, depicting the lateral displacement at the top of the wall as a function of the applied lateral force. The maximum push and pull direction strengths of 52 kN and -50 kN were recorded during experimental testing. Similar to Walls 1-4, Wall 5 was classified as failing in a diagonal tension mode. The desirable behaviour of this perforated nominally reinforced partially grout-filled concrete masonry wall was created by the solid filled bond beam at the top of the wall, which caused a frame-type action at latter stage of testing. As shown in Figure 5.9, Wall 5 exhibited significant non-symmetrical force-displacement response due to the non-symmetrical wall construction. This was correlated with the different geometry of crack patterns that formed in the two directions of loading. In addition, inspection of the wall condition at the end of testing strongly indicated that the wall cracking patterns aligned well with the load paths by which shear force was transferred to the foundation in the strut mechanism. Consequently, this observation further supports the use of strut-and-tie analysis as the tool to evaluate the strength of perforated partially grout-filled masonry walls that are nominally reinforced. The wall cracking pattern at end of testing is presented in Figure 5.10.

As shown in Figure 5.9, the strut-and-tie analysis correctly established a stronger wall strength in the push direction than that in the pull direction. This increased strength in the push direction was expected due to presence of the extended trimming reinforcement in the right side panel. It was established that the maximum strength achieved by Wall 5 was about 39% and 34% higher than the bracing capacity prescribed by NZS 4229:1999 in the respective push and pull directions. The maximum strengths recorded during experimental testing were about 16% and 35% higher than the predicted $F_{n,ST}$ in the respective push and pull directions.

The yield displacement (Δ_y) for this partially grouted wall was evaluated to be 0.84 mm and 0.66 mm in the respective push and pull directions. The test wall was defined as failing during the second push cycle to displacement ductility 4, giving it a ductility capacity μ_{av} of 2.0.

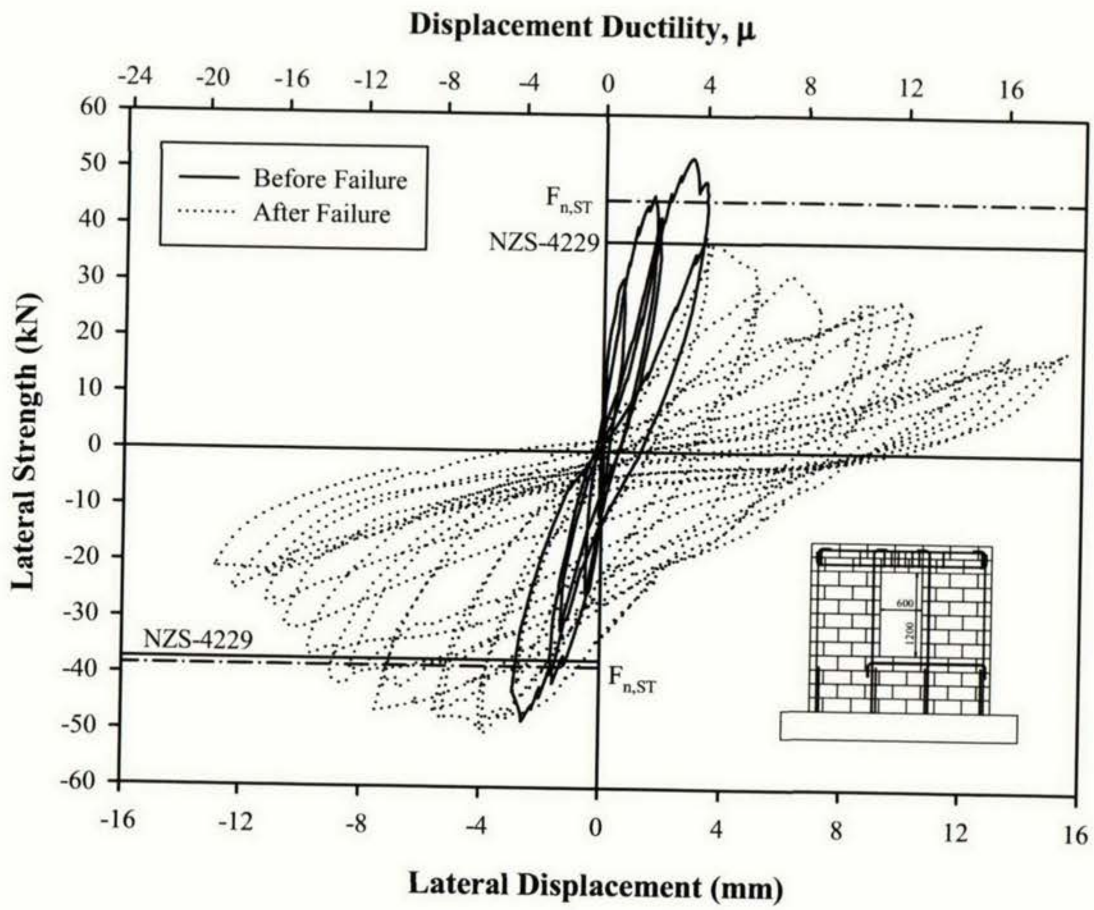

Figure 5.9 Force-displacement history for Wall 5.

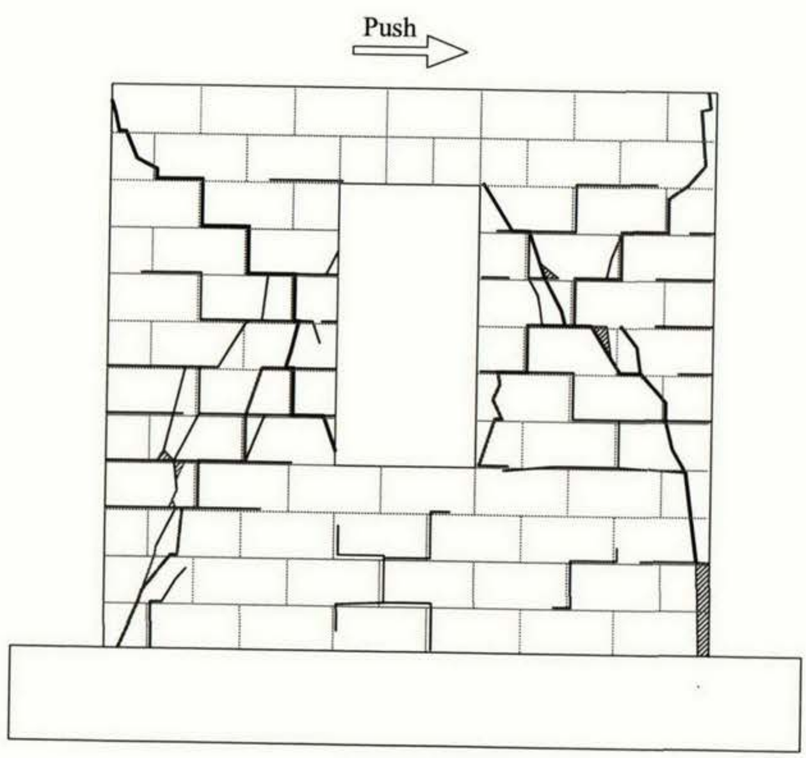

Figure 5.10 Wall 5 cracking pattern at end of testing.

5.6 Wall 6

The measured force-displacement curve for Wall 6 is presented in Figure 5.11. The maximum strengths of 94.3 kN and -94.6 kN were measured during the first cycle to displacement ductility 2 and 4 in the respective push and pull cycles. Wall 6 was classified as failing in a diagonal tension mode, characterised by gradual and fairly symmetrical strength degradation in both directions of loading. This desirable behaviour was created by the solid filled bond beam at the top of the wall, which caused a frame-type action at latter stage of testing. Similar to other test results, the force-displacement plot in Figure 5.11 consistently illustrated a pinched shape. The yield displacement (Δ_y) for this partially grouted wall was evaluated to be 1.83 mm. The test wall was defined as failing during the second push cycle to displacement ductility 4, giving it a ductility capacity μ_{av} of 2.0.

By comparing the strengths recorded for Walls 2, 4 and 6, it was established that double bending of the central pier significantly increased the lateral strength of Wall 6. It was identified that the maximum strength developed by Wall 6 was at least double that recorded for Walls 2 and 4. As shown in Figure 5.12, the diagonal cracking pattern on this wall aligned well with the load paths by which shear force was transferred to the foundation in the strut mechanism. This observation supports the use of strut-and-tie analysis as the tool to evaluate the strength of walls with reinforcement details complying with the specifications of NZS 4229:1999. From Table 4.1, it was shown that failure of the simplified strut-and-tie model (as indicated by symbol $F_{n,st}$) to account for the double bending of the central pier had resulted in significant under-prediction of wall strength. Figure 5.11 illustrates that a significantly improved strength prediction was attained when double bending of the central pier was adequately considered in the $F_{n,ST}$ and $F_{n,FR}$ presented in Figures 4.4f and 4.8f, resulted in $F_{max}/F_{n,ST}$ and $F_{max}/F_{n,FR}$ of about 1.18 and 1.08 respectively. Similarly, failure of NZS 4229:1999 to account for the extra strength generated by the central pier resulted in significant under-prediction of wall strength by the current standard. It was established that the maximum strength achieved by Wall 6 was about 69% higher than the bracing capacity prescribed by NZS 4229:1999, therefore suggesting that NZS 4229:1999 is additionally conservative for walls that have inner piers that undergo double bending. The wall maximum strength recorded during testing was about 27% less than that predicted from a full plastic collapse analysis ($F_{n,fr}$), therefore supporting the assumption of pins forming at bond beam centre of the outer piers.

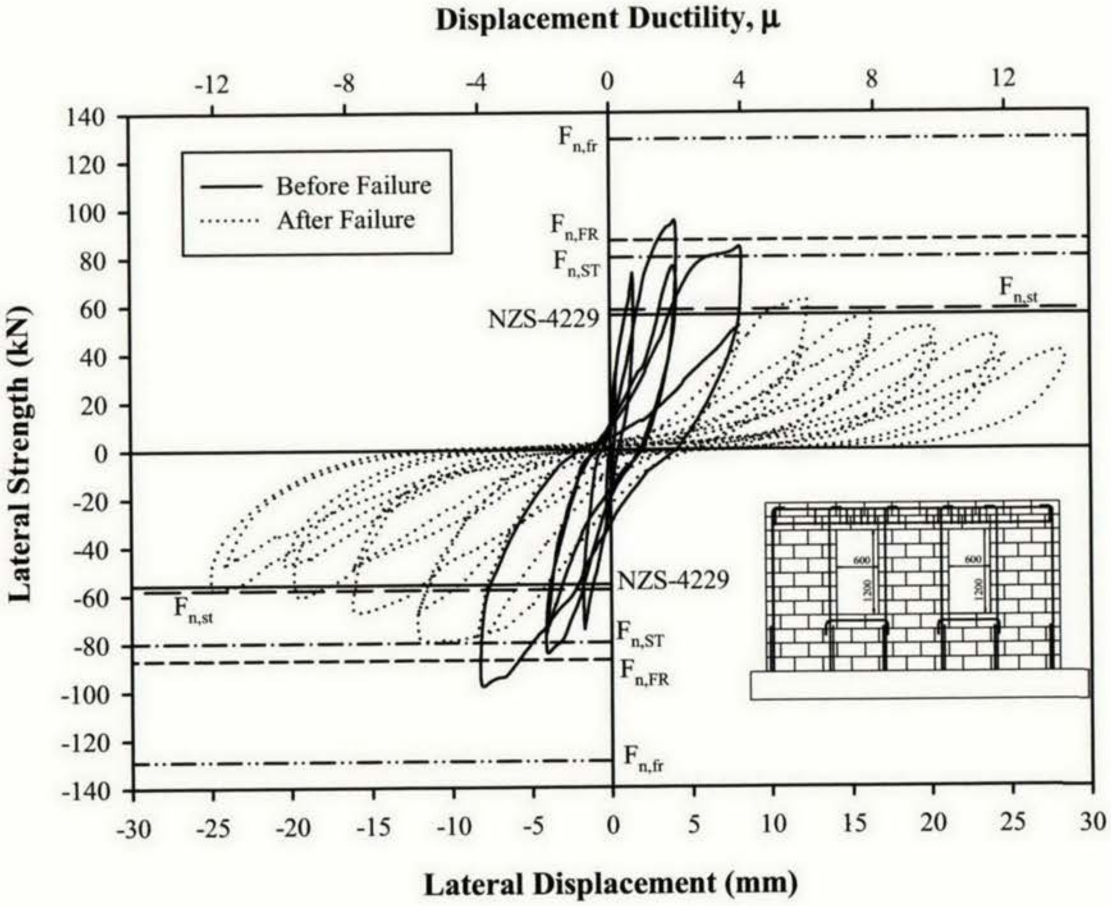

Figure 5.11 Force-displacement history for Wall 6.

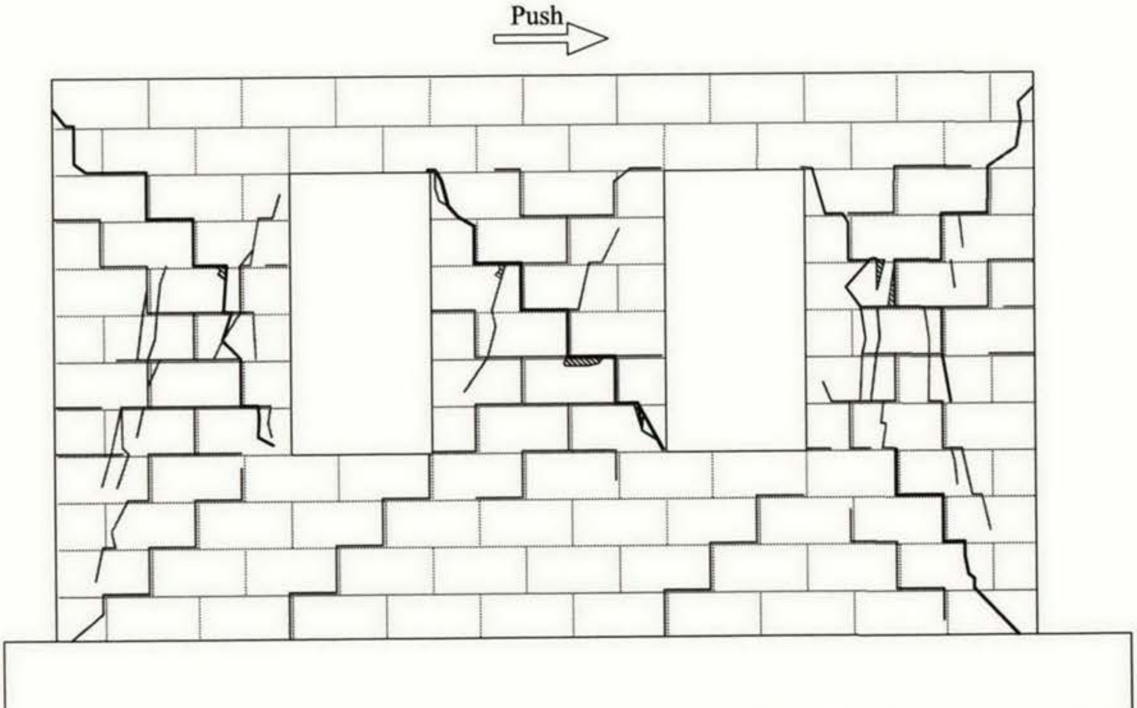

Figure 5.12 Wall 6 cracking pattern at end of testing.

5.7 Wall 7

The measured force-displacement curve for Wall 7 is presented in Figure 5.13, depicting the lateral displacement at the top of the wall as a function of the applied lateral force. The maximum push and pull direction strengths of 82.8 kN and -82.5 kN were measured during the first cycle to displacement ductility 4. Despite the presence of widely open diagonal cracks, the wall exhibited a gradual and fairly symmetrical strength degradation in both loading directions. Consequently, it was possible to classify Wall 7 as having a diagonal tension failure mode. This desirable behaviour of the nominally reinforced partially grout-filled concrete masonry wall with openings was created by the solid filled bond beam at the top of the wall, which caused a frame-type action at latter stage of testing.

Similar to Wall 6, double bending of the central pier in Wall 7 resulted in a significantly higher strength than previously reported for the walls with a single opening. The wall cracking pattern shown in Figure 5.14 illustrated that diagonal cracks aligned well with the load paths by which shear force was transferred to the foundation in the strut mechanism. This observation supports the use of strut-and-tie analysis as the tool to evaluate the strength of walls with reinforcement details complying with the specifications of NZS 4229:1999. As shown in Figure 5.13, the values of $F_{n,st}$ and NZS 4229:1999 failed to account for double bending of the central pier and resulted in significant under-prediction of wall strength, giving $F_{max}/F_{n,st} > 1.65$ and $F_{max}/F_{code} > 1.67$. Consequently, the force-displacement curve presented in Figure 5.13 indicates the conservatism of F_{code} and $F_{n,st}$ for masonry walls containing a central pier that are allowed to form plastic hinges on both ends of the inner piers. This is illustrated in the same figure, where a significantly improved strength prediction was attained when double bending of the central pier was accounted for in the strut-and-tie models presented in Figures 4.4g and 4.5g, resulted in $F_{max}/F_{n,ST}$ of 1.34 and 1.08 in the push and pull directions respectively. Experimental result of Figure 5.13 illustrate that strength prediction from the full plastic collapse analysis over-predicted the wall strength by about 38%.

The average yield displacement (Δ_y) for this partially grouted wall was evaluated to be 1.89 mm. The test wall was defined as failing during the first pull cycle to displacement ductility 6, giving it a ductility capacity μ_{av} of 3.75.

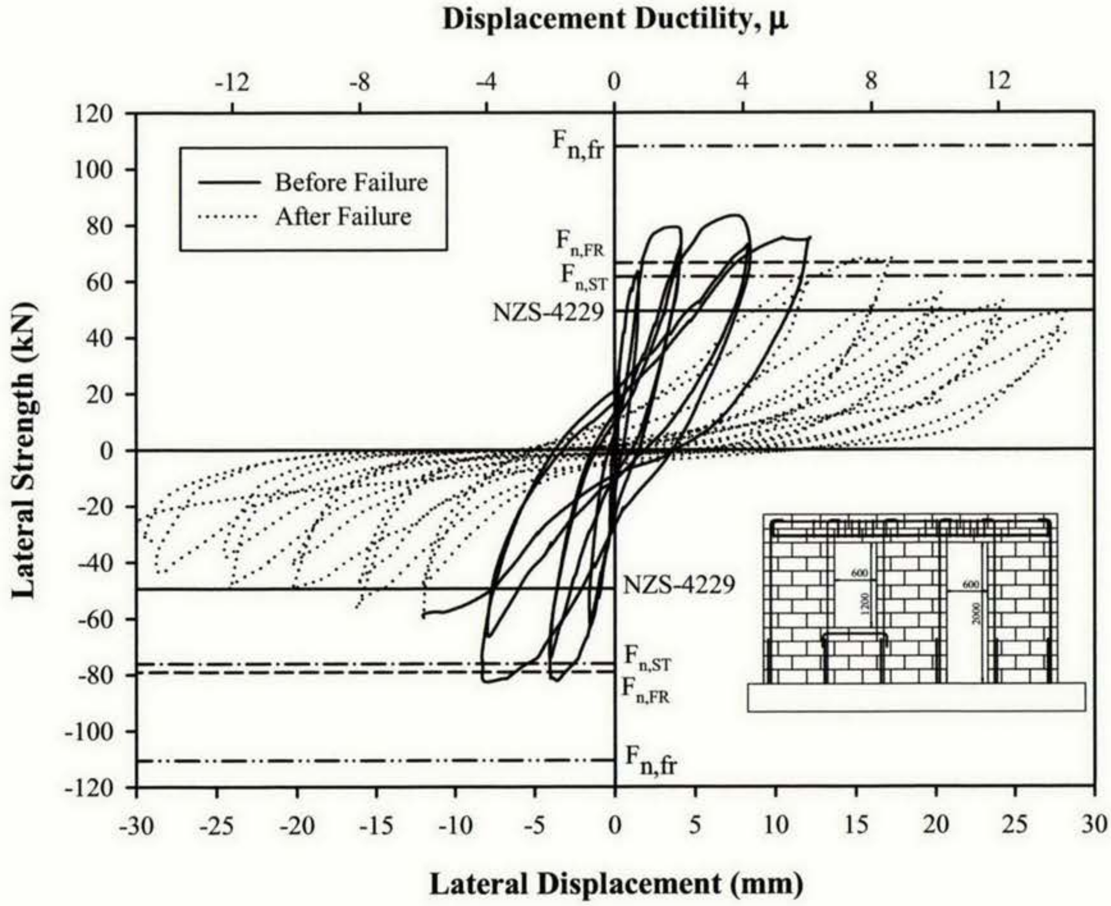

Figure 5.13 Force-displacement history for Wall 7.

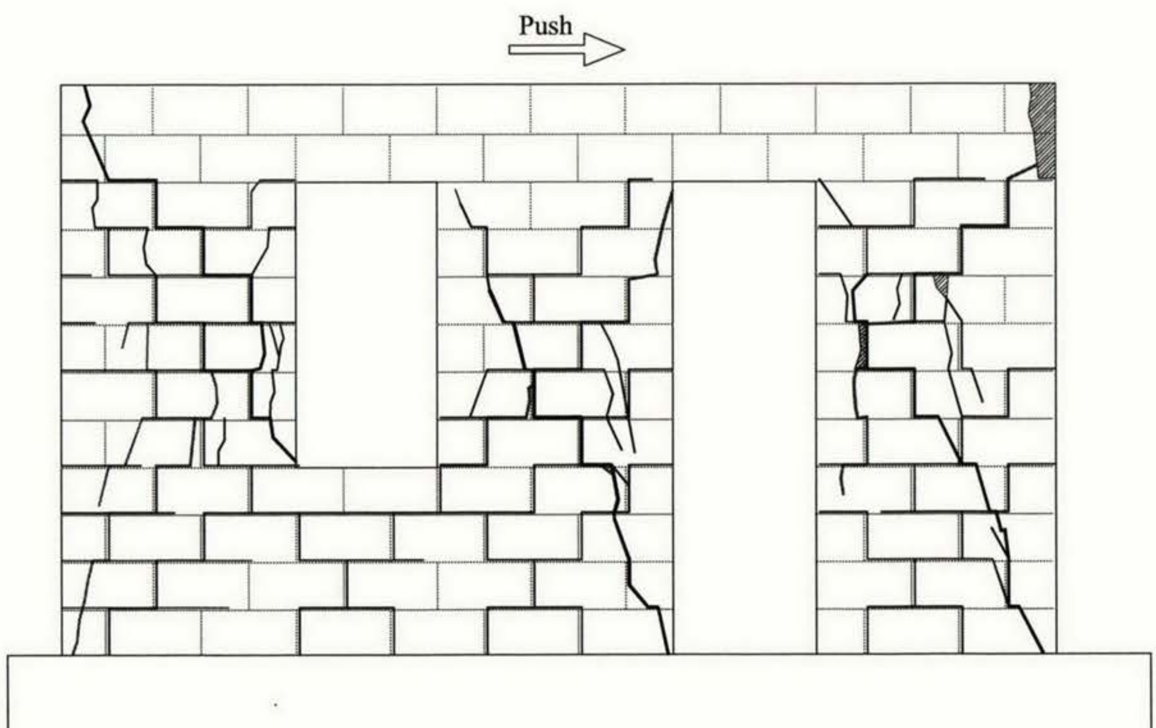

Figure 5.14 Wall 7 cracking pattern at end of testing.

5.8 Wall 8

The force-displacement history of Wall 8 is shown in Figure 5.15. The maximum push and pull direction strengths of 82.7 kN and -93.2 were measured during the first cycle to displacement ductility 4. Despite the lack of distributed horizontal shear reinforcement and the fact that the wall was partially grout-filled, the wall exhibited gradual strength degradation in both loading directions. Consequently, it was possible to classify Wall 7 as having a failure mode of diagonal tension. This type of failure was characterised by the development of early horizontal flexural cracking, which was later exaggerated by diagonal cracking that extended throughout the wall panels. The desirable behaviour of this perforated masonry wall was created by the solid filled bond beam at the top of the wall, which caused a frame-type action at latter stage of testing. This notion was supported by the absence of significant structural damage in the bond beam. Similar to Walls 1-7, the force-displacement plot in Figure 5.15 consistently illustrates a pinched shape. This was primarily due to the presence of significant shear deformation in this type of masonry construction. As shown in Figure 5.15, the conservatism of NZS 4229:1999 was higher in the pull direction than in the push direction. Higher strength in the pull direction was due to the presence of an extended trimmer reinforcing bar on one side of the window opening. Consequently, the experimental result of Wall 8 successfully illustrates that increased conservatism over NZS 4229:1999 bracing values will result when the length of trimmer reinforcement is extended below an opening. Experimental results shown in Figure 5.15 illustrate that measured strengths in both the push and pull directions closely matched those predicted from $F_{n,ST}$ and $F_{n,FR}$.

It was illustrated in Figure 5.16 that the diagonal cracking patterns on this wall aligned well with the load paths by which shear force was transferred to the foundation in the strut mechanism. This observation supports the use of strut-and-tie analysis as the tool to evaluate the strength of walls with reinforcement details complying with the specifications of NZS 4229:1999. However, the recorded wall strengths were 34% and 17% higher than the $F_{n,ST}$ predicted in the push and pull directions. Due to the non-symmetrical arrangement of trimming reinforcement, the yield displacements (Δ_y) for this partially grouted wall were evaluated to be 1.52 mm and 1.67 mm in the push and pull directions respectively. However, due to the slight difference of yield displacements for the two loading directions, an average Δ_y of 1.60 mm was adopted as the yield displacement for the two loading directions for convenience. The test wall was defined as failing during the second push cycle to displacement ductility 4, giving it a ductility capacity μ_{av} of 2.0.

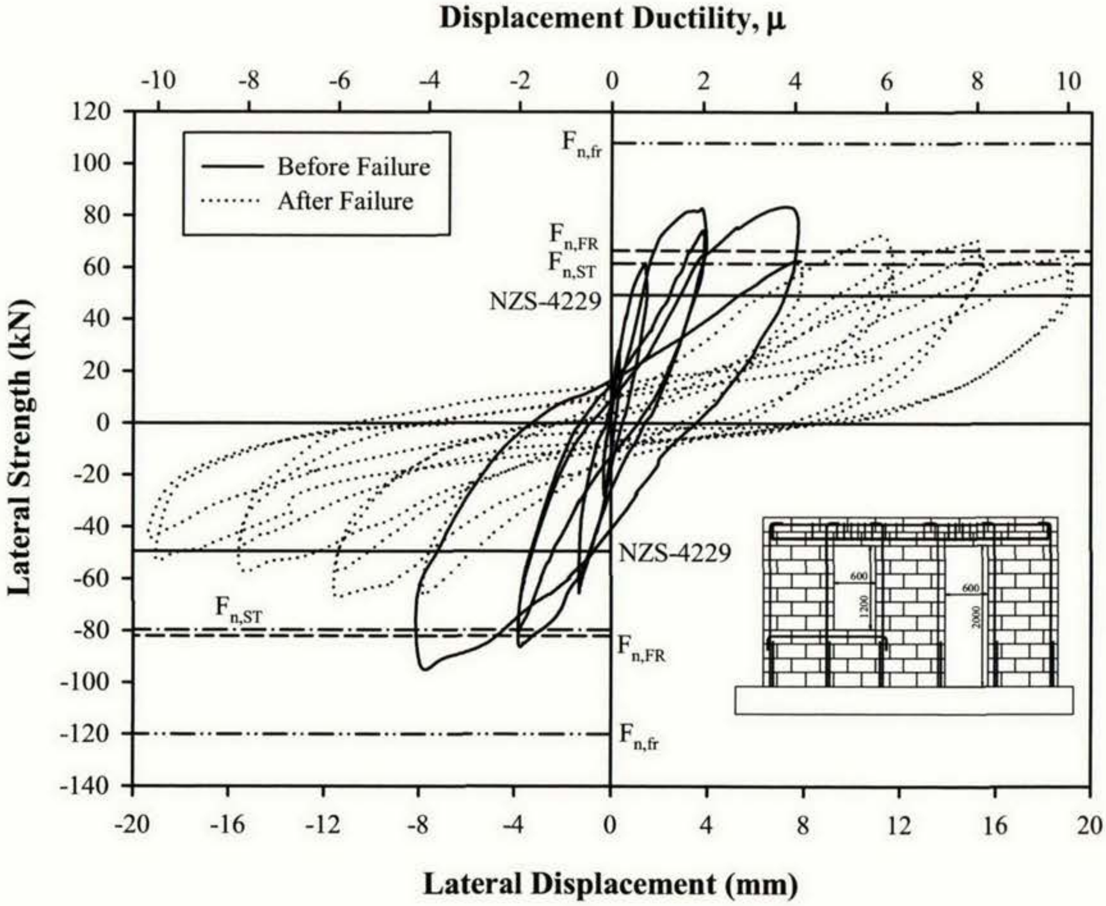

Figure 5.15 Force-displacement history of Wall 8.

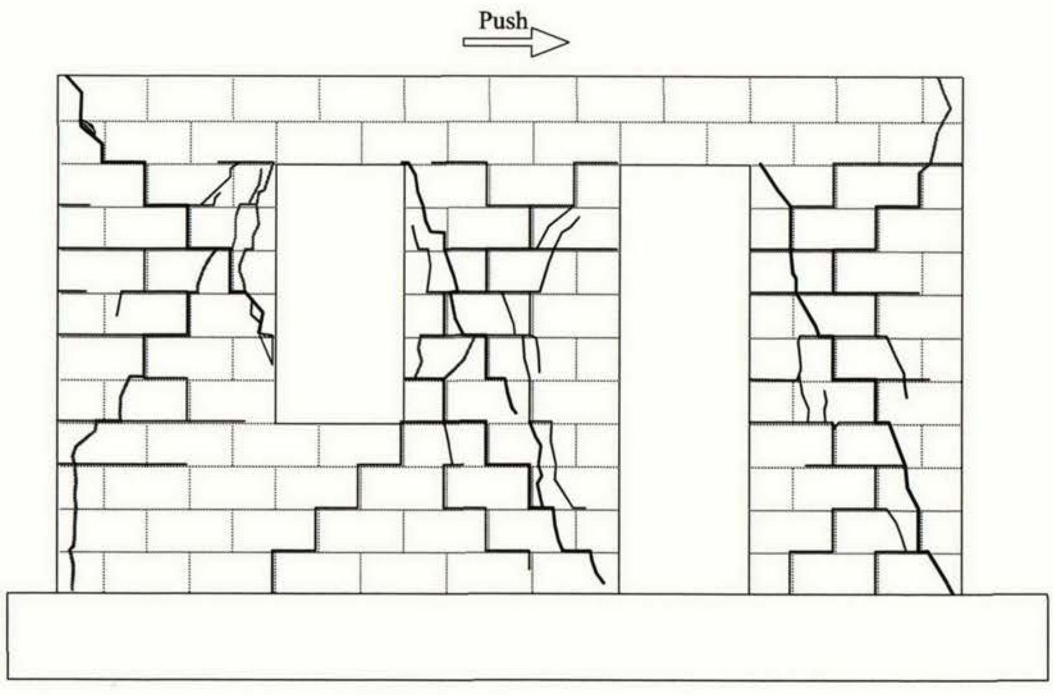

Figure 5.16 Wall 8 cracking pattern at end of testing.

5.9 Wall 9

The force-displacement history of Wall 9 is shown in Figure 5.17. The maximum push and pull direction strengths of 125.3 kN and -114.6 kN were measured during the first cycle to displacement ductility 14. The average yield displacement (Δ_y) for this partially grouted wall was evaluated to be 1.07 mm. The test wall was defined as failing during the second push cycle to displacement ductility 14, giving it a ductility capacity of $\mu_{av} > 6.0$.

As shown in Figure 5.17, the maximum strength achieved by Wall 9 was 43% higher than the values of $F_{n,st}$ obtained from the simple strut-and-tie model shown in Figure 4.2i. This higher strength was due to the solid filled bond beam constructed on top of the control joint. Consequently, the (un-debonded) continuous bond beam caused a frame-type action between the two piers, therefore allowing partial shear transfer. This notion was supported by the absence of significant structural damage in the bond beam. In addition, double bending of the solid filled bond beam (above the control joint) allowed it to generate some strength and subsequently led to yielding of the D12 reinforcing bar adjacent to the compression edge (as shown by the $F_{n,ST}$ model presented in Figure 4.4i). Furthermore, closing of the control joint at the wall mid-height position at latter stage of testing permitted additional shear transfer between the two piers. The maximum strengths recorded by the wall were 18% and 8% higher than the predicted value of $F_{n,ST}$ in the respective push and pull loading directions.

Despite the presence of widely open diagonal cracks, the wall exhibited a gradual and fairly symmetrical strength degradation in both directions of loading. Consequently, it was possible to classify Wall 9 as having a diagonal tension failure mode. This type of failure was characterised by the development of early horizontal flexural cracking on the pier tension edges, which was later exaggerated by diagonal cracking that extended throughout the wall panels. This desirable strength behaviour was created by the solid filled bond beam that was constructed continuously (un-debonded) above the control joint, causing a frame-type action at latter stage of testing. It is noted that no comment is implied on the ability of this bond beam/shrinkage control joint detail to satisfactorily accommodate shrinkage strains.

Similar to Walls 1-8, the force-displacement plot in Figure 5.17 consistently illustrated a pinched shape. This was primarily due to the presence of significant shear deformation (as discussed in section B.1.4) in this type of masonry construction. It was also observed that less hysteretic energy was expended during the second cycle to any displacement level, when compared with the first displacement cycle. This is illustrated by the more pinched hysteresis loops of the second cycle.

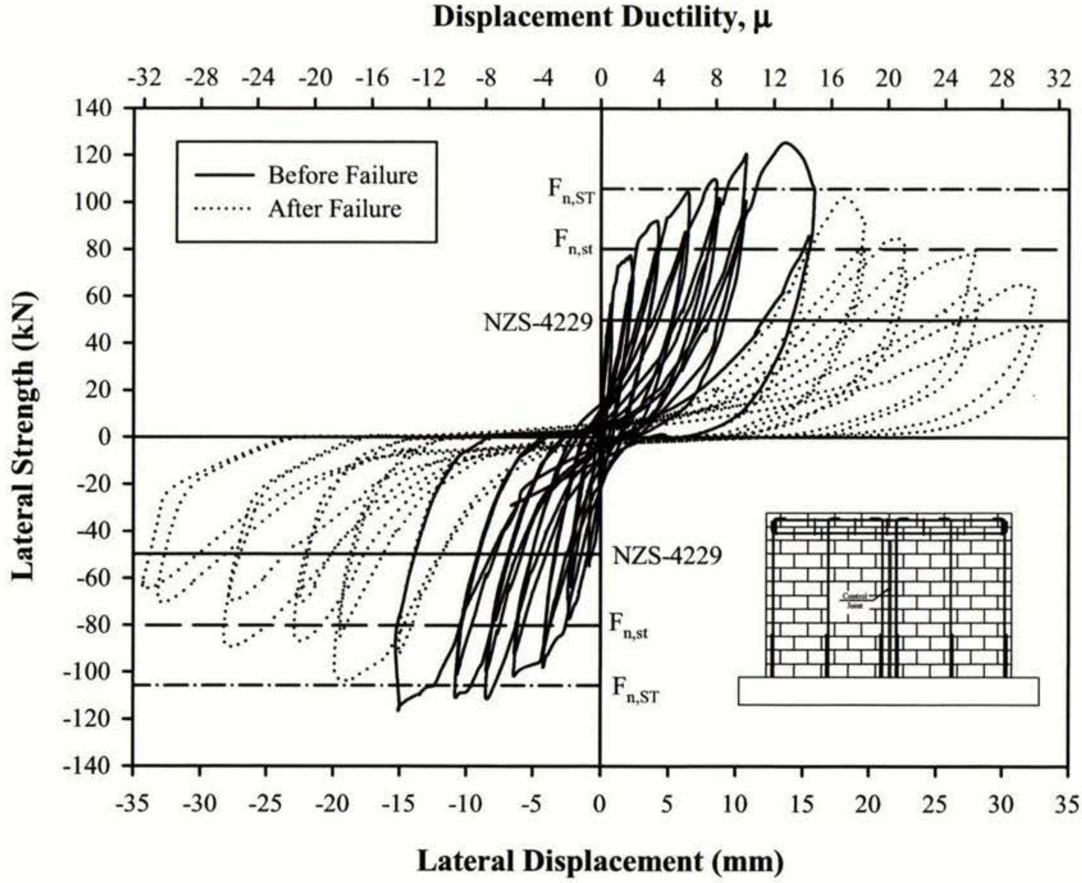

Figure 5.17 Force-displacement history for Wall 9.

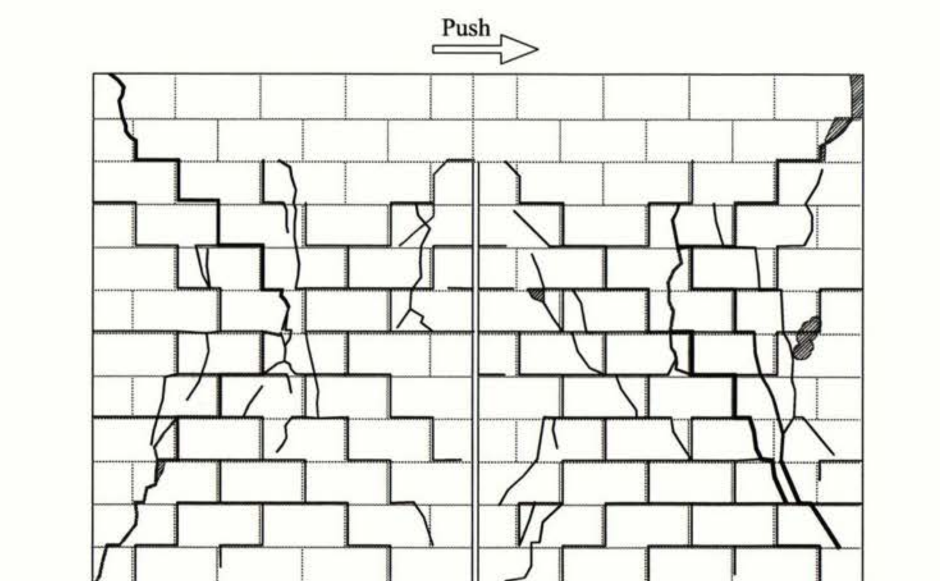

Figure 5.18 Wall 9 cracking pattern at end of testing.

5.10 Wall 10

The force-displacement history of Wall 10 is shown in Figure 5.19, depicting the lateral displacement at the top of the wall as a function of the applied lateral force. The nominal strength $F_{n,st}$ and the strength value derived from NZS 4229:1999 (denoted NZS-4229) are included in this plot. Also shown in this plot is the theoretical failure point, corresponding to the cycle in which the peak strength failed to exceed 80% of the maximum previously attained strength.

The maximum push and pull direction strengths of 89.0 kN and -84.6 kN were measured during the first cycle to displacement ductility 4. The average yield displacement (Δ_y) for this partially grouted wall was evaluated to be 2.10 mm. The test wall was defined as failing during the second push cycle to displacement ductility 6, giving it a ductility capacity μ_{av} of 4.5. As shown in Figure 5.19, the maximum strength achieved by Wall 10 was about 10% higher than the $F_{n,st}$ predicted.

Despite the presence of widely open diagonal cracks, the wall exhibited gradual and fairly symmetrical strength degradation in both directions of loading. Consequently, it was possible to classify Wall 10 as having a diagonal tension failure mode. This type of failure was characterised by the development of early horizontal flexural cracking on the pier tension edges, which was later exaggerated by diagonal cracking that extended throughout the wall panels.

Similar to the other walls previously reported, the force-displacement plot in Figure 5.19 consistently illustrated a pinched shape. This was primarily due to the presence of significant shear deformation in this type of masonry construction. It was also observed that less hysteretic energy was expended during the second cycle to any displacement level, when compared with the first displacement cycle. This is illustrated by the more pinched hysteresis loops of the second cycle.

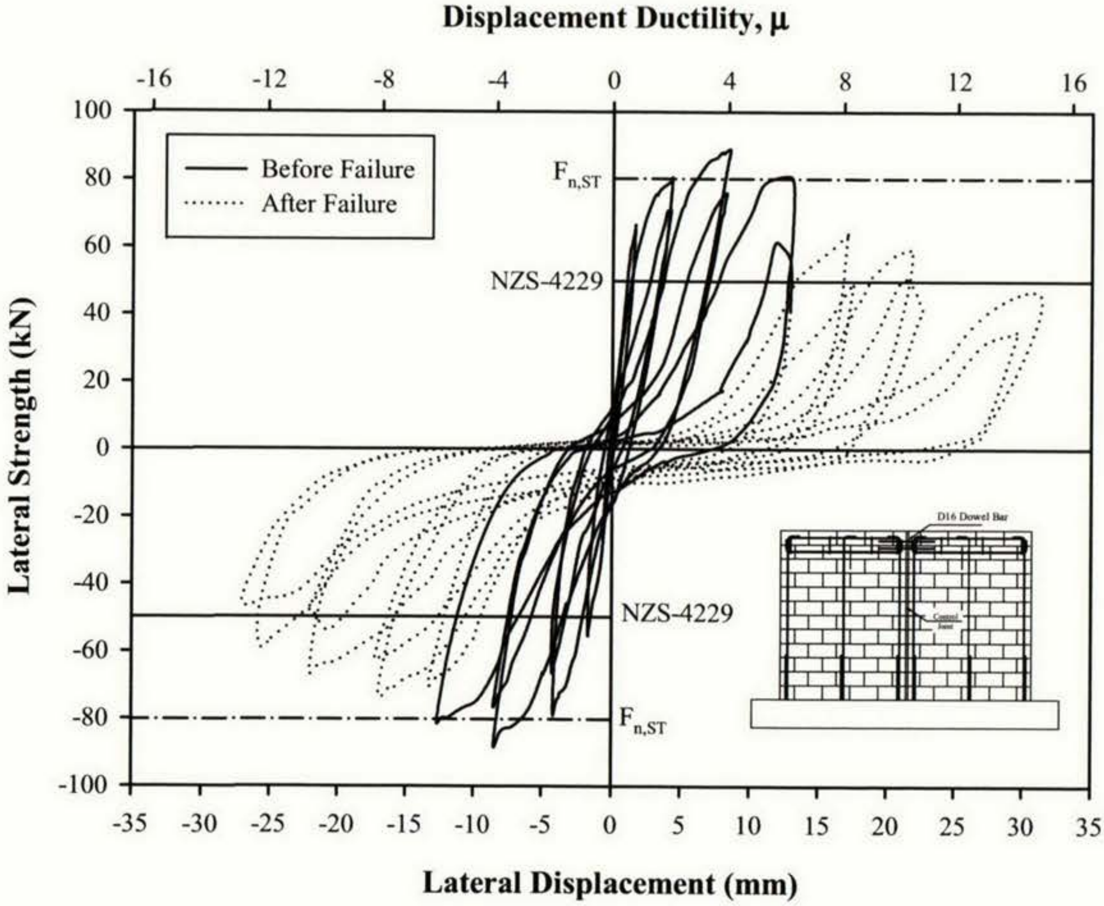

Figure 5.19 Force-displacement history for Wall 10.

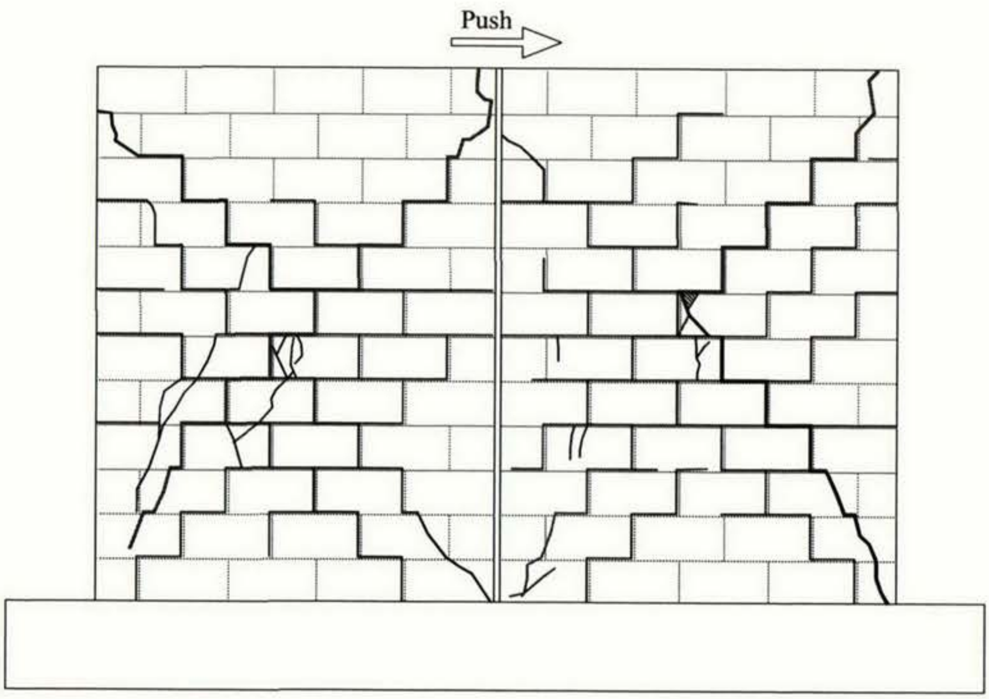

Figure 5.20 Wall 10 cracking pattern at end of testing.

Chapter 6

Discussion of Test Results

6.1 Introduction

The primary objective of this study was to validate the adequacy of NZS 4229:1999 in addressing the bracing capacity of masonry walls containing openings. As shown in Figure 3.4, design of the eight perforated masonry wall specimens was conceived to facilitate comparison of wall behaviour between two or more walls with respect to variation of a given design parameter. These eight partially grouted concrete masonry walls had variations in trimming reinforcement detailing, including those complying with NZS 4229:1999, and a range of penetration geometries. In addition, experimental works previously conducted at the University of Auckland (see Figures 2.2 and 2.3) are included in this part of the study to supplement the experimental results presented in Chapter 4. The two 15 series concrete masonry walls tested by Brammer (1995) are valuable to provide comparison of behaviour between perforated walls and those of solid built walls (i.e. without opening). A parallel issue is the influence which shrinkage control joints have on the bracing capacity of partially grouted concrete masonry walls. NZS 4229:1999 prescribed a procedure to account for shrinkage control joints, but this detail has never been verified through structural testing. Consequently, experimental testing on two partially grout-filled concrete masonry walls was conducted to validate the structural adequacy of the shrinkage control joint detail published in NZS 4229:1999.

The figures in this section are limited to force-displacement (F-D) envelopes. These are curves that relate the peak strength recorded in the first cycle for each displacement ductility level. The F-D envelopes are arranged in groups to show the effect of a particular parameter. A full set of curves for each test is presented in Chapter 5.

6.2 Result Summary

It is noteworthy that the general nature of the force-displacement responses presented in Chapter 5 are significantly similar to those reported by Brammer (1995) and Davidson (1996). From the F-D curves illustrated in Chapter 5, a number of general characteristics of Walls 1-10 can be identified:

1. The maximum strength was typically developed during the first excursion to $\mu = 4$. Following this, cracking became significant in some walls and strength degradation began.
2. The partially grouted concrete masonry walls detailed in Figures 3.4 and 3.5 exhibited gradual strength and stiffness degradation, and in no case did any wall suffer from sudden failure. This desirable behaviour of the nominally reinforced partially grouted masonry walls with openings was created by the solid filled bond beam at the top of the walls, which caused a frame-type action at latter stage of testing.
3. From the wall cracking pattern diagrammatically shown in Chapter 5, it is clearly illustrated that the absence of major damage in the solid grout-filled bond beam supported the notion of frame-type action being developed at later stage of the test. This leads to considerable inelastic displacement capacity of the partially grouted masonry walls, where μ_{av} was measured to consistently be above 2.0.
4. The force-displacement plots consistently illustrated a pinched shape. This was primarily due to the presence of significant shear deformation in this type of masonry construction (please refer to Appendices A and B for relevant information).
5. Less hysteretic energy was expended during the second cycle to any displacement level, when compared with the first displacement cycle. This is illustrated by the more pinched hysteresis loops of the second cycle.

Table 6.1 shows key test results for each wall. The results are given for both directions of loading. F_{max} corresponds to the maximum wall strength measured in the test, and Δ_y is the evaluated yield displacement of the tested walls. μ_{max} is defined as the displacement ductility level at which maximum strength was measured and μ_{av} is the available displacement ductility factor, which according to Park (1989) is the ductility level at which a test element has sustained less than 20% loss in peak strength after four complete (bi-directional) loading cycles to μ_{av}.

Due to the lack of distributed horizontal shear reinforcement, all walls presented in Table 6.1 were reported to fail in a diagonal tension mode. This was preferable to the hinge-sliding mode, where the lateral force was resisted only by dowel action of the vertical reinforcement once a crack opened up along the entire length of the wall/foundation interface (Priestley, 1976).

The μ_{av} values recorded in Table 6.1 show that the largest recorded ductility capacity for the perforated masonry walls corresponded to a wall length of 2600 mm, and reduced significantly for the 4200 mm long perforated masonry walls. It was observed from experimental testing that the 4200 mm long masonry walls displayed greater cracking than the 2600 mm long walls. Consequently, it was deduced that the lower observed ductility rating for the 4200 mm long walls occurred because of the rapid-developing wide cracks that contribute to shear displacement, accelerating initiation if the diagonal tension mode of failure and subsequent strength degradation.

6.3 Depth of Openings

Test results from this study successfully illustrate correlation between the reduction of wall strength and depth of openings (h_{op}) on masonry walls. This is shown in Table 6.1 and Figure 6.1 by the consistent reduction of $F_{max}/F_{n,no\text{-}op}$ ratios when the depth of openings were increased in the 2600 mm and 4200 mm long masonry walls that were constructed according to NZS 4229:1999 specifications. This reduction of wall strength could also be identified in the F-D envelopes presented in Figures 6.2 and 6.4. In Figure 6.2, it is shown that the lateral strength of the 2600 mm long walls reduced from the maximum of 76.5 kN in the case of Wall B1 (without opening), to 50.2 kN when a window opening of 600 x 800 was included in Wall 1. The same figure also shows further reduction of wall strength to 41.2 kN and 34.4 kN when the depth of openings was increased to 1200 mm and 2000 mm in Walls 2 and 3 respectively. As diagrammatically illustrated in the strut-and-tie models presented in Figure 6.3, the further reduction of strength in Walls 2 and 3 (compared to Wall 1) was because of the steepened diagonal struts on the left piers when the depth of openings increased. While the diagonal strut on the right piers remained unchanged for these three walls, the steepened diagonal struts on the left piers resulted in reduction of horizontal shear components that could be resisted by the left piers, consequently leading to the overall reduction of lateral strength in Walls 2 and 3.

Table 6.1 Summary of test results for the 2600 mm long masonry walls.

Wall	Specimen	h_{op}/h_w	f'_m	$F_{n,no\text{-}op}$	F_{max}	$\frac{F_{max}}{F_{n,no-op}}$	Δ_y	μ_{max}	μ_{av}
Current research	1	0.33	16.2	77.3	+50.2 -49.0	0.65	0.82	+6 -4	>6.0
	2	0.5	12.9	77.0	+41.2 -38.7	0.54	0.57	±4	>6.0
	3	0.83	14.4	77.1	+33.3 -34.4	0.45	1.07	±4	>6.0
	4	0.5	16.5	77.3	+47.4 -48.8	0.63	1.15	+2 -4	4.5
	5	0.5	18.9	77.5	+52.4 -50.4	0.68	+0.84 -0.66	+4 -6	2.0
	6	0.5	16.5	191.4	+94.3 -94.6	0.49	1.83	+2 -4	2.0
	7	0.83*	18.0	191.6	+82.8 -82.5	0.43	1.89	±4	3.8
	8	0.83*	18.0	191.6	+82.7 -93.2	0.49	1.60	±4	2.0
	9	0	23.8	105.8	+125.3 -114.6	1.18	1.07	±14	>6.0
	10	0	23.8	82.1	+89.0 -84.6	1.08	2.10	±4	4.5
Previous	B1	0	---	75.0	76.5	1.02	1.57	---	5.4
	B2	0	---	213.1	179.9	0.84	3.60	---	1.0
	D1	0.83*	---	174.0	89.0	0.51	1.00	---	6.0
Units		---	MPa	kN	kN	---	mm	---	---

Note:

1. * h_{op}/h_w ratio according to the largest opening on the wall
2. B1 is the 2600 x 2400 x 140 concrete masonry wall tested by Brammer (1995), see Figure 2.2a.
3. B2 is the 4200 x 2400 x 140 concrete masonry wall tested by Brammer (1995), see Figure 2.2b.
4. D1 is the 4200 x 2400 x 190 perforated concrete masonry wall tested by Davidson (1996), see Figure 2.3.

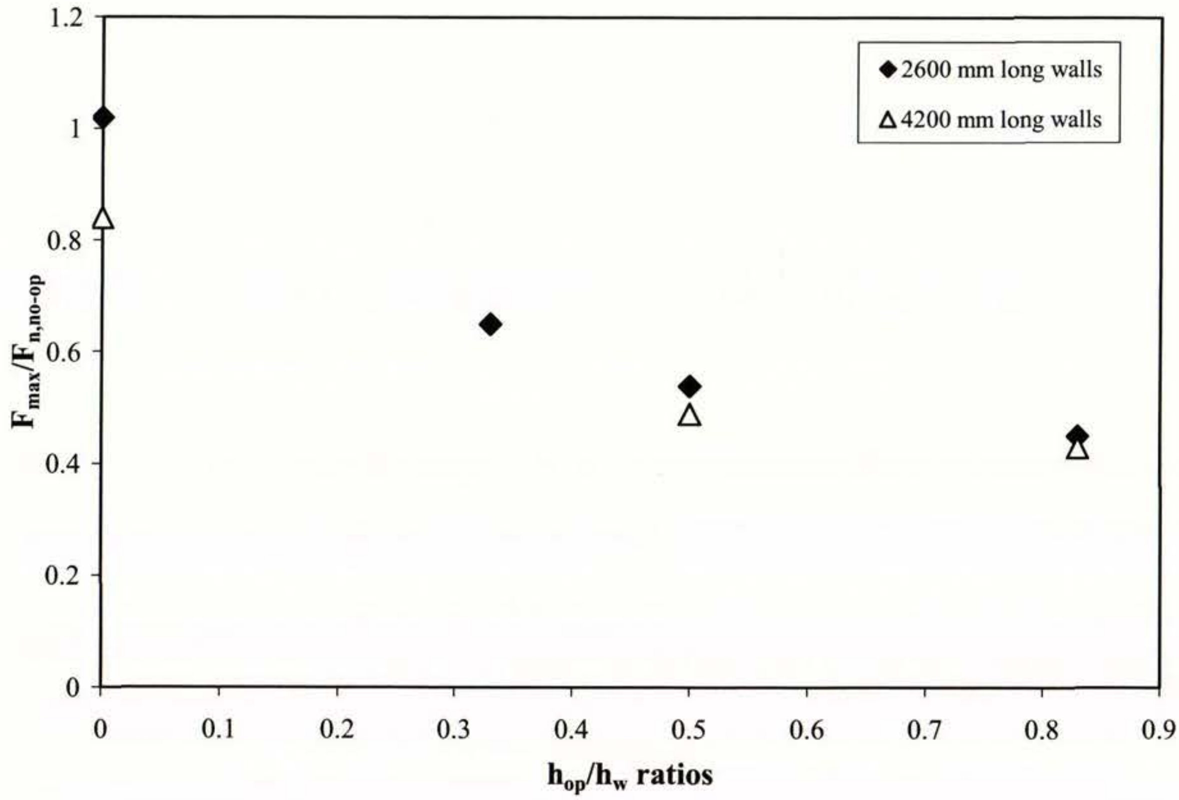

Figure 6.1 Effect of opening for walls constructed according to NZS 4229:1999 specifications.

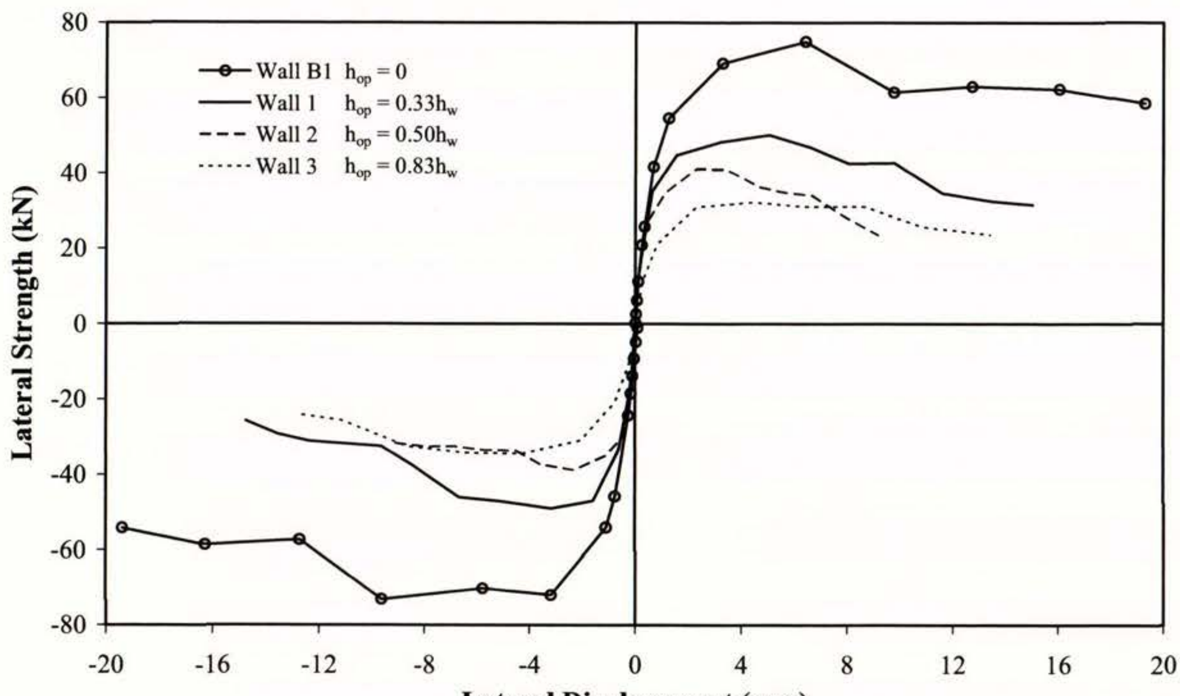

Figure 6.2 Effect of opening on the 2600 mm long walls.

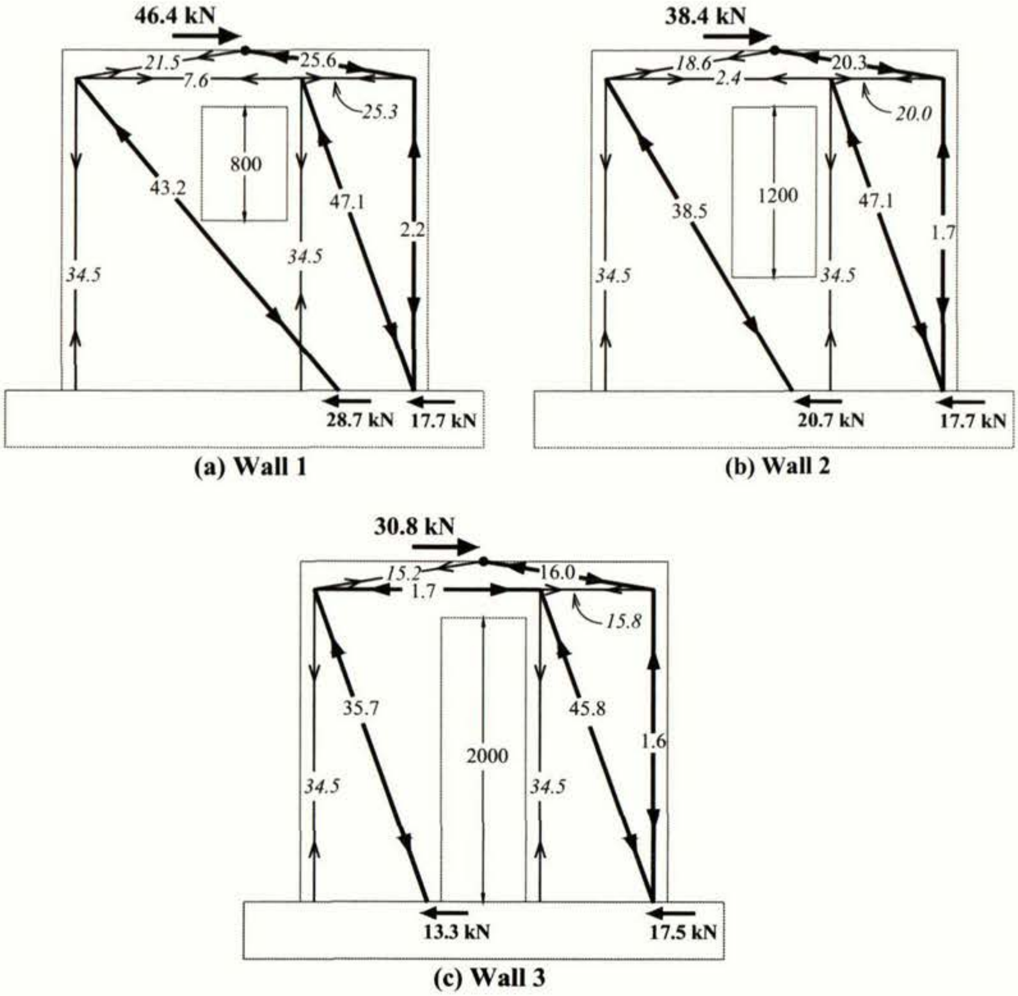

Figure 6.3 Strut-and-tie models in push direction.

Similarly, the reduction of lateral strength in the 4200 mm long walls is also evident in Figure 6.4. As compared to the strength recorded in Wall B2, it is shown that the wall lateral strength was almost halved when openings were introduced on the 4200 mm long masonry walls. In addition, by comparing the lateral strengths of Walls 6 and 7, it is shown that the introduction of a door opening resulted in the reduction of strength from 94 kN to 83 kN in Wall 7 (about 12% reduction of strength). Please note that the test results of Walls 4, 5 and 8 are not included in Figures 6.1-6.4 because the detailing of trimming reinforcement in these walls differed from that specified in NZS 4229:1999. The primary objective of Figures 6.1-6.3 is to illustrate the effect of openings on the lateral strength of perforated masonry walls constructed according to NZS 4229:1999 specifications.

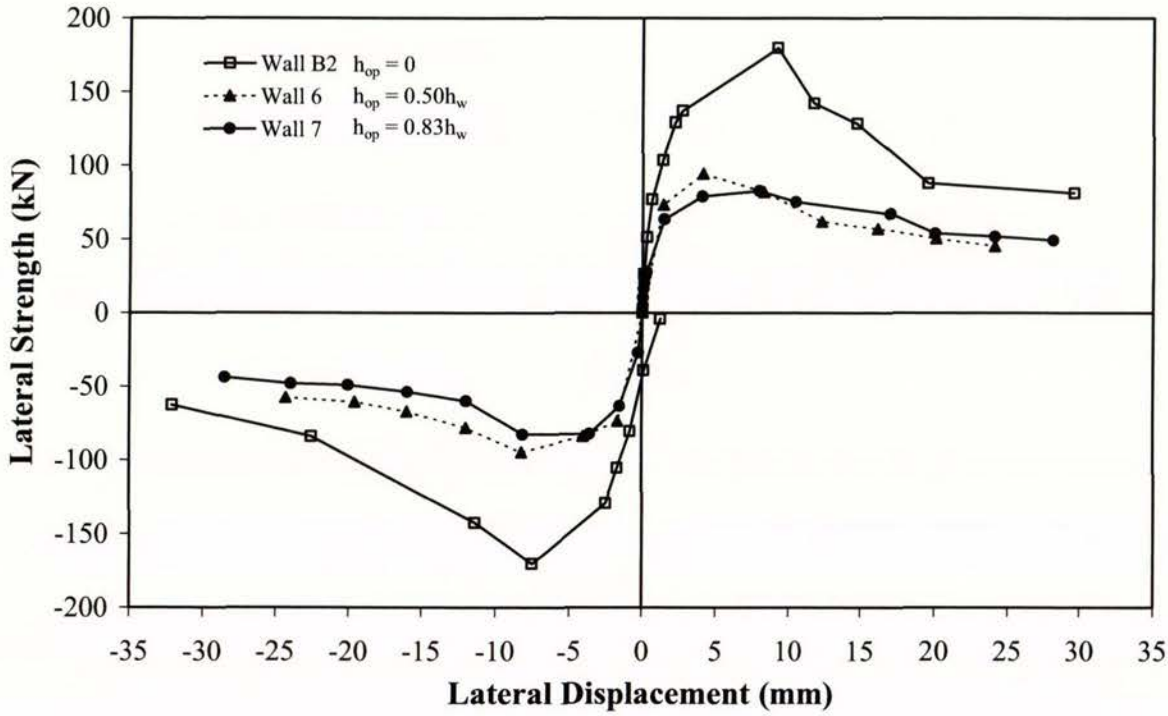

Figure 6.4 Effect of openings on the 4200 mm perforated masonry walls.

6.3 Effect of Trimming Reinforcement

The effect of trimming reinforcement on the lateral strength of perforated masonry walls is discussed in this subsection. It was illustrated in Chapter 5 that the use of extended D16 trimming reinforcement could affect the wall ultimate strength considerably. This is shown by the increase in magnitude of the $F_{max}/F_{n,no\text{-}op}$ ratios presented in Table 6.1 when the trimming reinforcement was extended below the window openings in the 2600 mm and 4200 mm long masonry walls. This increase of wall strength can also be identified in the F-D envelopes presented in Figures 6.5 and 6.6. Figure 6.5 shows the force-displacement envelopes for Walls 2, 4 and 5. These three partially grout-filled masonry walls were constructed to identical geometries and consisted of identical longitudinal and bond beam reinforcement, with the only difference being the length of trimming reinforcement used in each wall. The trimming reinforcement in Wall 2 (see Figure 3.4) was detailed according to the specifications of NZS 4229:1999, but Walls 4 and 5 were detailed with extended trimming reinforcement. As shown in Figure 3.4, the trimming reinforcement in Wall 5 was only extended to the outermost vertical reinforcement on one side of the wall, therefore resulting in higher strength being predicted in the push direction than in the pull direction. The force-displacement envelopes in Figure 6.5 clearly illustrate the increase of lateral strength from the maximum of 41.2 kN for Wall 2 to 47.7 kN and 52.4 kN when the trimming reinforcement was extended beneath the window opening in Walls 4 and 5, therefore resulting in strength increases of about 18% and 27% respectively. However, the effect of the extended trimming reinforcement in the pull direction could not be properly observed in Wall 5. Although a lesser strength was predicted in the pull direction for Wall 5, a maximum strength of about 50 kN was recorded despite the absence of extended trimming reinforcement on the left pier. As shown in Table 6.1, this maximum strength in Wall 5 was larger than that recorded in the pull direction for Wall 4, although an extended trimming reinforcement bar was present on the left pier in Wall 4. Consequently, this observation confirms that Wall 5 may have developed strength in its pull direction that was substantially higher than specimens of similar construction. Discarding the experimental result of Wall 5, the effect of trimming reinforcement in increasing wall strength (pull direction) could be undoubtedly demonstrated by the experimental results of Walls 2 and 4. It was shown that a strength increase of about 26% was recorded in Wall 4, as compared to Wall 2, when extended trimming reinforcement was present in the left pier.

Strength increase due to the extended trimming reinforcement in the 4200 mm perforated masonry walls is shown in Figure 6.6. Although the test result reported by Davidson (1996) is presented in Figure 6.6, it is not suitable for use as a wall strength comparison. This is because the reinforcing steel used in Davidson's wall construction was inconsistent with the reinforcing steel used in the current study. Davidson employed $f_y = 275$ MPa reinforcing steel in his wall construction, therefore resulting in a lower wall strength than if $f_y = 300$ MPa reinforcing steel was used. Figure 6.6 is valuable to show the significantly similar nature of the force-displacement response of the three 4200 mm long perforated masonry walls. This provides further credibility to the performance of partially grout-filled masonry construction. Similar to Figure 6.5, the force-displacement envelopes in Figure 6.6 illustrate an increase in wall pull strength from 82.5 kN for Wall 7 to 93.2 kN when the trimming reinforcement of Wall 8 was extended to the outermost vertical reinforcement in the left pier (see Figure 3.4), resulting in a strength increase of about 12% in the pull direction.

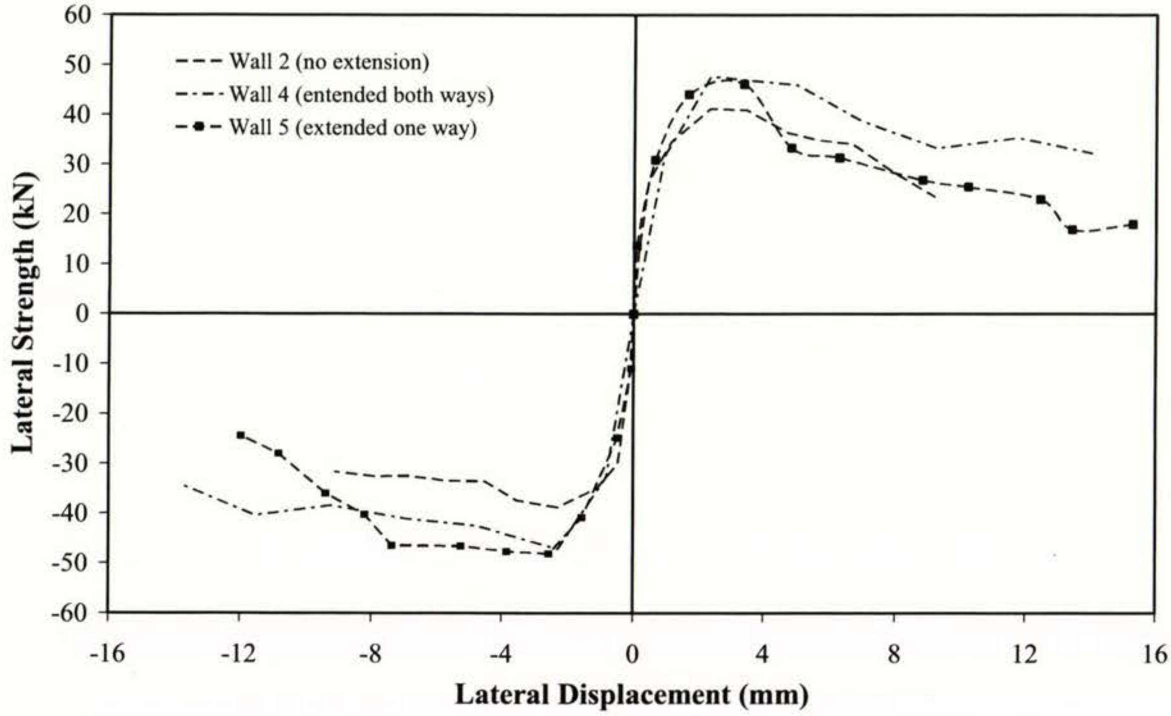

Figure 6.5 Effect of trimming reinforcement on the 2600 mm long perforated masonry walls.

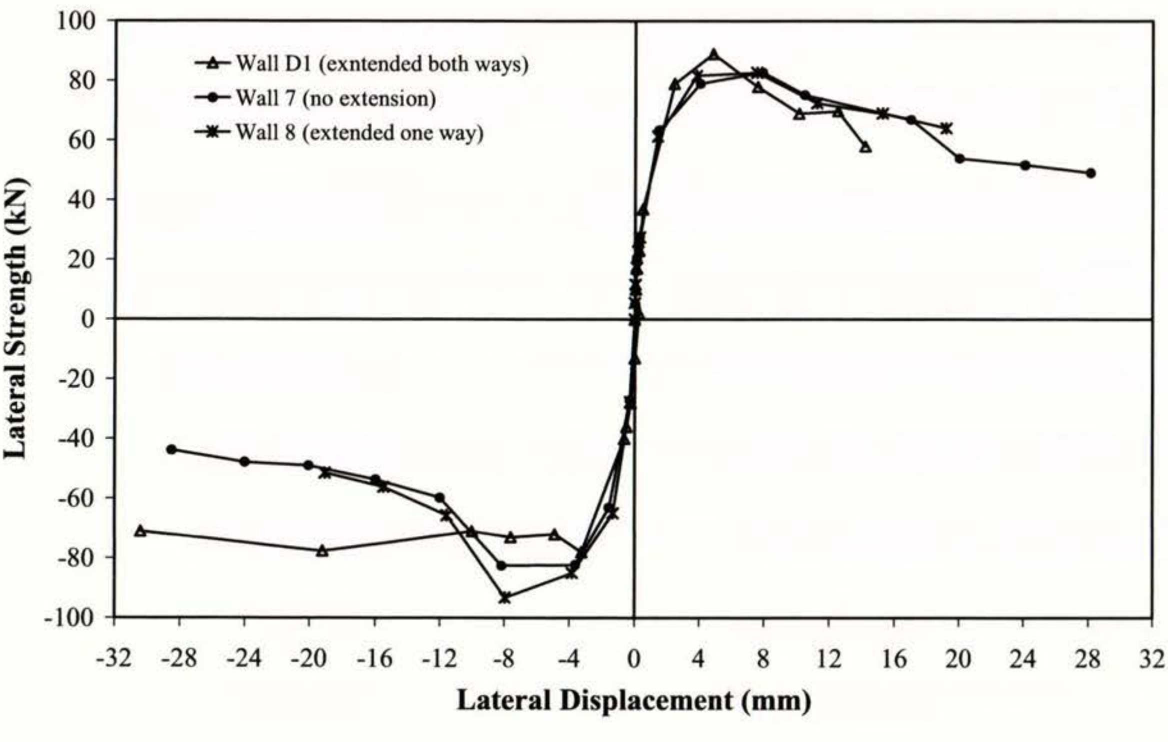

Figure 6.6 Effect of trimming reinforcement on the 4200 mm long perforated masonry walls.

6.4 Effect of Shrinkage Control Joint

Figure 6.7 shows the force-displacement envelopes of the two walls containing a shrinkage control joint at wall centre. It is clearly illustrated that the lateral strength of Wall 9, which had a control joint constructed in accordance with the specifications of NZS 4229:1999, exceeded the maximum strength recorded in Wall 10 by about 38%. This higher strength was due to the solid filled bond beam constructed on top of the control joint. Consequently, the (un-debonded) continuous bond beam caused a frame-type action between the two piers, therefore allowing partial shear transfer. This notion was supported by the absence of significant structural damage in the bond beam. In addition, double bending of the solid filled bond beam (above the control joint) allowed it to generate some strength and subsequently led to the yielding of D12 reinforcing bar adjacent to the compression edge (as shown by the $F_{n,ST}$ model presented in Figure 4.4i). Furthermore, closing of the control joint at the wall mid-height position at latter stage of testing permitted additional shear transfer between the two piers. It is also shown in Table 6.1 that the control joint detailed according to the NZS 4229:1999 procedure resulted in a F_{max}/F_{code} ratio of 2.52 for Wall 9, while a F_{max}/F_{code} ratio of 1.79 was measured for Wall 10 that had a control joint extended up the full height of the wall. Consequently, it is concluded that there is additional conservatism in the standard when the control joint is constructed according to the specifications of NZS 4229:1999.

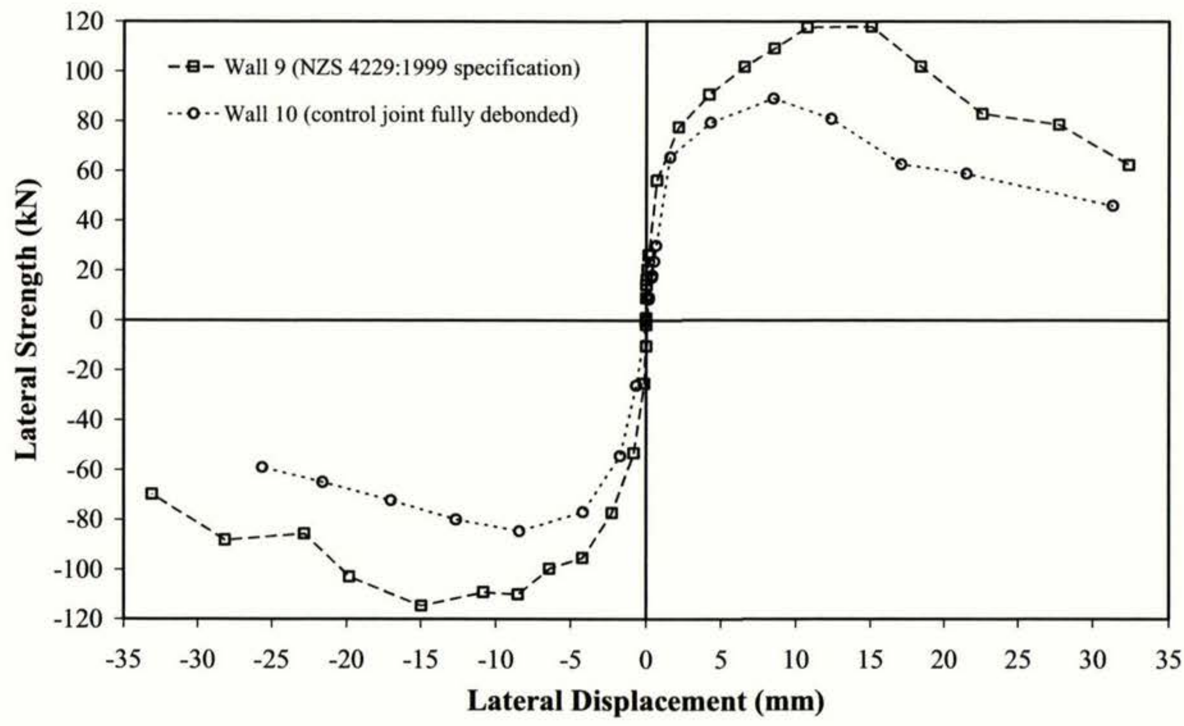

Figure 6.7 Effect of shrinkage control joint on partially grout-filled masonry walls.

Apart from the difference in strength shown in Figure 6.7, both Walls 9 and 10 shared similar force-displacement responses, with gradual strength and stiffness degradation. Consequently, the results attained from this study successfully demonstrated that the NZS 4229:1999 procedure for accounting for shrinkage control joints has resulted in adequate structural performance.

6.5 Wall Strength Prediction

The test results of Walls 1-5 presented in Table 6.2 clearly demonstrate that the size of openings and the arrangement of trimming reinforcement significantly affect the lateral strength of perforated masonry walls. For the small window opening in Wall 1, the measured strength was slightly less than that prescribed by NZS 4229:1999, resulting in F_{max}/F_{code} = 0.97. However, it was successfully illustrated in Chapter 5 that the conservatism of NZS 4229:1999 increases with the depth of opening, and for a full depth opening (e.g. a door in Wall 3) the NZS 4229:1999 prediction had significant conservatism. As shown in Figure 6.8, it is illustrated that a 50% increase in the number of piers for the 4200 mm long walls resulted in approximately 100% increase in lateral strength when compared to the strengths recorded for the 2600 mm long walls. It is therefore established that double bending of the central pier significantly increased the lateral strength of perforated walls. Consequently, failure of NZS 4229:1999 to account for the extra strength generated by double bending of the central pier resulted in significant under-prediction of strengths recorded in Walls 6-8. As shown in Table 6.2, ratios of $0.97 \leq F_{max}/F_{code} \leq 1.40$ and $1.68 \leq F_{max}/F_{code} \leq 1.89$ were observed for the 2600 mm and 4200 mm long perforated walls included in this study. This observation subsequently lead to the preliminary conclusion that NZS 4229:1999 is only non-conservative for walls containing single opening with a depth of less than 1200 mm, but significant conservatism of the standard would result for walls that have more than one opening where the inner piers can undergo double bending.

Comparisons of $F_{max}/F_{n,st}$, $F_{max}/F_{n,ST}$, $F_{max}/F_{n,fr}$ and $F_{max}/F_{n,FR}$ are presented in Table 6.2 and Figure 6.9. It is shown that the simplified strut-and-tie method was reasonably accurate in predicting the lateral strength of the 2600 mm long perforated masonry walls, with $F_{max}/F_{n,st}$ varying from 1.12 to 1.28 (excluding the experimental result obtained in the pull direction for Wall 5). However, the effectiveness of this method was significantly reduced when predicting the strengths of the 4200 mm long masonry walls included in this study. This was shown by the consistent under-prediction of strengths for Walls 6-8 by about 60% when the simplified strut-and-tie method was used. Similar to NZS 4229:1999, this under-prediction of wall strength by $F_{n,st}$ was due to the fact that double bending of the central pier was not accounted for in the simplified strut-and-tie models. When using the improved strut-and-tie method, it is illustrated in Figure 6.9c that significantly improved strength predictions were attained when double bending of the central pier and when wall self-weight were considered in models presented in Figures 4.4 and 4.5, resulted in average $F_{max}/F_{n,ST}$ values of about 1.10 for the 2600 mm long walls (excluding Wall 5 pull direction) and 1.22 for the 4200 mm long masonry walls. The diagonal cracking patterns (see Chapter 5) on the perforated walls were observed to align well with the load paths by which shear force was assumed to be transferred to the foundation in the strut mechanism. This observation supports use of the strut-and-tie method as the tool to evaluate the strength of nominally reinforced masonry walls with openings.

The full plastic collapse analysis, as shown by the $F_{max}/F_{n,fr}$ ratios presented in Figure 6.9d, was shown to significantly over-predict the lateral strengths of all perforated walls included in this study, with $0.48 \leq F_{max}/F_{n,fr} \leq 0.63$ and $0.73 \leq F_{max}/F_{n,fr} \leq 0.78$ for the 2600 mm and 4200 mm long walls respectively. It is therefore successfully illustrated that a full plastic mechanism would not develop in the nominally reinforced perforated masonry walls. Consequently, test results from this study indicated that lateral strength prediction of perforated walls using the full plastic collapse analysis can lead to unsafe design for masonry walls constructed according to specifications of NZS 4229:1999. Finally, the $F_{max}/F_{n,FR}$ values presented in Table 6.2 and Figure 6.9e show that strength predictions using the modified plastic collapse analysis have resulted in accuracy that closely matches predictions using the improved strut-and-tie models. It is successfully illustrated that significantly improved strength predictions were attained when single bending of the outer piers was considered in models presented in Figures 4.8 and 4.9, resulted in $1.12 \leq F_{max}/F_{n,FR} \leq 1.40$ and $1.09 \leq F_{max}/F_{n,FR} \leq 1.25$ for the respective 2600 mm and 4200 mm long masonry walls.

Based on the values for $F_{max}/F_{n,st}$, $F_{max}/F_{n,ST}$, $F_{max}/F_{n,fr}$ and $F_{max}/F_{n,FR}$ presented in Tables 6.2 and Figure 6.9, it is shown that the simplified strut-and-tie method ($F_{n,st}$) is only accurate in predicting the lateral strength of perforated walls that have a single opening and the conservatism of $F_{n,st}$ is significantly increased when two openings are present in a masonry wall. Consequently, test results show the $F_{n,st}$ method can lead to a non-economic cost design for masonry walls that contain more than one opening, which could subsequently lead to the reduced popularity of masonry as a constructional material. Conversely, the full plastic collapse analysis ($F_{n,fr}$) was shown to consistently over-predict the strength of all perforated walls included in this study and therefore indicating that this analysis method could lead to unsafe design for partially grout-filled masonry walls constructed according to NZS 4229:1999 specifications.

Of the strength prediction methods discussed in section 4.1, the improved strut-and-tie method ($F_{n,ST}$) and modified plastic collapse analysis ($F_{n,FR}$) were shown to predict the lateral strength of the perforated walls with significantly improved accuracy. This is shown by the average $F_{max}/F_{n,ST}$ ratio of 1.15 and $F_{max}/F_{n,FR}$ ratio of 1.18 for the eight perforated walls included in this study. Hence, it is strongly recommended that the strength prediction of partially grout-filled perforated masonry walls with reinforcement details similar to those shown in Figure 3.4 be conducted according to the improved strut-and-tie model ($F_{n,ST}$) or the modified plastic collapse analysis ($F_{n,FR}$). Although the $F_{n,ST}$ method is shown to produce strength prediction accuracy that is slightly better than the $F_{n,Fr}$ method, the $F_{n,ST}$ method would normally require computer software, such as SAP2000, in order to quickly produce an accurate answer. Conversely, the modified plastic collapse analysis is significantly easier to

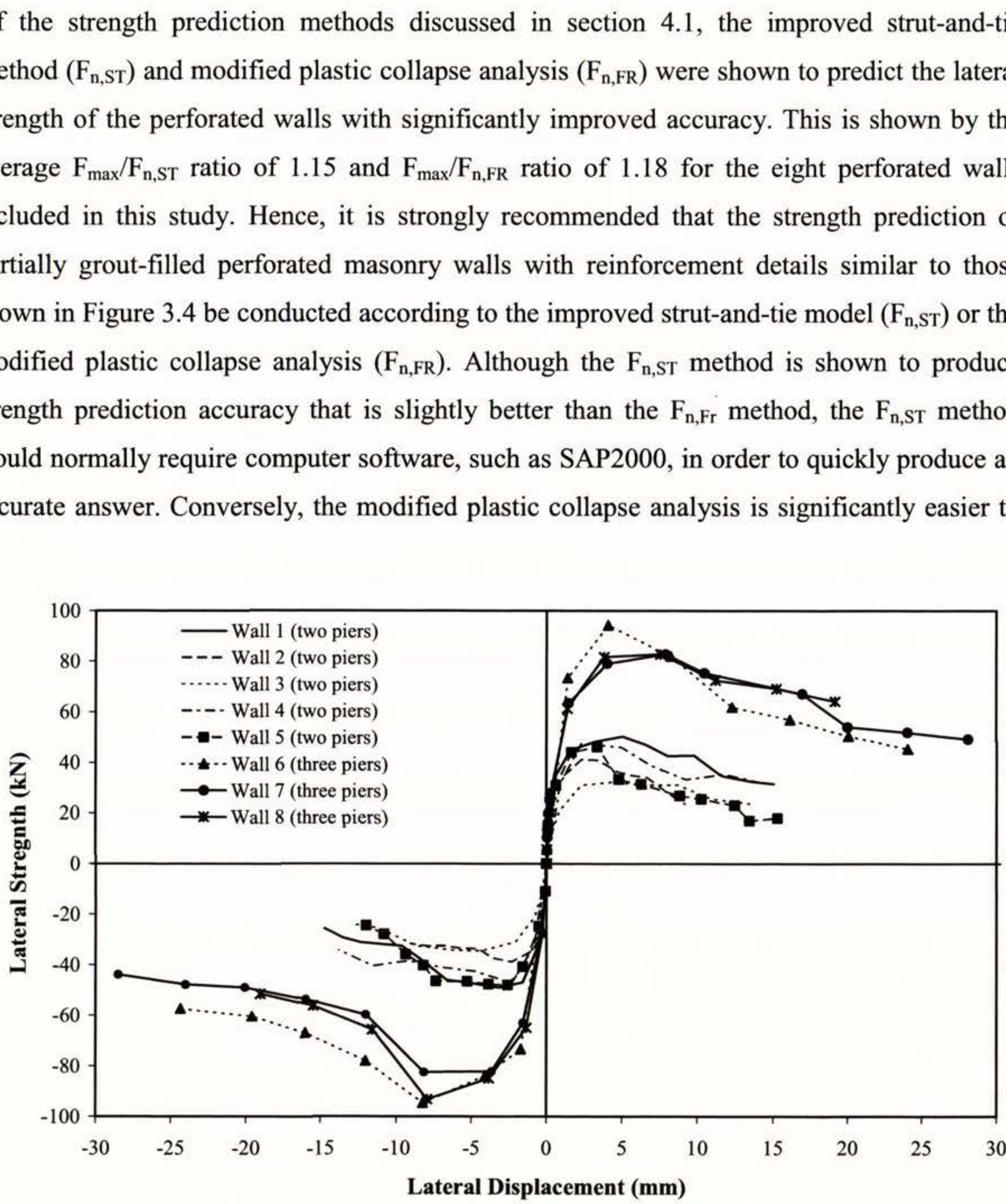

Figure 6.8 Effect of double bending of central pier on wall strength.

Table 6.2 Summary of test results and wall strength predictions

Wall	Specimen	Prediction					Test Result					
		$F_{n,st}$	$F_{n,ST}$	$F_{n,fr}$	$F_{n,FR}$	F_{code}	F_{max}	$\frac{F_{max}}{F_{n,st}}$	$\frac{F_{max}}{F_{n,ST}}$	$\frac{F_{max}}{F_{n,fr}}$	$\frac{F_{max}}{F_{n,FR}}$	$\frac{F_{max}}{F_{code}}$
Current research	1	44.7	46.4	103.6	44.7	51.8	+50.2 -49.0	1.12	1.08	0.48	1.12	0.97
	2	35.9	38.4	80.6	35.9	37.3	+41.2 -38.7	1.15	1.07	0.51	1.15	1.10
	3	28.0	30.8	61.4	27.9	24.3	+33.3 -34.4	1.23	1.11	0.56	1.23	1.42
	4	41.0	44.7	94.4	40.9	37.3	+47.4 -48.8	1.19	1.09	0.52	1.19	1.31
	5	+41.0 -35.9	44.7 -38.4	94.4 -80.6	40.9 -35.9	37.3	+52.4 -50.4	1.28* 1.40**	1.17* 1.31**	0.56* 0.63**	1.28* 1.40**	1.40
	6	58.0	79.9	129.2	87.0	55.9	+94.3 -94.6	1.63	1.18	0.73	1.09	1.69
	7	50.0	61.6 -76.1	108.0 -110.5	66.5 -79.2	49.4	+82.8 -82.5	1.66	1.34* 1.08**	0.77* 0.75**	1.25* 1.04**	1.68
	8	50.0 -55.0	61.6 -79.7	108.0 -119.9	66.5 -81.7	49.4	+82.7 -93.2	1.66* 1.69**	1.34* 1.17**	0.77* 0.78**	1.24* 1.14**	1.89
	9	80.2	105.8	---	---	49.8	+125.3 -114.6	1.56	1.18	---	---	2.52
	10	80.2	82.1	---	---	49.8	+89.0 -84.6	1.11	1.08	---	---	1.79
Previous	B1	---	75.0	---	---	46.0	76.5	---	1.02	---	---	1.66
	B2	---	213.1	---	---	85.6	179.9	---	0.84	---	---	2.10
	D1	49.5	75.5	111.8	74.9	50.1	89.0	1.80	1.18	0.80	1.19	1.78
	Units	kN	kN	kN	kN	kN	kN	---	---	---	---	----

Note:

1. * indicates push direction.
2. ** indicates pull direction.
3. B1 is the 2600 x 2400 x 140 concrete masonry wall tested by Brammer (1995), see Figure 2.2a.
4. B2 is the 4200 x 2400 x 140 concrete masonry wall tested by Brammer (1995), see Figure 2.2b.
5. D1 is the 4200 x 2400 x 190 perforated concrete masonry wall tested by Davidson (1996), see Figure 2.3.

perform and can be carried out without the use of complicated computer software. The $F_{n,FR}$ method can be performed once the capacity of individual member, such as those shown in Appendix D, is calculated. Consequently, the modified plastic collapse analysis can be used as an alternative to the strut-and-tie method when analysing the lateral strength capacities of partially grout-filled perforated concrete masonry walls that were constructed according to NZS 4229:1999 specifications.

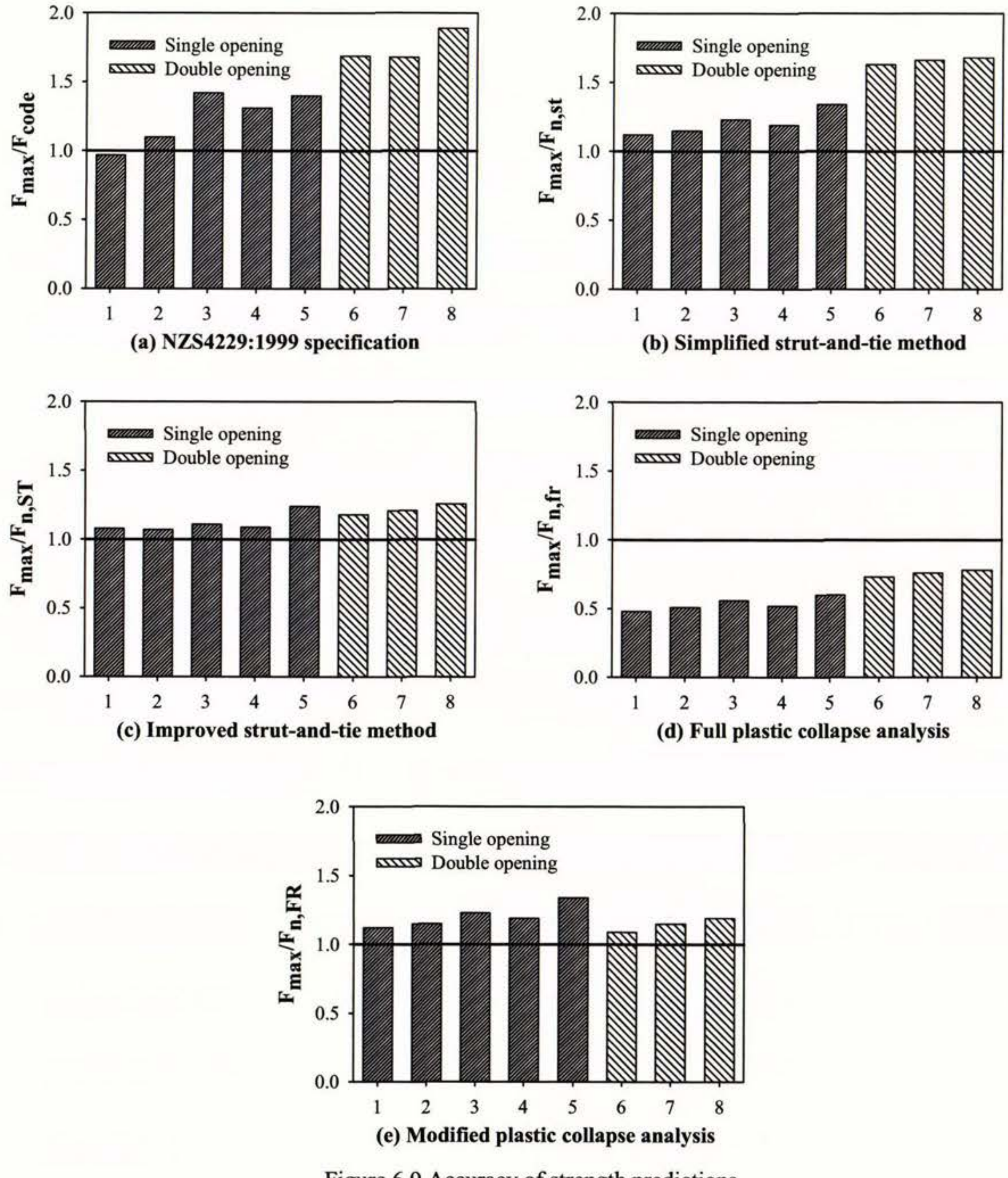

Figure 6.9 Accuracy of strength predictions.

6.6 Possible Amendment to NZS 4229:1999

Due to the lack of distributed horizontal shear reinforcement, all perforated walls included in this experimental study were observed to fail in a diagonal tension mode. As reported in Chapter 5, the diagonal cracking patterns identified on the walls were observed to align well with the load paths by which shear force is transferred to the foundation in the strut mechanism. Furthermore, vertical compressive cracks similar to vertical struts shown in strut-and-tie models, were also identified beneath the trimming reinforcement in Walls 4, 5 and 8. These observations further support the use of strut-and-tie analysis as the tool to evaluate the strength of walls with reinforcement details similar to those specified by NZS 4229:1999. Consequently, crack patterns observed from the wall tests suggested that NZS 4229:1999 incorrectly defines the bracing geometries for walls constructed according to its specification and it might be non-conservative for NZS 4229:1999 to assume that the base of the cantilevered piers on either side of an opening corresponds to the level of the penetration sill, i.e. it is non-conservative for NZS 4229:1999 to define bracing capacity geometry based upon the vertical dimension of the smallest adjacent penetration.

Ingham et al. (2001) reported that NZS 4229:1999 significantly underestimates the capacity of full-height bracing panels. The total bracing capacity of most bracing lines is primarily derived from the capacity of a limited number of large bracing panels. Consequently, any code overestimation of the capacity of small bracing panels, such as that tested in Wall 1, will be readily compensated for. The code-predicated values for the capacity of the complete bracing line can therefore be expected to have considerable conservatism. Nevertheless, failure of NZS 4229:1999 to correctly identify the bracing geometries is of some concern and the matter clearly warrants attention to determine if an amendment to the standard is required.

There are several possible amendments that could be introduced to the standard. These amendments include the use of the strut-and-tie method to correctly identify the bracing geometry or adopting bracing panel dimensions based upon the geometry of the largest adjacent wall openings. Recalling that NZS 4229:1999 is primarily targeted for use by architects and draftspersons, rather than structural engineers, the adoption of strut-and-tie models to identify bracing geometry would increase the complexity of the standard, therefore restricting the effective use of NZS 4229:1999 by non-engineering professions. Also, the adoption of the second mentioned amendment would significantly increase the conservatism of NZS 4229:1999 and result in reduced efficiency of the standard, which would ultimately lead to the perception that reinforced concrete masonry is an expensive form of construction when compared with competing products and systems. Consequently, it is considered that these two amendments may not well suit the primary purpose of NZS 4229:1999. Other possible amendments to the standard, if required, are presented in the following sub-sections.

6.6.1 Extended Trimming Reinforcement

Another possible solution is to prescribe an extended trimming reinforcement detail as shown in Figure 6.10. This amendment has the advantage of requiring minimum education, and therefore could be easily adopted by users of this standard. In addition, as shown by the simplified strut-and-tie model in Figure 6.10, this amendment would result in bracing geometries that are identical to those currently prescribed by NZS 4229:1999, therefore resulting in the same level of conservatism as the current standard.

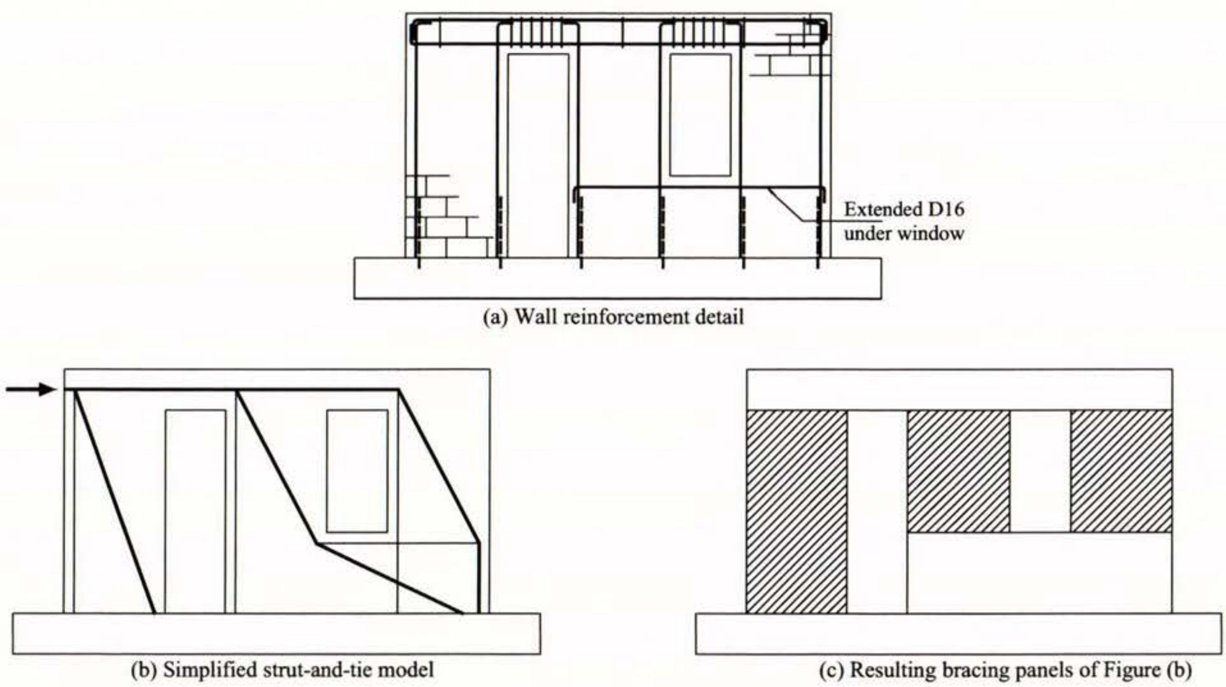

Figure 6.10 Proposed amendment to trimming reinforcement.

However, the detailing of trimming reinforcement such as that shown in Figure 6.10 may only be feasible for partially grout-filled masonry walls that have closely spaced penetrations. For a partially filled masonry wall that has constructional geometry similar to that shown in Figure 6.11, an issue regarding the length of extension to the trimming reinforcement may arise. In order to achieve bracing geometries specified by the standard, the trimming reinforcement, as illustrated in Figure 6.11a, needs to be extended to cover the whole length of the wall. For a partial extension of trimming reinforcement such as that shown in Figure 6.11b, it is unlikely to produce bracing geometries that are significantly different from the bracing geometries of a wall that is reinforced with NZS 4229:1999 specified trimming reinforcement. In addition, it is noted that by extending trimming reinforcement such as those shown in Figure 6.11, it may make such walls more difficult and more expensive to construct. This is because the construction of such walls may require at least two phases in order to ascertain that full grouting is achieved for the masonry core containing the trimming reinforcement. Such construction procedure may increase the cost of construction and this may potentially reduce the popularity of masonry construction.

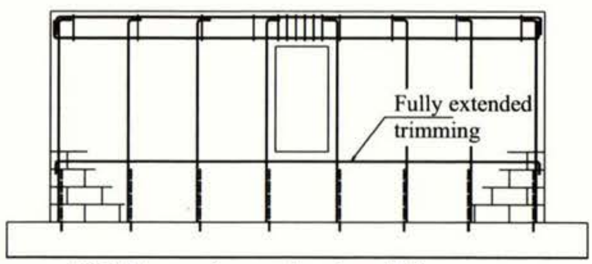

(a) Full extension to trimming reinforcement

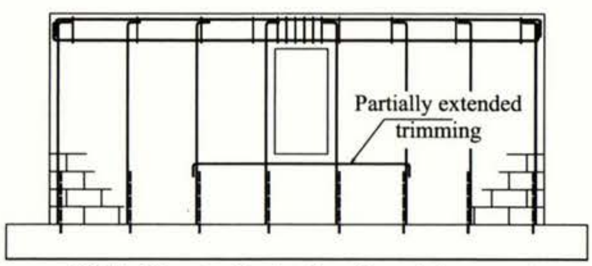

(b) Partial extension to trimming reinforcement

Figure 6.11 Extension to trimming reinforcement.

6.6.2 Amendment to NZS 4229:1999 bracing capacity

This subsection examines the degree of non-conservatism of the NZS 4229:1999 prescribed bracing capacity. As discussed in section 6.5, it was found that NZS 4229:1999 is only non-conservative for walls containing a single opening with a depth of less than 1200 mm, with the conservatism significantly increasing when the masonry walls contain more than one opening. Consequently, this subsection will examine only the adequacy of NZS 4229:1999 in prescribing the bracing capacities for masonry walls containing a single opening. This investigation is accomplished by comparing predictions derived using the NZS 4229:1999 prescribed bracing capacities with those predicted using the modified plastic collapse analysis ($F_{n,FR}$). The $F_{n,FR}$ method is selected instead of the improved strut-and-tie analysis due to the fact that $F_{n,FR}$ is significantly easier to perform and it was successfully shown that wall strength predictions using the $F_{n,FR}$ closely matched the test results of the perforated masonry walls tested in this study.

As shown in Figure 6.12, the masonry walls included in this investigation had a single opening of varying depth and piers of varying length. In all cases, the walls were considered to be 140 mm thick and of partially grout-filled construction. The D12 longitudinal reinforcement was of f_y = 300 MPa and spaced at maximum spacing of 800 mm centres, with f'_m = 12.0 MPa being assumed. NZS 4229:1999 recommended that vertical control joints should be placed at not more than 6.0 m centres. Consequently, only perforated masonry walls with length less than 6.0 m are included in the following investigation. The wall strengths predicted according to the two mentioned methods are summarised in Tables 6.3-6.5. Included in the same tables are the NZS 4229:1999 prescribed bracing capacities for the corresponding walls when they have no opening. These values are identified as $F_{code,no\text{-}op}$ in the tables.

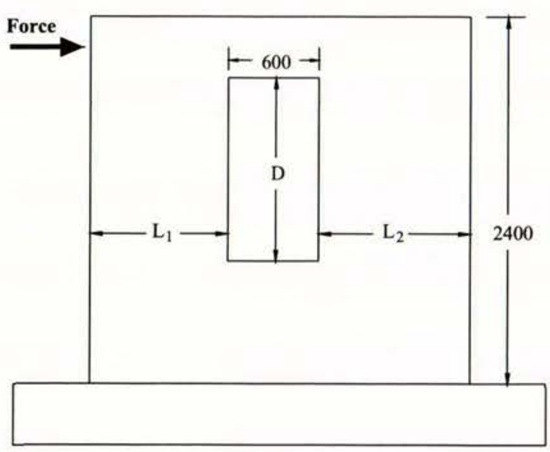

Figure 6.12 Masonry wall with varying pier lengths and opening depth.

From the predicted strengths presented in Tables 6.3-6.5 and Figure 6.13a, it is found that the bracing capacities prescribed by the current standard is non-conservative when L_1 is less than 1200 mm long and when the opening is not more than 1000 mm deep. As shown by the $F_{n,FR}/F_{code}$ ratios presented in Tables 6.3-6.5, the conservatism of NZS 4229:1999 increases when the depth of opening and the length of L_1 increase. In addition, it is shown that the standard would remain conservative when L_1 is at least 1200 mm regardless of the size of opening. Consequently, it is deduced from this study that the standard is only non-conservative when the depth of a single opening is less than 1200 mm and when one of the adjacent piers is less than 1200 mm in length.

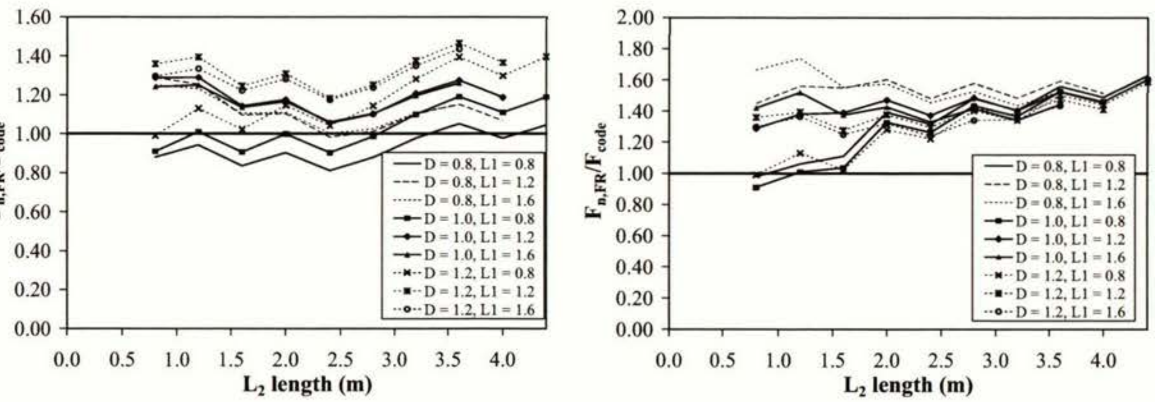

(a) $F_{n,FR}/F_{code}$ (b) $F_{n,FR}/F_{code,amd}$

Figure 6.13 Comparison of predicted strengths.

As shown in Tables 6.3-6.5, a significant number of the walls included in this part of study, the summation of capacity of small bracing panels (F_{code}) is more than the bracing capacity currently prescribed by the standard for the corresponding solid built walls ($F_{code,no\text{-}op}$). Consequently, one possible solution to the current problem is to limit the bracing capacity of any masonry wall containing a single opening of less than 1200 mm deep, to be no more than the capacity currently prescribed by NZS 4229 for the corresponding solid built masonry wall, i.e. $F_{code} \leq F_{code,no\text{-}op}$. This proposed procedure has the advantage of requiring minimum education without further reducing the bracing capacity values currently prescribed by the standard. A comparison of the $F_{n,FR}$ predicted wall strength with the standard predicted bracing capacity using the newly proposed procedure is presented in Tables 6.3-6.5 as $F_{n,FR}/F_{code,amd}$ and diagrammatically illustrated in Figure 6.13b. It is shown that the new procedure significantly reduces the over-prediction of strength by NZS 4229:1999.

6.6.2 No Amendment to NZS 4229:1999

Within a bracing line, a structural wall is divided into bracing panels of various heights and lengths as dictated by wall openings, control joints and wall ends. As shown in Figure 6.14, the total bracing capacity of most bracing lines is primarily derived form the capacity of a limited number of large bracing panels. As previously reported, NZS 4229:1999 significantly

Table 6.3 Strength predictions for walls with 800 mm deep single opening

L_1 (m)	L_2 (m)	$F_{n,FR}$ (kN)	F_{code} (kN)	$F_{code,no\text{-}op}$ (kN)	$F_{n,FR}/F_{code}$	$F_{n,FR}/F_{code,amd}$
0.8	0.8	33.9	38.5	34.6	0.88	0.98
	1.2	48.8	51.8	46.0	0.94	1.06
	1.6	58.0	69.5	52.3	0.83	1.11
	2	81.8	90.5	58.6	0.90	1.40
	2.4	94.1	116.0	71.5	0.81	1.32
	2.8	126.8	144.5	85.6	0.88	1.48
	3.2	142.2	145.5	101.1	0.98	1.41
	3.6	183.8	174.8	117.9	1.05	1.56
	4	202.4	207.0	135.9	0.98	1.49
	4.4	252.8	242.0	155.3	1.04	1.63
1.2	0.8	66.7	51.8	46.0	1.29	1.45
	1.2	81.6	65.0	52.3	1.26	1.56
	1.6	90.8	82.8	58.6	1.10	1.55
	2.0	114.6	103.8	71.5	1.10	1.60
	2.4	126.9	129.3	85.6	0.98	1.48
	2.8	159.6	157.8	101.1	1.01	1.58
	3.2	175.0	158.8	117.9	1.10	1.48
	3.6	216.6	188.0	135.9	1.15	1.59
	4.0	235.2	220.3	155.3	1.07	1.51
1.6	0.8	87.0	69.5	52.3	1.25	1.66
	1.2	101.9	82.8	58.6	1.23	1.74
	1.6	111.1	100.5	71.5	1.11	1.55
	2.0	134.9	121.5	85.6	1.11	1.58
	2.4	147.2	147.0	101.1	1.00	1.46
	2.8	179.9	175.5	117.9	1.03	1.53
	3.2	195.3	176.5	135.9	1.11	1.44
	3.6	236.9	205.8	155.3	1.15	1.53

Table 6.4 Strength predictions for walls with 1000 mm deep single opening

L_1 (m)	L_2 (m)	$F_{n,FR}$ (kN)	F_{code} (kN)	$F_{code,no-op}$ (kN)	$F_{n,FR}/F_{code}$	$F_{n,FR}/F_{code,amd}$
0.8	0.8	30.0	33.0	34.6	0.91	0.91
	1.2	44.9	44.5	46.0	1.01	1.01
	1.6	54.1	59.8	52.3	0.91	1.04
	2	77.9	78.0	58.6	1.00	1.33
	2.4	90.2	100.0	71.5	0.90	1.26
	2.8	122.9	124.8	85.6	0.99	1.44
	3.2	138.3	125.8	101.1	1.10	1.37
	3.6	179.9	151.0	117.9	1.19	1.53
	4	198.5	178.8	135.9	1.11	1.46
	4.4	249.0	209.3	155.3	1.19	1.60
1.2	0.8	57.3	44.5	46.0	1.29	1.29
	1.2	72.3	56.0	52.3	1.29	1.38
	1.6	81.5	71.3	58.6	1.14	1.39
	2.0	105.3	89.5	71.5	1.18	1.47
	2.4	117.6	111.5	85.6	1.05	1.37
	2.8	150.3	136.3	101.1	1.10	1.49
	3.2	165.7	137.3	117.9	1.21	1.41
	3.6	207.2	162.5	135.9	1.28	1.52
	4.0	225.8	190.3	155.3	1.19	1.45
1.6	0.8	74.3	59.8	52.3	1.24	1.42
	1.2	89.2	71.3	58.6	1.25	1.52
	1.6	98.4	86.5	71.5	1.14	1.38
	2.0	122.2	104.8	85.6	1.17	1.43
	2.4	134.5	126.8	101.1	1.06	1.33
	2.8	167.2	151.5	117.9	1.10	1.42
	3.2	182.6	152.5	135.9	1.20	1.34
	3.6	224.1	177.8	155.3	1.26	1.44

Table 6.5 Strength predictions for walls with 1200 mm deep single opening

L_1 (m)	L_2 (m)	$F_{n,FR}$ (kN)	F_{code} (kN)	$F_{code,no-op}$ (kN)	$F_{n,FR}/F_{code}$	$F_{n,FR}/F_{code,amd}$
0.8	0.8	27.2	27.5	34.6	0.99	0.99
	1.2	42.1	37.3	46.0	1.13	1.13
	1.6	51.4	50.3	52.3	1.02	1.02
	2	75.1	65.5	58.6	1.15	1.28
	2.4	87.5	84.0	71.5	1.04	1.22
	2.8	120.1	105.0	85.6	1.14	1.40
	3.2	135.6	105.8	101.1	1.28	1.34
	3.6	177.1	127.0	117.9	1.39	1.50
	4	195.7	150.8	135.9	1.30	1.44
	4.4	246.2	176.3	155.3	1.40	1.59
1.2	0.8	50.7	37.3	46.0	1.36	1.36
	1.2	65.6	47.0	52.3	1.40	1.40
	1.6	74.8	60.0	58.6	1.25	1.28
	2.0	98.6	75.3	71.5	1.31	1.38
	2.4	110.9	93.8	85.6	1.18	1.30
	2.8	143.6	114.8	101.1	1.25	1.42
	3.2	159.0	115.5	117.9	1.38	1.38
	3.6	200.5	136.8	135.9	1.47	1.48
	4.0	219.2	160.5	155.3	1.37	1.41
1.6	0.8	65.2	50.3	52.3	1.30	1.30
	1.2	80.1	60.0	58.6	1.33	1.37
	1.6	89.3	73.0	71.5	1.22	1.25
	2.0	113.1	88.3	85.6	1.28	1.32
	2.4	125.4	106.8	101.1	1.17	1.24
	2.8	158.1	127.8	117.9	1.24	1.34
	3.2	173.5	128.5	135.9	1.35	1.35
	3.6	215.0	149.8	155.3	1.44	1.44

underestimates the capacity of full height bracing panels. Consequently, any code overestimation of capacity of small bracing panels, such as that shown in Figure 6.12 will be readily compensated for.

The following examples show that considerable conservatism is maintained in the code-predicated values for the capacity of the complete bracing line. A summary of predicted strengths are included in Tables 6.6 and 6.7. The predicted $F_{n,FR}$ values for the two loading directions are also included.

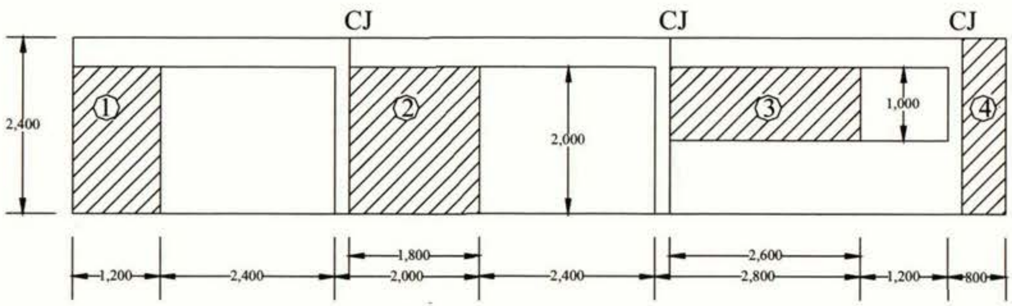

(a) Design example 1

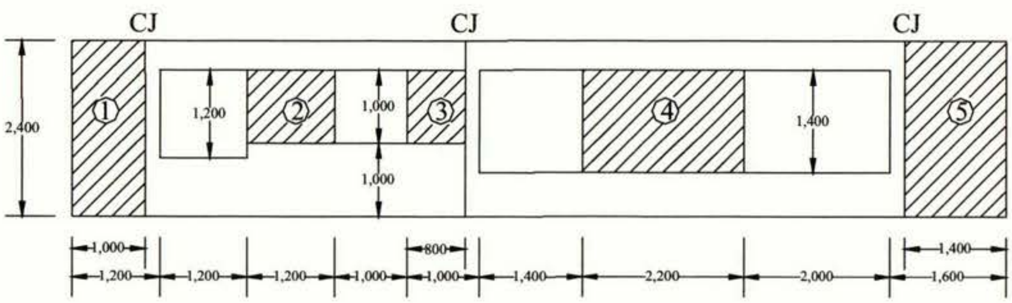

(b) Design example 2

Figure 6.14 Bracing panel for design example.

Table 6.6 Bracing capacity for design example 1

Bracing Panel	F_{code} (kN)	$F_{n,FR}$ (kN)	
		Push	Pull
1	15.3	25.5	25.5
2	29.0	39.4	39.4
3	83.5	129.8	70.8
4	7.8	9.7	9.7
Total	135.5	204.4	145.4

Table 6.7 Bracing capacity for design example 2

Bracing Panel	F_{code} (kN)	$F_{n,FR}$ (kN)	
		Push	Pull
1	10.4	12.6	12.6
2	28.0	46.8	40.1
3	16.5	10.6	19.4
4	54.8	88.8	88.8
5	16.8	27.6	27.6
Total	126.5	186.4	188.5

The two design examples successfully illustrated that any code overestimation of capacity of small bracing panels, such as Panels 3 in both examples is readily compensated for by the significant underestimation of the bracing capacity of the larger bracing panels. Based on the design examples presented above, it is proposed that an amendment to the NZS 4229:1999 specified bracing capacities may not be necessary.

Chapter 7

Conclusion

This section concludes the findings of the cyclic load tests conducted on partially grout-filled concrete masonry walls. The test matrix described in Chapter 3 allowed for meaningful comparison of test specimens, and provided valuable information for the parameters being investigated in this study.

Based on testing of the 10 partially grout-filled concrete masonry walls reported in Chapter 5, the following conclusions are made:

1. It was observed that the perforated partially grouted concrete masonry walls tested at the University of Auckland exhibited gradual strength and stiffness degradation, and in no case did any wall suffer from sudden failure. This desirable behaviour of the nominally reinforced partially grouted masonry walls with openings was attributed to the solid filled bond beam at the top of the walls, which caused frame-type action at latter stages of testing. This leads to considerable inelastic displacement capacity of the partially grouted masonry walls, where μ_{av} was measured to consistently be above 2.0.
2. The test results clearly demonstrated that the size of openings significantly affect the lateral strength of the tested walls. It was shown that the reduction of wall strength corresponded to the increased depth of an opening. This reduction of strength was because of the steepened diagonal strut when the depth of openings increase. This in turn leads to a reduction of the horizontal shear component that could be resisted by the masonry piers, which resulted in the overall reduction of lateral strength in the perforated masonry walls.
3. It was successfully demonstrated that extension of the trimming reinforcement below the window had the effect of increasing wall strength.
4. The diagonal cracking patterns on the perforated masonry walls were observed to align well with the load paths by which shear force was assumed to be transferred to the foundation in the strut mechanism. This observation further supported the use of the strut-and-tie method of analysis as the tool to evaluate the strength of nominally reinforced masonry walls with openings.

5. Strength prediction using the improved strut-and-tie method and the modified plastic collapse analysis were found to closely match the experimental results of the perforated walls tested in this study. Strength prediction by the simplified strut-and-tie method was found to closely match the test results of masonry walls with a single opening, but significant underestimation of strength by this method was found for walls with double openings. The full plastic collapse analysis was found to significantly over-predict the strength of all perforated walls included in this study.
6. It was established that NZS 4229:1999 fails to correctly identify the geometry of bracing panels on perforated masonry walls. This resulted in the over-prediction of strength of walls containing a small opening. It was shown in the experimental study that the conservatism of NZS 4229:1999 would increase when the depth of opening is increased.
7. Possible amendments to NZS 4229:1999 are presented in section 6.6 for consideration.
8. It was successfully demonstrated that the NZS 4229:1999 detail for the shrinkage control joint results in adequate structural performance. In addition, shrinkage control joints constructed in accordance with the NZS 4229:1999 prescription result in a masonry wall that has significantly higher wall strength and exhibits gradual strength and stiffness degradation. This increase in strength is due to pier double bending that is not considered by the standard.

Chapter 8

Reference

Beck, J.K., Curtin, W.G., and Shaw, G. (1988), "Design of Reinforced and Prestressed Masonry", Thomas Telford, Loondon.

Brammer, D.R. (1995), "The Lateral Force-Deflection Behaviour of Nominally Reinforced Masonry Walls", ME Thesis, Department of Civil and Resource Engineering, University of Auckland.

Davidson, B.J. (1996), "In-Plane Cyclic Loading of Nominally Reinforced Masonry Walls with Openings", New Zealand Concrete Society Conference, Wairakei, New Zealand, pp. 120-129.

Dowrick, D.J. (1998), "Damage and Intensities in the Magnitude 7.8 1931 Hawke's Bay, New Zealand, Earthquake", Bulletin of NZSEE, Vol. 30, No. 2.

Elshafie, H., Hamid, A., and Nasr, E. (2002), "Strength and Stiffness of Masonry Shear Walls with Openings", The Masonry Society Journal, pp. 49-60.

Hart, G. C., Hong, W., and Englekirk, R. (1988), "Structural Component Model of Flexural Walls", Fourth Meeting of the U.S.-Japan Joint Technical Coordination Committee on Masonry Research, San Diego.

Hiraishi, H. (1984), "Evaluation of Shear and Flexural Deformation of Flexural Type Shear Walls", Bulletin of NZSEE, Vol. 17, No. 2, pp. 135-144.

Ingham, J.M., Davidson, B.J., Brammer, D.R., and Voon, K.C. (2001), "Testing and Codification of Partially Grout-filled Nominally-reinforced Concrete Masonry Subjected to In-plane Cyclic Loads", The Masonry Society Journal, Vol. 19, No. 1, pp. 83-96.

Leiva, G., Merrymann, M., and Klingner, R. E. (1990a), " In-Plane Seismic Resistance of Two-Story Concrete Masonry Coupled Walls", Fifth North American Masonry Conference, University of Illinois, Urbana-Champagne, pp. 333-345.

Leiva, G., Merryman, M., and Klingner, R.E. (1990b), "Design Philosophies for Two-Storey Concrete Masonry Walls with Door and Window Openings", Fifth North American Masonry Conference, University of Illinois, Urbana-Champagne, pp. 287-295.

Leiva, G., and Klingner, R. E. (1994), "Behaviour and Design of Multistory Masonry Walls under In-Plane Seismic Loading", The Masonry Society Journal, Vol. 12, No. 1, pp. 12-24.

Liddell, D., Ingham, J. M., and Davidson, B. J. (2000), "Influence of Loading History on Ultimate Displacement of Concrete Structures", School of Engineering Report No. 597, University of Auckland.

NZS 4229:1999, "Concrete Masonry Buildings Not Requiring Specific Engineering Design", Standards Association of New Zealand. Wellington.

NZS 4230:2004, "Design of Reinforced Concrete Masonry Structures", Standards Association of New Zealand, Wellington.

Park, R. (1989), "Evaluation of Ductility of Structures and Structural Assemblages for Laboratory Testing," Bulletin of the NZSEE, Vol. 22, No. 3. 1989, pp. 155-166.

Priestley, M. J. N. (1976), "Cyclic Testing of Heavily Reinforced Concrete Masonry Shear Walls", Department of Civil Engineering, University of Canterbury, New Zealand, Research Report 76-12.

Scott, E.F. (1999), "A Report on the Relief Organisation in Hastings Arising out of the [Magnitude 7.8] Earthquake in Hawke's Bay [New Zealand] on February 3, 1931", Bulletin of NZSEE, Vol. 32, No. 4, pp. 246-256.

Singh, S.S., Cooke, N., and Bull, D.K. (1999), "Out-of-Plane Performance of a Partially Filled Reinforced Concrete Masonry Wall with Ribraft TM Floor", Bulletin of NZSEE, Vol. 32, No. 2, pp. 990-101.

Voon, K. C., and Ingham, J. M. (2003), "Shear Strength of Concrete Masonry Walls" School of Engineering Report No. 611, University of Auckland.

Wu, H., and Li, B. (2003), "Investigating the Load Paths of RC Shear Wall with Openings under Reversed Cyclic Loadings", Pacific Conference on Earthquake Engineering, New Zealand.

Yanez, F.V., Park, R., and Paulay, T. (1991), "Seismic Behaviour of Reinforced Concrete Structural Walls with Irregular Openings", Pacific Conference on Earthquake Engineering, New Zealand, pp. 3303-3308.

Zhang, Z.D. (1998), "Out-of-Place Performance of Partially Grouted Reinforced Concrete Masonry Walls under Simulated Seismic Loading", ME Thesis, University of Canterbury.

Appendix A

Experimental Results – Series A "Walls with Openings"

Eight partially grout-filled nominally reinforced concrete masonry walls with openings were tested under cyclic lateral loading in the Civil Engineering Test Hall at the University of Auckland. All eight concrete masonry walls were constructed of 15 series CMUs, which resulted in an effective wall thickness of 60 mm for a partially grout-filled wall. These walls were constructed to the same height of 2.4 m but varied in length. In addition, these walls had variations in trimming reinforcement detailing, and a range of opening geometries. The objectives of this research were to study the performance of concrete masonry walls with openings under seismic loading conditions and to validate the adequacy of NZS 4229:1999 in addressing the bracing capacity of these types of masonry walls.

The experimental results of these eight concrete masonry walls are presented here. These results played a significant role in formulating the conclusions of this report. For information about wall construction, test set-up, testing procedure and data reduction please refer to Chapters 3 and 4. This report defines displacement in the push direction as positive while displacement in the pull direction as negative.

A.1 Wall 1

This section describes the laboratory test of Wall 1. The wall geometry and reinforcement details are shown in Figure A.1.1. The wall nominal shear (V_n) and flexural (F_n) strengths, calculated according to the shear expressions and $F_{n,st}$ described in Chapter 4, were established to be 44.7 kN and 81.0 kN respectively.

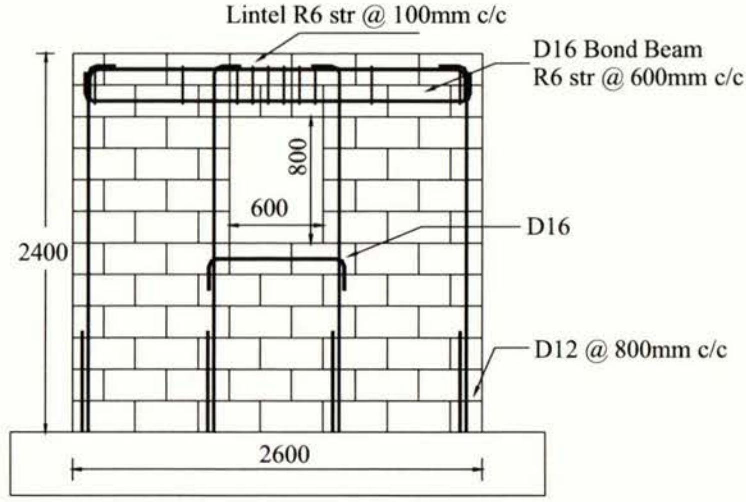

Figure A.1.1 Wall 1 geometry and reinforcing details.

A.1.1 Pre-test

The masonry wall was tested on the 15^{th} days after construction. Instrumentation was attached to the wall according to section 3.5.1. Prior to wall testing the wall was inspected, with no cracks or structural defects being identified.

A.1.2 Testing

<u>$^3/_4$ F_n push,</u>

An applied force of 35.2 kN was recorded when the wall was being pushed away (towards the right) from the strong wall. A corresponding displacement of 0.63 mm was recorded for this loading cycle. There was no clear evidence of cracking.

<u>$^3/_4$ F_n pull,</u>

A maximum strength of -33.1 kN was recorded at the displacement of -0.60 mm. No cracking was identified.

According to the procedure outlined in section 4.5, the measured lateral forces for the two directions of loading resulted in an average yield displacement of:

$$\Delta_y = \frac{4}{3}\left(\frac{.063 + 0.60}{2}\right) = 0.82 \text{ mm}$$

μ_2 push, 1st cycle

A maximum strength of 44.8 kN was recorded at the conclusion of this load cycle. An uplift of about 0.1 mm was recorded at the tension toe, resulted in a 300 mm horizontal crack along the wall-foundation interface. Hairline horizontal cracks were identified on mortar beds at the tension edge of the left pier. Also identified were diagonal cracks on both piers at this loading level. The wall cracking patterns at this stage of testing is shown in Figure A.1.2.

μ_2 pull, 1st cycle

Cracking patterns mirroring to those formed in the previous push cycle were identified. A maximum strength of -47 kN was measured at the conclusion of this load cycle.

μ_2 push, 2nd cycle

The wall responded similarly to observations made in the previous push cycle. A maximum strength of 42.7 kN was recorded. No new cracking was identified.

μ_2 pull, 2nd cycle

Minor elongations to diagonal cracks formed in the previous pull cycle were observed. A maximum strength of -40.6 kN was recorded.

μ_4 push, 1st cycle

A maximum strength of 48.3 kN was measured at the conclusion of this load cycle. Apart from extension of existing diagonal cracks, two new diagonal cracks were identified on each pier. The wall tension toe was measured to uplift 0.12 mm, and the maximum diagonal crack width was measured to be about 1.50 mm.

μ_4 pull, 1st cycle

A maximum strength of -49 kN was recorded in this load cycle. Apart from the formation of new diagonal cracks on both piers, elongations to previously formed diagonal cracks were also identified, with crack widths up to 1.0 mm.

μ_4 push, 2nd cycle

A maximum strength of 42.3 kN was measured. No new cracking or crack extensions were identified.

μ_4 pull, 2nd cycle

No new cracking, but elongations to diagonal cracks (towards compression toe) on the left pier were observed. A maximum strength of -46.5 kN was recorded.

μ_6 push, 1st cycle

A maximum strength of 50.2 kN was recorded at a displacement of 5.06 mm. No new cracks, but elongation and widening of diagonal cracks formed in previous push cycles were identified, with crack width up to 3.2 mm. The face shells and mortar beds along diagonal cracks showed sign of distress.

μ_6 pull, 1st cycle

The wall responded similarly to observations made in the previous push cycle. A maximum strength of -47.1 kN was recorded at the displacement of -5.03 mm. No new cracks were identified, but widening of diagonal cracks was observed with crack width up to 5.0 mm.

μ_6 push, 2nd cycle

A maximum strength of 47.7 kN was recorded at the displacement of 5.08 mm. No new cracks were identified.

μ_6 pull, 2nd cycle

The wall responded similarly to observation made in the previous push cycle. A maximum strength of -41.8 kN was recorded for this load step. No new crack was identified.

μ_8 push, 1st cycle

A maximum strength of 47.0 kN was recorded at the displacement of 6.60 mm. Further elongation and widening of diagonal cracks were identified, causing degradation of masonry along the diagonal cracks. Maximum crack width was measured to be about 6.70 mm

μ_8 pull, 1st cycle

The wall responded similarly to observations made in the previous push cycle. Elongation and widening of previously formed diagonal cracks were identified. As shown in Figure A.1.3, the diagonal cracking patterns aligned well with the load paths by which shear force was transferred to the foundation in the strut mechanism (see section 4.1.2 for strut-and-tie models). A maximum strength of -46 kN was recorded at the displacement of -6.65 mm. An uplift of 0.18 mm was measured at the wall tension toe.

<u>μ_8 push, 2nd cycle</u>

Response was dominated by the elongation and widening of the diagonal cracks formed in previous cycles. The face shells in the window toe corner (on right pier) detached from the grout core due to significant degradation of masonry along the diagonal cracks. A maximum strength of 43 kN was recorded at a displacement of 6.78 mm.

<u>μ_8 pull, 2nd cycle</u>

The response was the very much similar to that observed in the previous cycle. A maximum strength of -41.1 kN was recorded at a corresponding displacement of -7.15 mm.

<u>μ_{10} push, 1st cycle</u>

A maximum strength of 42.6 kN was recorded at the displacement of 8.1 mm. No new cracking was identified. The wall response was dominated by the degradation and widening of previously formed diagonal cracks. A maximum crack width of about 12 mm was measured.

<u>μ_{10} pull, 1st cycle</u>

The wall response was similar to observations made in the previous push cycle. A maximum strength of -37.3 kN was measured at a displacement of -8.5 mm. This strength corresponded to about 76% of the maximum strength achieved in the pull direction. Hence the wall was defined as failing according to the test procedure outlined in section 4.5.

<u>μ_{10} push, 2nd cycle</u>

A maximum strength of 37.4 kN was measured at the displacement of 8.1 mm. No new cracks or extensions of cracks were identified.

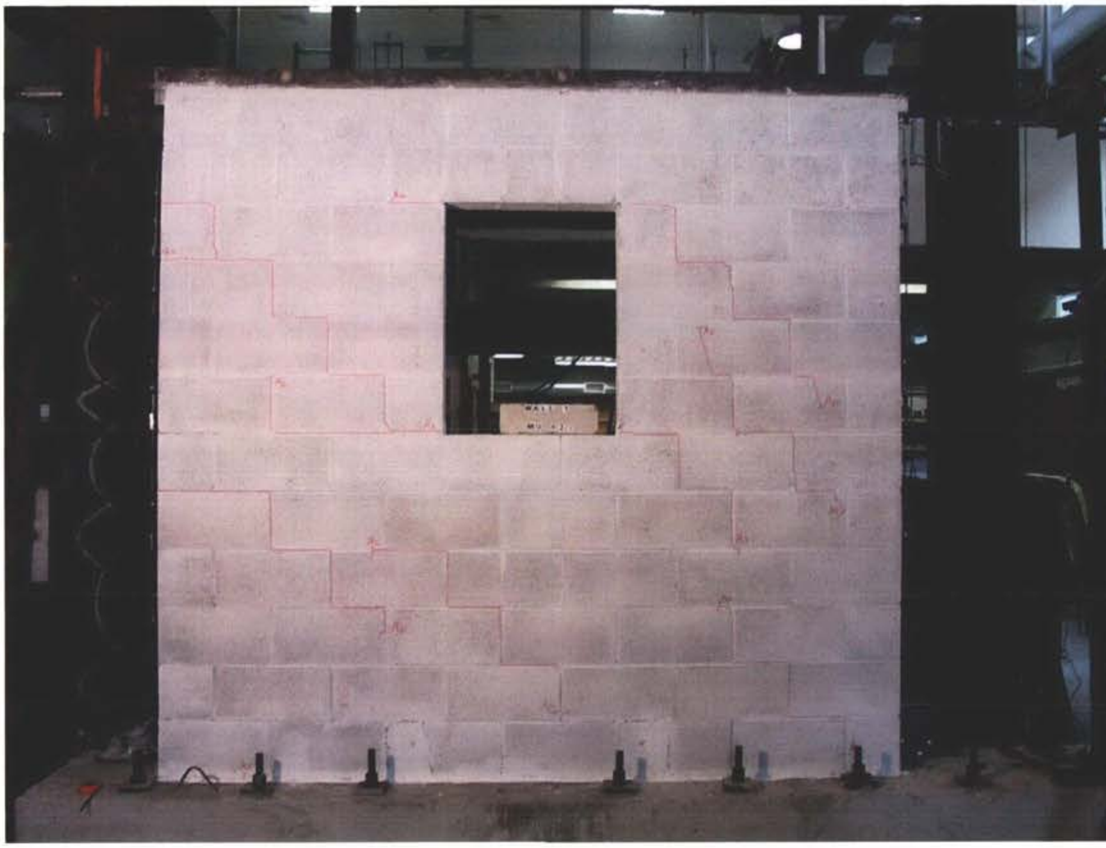

Figure A.1.2 Condition of test wall at end of first ductility 2 push cycle.

Figure A.1.3 Condition of test wall at end of first ductility 8 pull cycle.

μ_{10} pull, 2nd cycle

The wall response was similar to observations made in the previous push cycle. A maximum strength of -31.7 kN was recorded at a displacement of -8.2 mm.

μ_{12} push, 1st cycle

A maximum strength of 42.8 kN was recorded at a displacement of 9.8 mm. Further widening of diagonal crack on the left pier resulted in the spalling of face shell from the wall edge at bond beam layer (see Figure A.1.4). However, upon closed observation, it was established that the spalling of face shell would result in insignificant structural damage to the bond beam.

μ_{12} pull, 1st cycle

The wall response was dominated by further widening of diagonal cracks formed in previous cycles, with crack width up to 17 mm. A maximum strength of -32.5 kN was measured at the displacement of -9.6 mm. The wall cracking patterns at this loading stage is depicted in Figure A.1.4.

μ_{12} push, 2nd cycle

No new cracks or crack extensions were identified. A maximum strength of 35.6 kN was measured at a displacement of 9.9 mm.

μ_{12} pull, 2nd cycle

No new crack or crack extensions were identified. A maximum strength of -25.3 kN was measured at a displacement of -10.3 mm.

μ_{14} push, 1st cycle

No new crack or crack extensions were identified. A maximum strength of 34.7 kN was measured at a displacement of 11.6 mm. As shown in Figure A.1.5, further widening of cracks had resulted in the spalling of face shell along diagonal cracks.

Figure A.1.4 Condition of test wall after cycling to displacement ductility 12.

Figure A.1.5 Condition of test wall after first push cycle to ductility 14.

μ_{14} pull, 1st cycle

The wall responded similarly to observations made in the previous push cycle. A maximum strength of -31.1 kN was recorded at a displacement of -12.4 mm.

μ_{14} push, 2nd cycle

No new cracks or crack extensions were identified. A maximum strength of 32.6 kN was recorded at 12.3 mm.

μ_{14} pull, 2nd cycle

No new cracks or crack extensions were identified. A maximum strength of -25.7 kN was recorded at the displacement of -12.2 mm.

μ_{16} push, 1st cycle

The wall developed a maximum strength of 32.5 kN at a displacement of 13.2 mm. No new cracking was identified, but further widening of diagonal cracks was observed.

μ_{16} pull, 1st cycle

The wall responded similarly to observations made in the previous push cycle. A maximum strength of -29.2 kN was recorded at a displacement of -13.5 mm.

μ_{16} push, 2nd cycle

Further widening of diagonal cracks was observed. A maximum strength of 30.8 kN was recorded for this loading cycle.

μ_{16} pull, 2nd cycle

A maximum strength of -25.4 kN was recorded. No new cracking was identified.

μ_{18} push, 1st cycle

The wall response was dominated by the widening of diagonal cracks. No new cracking was identified. A maximum strength of 31.6 kN was measured in this semi-cycle of loading. This strength corresponded to 63% of the maximum force recorded in the pushing direction.

μ_{18} pull, 1st cycle

The wall responded similarly to observations made in previous push cycle. A maximum strength of -25.7 kN was recorded at a displacement of -14.7 mm.

μ_{18} push, 2nd cycle

A maximum strength of 28.3 kN was recorded. No new cracking was identified.

μ_{18} pull, 2nd cycle

A maximum strength of -18.8 kN was recorded. No new cracking was identified.

A.1.3 Summary Behaviour

The force-displacement history of Wall 1 is shown in Figure A.1.6. The maximum push direction strength of 50.2 kN was measured during the first push cycle to displacement ductility six, and the maximum pull direction of -49.0 kN was measured during the first pull cycle to displacement ductility four. The average yield displacement (Δ_y) for this partially grouted wall was evaluated to be 0.82 mm. The test wall was defined as failing during the first pull cycle to displacement ductility 10, giving it a ductility capacity of $\mu_{av} > 6.0$.

Due to the lack of distributed horizontal shear reinforcement and the fact that the wall was partially grout-filled, the test wall was observed to fail in a diagonal tension mode. This type of failure was characterised by the development of early horizontal flexural cracking, which was later exaggerated by diagonal cracking that extended throughout the wall panels. It was observed during experimental testing that the (diagonal) cracking patterns of this wall aligned well with the load paths by which shear force was transferred to the foundation in the strut mechanism (see Figures A.1.5).

The nominal strength F_n derived using the simplified strut-and-tie analysis, along with the strength value derived from NZS 4229:1999 (denoted NZS-4229) are included in Figure A.1.6. Also shown in this plot is the theoretical failure point, corresponding to the cycle in which the peak strength failed to exceed 80% of the maximum previously attained strength. From Figure A.1.6, it was observed that Wall 1 did not achieve the bracing capacity prescribed by NZS 4229:1999, therefore indicating that the existing standard may be non-conservative in its treatment of walls containing small opening. The wall maximum strength recorded during experimental testing was about 10% higher than that predicted using the strut-and-tie analysis.

The force-displacement plot of Figure A.1.6 indicates that despite significant stiffness degradation, Wall 1 exhibited gradual strength degradation. This desirable behaviour of the nominally reinforced partially grout-filled concrete masonry wall with openings was created by the solid filled bond beam at the top of the wall, which caused a frame-type action at latter stage of testing. This notion was supported by the absence of significant structural damage in the bond beam. Furthermore, the force-displacement plot in Figure A.1.6 consistently illustrated a pinched shape. This was primarily due to the presence of significant shear deformation in this type of masonry construction (see section A.1.4). It was also observed that less hysteretic energy was expended during the second cycle to any displacement level, when compared with the first displacement cycle. This is illustrated by the more pinched hysteresis loops of the second cycle.

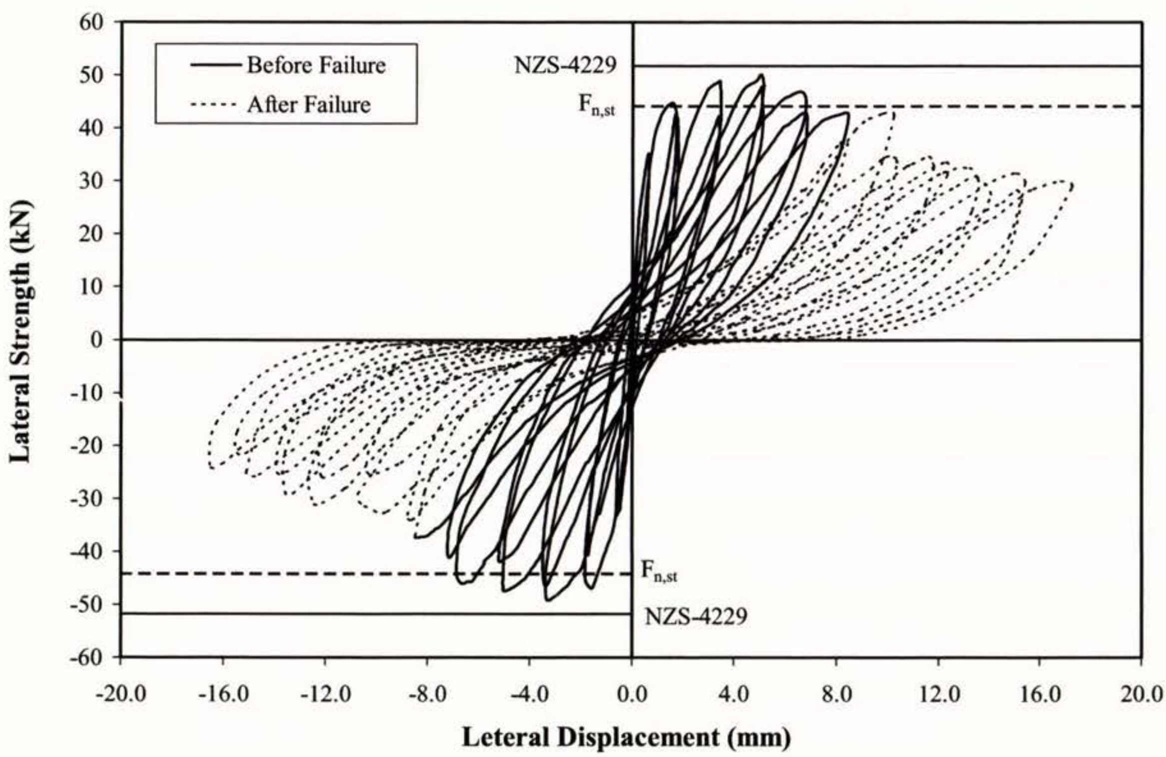

Figure A.1.6 Force-displacement behaviour for Wall 1.

A.1.4 Panel Displacement Components

The total horizontal displacement of the wall was decomposed into four components according to the procedure outlined in section 3.9 with the results as shown in Figure A.1.7. It is seen that shear displacement was the single most dominant deformation mode. The rocking, sliding and flexural displacement components were insignificant throughout the test. It is noted that the summed up deformation (rocking + sliding + flexural + shear) approximately match the overall displacement measured at the loading beam. Ideally, the line representing the sum of components should coincide with the line representing the lateral displacement measured at the loading beam. Figure A.1.7 provides an indication of the relative size of each displacement component at various stages of the displacement envelope.

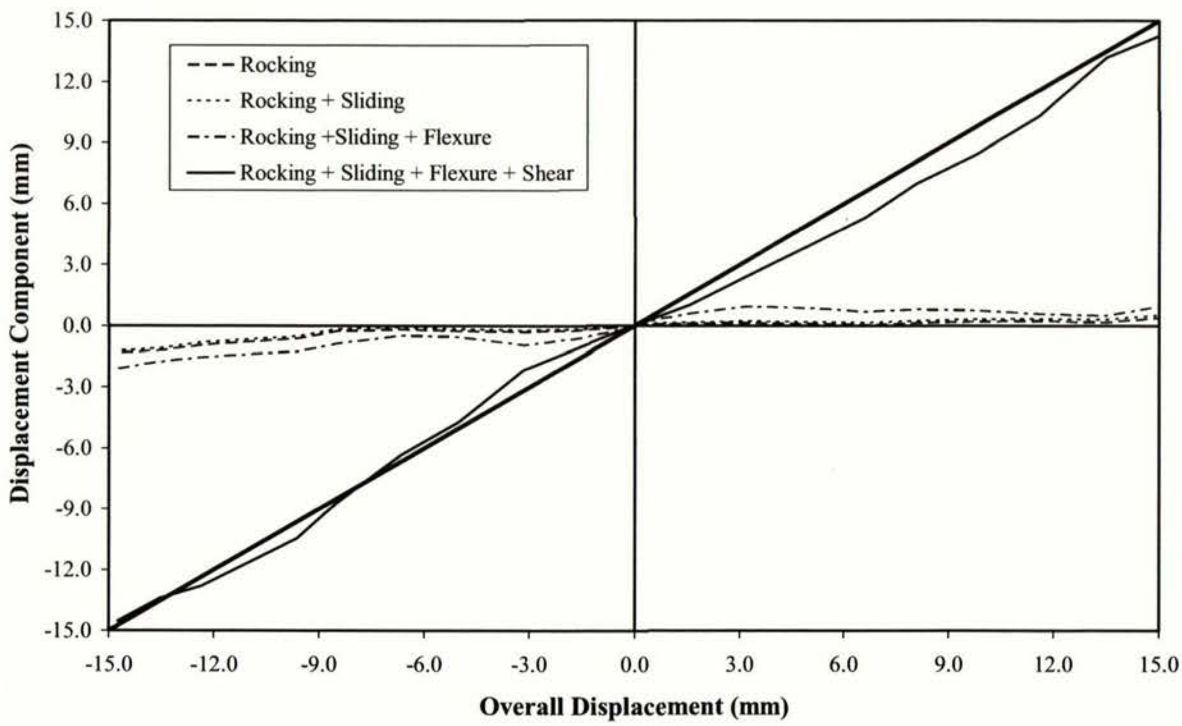

Figure A.1.7 Components of displacement.

A.2 Wall 2

This section describes the laboratory test of Wall 2. The wall geometry and reinforcement details are shown in Figure A.2.1. The wall nominal shear (V_n) and flexural (F_n) strengths, calculated according to the shear expressions and $F_{n,st}$ described in Chapter 4, were established to be 35.9 kN and 69.1 kN respectively.

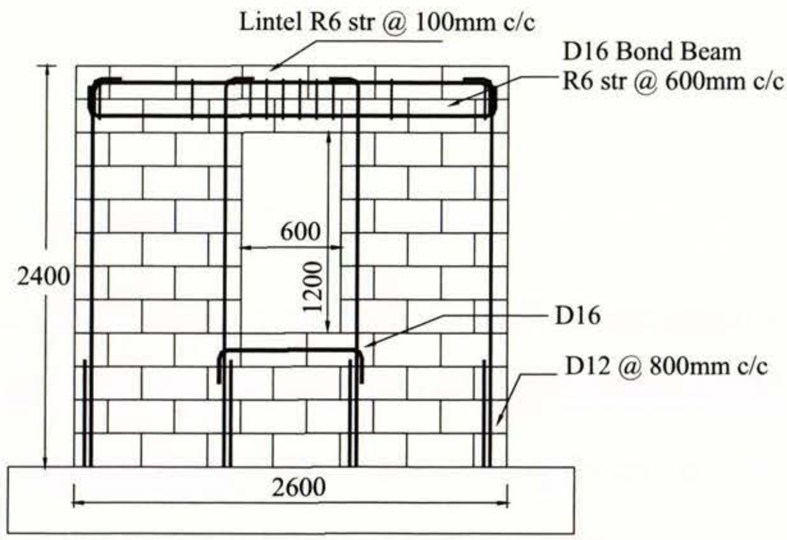

Figure A.2.1 Wall 2 geometry and reinforcing details.

A.2.1 Pre-test

The masonry wall was tested on the 14th days after construction. Instrumentation was attached to the wall according to section 3.5.1. Prior to wall testing the wall was inspected, with no cracks or structural defects being identified.

A.2.2 Testing

<u>$^3/_4$ F_n push,</u>

An applied force of 26.6 kN was recorded when the wall was being pushed away (towards the right) from the strong wall. A corresponding displacement of 0.43 mm was recorded for this loading cycle. No clear evidence of cracking.

<u>$^3/_4$ F_n pull,</u>

A maximum strength of -26.8 kN was recorded at the displacement of -0.42 mm. Again, no cracking was identified.

According to the procedure outlined in section 4.5, the measured lateral forces for the two directions of loading resulted in an average yield displacement of:

$$\Delta_y = \frac{4}{3}\left(\frac{.043 + 0.42}{2}\right) = 0.57 \text{ mm}$$

μ_2 push, 1st cycle

A maximum strength of 34.7 kN was recorded at the displacement of 1.13 mm. An uplift of about 0.1 mm was recorded at the tension toe. Five hairline horizontal cracks (maximum crack width about 0.2 mm) were identified on the mortar beds at wall tension edges. Also identified were hairline diagonal cracks along the mortar joints.

μ_2 pull, 1st cycle

A maximum strength of -40.0 kN was recorded at the displacement of -1.11 mm. The wall responded similarly to observations made in the previous cycle. Cracking patterns mirrored to those formed in the previous push cycle were identified.

μ_2 push, 2nd cycle

A maximum strength of 32.5 kN was recorded at the conclusion of this loading cycle. No new cracking or extensions to previously formed cracks were identified.

μ_2 pull, 2nd cycle

A maximum strength of -28.5 kN was recorded for this loading cycle. No new cracking was identified.

μ_4 push, 1st cycle

A maximum strength of 41.2 kN was measured at the displacement of 2.33 mm. This strength was about 10% more than that prescribed by NZS 4229:1999. No new cracking was identified, but extensions to cracks formed in the previous push cycles were identified, with crack width up to 0.4 mm. Despite the extension of diagonal crack to reach the bond beam on the left pier, it was established that such crack would induce insignificant structural damage to the bond beam. Minor crushing of mortar was observed along diagonal cracks at the completion of this loading stage. An uplift of 0.18 mm was measured at the tension toe.

μ_4 pull, 1st cycle

A "splitting" noise was heard when the wall was being pulled to a displacement of about -1.5 mm due to the widening of diagonal cracks formed in the previous pull cycles, but no strength loss was observed. The wall strength continued to increase to a maximum of -38.7 kN at the end of this loading stage. Upon close observation, it was established that wall cracking patterns were very similar to those observed in the previous push cycle. A maximum crack width of about 0.5 mm was identified. Also observed was the sign of crushing of mortar along diagonal cracks. The maximum strength developed in this pull cycle was about 4% more than that prescribed by NZS 4229:1999. See Figure A.2.2 for cracking patterns at this stage of loading.

μ_4 push, 2nd cycle

A maximum strength of 36.2 kN was measured. No new cracking or crack extensions were identified.

μ_4 pull, 2nd cycle

A maximum strength of -32.8 kN was recorded at the displacement of -2.24 mm. No new cracking or crack extensions were identified.

μ_6 push, 1st cycle

A maximum strength of 41.0 kN was recorded at the displacement of 3.43 mm. No new cracks, but elongations and widening of diagonal cracks formed in previous push cycles were identified, with crack width up to 0.6 mm.

μ_6 pull, 1st cycle

The wall responded similarly to observations made in the previous push cycle. A maximum strength of -37.4 kN was recorded at the displacement of -3.55 mm. No new cracks were identified, but further elongations and widening of diagonal cracks were observed.

μ_6 push, 2nd cycle

A maximum strength of 38.7 kN was recorded at the displacement of 3.55 mm. No new cracks were identified, but further widening of diagonal cracks were identified with crack width up to 2.5 mm.

μ_6 pull, 2nd cycle

The wall responded similarly to observations made in the previous push cycle. A maximum strength of -32.8 kN was recorded for this load step. No new crack was identified.

μ_8 push, 1st cycle

A maximum strength of 37.0 kN was recorded at the displacement of 4.59 mm. No new cracking was identified. Further elongations and widening of diagonal cracks were observed, maximum crack of about 4.0 mm was measured.

μ_8 pull, 1st cycle

The wall responded similarly to observations made in the previous push cycle. Elongation and widening of previously formed diagonal cracks were identified. A maximum strength of -33.6 kN was recorded at the displacement of -4.52 mm.

μ_8 push, 2nd cycle

No new cracking or crack extensions were identified. A maximum strength of 35.0 kN was recorded at the displacement of 4.69 mm.

μ_8 pull, 2nd cycle

A maximum strength of -32.8 kN was recorded at the corresponding displacement of -4.76 mm. No new cracking or crack extensions were identified.

μ_{10} push, 1st cycle

A maximum strength of 34.8 kN was recorded at the displacement of 5.65 mm. No new cracking was identified. The wall response was dominated by the degradation and widening of previously formed diagonal cracks. Maximum crack width of about 6.5 mm was measured. See Figure A.2.3 for wall cracking patterns at this stage of testing.

μ_{10} pull, 1st cycle

The wall response was similar to observations made in the previous push cycle. A maximum strength of -33.5 kN was measured at the displacement of -5.7 mm.

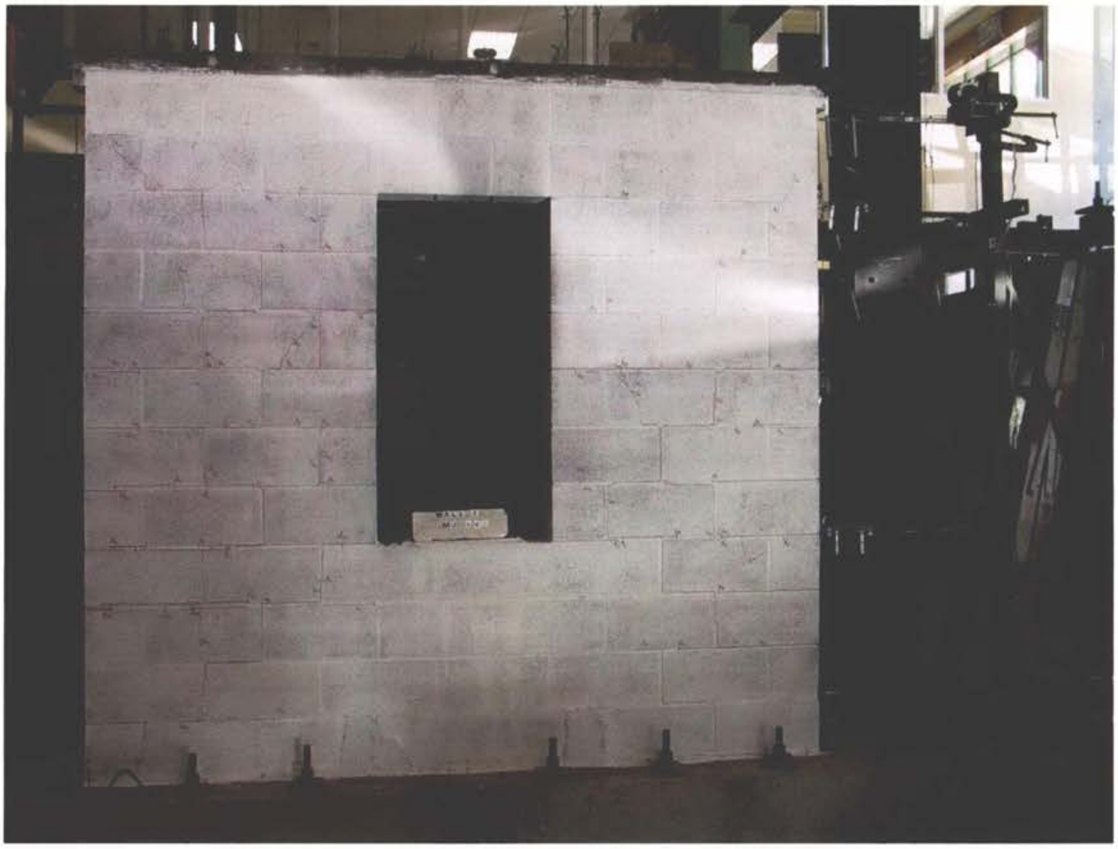

Figure A.2.2 Condition of test wall at end of first ductility 4 pull cycle.

Figure A.2.3 Condition of test wall at end of first ductility 10 push cycle.

μ_{10} push, 2nd cycle

A maximum strength of 30.7 kN was measured at the displacement of 5.68 mm. No new cracks or crack extensions were identified. This strength corresponded to about 75% of the maximum strength achieved in the push direction. Hence the wall was defined as failing according to the test procedure outlined in section 4.5.

μ_{10} pull, 2nd cycle

The wall response was similar to observations made in previous push cycle. A maximum strength of -31.5 kN was recorded at the displacement of -5.8 mm.

μ_{12} push, 1st cycle

A maximum strength of 34.1 kN was recorded at the displacement of 6.67 mm. No new crack, but further widening of diagonal crack with crack width up to 8.0 mm being identified.

μ_{12} pull, 1st cycle

The wall response was dominated by further widening of diagonal cracks formed in previous cycles, with crack width up to 10.1 mm. A maximum strength of -32.5 kN was measured at the displacement of -6.84 mm.

μ_{12} push, 2nd cycle

No new cracks or crack elongations were identified. Further widening of diagonal cracks was observed, with crack width up to 10 mm. A maximum strength of 29.6 kN was measured at the displacement of 6.93 mm. The wall condition at this stage of testing is presented in Figure A.2.4.

μ_{12} pull, 2nd cycle

Similar to previous push cycle, no new cracks or crack alongations were identified. A maximum strength of -30.2 kN was measured at the displacement of -6.78 mm. As shown in Figure A.2.4, the diagonal cracking patterns aligned well with the load path by which shear force was transferred to the foundation in the strut mechanism.

μ_{14} push, 1st cycle

Widening of diagonal cracks (maximum crack width about 12 mm) was observed to cause further deterioration of the right pier compression toe. However, tapping the masonry face shell to indicate that no face shell delamination at the compression toe, i.e. compression toe was still intact. Degradation of masonry along diagonal cracks caused minor spalling of face shell and mortar. A maximum strength of 28.1 kN was recorded at the displacement of 7.97 mm.

μ_{14} pull, 1st cycle

The wall responded similarly to observations made in the previous push cycle. A maximum strength of -32.6 kN was recorded at the displacement of -7.93 mm.

μ_{14} push, 2nd cycle

No new cracks or crack elongations were identified. A maximum strength of 22.9 kN was recorded at 7.89 mm.

μ_{14} pull, 2nd cycle

No new cracks or crack elongations were identified. A maximum strength of -30.5 kN was recorded at the displacement of -8.15 mm.

μ_{16} push, 1st cycle

The wall developed a maximum strength of 23.5 kN at the displacement of 9.19 mm. This strength corresponded to 57% of the maximum strength recorded in the pushing direction. No new cracking was identified, but further widening of diagonal cracks was observed.

μ_{16} pull, 1st cycle

The wall responded similarly to observations made in the previous push cycle. A maximum strength of -31.6 kN was recorded at the displacement of -9.10 mm. Figure A.2.5 shows the wall cracking patterns at this stage of testing.

μ_{16} push, 2nd cycle

Further widening of diagonal cracks was observed. A maximum strength of 21.6 kN was recorded at the displacement of 9.04 mm.

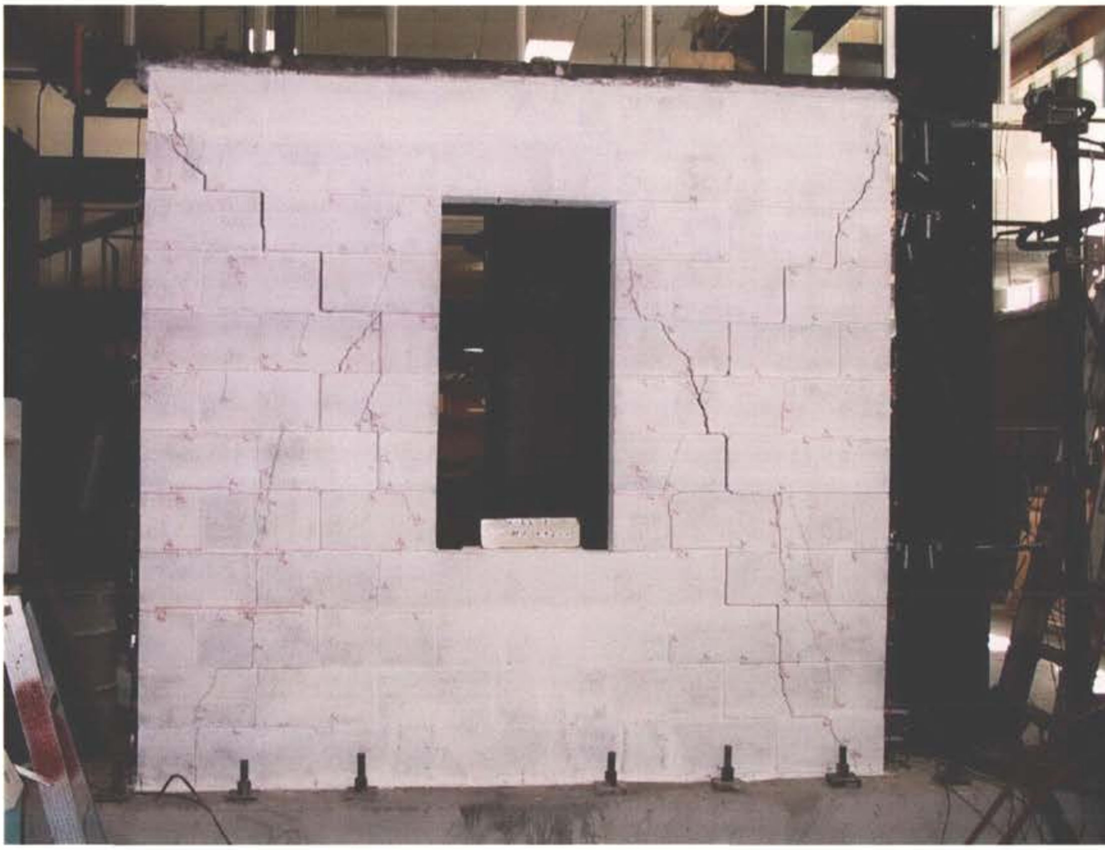

Figure A.2.4 Condition of test wall after cycling to displacement ductility 12.

Figure A.2.5 Condition of test wall after cycling to displacement ductility 16.

μ_{16} pull, 2nd cycle

A maximum strength of -29.7 kN was recorded at the displacement of -9.23 mm. No new cracking was identified.

A.2.3 Summary Behaviour

The measured force-displacement curve for Wall 2 is presented in Figure A.2.6, depicting the lateral displacement at the top of the wall as a function of the applied lateral force. The maximum push and pull direction strengths of 41.2 kN and -38.7 kN were measured during the first cycle to displacement ductility 4. Despite the presence of widely open diagonal cracks, the wall exhibited a gradual and fairly symmetrical strength degradation of strength in both direction of loading. Consequently, it was possible to classify Wall 2 as having a failure mode of diagonal tension. The desirable behaviour of this nominally reinforced partially grout-filled concrete masonry walls with openings was created by the solid filled bond beam at the top of the walls, which caused a frame-type action at latter stage of testing.

As shown in Figure A.2.6, it was established that the maximum strength achieved by Wall 2 was at least 4% higher (pulling direction) than the bracing capacity prescribed by NZS 4229:1999, therefore suggesting that the conservatism of NZS 4229:1999 increases as the depth of penetration increases (the window in this wall had a depth of 1200 mm as compared to that of 800 mm in Wall 1). The wall nominal strength predicted using the simplified strut-and-tie analysis was about 9% less than the maximum strength achieved by the wall.

As shown in Figures A.2.2 to A.2.5, the diagonal cracking patterns on this wall aligned well with the load paths by which shear force was transferred to the foundation in the strut mechanisms. This observation supports the use of strut-and-tie analysis as the tool to evaluate the strength of walls with reinforcement details complying to the specifications of NZS 4229:1999.

Similar to Figure A.1.6, the force-displacement plot in Figure A.2.6 consistently illustrated a pinched shape. This was primarily due to the presence of significant shear deformation in this type of masonry construction. It was also observed that less hysteretic energy was expended during the second cycle to any displacement level, when compared with the first displacement cycle. This is shown by the more pinched hysteresis loops of the second cycle.

The average yield displacement (Δ_y) for this partially grouted wall was evaluated to be 0.57 mm. The test wall was defined as failing during the second push cycle to displacement ductility 10, giving it a ductility capacity of $\mu_{av} > 6.0$.

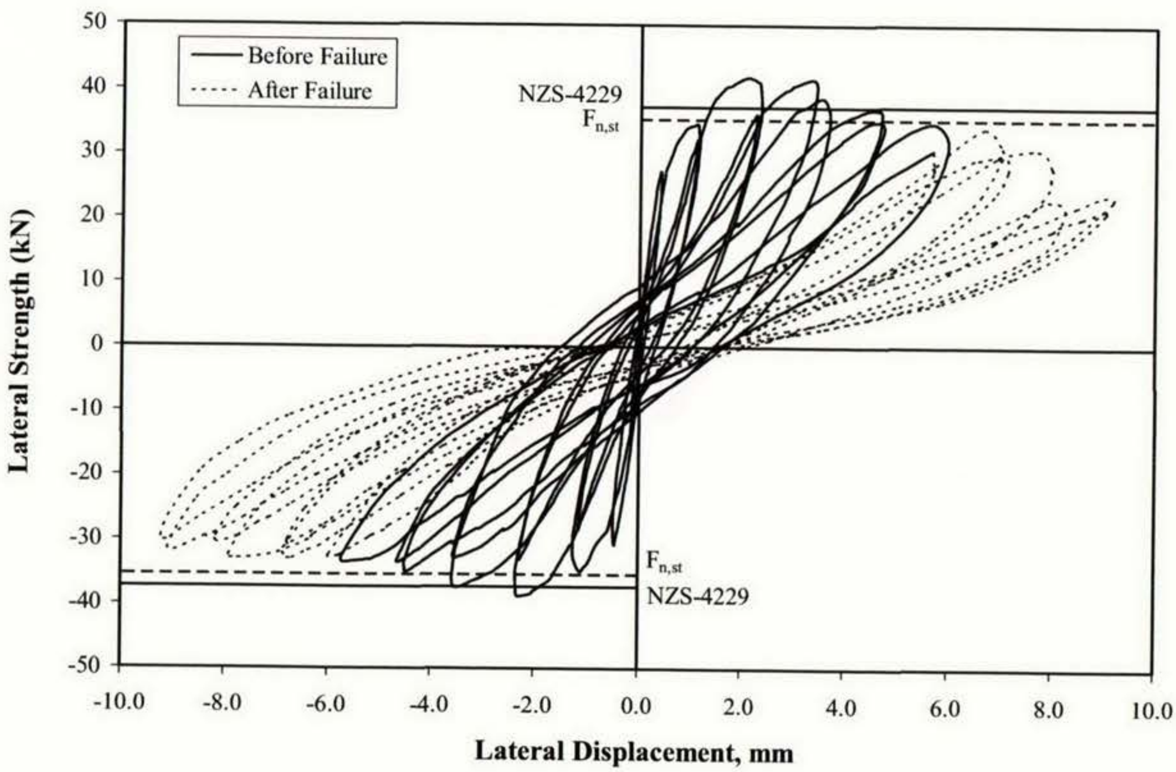

Figure A.2.6 Force-displacement behaviour of Wall 2.

A.2.4 Panel Displacement Components

The total horizontal displacement of the wall was decomposed into four components according to the procedure outlined in section 4.7 with the results shown in Figure A.2.7. From the rocking, sliding, flexure and shear deformation components plotted in Figure A.2.7, it is shown that the rocking and sliding deformations were negligible throughout the test and the shear displacement was the single most dominant deformation mode. The influence of flexural component of deformation was significant only at low displacement level. As shown in Figure A.2.7, it is illustrated that the shear displacement tends to increase with a concurrent decrease in the flexural displacement once the wall was pushed/pulled beyond the displacement of ± 4.0 mm.

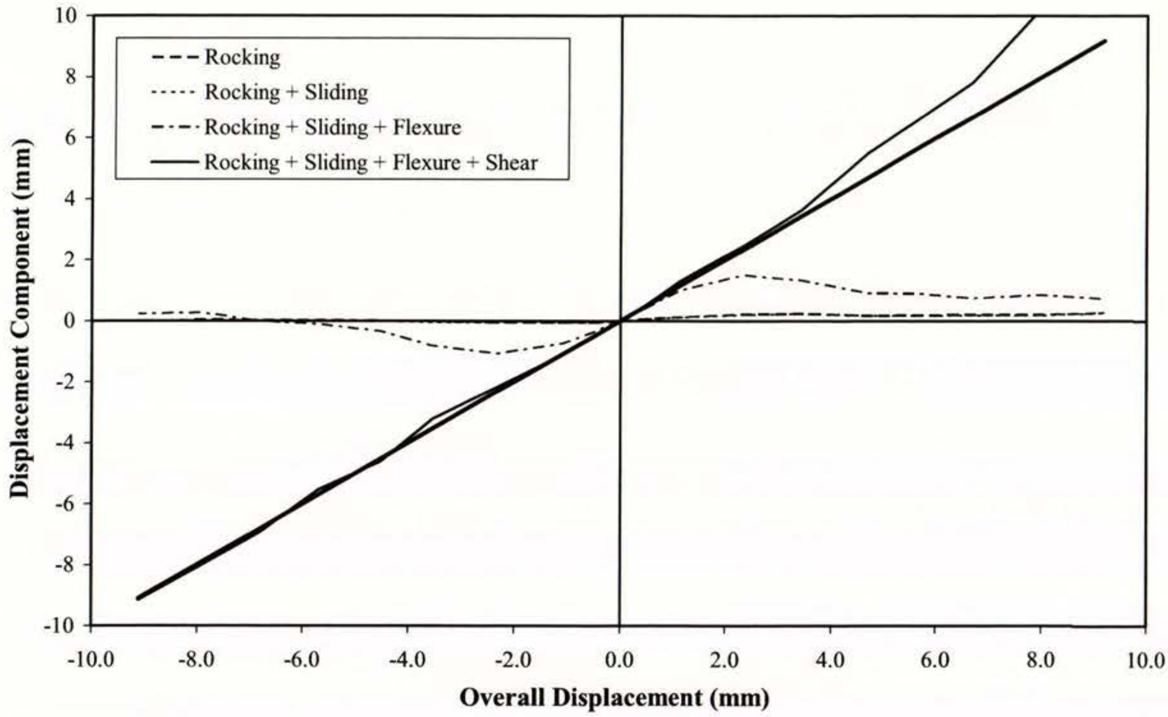

Figure A.2.7 Components of displacement.

A.3 Wall 3

This section describes the laboratory test of Wall 3. The wall geometry and reinforcement details are shown in Figure A.3.1. The wall nominal shear (V_n) and flexural (F_n) strengths, calculated according to the shear expressions and $F_{n,st}$ described in Chapter 4, were established to be 28.0 kN and 73.0 kN respectively.

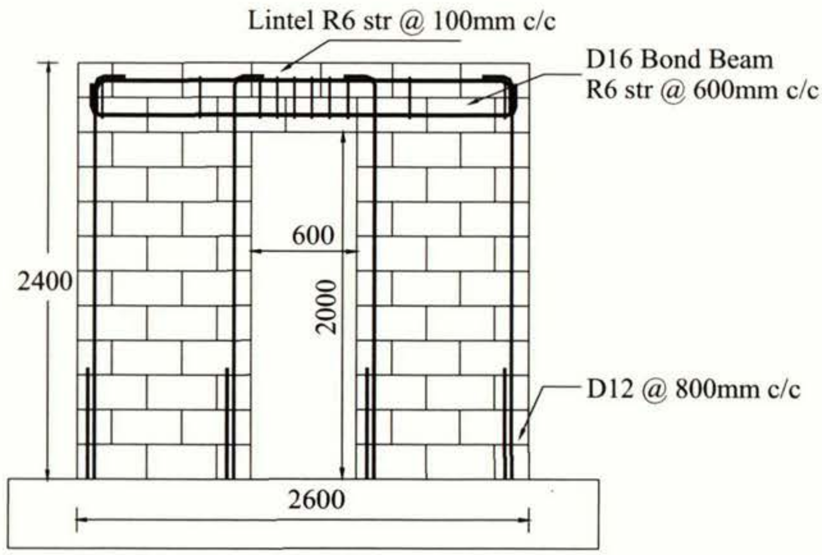

Figure A.3.1 Wall 3 geometry and reinforcing details.

A.3.1 Pre-test

The masonry wall was tested on the 15th days after construction. Instrumentation was attached to the wall according to section 3.5.1. Prior to wall testing the wall was inspected, with no cracks or structural defects being identified.

A.3.2 Testing

<u>$^3/_4$ F_n push,</u>

An applied force of 21.2 kN was recorded when the wall was pushed away (towards the right) from the strong wall. A corresponding displacement of 0.85 mm was recorded for this loading cycle. No clear evidence of cracking.

<u>$^3/_4$ F_n pull,</u>

A maximum strength of -20.9 kN was recorded at the displacement of -0.77 mm. No cracking was identified.

According to the procedure outlined in section 4.5, the measured lateral forces for the two directions of loading resulted in an average yield displacement of:

$$\Delta_y = \frac{4}{3}\left(\frac{0.85+0.77}{2}\right) = 1.07 \text{ mm}$$

<u>μ_2 push, 1st cycle</u>

A maximum strength of 31.0 kN was recorded at the displacement of 2.31 mm. Hairline diagonal cracks were identified (four cracks on left pier and three cracks on right pier), with maximum crack width of about 0.2 mm.

<u>μ_2 pull, 1st cycle</u>

The wall responded similarly to observations made in the previous cycle, diagonal cracking patterns mirrored to those formed in the previous push cycle were identified. A maximum strength of -30.9 kN was measured at the displacement of -2.06 mm.

<u>μ_2 push, 2nd cycle</u>

A maximum strength of 29.5 kN was recorded at the conclusion of this loading cycle. No new cracking, the diagonal cracks were observed to widen slightly to a maximum width of about 0.3 mm.

<u>μ_2 pull, 2nd cycle</u>

A maximum strength of -30.0 kN was recorded for this loading cycle. Similar to previous push cycle, no new cracking was identified.

<u>μ_4 push, 1st cycle</u>

A maximum strength of 32.3 kN was measured at the displacement of 4.46 mm. One new diagonal cracking was identified on each panel, accompanied by the elongations to cracks formed in previous push cycles. It was identified that widening of diagonal cracks had been taken place during this load cycle, with crack width up to 1.5 mm being identified.

μ_4 pull, 1st cycle

The wall responded similarly to observations made in the previous push cycle. A maximum strength of -34.4 kN was recorded at the displacement of -4.28 mm. Extensions to diagonal cracks formed in previous pull cycles were identified, of particular significant was the elongation of diagonal cracks towards the bond beam corner (close to wall edge) on top of the right pier. However, it was established that the diagonal crack on the bond beam was insignificant to adversely affect the structural performance of the bond beam. Widening of previously formed diagonal cracks were observed, with crack width up to 3 mm being identified. The maximum strength developed in this pull cycle was about 42% more than that prescribed by NZS 4229:1999 and about 23% higher than the predicted $F_{n,st}$.

μ_4 push, 2nd cycle

A maximum strength of 29.3 kN was measured at the displacement of 4.2 mm. No new cracking or crack elongations were identified.

μ_4 pull, 2nd cycle

A maximum strength of -33.0 kN was recorded at the displacement of -4.44 mm. Extensions to existing diagonal cracks were identified. Also observed was the widening of diagonal cracks to a maximum width of about 4.5 mm.

μ_6 push, 1st cycle

A maximum strength of 31.1 kN was recorded at the displacement of 6.4 mm. Degradation of masonry along diagonal cracks were observed to cause minor spalling of face shell and mortar. No new crack, but elongation and widening of diagonal cracks were identified.

μ_6 pull, 1st cycle

The wall responded similarly to observations made in the previous push cycle. A maximum strength of -34.2 kN was recorded at the displacement of -6.4 mm. No new cracking was identified, but further elongations and widening of diagonal cracks were observed, with crack width up to 7.5 mm. The wall condition at this stage of testing is shown in Figure A.3.2.

Figure A.3.2 Condition of test wall at end of first ductility 6 pull cycle.

μ_6 push, 2nd cycle

A maximum strength of 30.1 kN was recorded at the displacement of 6.69 mm.

μ_6 pull, 2nd cycle

A maximum strength of -32.7 kN was recorded for this load step. No new crack was identified.

μ_8 push, 1st cycle

A maximum strength of 31.1 kN was recorded at the displacement of 8.68 mm. No new cracking was identified. Further elongations and widening of diagonal cracks were observed, maximum crack width of about 11 mm was measured.

μ_8 pull, 1st cycle

Similar to the previous push cycle, elongations and widening of previously formed diagonal cracks were identified. A maximum strength of -32.5 kN was recorded at the displacement of -8.65 mm.

μ_8 push, 2[nd] cycle

No new cracking or crack extensions were identified. A maximum strength of 28.7 kN was recorded at the displacement of 9.05 mm. The wall condition at this stage of testing is shown in Figure A.3.3.

μ_8 pull, 2[nd] cycle

A maximum strength of -25.9 kN was recorded at the displacement of -9.04 mm. Spalling of mortar due to grinding movement of masonry along crack paths was observed to take place. Maximum crack width of about 15 mm was measured. This strength corresponded to about 75% of the maximum strength achieved in the pull direction. Hence, the wall was defined as failing according to the test procedure outlined in section 4.5.

μ_{10} push, 1[st] cycle

A maximum strength of 25.7 kN was recorded at the displacement of 10.8 mm. The wall response was dominated by the degradation of masonry and widening of existing diagonal cracks. Spalling of masonry face shells and mortar along diagonal cracks were also identified.

μ_{10} pull, 1[st] cycle

The wall response was similar to observations made in the previous push cycle. A maximum strength of -25.3 kN was measured at the displacement of -11.2 mm.

μ_{10} push, 2[nd] cycle

A maximum strength of 23.3 kN was measured at the displacement of 11.9 mm. Similar to previous push cycle, the wall response was dominant by the widening of diagonal cracks and degradation of masonry (face shells and mortar) along the crack paths. The wall condition at this stage of testing is shown in Figure A.3.4.

μ_{10} pull, 2[nd] cycle

The wall response was similar to observations made in the previous push cycle. A maximum strength of -22.3 kN was recorded at the displacement of -10.97 mm.

μ_{12} push, 1[st] cycle

A maximum strength of 22.8 kN was recorded at the displacement of 13.4 mm.

Figure A.3.3 Condition of test wall at end of second ductility 8 push cycle.

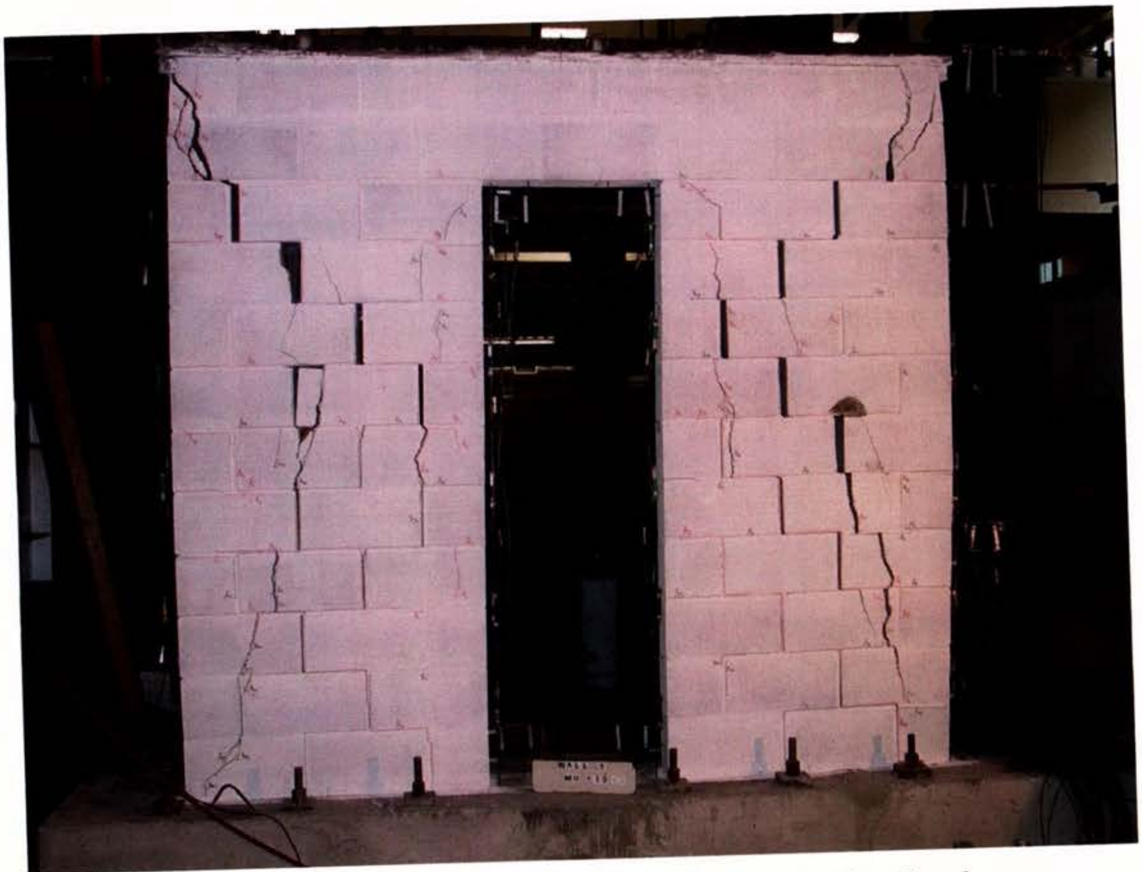

Figure A.3.4 Condition of test wall at end of second ductility 10 push cycle.

μ_{12} pull, 1st cycle

A maximum strength of -23.9 kN was measured at the displacement of -12.8 mm. This strength corresponded to about 70% of the maximum strength recorded in the pull direction.

A.3.3 Summary Behaviour

The measured force-displacement curve for Wall 3 is presented in Figure A.3.5, depicting the lateral displacement at the top of the wall as a function of the applied lateral force. The maximum push and pull direction strengths of 33.3 kN and -34.4 kN were measured during the first cycle to displacement ductility 4. This wall was classified to fail in a diagonal tension mode. This failure mode was characterised by the gradual and fairly symmetrical strength degradation of strength in both direction of loading and the presence of widely open diagonal cracks on both piers. The desirable behaviour of this nominally reinforced partially grout-filled concrete masonry wall was created by the solid filled bond beam at the top of the wall, which caused a frame-type action at latter stage of testing.

As shown in Figure A.3.5, it was established that the maximum strength achieved by Wall 3 was at least 37% higher than the bracing capacity prescribed by the current NZS 4229:1999, therefore further suggesting that the conservatism of NZS 4229:1999 to increase as the depth of penetration increased (this wall had an opening of 2000 mm deep, as compared to the depth of window openings of 800 mm and 1200 mm in Walls 1 and 2 respectively). The maximum strength recorded during experimental testing was about 19% higher than the strength predicted according to $F_{n,st}$.

As shown in Figures A.3.2 to A.3.4, the diagonal cracking patterns on this wall aligned well with the load paths by which shear force was transferred to the foundation in the strut mechanism. This observation supports the use of strut-and-tie analysis as the tool to evaluate the strength of walls with reinforcement details complying to specifications of NZS 4229:1999.

The average yield displacement (Δ_y) for this partially grouted wall was evaluated to be 1.07 mm. The test wall was defined as failing during the second pull cycle to displacement ductility 8, giving it a ductility capacity of $\mu_{av} > 6.0$.

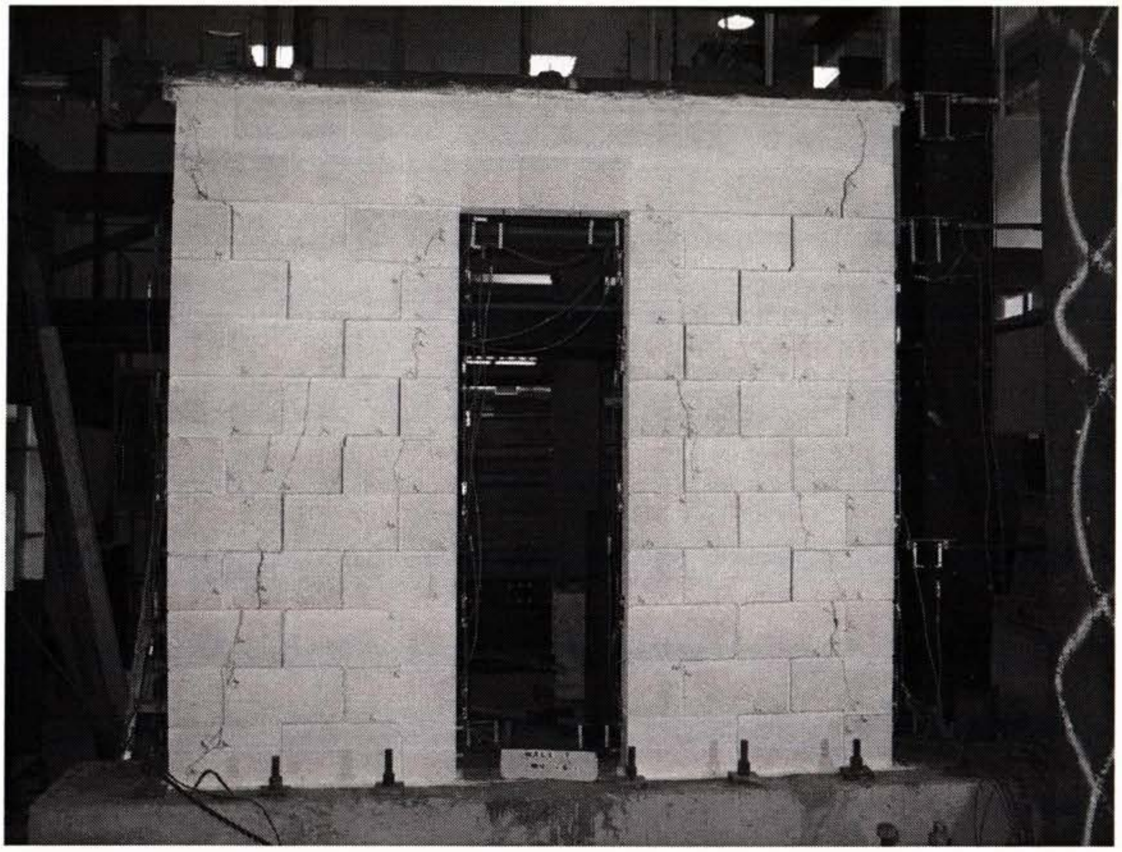

Figure A.3.2 Condition of test wall at end of first ductility 6 pull cycle.

μ_6 push, 2^{nd} cycle

A maximum strength of 30.1 kN was recorded at the displacement of 6.69 mm.

μ_6 pull, 2^{nd} cycle

A maximum strength of -32.7 kN was recorded for this load step. No new crack was identified.

μ_8 push, 1^{st} cycle

A maximum strength of 31.1 kN was recorded at the displacement of 8.68 mm. No new cracking was identified. Further elongations and widening of diagonal cracks were observed, maximum crack width of about 11 mm was measured.

μ_8 pull, 1^{st} cycle

Similar to the previous push cycle, elongations and widening of previously formed diagonal cracks were identified. A maximum strength of -32.5 kN was recorded at the displacement of -8.65 mm.

μ_8 push, 2nd cycle

No new cracking or crack extensions were identified. A maximum strength of 28.7 kN was recorded at the displacement of 9.05 mm. The wall condition at this stage of testing is shown in Figure A.3.3.

μ_8 pull, 2nd cycle

A maximum strength of -25.9 kN was recorded at the displacement of -9.04 mm. Spalling of mortar due to grinding movement of masonry along crack paths was observed to take place. Maximum crack width of about 15 mm was measured. This strength corresponded to about 75% of the maximum strength achieved in the pull direction. Hence, the wall was defined as failing according to the test procedure outlined in section 4.5.

μ_{10} push, 1st cycle

A maximum strength of 25.7 kN was recorded at the displacement of 10.8 mm. The wall response was dominated by the degradation of masonry and widening of existing diagonal cracks. Spalling of masonry face shells and mortar along diagonal cracks were also identified.

μ_{10} pull, 1st cycle

The wall response was similar to observations made in the previous push cycle. A maximum strength of -25.3 kN was measured at the displacement of -11.2 mm.

μ_{10} push, 2nd cycle

A maximum strength of 23.3 kN was measured at the displacement of 11.9 mm. Similar to previous push cycle, the wall response was dominant by the widening of diagonal cracks and degradation of masonry (face shells and mortar) along the crack paths. The wall condition at this stage of testing is shown in Figure A.3.4.

μ_{10} pull, 2nd cycle

The wall response was similar to observations made in the previous push cycle. A maximum strength of -22.3 kN was recorded at the displacement of -10.97 mm.

μ_{12} push, 1st cycle

A maximum strength of 22.8 kN was recorded at the displacement of 13.4 mm.

Figure A.3.3 Condition of test wall at end of second ductility 8 push cycle.

Figure A.3.4 Condition of test wall at end of second ductility 10 push cycle.

μ_{12} pull, 1st cycle

A maximum strength of -23.9 kN was measured at the displacement of -12.8 mm. This strength corresponded to about 70% of the maximum strength recorded in the pull direction.

A.3.3 Summary Behaviour

The measured force-displacement curve for Wall 3 is presented in Figure A.3.5, depicting the lateral displacement at the top of the wall as a function of the applied lateral force. The maximum push and pull direction strengths of 33.3 kN and -34.4 kN were measured during the first cycle to displacement ductility 4. This wall was classified to fail in a diagonal tension mode. This failure mode was characterised by the gradual and fairly symmetrical strength degradation of strength in both direction of loading and the presence of widely open diagonal cracks on both piers. The desirable behaviour of this nominally reinforced partially grout-filled concrete masonry wall was created by the solid filled bond beam at the top of the wall, which caused a frame-type action at latter stage of testing.

As shown in Figure A.3.5, it was established that the maximum strength achieved by Wall 3 was at least 37% higher than the bracing capacity prescribed by the current NZS 4229:1999, therefore further suggesting that the conservatism of NZS 4229:1999 to increase as the depth of penetration increased (this wall had an opening of 2000 mm deep, as compared to the depth of window openings of 800 mm and 1200 mm in Walls 1 and 2 respectively). The maximum strength recorded during experimental testing was about 19% higher than the strength predicted according to $F_{n,st}$.

As shown in Figures A.3.2 to A.3.4, the diagonal cracking patterns on this wall aligned well with the load paths by which shear force was transferred to the foundation in the strut mechanism. This observation supports the use of strut-and-tie analysis as the tool to evaluate the strength of walls with reinforcement details complying to specifications of NZS 4229:1999.

The average yield displacement (Δ_y) for this partially grouted wall was evaluated to be 1.07 mm. The test wall was defined as failing during the second pull cycle to displacement ductility 8, giving it a ductility capacity of $\mu_{av} > 6.0$.

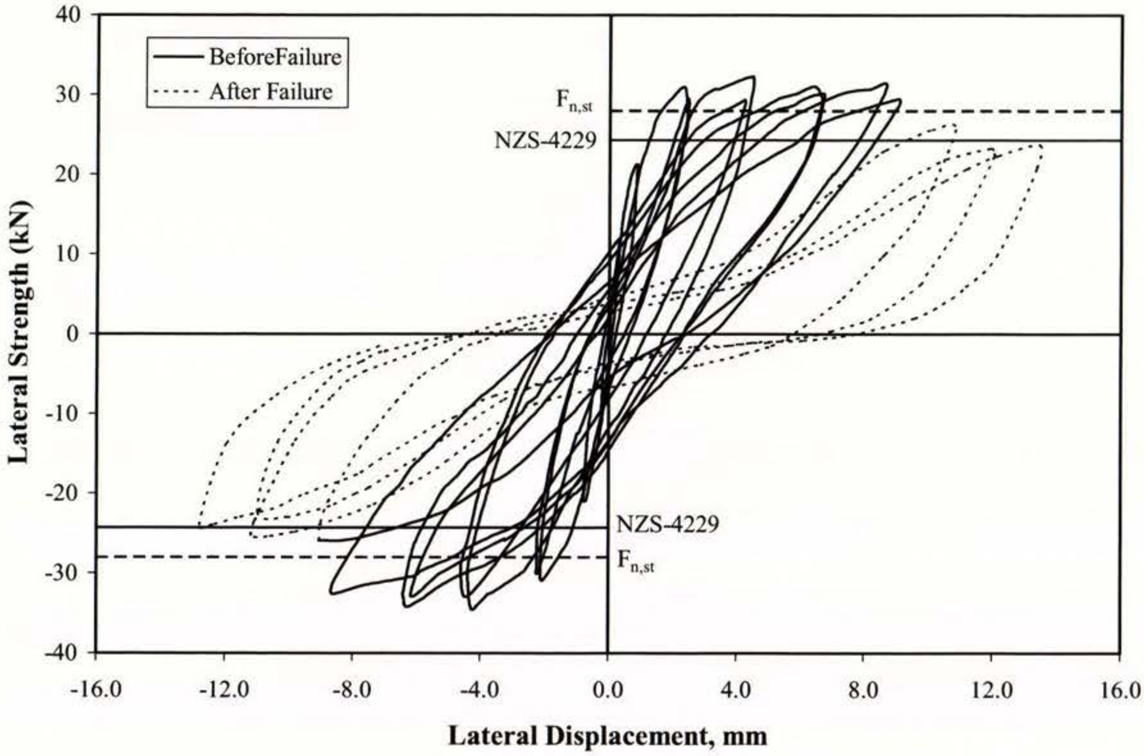

Figure A.3.5 Force-displacement behaviour of Wall 3.

A.3.4 Panel Displacement Components

The total horizontal displacement of the wall was decomposed into four components according to the procedure outlined in section 4.7 with the results shown in Figure A.3.6. From the rocking, sliding, flexure and shear deformation components plotted in Figure A.3.6, it is shown that the rocking and sliding deformations were negligible throughout the test and the influence of flexural component of deformation was significant only at low displacement level. As shown in Figure A.3.6, the magnitude of shear displacement grew significantly once the wall was being pushed/pulled beyond the lateral displacement of ± 2.0 mm. Also illustrated in the figure is the decrease in flexural displacement in the pushing direction once the wall was pushed beyond the displacement of 4.0 mm.

Figure A.3.6 shows that the summed up deformation (rocking + sliding + flexural + shear) approximately match the overall displacement measured at the loading beam. The figure provides an indication of the relative size of each displacement component at various stages of the displacement envelope.

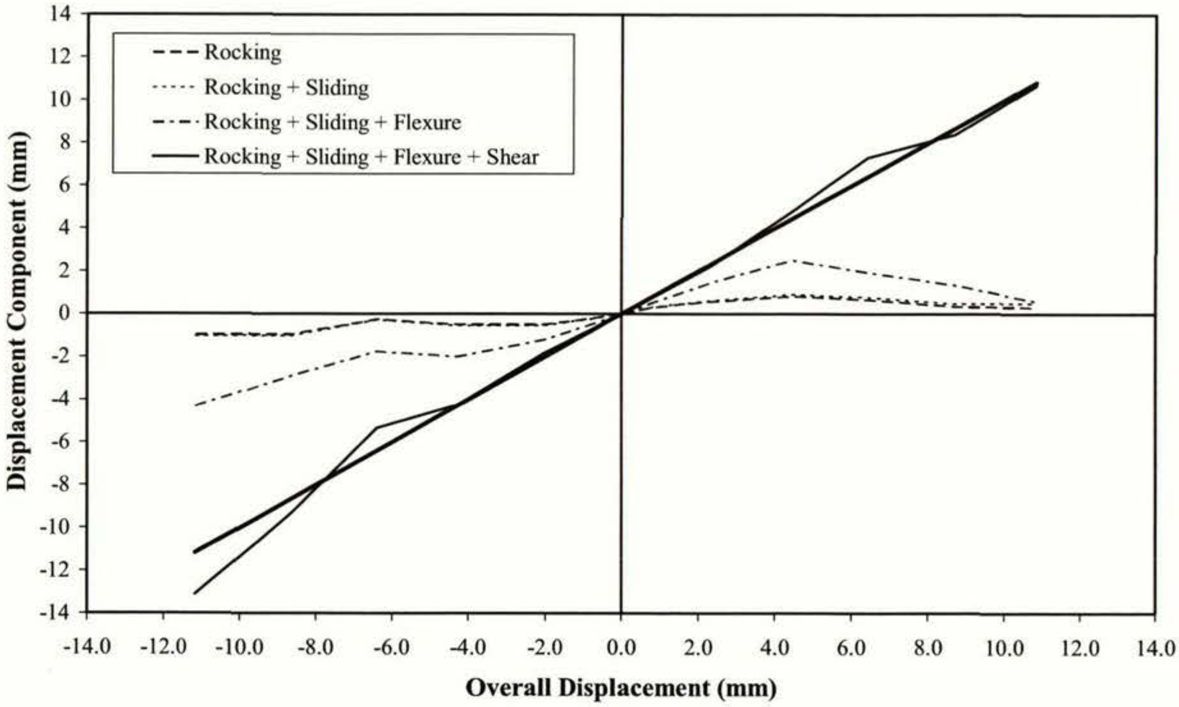

Figure A.3.6 Components of displacement.

A.4 Wall 4

This section describes the laboratory test of Wall 4. As shown in Figure A.4.1, this wall had the same opening geometry as Wall 2, but with an extended trimming reinforcement below both sides of window opening. The wall nominal shear (V_n) and flexural (F_n) strengths, calculated according to the shear expressions and $F_{n,st}$ described in Chapter 4 were established to be 78.1 kN and 41.0 kN respectively.

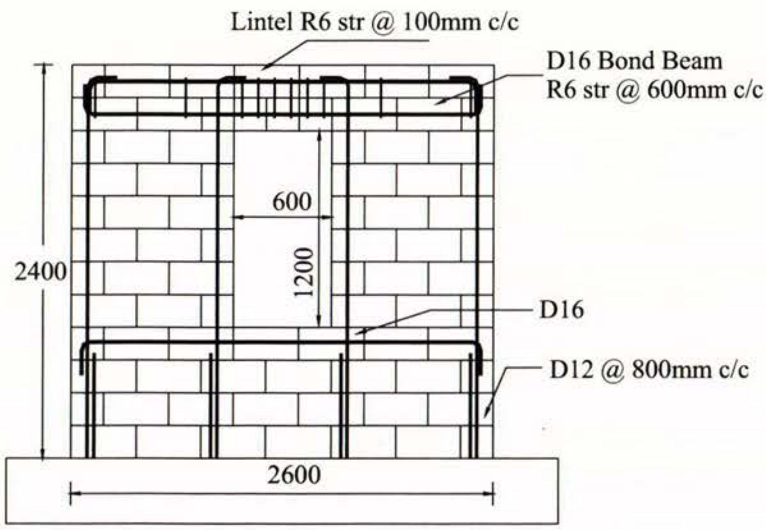

Figure A.4.1 Wall 4 geometry and reinforcing details.

A.4.1 Pre-test

The masonry wall was tested on the 30th days after construction. Instrumentation was attached to the wall according to section 3.5.1. Prior to wall testing the wall was inspected, with no cracks or structural defects being identified.

A.4.2 Testing

<u>$^3/_4$ F_n push,</u>

An applied force of 31.0 kN was recorded when the wall was pushed away (towards the right) from the strong wall. A corresponding displacement of 0.90 mm was recorded for this loading cycle. No clear evidence of cracking.

<u>$^3/_4$ F_n pull,</u>

A maximum strength of -31.6 kN was recorded at the displacement of -0.82 mm. No cracking was identified.

According to the procedure outlined in section 4.5, the measured lateral forces for the two directions of loading resulted in an average yield displacement of:

$$\Delta_y = \frac{4}{3}\left(\frac{0.90 + 0.82}{2}\right) = 1.15 \text{ mm}$$

μ_2 push, 1^{st} cycle

A maximum strength of 47.7 kN was recorded at the displacement of 2.33 mm. Seven hairline diagonal cracks were identified above the fully grouted horizontal flue containing the extended D16 trimming reinforcing steel (three diagonal cracks on the left pier and one diagonal crack on the right pier). One of the diagonal cracks initiated from the left side wall tension edge (about 50^o to the horizontal) and reached the wall base below the window opening. A maximum crack width of about 0.35 mm was measured.

μ_2 pull, 1^{st} cycle

The wall responded similarly to observations made in the previous push cycle. Diagonal cracking patterns mirrored to those formed in the previous push cycle were identified. A maximum strength of -47.1 kN was measured at the displacement of -2.29 mm.

μ_2 push, 2^{nd} cycle

A maximum strength of 39.6 kN was recorded at the displacement of 2.80 mm. No new cracking, the diagonal cracks were observed to widen slightly to a maximum width of about 0.50 mm.

μ_2 pull, 2^{nd} cycle

A maximum strength of -43.8 kN was recorded for this loading cycle. Similar to the previous push cycle, no new cracking was identified.

μ_4 push, 1^{st} cycle

A maximum strength of 46.0 kN was measured at the displacement of 4.95 mm. No new diagonal cracking, but elongations to existing cracks were identified. Of particular significant was the development of vertical crack beneath the trimming reinforcement on right pier. This vertical crack was similar to the vertical strut shown in Figure 4.2d. Also identified was the widening of previously formed diagonal cracks, with crack width up to 3.0 mm being identified. The wall cracking patterns at this stage of testing is shown in Figure A.4.2.

μ_4 pull, 1st cycle

The wall responded similarly to observations made in the previous push cycle. A maximum strength of -48.8 kN was recorded for this pulling cycle. Extensions to diagonal cracks formed in previous pull cycles were identified. Of particular significant was the elongation of diagonal cracks towards the bond beam corner (close to wall edge) above the right pier and the development of vertical crack beneath the trimming reinforcement on the left pier compression side. Diagonal crack on the bond beam was established to be insignificant to affect the structural performance of the bond beam. Widening of previously formed diagonal cracks were observed, with crack width up to 3.5 mm being identified. The wall condition at this stage of testing is shown in Figure A.4.2.

μ_4 push, 2nd cycle

A maximum strength of 38.1 kN was measured at the displacement of 4.95 mm. No new cracking was identified, but the vertical crack on the right pier was observed to further elongate to reach the compression toe. Hand tapping the face shells revealed the compression toe was still intact (solid sound during tapping) at this stage of testing.

μ_4 pull, 2nd cycle

A maximum strength of -41.5 kN was recorded at the displacement of -4.61 mm. The wall responded similarly to observations made in the previous push cycle.

μ_6 push, 1st cycle

A maximum strength of 38.8 kN was recorded at the displacement of 6.94 mm. Further widening of previously formed diagonal cracks and degradation of masonry at the compression toe region (right side wall panel) were observed. A maximum crack width of 9.5 mm was measured at the conclusion of this load stage.

μ_6 pull, 1st cycle

The wall responded similarly to observations made in the previous push cycle. A maximum strength of -42.5 kN was recorded at the displacement of -6.93 mm. No new crack was identified, but further elongations and widening of existing diagonal cracks were observed.

μ_6 push, 2nd cycle

A maximum strength of 29.2 kN was recorded at the displacement of 6.94 mm. This strength corresponded to about 61% of the maximum strength achieved in the pull direction. Hence the wall was defined as failing according to the test procedure outlined in section 4.5.

μ_6 pull, 2nd cycle

A maximum strength of -32.7 kN was recorded for this load step. No new cracking was identified.

μ_8 push, 1st cycle

A maximum strength of 33.3 kN was recorded at the displacement of 9.24 mm. No new cracking was identified. Further elongations and widening of previously formed cracks were observed, maximum crack of about 13 mm was measured.

μ_8 pull, 1st cycle

Similar to the previous push cycle, elongations and widening of previously formed diagonal cracks were identified. A maximum strength of -38.4 kN was recorded at the displacement of -9.21 mm.

μ_8 push, 2nd cycle

No new cracking or extensions of cracks were identified. A maximum strength of 31.5 kN was recorded at the displacement of 9.25 mm. See Figure A.4.3 for wall condition at this stage of testing

μ_8 pull, 2nd cycle

A maximum strength of -36.8 kN was recorded at the displacement of -9.22 mm. Minor spalling of mortar was observed, this was caused by the grinding movement of masonry along the crack paths.

Figure A.4.2 Condition of test wall at end of first ductility 4 pull cycle.

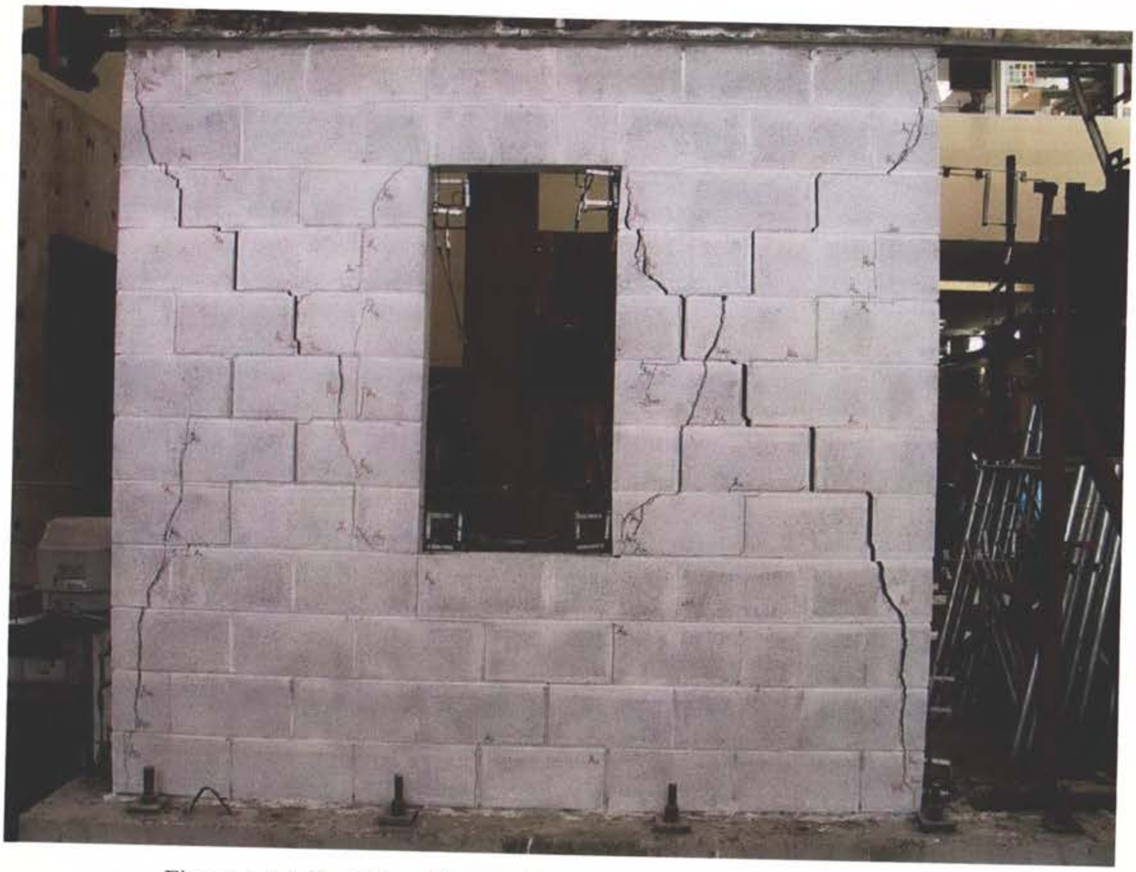

Figure A.4.3 Condition of test wall at end of second ductility 8 push cycle

μ_{10} push, 1st cycle

A maximum strength of 35.4 kN was recorded at the displacement of 11.77 mm. The wall response was dominated by the widening of existing cracks, with maximum crack width of about 19 mm being measured.

μ_{10} pull, 1st cycle

The wall response was similar to observations made in the previous push cycle. A maximum strength of -40.3 kN was measured at the displacement of -11.54 mm.

μ_{10} push, 2nd cycle

A maximum strength of 34.1 kN was measured at the displacement of 11.82 mm.

μ_{10} pull, 2nd cycle

A maximum strength of -34.7 kN was recorded at the displacement of -11.37 mm.

μ_{12} push, 1st cycle

A maximum strength of 32.1 kN was recorded at the displacement of 14.14 mm. The wall response was dominated by the widening of existing cracks. The wall condition at this stage of testing is shown in Figure A.4.4.

μ_{12} pull, 1st cycle

A maximum strength of -34.2 kN was measured at the displacement of -13.8 mm. The wall responded similarly to observations made in the previous push cycle.

μ_{12} push, 2nd cycle

A maximum strength of 30.8 kN was recorded at the conclusion of this load stage.

μ_{12} pull, 1st cycle

A maximum strength of -32.5 kN was measured at the conclusion of this load stage.

Figure A.4.4 Condition of test wall at end of first ductility 12 push cycle.

A.4.3 Summary Behaviour

The measured force-displacement curve for Wall 4 is presented in Figure A.4.5, depicting the lateral displacement at the top of the wall as a function of the applied lateral force. The maximum push and pull direction strengths of 47.7 kN and -47.1 kN were measured during the first cycle to displacement ductility 2. This wall was classified to fail in a diagonal tension mode. This failure mode was characterised by the gradual and fairly symmetrical strength degradation of strength in both directions of loading, despite the presence of widely open diagonal cracks on both the left and right side wall panels. The desirable behaviour of this nominally reinforced partially grout-filled concrete masonry wall was created by the solid filled bond beam at the top of the wall, which caused a frame-type action at latter stage of testing.

As shown in Figure A.4.5, it was established that the maximum strength achieved by Wall 4 was about 27% higher than the bracing capacity prescribed by NZS 4229:1999, therefore suggesting that the conservatism of NZS 4229:1999 to increase when trimming reinforcement is extended below an opening (as compare to the F_{max}/F_{code} of 1.10 in Wall 2). The wall nominal strength predicted according to $F_{n,st}$ was about 15% less than the maximum strength achieved by the wall.

As shown in Figures A.4.2 to A.4.4, the diagonal cracking patterns on this wall aligned well with the load paths by which shear force was transferred to the foundation in the strut mechanism. Consequently, this observation further supports the use of strut-and-tie analysis as the tool to evaluate the strength of walls with reinforcement details complying with specification of NZS 4229:1999.

The average yield displacement (Δ_y) for this partially grouted wall was evaluated to be 1.15 mm. The test wall was defined as failing during the first push cycle to displacement ductility 6, giving it a ductility capacity μ_{av} of 4.5.

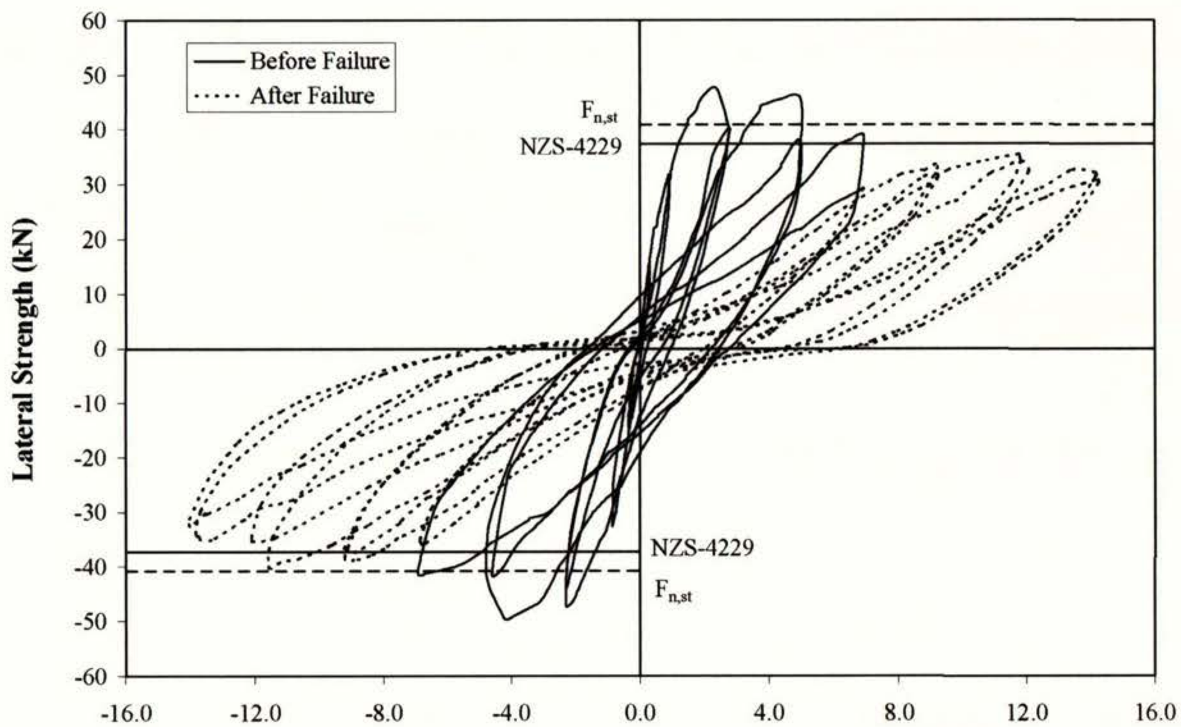

Figure A.4.5 Force-displacement behaviour of Wall 4.

A.4.4 Panel Displacement Components

The total horizontal displacement of the wall was decomposed into four components according to the procedure outlined in section 4.7 with the results shown in Figure A.4.6. It is shown that the shear deformation was the most dominant form of deformation, and the influence of rocking, sliding and flexural deformations were negligible throughout the test.

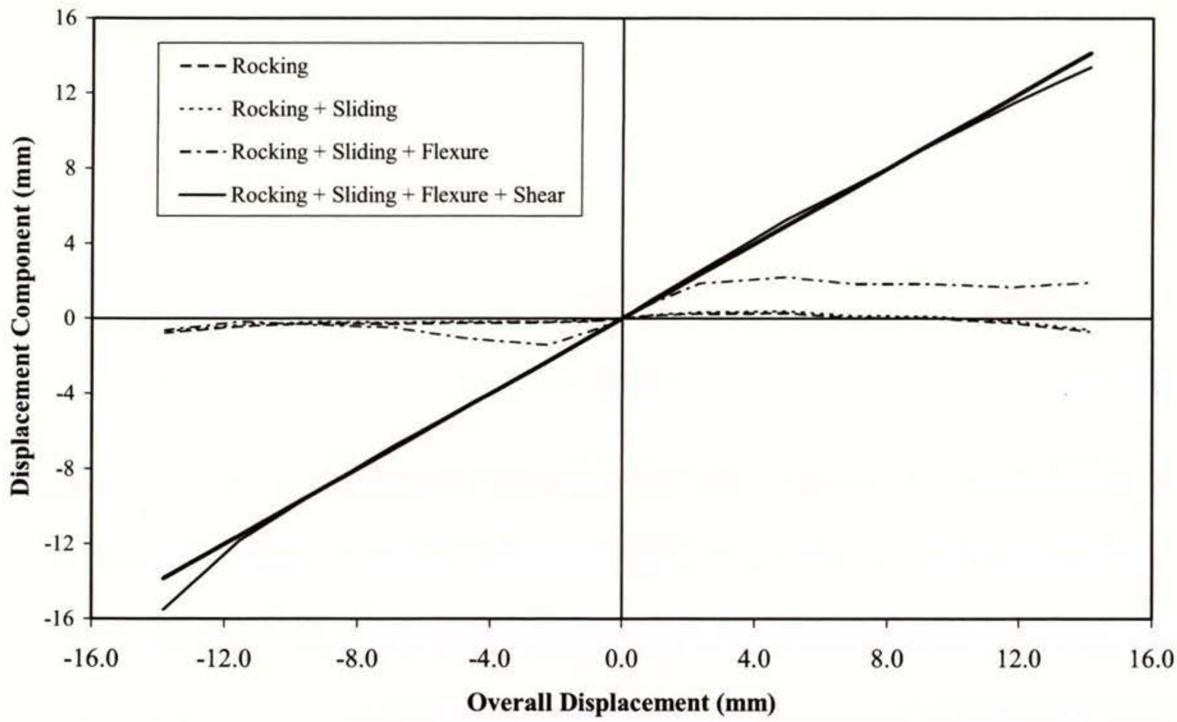

Figure A.4.6 Components of displacement.

A.5 Wall 5

This section describes the laboratory test of Wall 5. As shown in Figure A.5.1, this wall had an opening geometry identical to Wall 2, but the D-16 trimming reinforcement was only extended to the outermost vertical reinforcement on one side (right side) of the wall, resulting in an asymmetrical detailing of trimming reinforcement. The wall nominal shear strength (V_n) was evaluated to be 83.6 kN. The flexural (F_n) strengths, calculated according to $F_{n,st}$ described in section 4.1.2, were established to be 41.0 kN and 35.9 kN for the push and pull directions respectively.

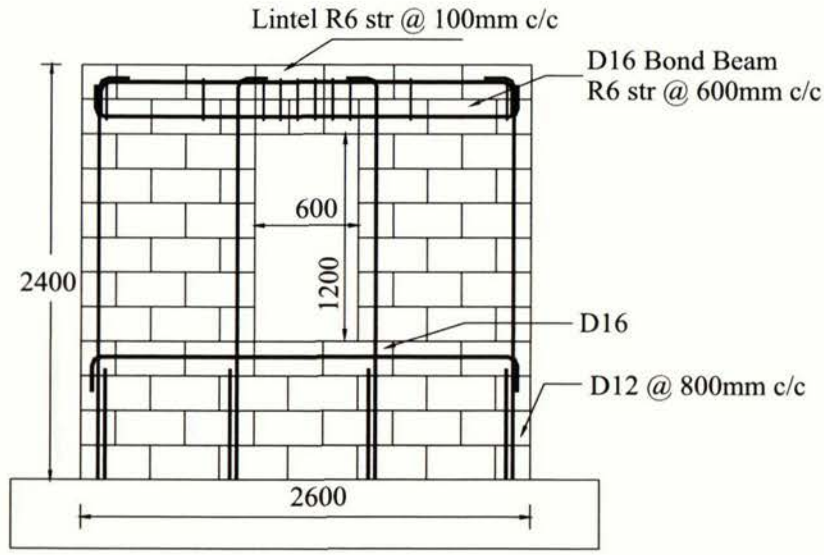

Figure A.5.1 Wall 5 geometry and reinforcing details.

A.5.1 Pre-test

The masonry wall was tested on the 19^{th} days after construction. Instrumentation was attached to the wall according to section 3.5.1. Prior to wall testing the wall was inspected, with no cracks or structural defects being identified.

A.5.2 Testing

<u>$^3/_4$ F_n push,</u>

An applied force of 30.8 kN was recorded when the wall was pushed away (towards the right) from the strong wall. A corresponding displacement of 0.63 mm was recorded for this loading cycle. No clear evidence of cracking.

According to the procedure outlined in section 3.8, the measured lateral forces for the pushing direction of loading resulted in a yield displacement of:

$$\Delta_y = \frac{4}{3} \times 0.63 = 0.84 \text{ mm}$$

$^3/_4$ F_n pull,

A maximum strength of -25.6 kN was recorded at the displacement of -0.50 mm. No cracking was identified.

According to the procedure outlined in section 4.5, the measured lateral forces for the pulling direction of loading resulted in a yield displacement of:

$$\Delta_y = \frac{4}{3} \times 0.5 = 0.66 \text{ mm}$$

μ_2 push, 1st cycle

A cracking noise was heard (due to diagonal crack opening) when the wall was pushed to a displacement of 1.2 mm. The opening of this diagonal crack did not cause strength loss. The wall continued to grow in strength until a maximum strength of 44.0 kN was recorded at the target displacement. At the completion of this loading stage, seven hairline horizontal cracks and one diagonal crack were identified.

μ_2 pull, 1st cycle

A maximum strength of -40.8 kN was measured at the displacement of -1.56 mm. Four diagonal cracks (two cracks on right pier, one on left pier and one below the window) were identified. A maximum crack width of about 0.1 mm was identified..

μ_2 push, 2nd cycle

A maximum strength of 41.2 kN was recorded at the displacement of 1.79 mm. Two new diagonal cracks and extensions to previously formed diagonal were identified.

μ_2 pull, 2nd cycle

A maximum strength of -31.9 kN was recorded for this loading cycle. No new cracking was identified.

μ_4 push, 1st cycle

In this push excursion towards the target displacement of 3.36 mm, significant widening of existing diagonal cracks (accompanied by cracking noise) occurred at the displacement of 2.85 mm, resulting in slight loss of strength and a sudden increase in lateral displacement. The peak strength measured was 52.4 kN at the displacement of 2.85 mm. At the final displacement of 3.37 mm, the strength measured was 46.1 kN. Two new diagonal cracks and a vertical crack beneath the trimming reinforced (adjacent to the compression wall edge) were identified at the completion of this loading stage. A maximum crack width of about 0.5 mm was identified.

μ_4 pull, 1st cycle

A maximum strength of -48.1 kN was measured at the displacement of -2.57 mm. Three new diagonal cracks and extensions to previously formed cracks were identified. The cracking patterns at this stage of testing aligned well with the load paths by which shear force was transferred to the foundation in the strut mechanism. The wall condition at this stage of testing is depicted in Figure A.5.2.

μ_4 push, 2nd cycle

A maximum strength of 38.2 kN was measured at the displacement of 3.32 mm. This strength corresponded to about 73% of the maximum strength achieved in the push direction. Hence the wall was defined as failing according to the test procedure outlined in section 4.5. Extensions to previously formed cracks were identified. No new cracking.

μ_4 pull, 2nd cycle

A maximum strength of -41.5 kN was recorded at the displacement of -4.61 mm. The wall responded similarly to observations made in the previous push cycle. Maximum crack width of about 1 mm was identified.

Figure A.5.2 Condition of test wall at end of first ductility 4 pull cycle.

μ_6 push, 1st cycle

A maximum strength of 37.4 kN was recorded when the wall was pushed to the displacement of 3.62 mm. This was immediate followed by the significant widening of previously formed cracks that resulted in slight drop in strength. Wall strength of 33.2 kN was recorded at the target displacement of this loading stage. No new cracking was identified, but extensions and widening of previously formed cracks were identified, with maximum crack width of about 2 mm. The vertical crack formed in previously cycle elongated to reach the compression toe. Upon tapping the face shell, it was established that masonry at the compression toe was still intact and face shell delamination had yet to take place.

μ_6 pull, 1st cycle

A maximum strength of -47.6 kN was recorded at the displacement of -3.85 mm. No new cracking was identified, but further elongations and widening of diagonal cracks were observed (diagonal cracks were observed to extend to the compression toe on the left side panel).

μ_6 push, 2nd cycle

A maximum strength of 29.3 kN was recorded at the displacement of 5.08 mm. Few extensions to previously formed cracks were identified.

μ_6 pull, 2nd cycle

A maximum strength of -49 kN was recorded at the displacement of -3.96 mm. No new cracks were identified. Widening of cracks was identified, with maximum crack width of about 5.5 mm.

μ_8 push, 1st cycle

A maximum strength of 33.3 kN was recorded at the displacement of 6.28 mm. No new cracking was identified. Further widening of previously formed cracks and degradation of compression toe were observed (as indicated by the widening of vertical crack). Maximum crack of about 7.0 mm was measured.

μ_8 pull, 1st cycle

Similar to previous push cycle, elongation and widening of existing diagonal cracks were identified. A maximum strength of -46.5 kN was recorded at the displacement of -5.26 mm. Spalling of masonry face shell along diagonal cracks were observed to take place. Maximum crack width of about 12 mm was identified.

μ_8 push, 2nd cycle

No new cracking or crack extensions were identified. A maximum strength of 24.8 kN was recorded at the displacement of 8.43 mm. Maximum crack width of about 18 mm was identified.

μ_8 pull, 2nd cycle

A maximum strength of -46.2 kN was recorded at the displacement of -5.45 mm.

μ_{10} push, 1st cycle

A maximum strength of 26.8 kN was recorded at the displacement of 8.82 mm. No new cracking was identified. The wall response was dominated by the widening of existing cracks.

μ_{10} pull, 1st cycle

A maximum strength of -46.4 kN was measured at the displacement of –7.38 mm. Grinding of masonry along crack paths caused the spalling of mortar. Maximum crack width of about 22 mm was identified.

μ_{10} push, 2nd cycle

The wall response was similar to observations made in the previous push cycle. A maximum strength of 26.9 kN was measured at the displacement of 9.78 mm.

μ_{10} pull, 2nd cycle

A maximum strength of -42.3 kN was recorded at the displacement of -6.65 mm.

μ_{12} push, 1st cycle

A maximum strength of 25.5 kN was recorded at the displacement of 10.24 mm. Similar to the previous loading cycle, the wall response was dominated by the widening of existing cracks.

μ_{12} pull, 1st cycle

A maximum strength of -40.2 kN was measured at the displacement of -13.8 mm.

μ_{12} push, 2nd cycle

A maximum strength of 18.4 kN was recorded at the conclusion of this load stage.

μ_{12} pull, 2nd cycle

A maximum strength of –39.1 kN was measured at the displacement of -8.11 mm.

μ_{14} push, 1st cycle

A maximum strength of 23.0 kN was recorded at the displacement of 12.44 mm. Widening of vertical crack below the fully grouted flue (trimming reinforcement) caused significant damage to compression toe.

μ_{14} pull, 1st cycle

A maximum strength of –36.0 kN was measured at the displacement of –9.38 mm. As shown in Figure A.5.3, vertical crack formed in previous push cycles resulted in the spalling of masonry at the tension toe region.

μ_{14} push, 2nd cycle

The wall response was similar to observations made in the previous push cycle. A maximum strength of 15.4 kN was measured at the displacement of 11.96 mm. The wall condition at this stage of testing is shown in Figure A.5.3.

Figure A.5.3 Condition of test wall at end of second ductility 14 push cycle.

μ_{14} pull, 2nd cycle

A maximum strength of -31.7 kN was recorded at the displacement of -9.94 mm.

μ_{16} push, 1st cycle

A maximum strength of 16.9 kN was recorded at the displacement of 10.24 mm. Similar to previous loading cycle, the wall response was dominated by the widening of existing cracks.

μ_{16} pull, 1st cycle

A maximum strength of -28.0 kN was measured at the displacement of -10.8 mm. No new crack, but further widening of existing cracks was identified.

μ_{16} push, 2nd cycle

A maximum strength of 15.7 kN was recorded at the displacement of 13.7 mm.

μ_{12} pull, 2nd cycle

A maximum strength of –22.6 kN was measured at the displacement of -11.1 mm.

A.5.3 Summary Behaviour

The measured force-displacement curve for Wall 5 is presented in Figure A.5.4, depicting the lateral displacement at the top of the wall as a function of the applied lateral force. The maximum push and pull direction strengths of 52 kN and -50 kN were recorded during experimental testing. Similar to Walls 1-4, Wall 5 was classified to fail in a diagonal tension mode. The desirable behaviour of this perforated nominally reinforced partially grout-filled concrete masonry wall was created by the solid filled bond beam at the top of the wall, which caused a frame-type action at latter stage of testing. As shown in Figure A.5.4, Wall 5 exhibited significant non-symmetrical force-displacement response due to the non-symmetrical arrangement of trimming reinforcement. This was correlated with different geometry of crack patterns formed in the two directions of loading. In addition, inspection of wall condition at end of testing strongly indicated that the wall cracking patterns aligned well with the load paths by which shear force was transferred to the foundation in the strut mechanisms. Consequently, this observation further supports the use of strut-and-tie analysis as the tool to evaluate the strength of perforated partially grout-filled masonry walls that were nominally reinforced.

As shown in Figure A.5.4, the strut-and-tie models correctly established a stronger wall strength in the pushing direction than that in the pulling direction. A stronger strength in the push direction was expected due to presence of the extended trimming reinforcement in the right side panel. It was established that the maximum strength achieved by Wall 5 was about 39% and 34% higher than the bracing capacity prescribed by NZS 4229:1999 in the respective pushing and pulling directions. The maximum strengths recorded during experimental testing were about 27% and 45% higher than those predicted according to $F_{n,st}$ in the respective pushing and pulling directions.

The yield displacement (Δ_y) for this partially grouted wall was evaluated to be 0.84 mm and 0.66 mm in the respectively pushing and pulling directions. The test wall was defined as failing during the second push cycle to displacement ductility 4, giving it a ductility capacity μ_{av} of 2.0.

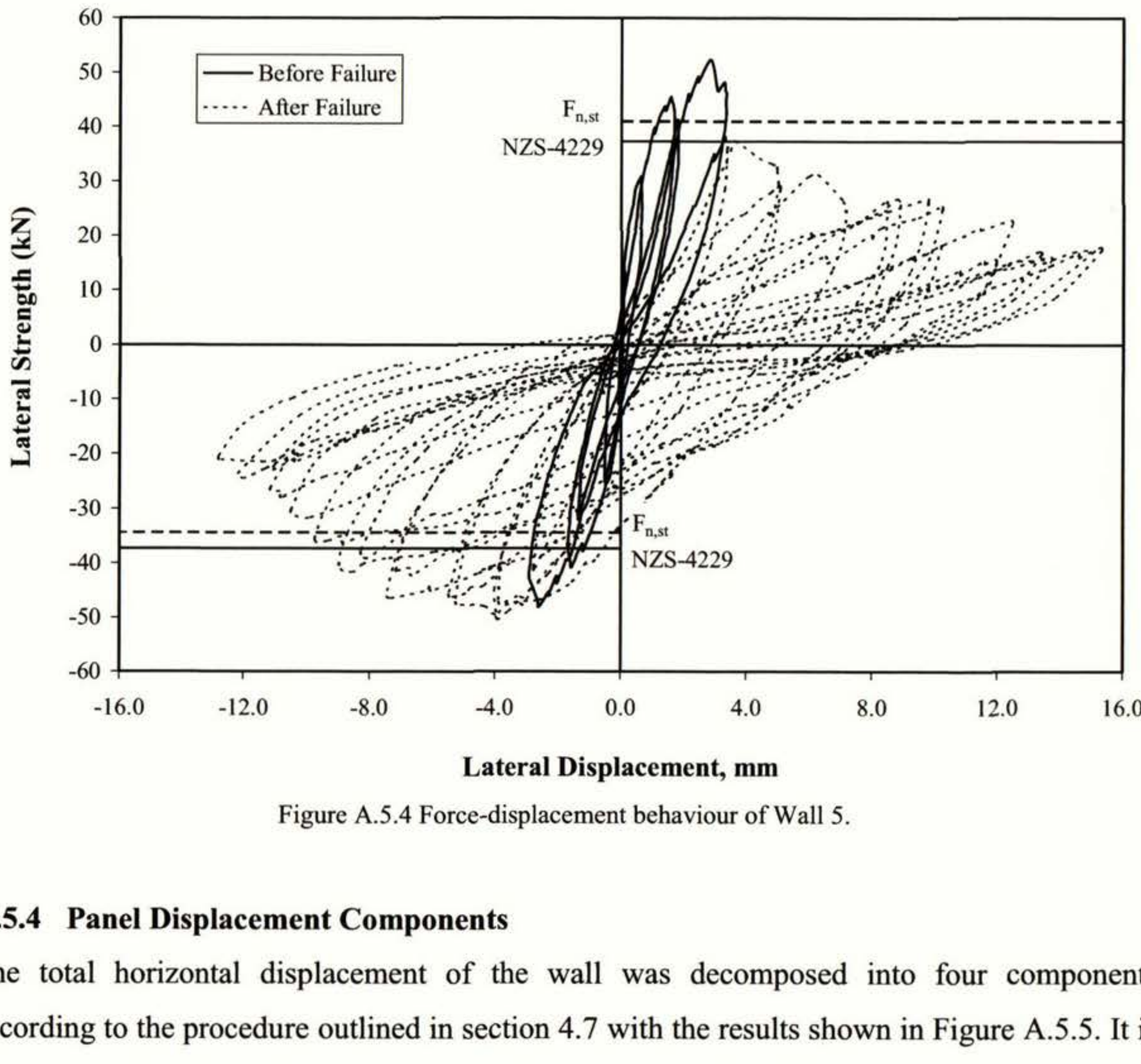

Figure A.5.4 Force-displacement behaviour of Wall 5.

A.5.4 Panel Displacement Components

The total horizontal displacement of the wall was decomposed into four components according to the procedure outlined in section 4.7 with the results shown in Figure A.5.5. It is shown that the shear deformation was the most dominant form of deformation. This observation correlated well with the development of significant diagonal shear cracking during the test. The influence of rocking, sliding and flexural deformations were negligible.

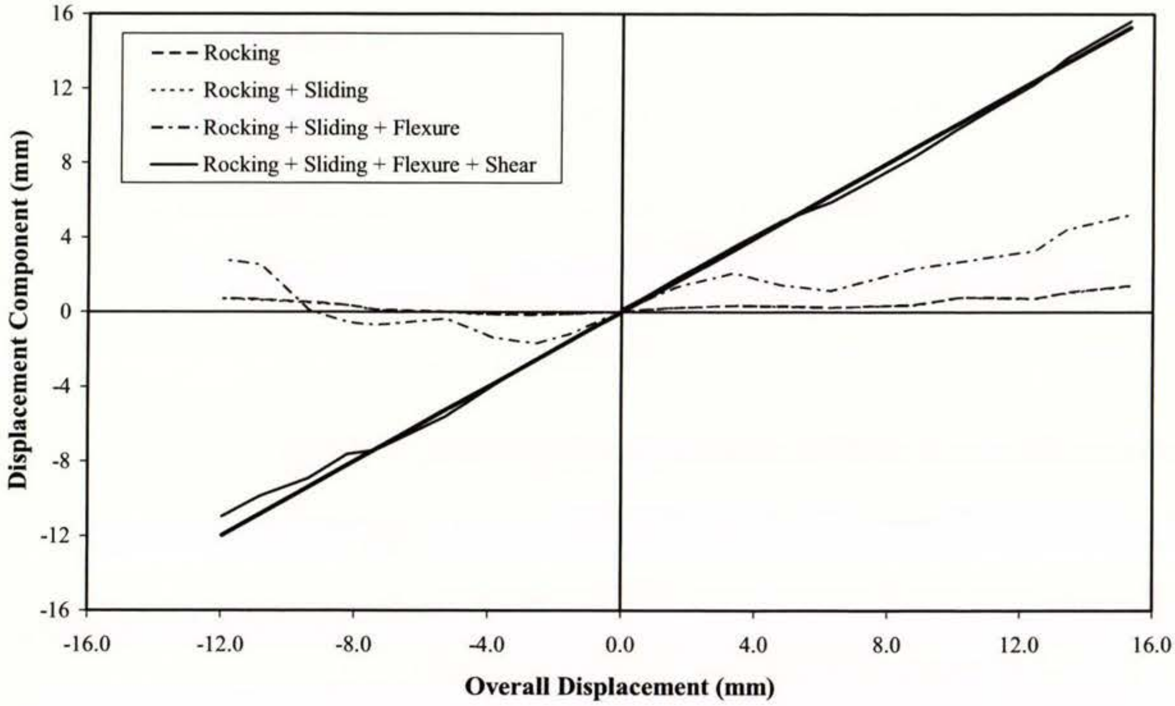

Figure A.5.5 Components of displacement.

A.6 Wall 6

This section describes the laboratory test of Wall 6. The wall geometry and reinforcement details are shown in Figure A.6.1. The wall nominal shear (V_n) and flexural (F_n) strengths, calculated according to the shear expressions and $F_{n,ST}$ described in Chapter 4, were established to be 117.1 kN and 79.9 kN respectively.

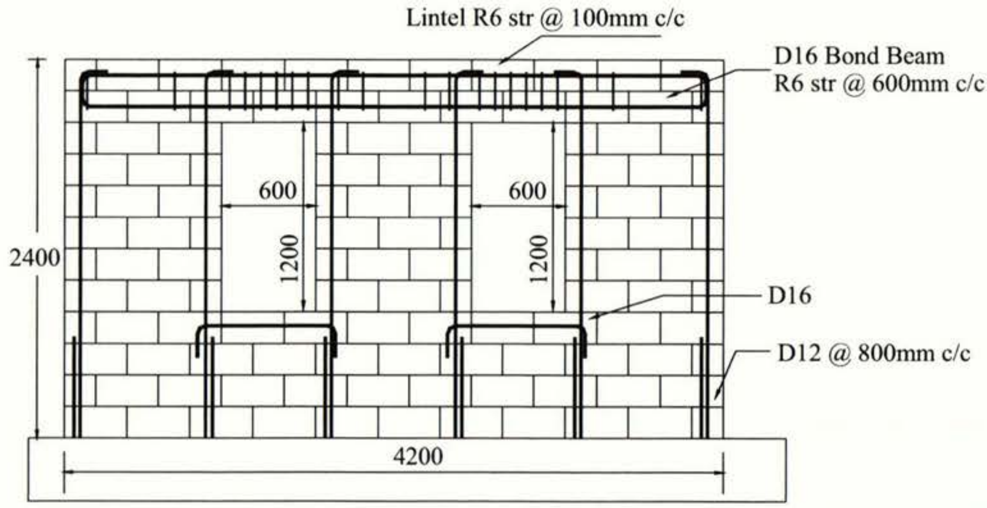

Figure A.6.1 Wall 6 geometry and reinforcing details.

A.6.1 Pre-test

The masonry wall was tested on the 21st days after construction. Instrumentation was attached to the wall according to section 3.5.1. Prior to wall testing the wall was inspected, with no cracks or structural defects being identified.

A.6.2 Testing

<u>$^3/_4$ F_n push,</u>

An applied force of 67.4 kN was recorded when the wall was being pushed away from the strong wall. A corresponding displacement of 1.40 mm was recorded for this loading cycle. Two diagonal cracks, with a maximum crack width of about 0.5 mm, were identified on all three piers.

<u>$^3/_4$ F_n pull,</u>

The wall responded similarly to observations made in the previous push cycle. A maximum strength of -67.5 kN was recorded at the displacement of -1.69 mm.

According to the procedure outlined in section 4.5, the measured lateral forces for the two directions of loading resulted in an average yield displacement of:

$$\Delta_y = \frac{1}{2}\left(\frac{80.0}{67.4}\times 1.40\right) + \frac{1}{2}\left(\frac{80.0}{67.5}\times 1.69\right) = 1.83 \text{ mm}$$

μ_2 push, 1st cycle

A maximum strength of 94.3 kN was recorded at the displacement of 4.07 mm. Extensions to previously formed cracks were identified, and cracks were widened to a maximum width of 2.5 mm. In addition, two new diagonal cracks were identified on the central pier.

μ_2 pull, 1st cycle

A maximum strength of -83.8 kN was recorded at the displacement of -4.07 mm. The wall responded similarly to observations made in the previous cycle. Cracking patterns significantly mirrored to those formed in the previous push cycle were identified. Maximum crack width of about 1.5 mm was identified.

μ_2 push, 2nd cycle

A maximum strength of 76.3 kN was recorded at the conclusion of this loading cycle. No new cracking or crack elongations were identified.

μ_2 pull, 2nd cycle

A maximum strength of -73.6 kN was recorded for this loading cycle. No new cracking was identified.

μ_4 push, 1st cycle

A maximum strength of 81.9 kN was measured at the displacement of 8.23 mm. No new cracking was identified, but elongations to existing cracks were identified, with crack width up to 6.5 mm. It was observed that diagonal crack on the left pier extended to reach the compression toe.

μ_4 pull, 1st cycle

The wall responded similarly to observations made in the previous push cycle. Diagonal cracks on the right side pier extended to the compression toe, no new cracking was identified. A maximum wall strength of – 94.6 kN was recorded at the displacement of -8.25 mm. Maximum crack width of about 8.0 mm was identified.

μ_4 push, 2nd cycle

A maximum strength of 51.4 kN was measured in this push excursion cycle. This strength corresponded to about 55% of the maximum strength achieved in the pushing direction. Hence, the wall was defined as failing according to the test procedure outlined in section 4.5. No new cracking or crack elongations were identified. Mortar crushing due to the grinding movement of masonry along the diagonal cracks was observed. The wall condition at this stage of testing is shown in Figure A.6.2.

μ_4 pull, 2nd cycle

A maximum strength of -77.0 kN was recorded at the displacement of -8.38 mm. The wall responded similarly to observations made in the previous push cycle.

μ_6 push, 1st cycle

A maximum strength of 61.8 kN was recorded at the displacement of 12.28 mm. No new crack. The wall response was dominant by the elongations and widening of existing diagonal cracks, with crack width up to 12.0 mm being identified. The wall condition at this stage of testing is shown in Figure A.6.3.

μ_6 pull, 1st cycle

The wall responded similarly to observations made in the previous push cycle. A maximum strength of –78.0 kN was recorded at the displacement of -12.01 mm. No new cracking was identified, but further elongations and widening of diagonal cracks were observed.

μ_6 push, 2nd cycle

A maximum strength of 42.3 kN was recorded at the displacement of 12.06 mm. No new cracking was identified, but further widening of diagonal cracks were identified with crack width up to 15 mm being identified.

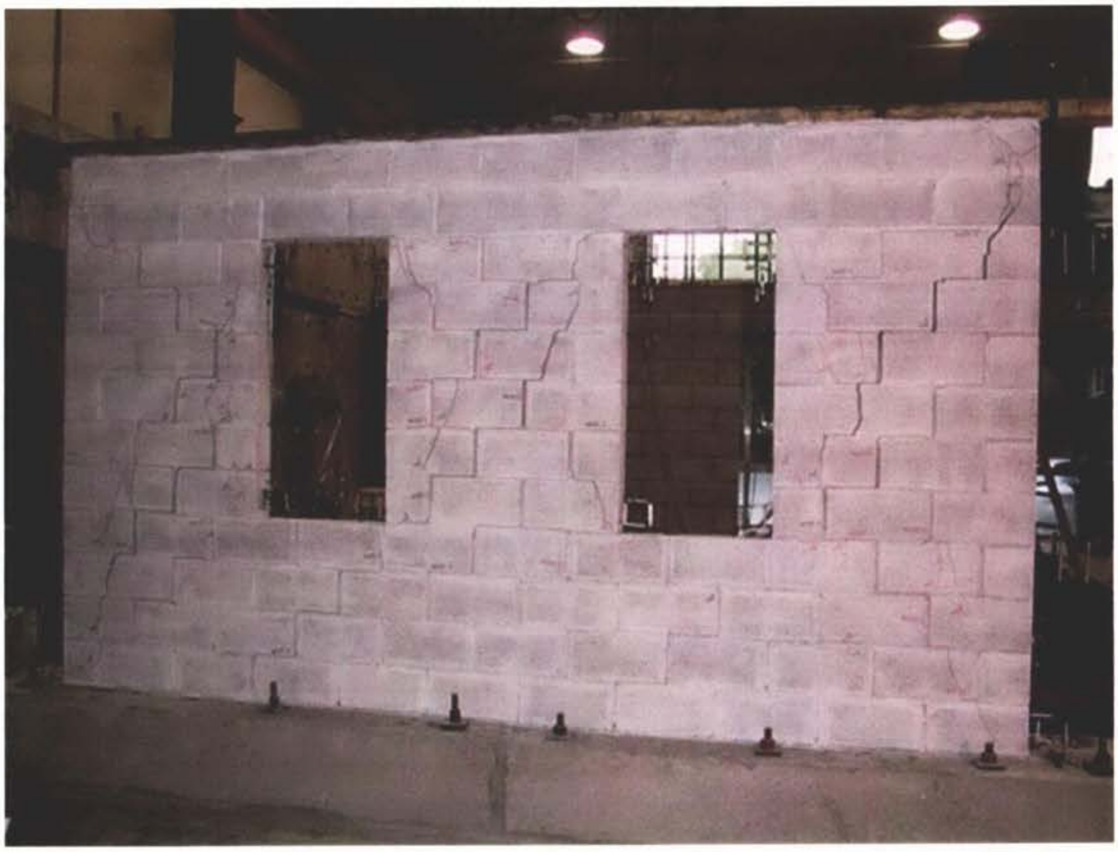

Figure A.6.2 Condition of test wall at end of second ductility 4 push cycle.

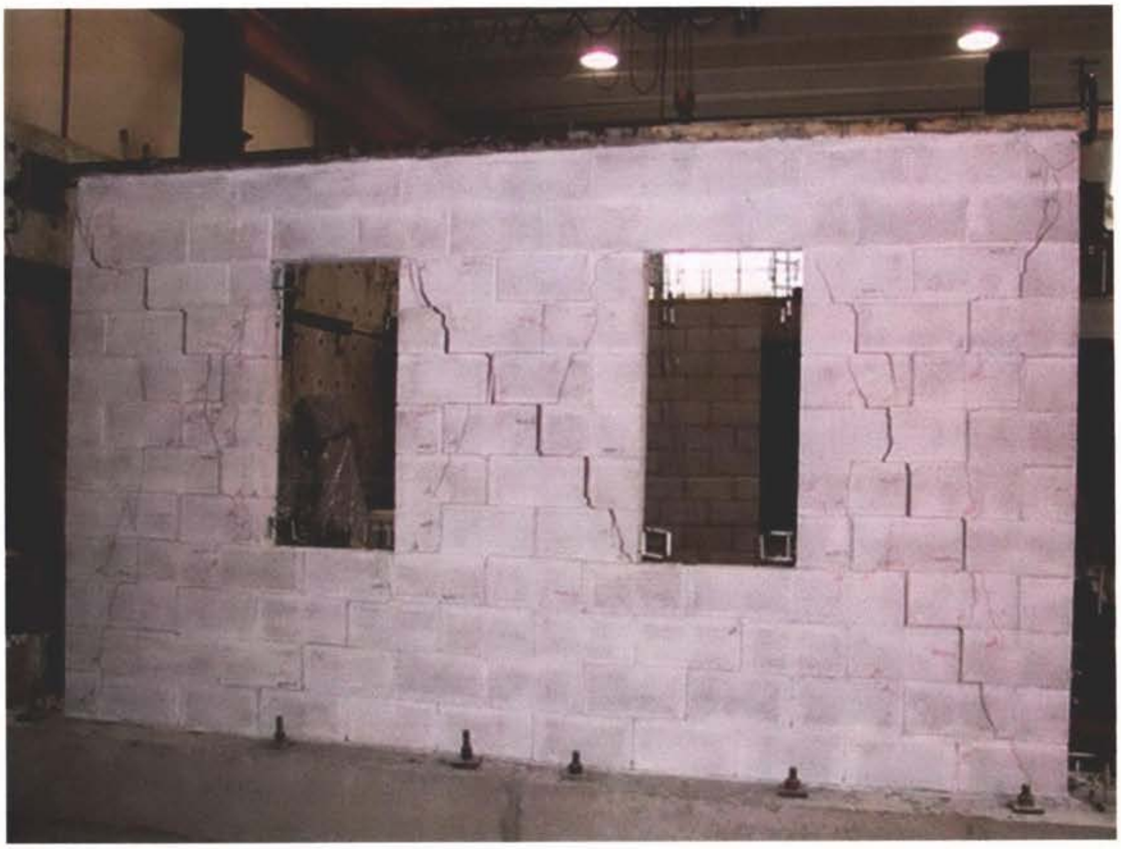

Figure A.6.3 Condition of test wall at end of first ductility 6 push cycle.

μ_6 pull, 2nd cycle

The wall responded similarly to observation made in the previous push cycle. A maximum strength of -67.2 kN was recorded for this load step. No new cracking was identified. Spalling of masonry face shell on the central pier was identified.

μ_8 push, 1st cycle

A maximum strength of 56.9 kN was recorded at the displacement of 16.14 mm. No new cracking was identified. Further elongations and widening of diagonal cracks were observed, maximum crack of about 17.5 mm was identified. The wall cracking pattern at this stage of testing (see Figure A.6.4) correlated well with the load paths by which shear force was transferred to the foundation according to the strut mechanisms shown in section 4.1.2.

μ_8 pull, 1st cycle

The wall responded similarly to observations made in the previous push cycle. Elongation and widening of previously formed diagonal cracks were identified. A maximum strength of -67 kN was recorded at the displacement of -16.0 mm.

μ_8 push, 2nd cycle

No new cracking or crack extensions were identified. A maximum strength of 44.3 kN was recorded at the displacement of 16.0 mm.

μ_8 pull, 2nd cycle

A maximum strength of -47.8 kN was recorded at the target displacement. No new cracking or crack elongations were identified.

μ_{10} push, 1st cycle

A maximum strength of 50.4 kN was recorded at the displacement of 20.1 mm. No new cracking was identified. The wall response was dominated by the degradation and widening of existing diagonal cracks. Maximum crack width of about 20.5 mm was measured.

μ_{10} pull, 1st cycle

The wall response was similar to observations made in the previous push cycle. A maximum strength of -50.4 kN was measured at the displacement of -19.6 mm.

Figure A.6.4 Condition of test wall at end of first ductility 8 push cycle.

Figure A.6.5 Condition of test wall at end of first ductility 12 pull cycle.

μ_{10} push, 2nd cycle

A maximum strength of 43.5 kN was measured at the displacement of 20.26 mm. No new cracking or crack extensions were identified.

μ_{10} pull, 2nd cycle

A maximum strength of -47.3 kN was recorded at the displacement of -20.2 mm.

μ_{12} push, 1st cycle

A maximum strength of 45.3 kN was recorded at the displacement of 24.09 mm. No new crack, but further widening of diagonal cracks with crack width up to 22.6 mm being identified.

μ_{12} pull, 1st cycle

The wall response was dominated by the further widening of existing diagonal cracks. A maximum strength of –57.4 kN was measured at the displacement of -24.35 mm. The wall condition at this stage of testing is shown in Figure A.6.5.

μ_{12} push, 2nd cycle

A maximum strength of 38.1 kN was measured at the displacement of 24.44 mm.

μ_{12} pull, 2nd cycle

A maximum strength of -47.2 kN was recorded at the target displacement. No new cracking was identified.

A.6.3 Summary Behaviour

The measured force-displacement curve for Wall 6 is presented in Figure A.6.6, depicting the lateral displacement at the top of the wall as a function of the applied lateral force. The maximum push direction strength of 94.3 kN was measured during the first cycle to displacement ductility 2 and the maximum pull direction strength of -94.6 kN was measured during the first cycle to displacement ductility 4. Despite the presence of widely open diagonal cracks, the wall exhibited a gradual and fairly symmetrical strength degradation of strength in both direction of loading. Consequently, it was possible to classify Wall 6 as having a failure mode of diagonal tension. The desirable behaviour of this nominally reinforced partially grout-filled concrete masonry wall was created by the solid filled bond beam at the top of the wall, which caused a frame-type action at latter stage of testing.

As shown in Figure A.6.6, it was established that the maximum strength achieved by Wall 6 was about 69% higher than the bracing capacity prescribed by NZS 4229:1999, therefore suggesting that the conservatism of NZS 4229:1999 to increase as the length of a perforated masonry wall increased. The wall maximum strength recorded during testing was about 18% more than that predicted using the improved strut-and-tie model.

As shown in Figures A.6.2 to A.6.5, the diagonal cracking pattern on this wall aligned well with the load paths by which shear force was transferred to the foundation in the strut mechanism. This observation supports the use of strut-and-tie analysis as the tool to evaluate the strength of walls with reinforcement details complying to specifications of NZS 4229:1999. However, it was noted that the maximum strength achieved by the wall was about 61% higher than that predicted using the simplified strut-and-tie method, therefore suggesting the conservatism of the simplified strut-and-tie analysis (similar to NZS 4229:1999) to increase as the wall length increases.

The force-displacement plot in Figure A.6.6 consistently illustrated a pinched shape. This was primarily due to the presence of significant shear deformation in this nominally reinforced partially grout-filled concrete masonry wall. It was also observed that less hysteretic energy was expended during the second cycle to any displacement level, when compared with the first displacement cycle. This is shown by the more pinched hysteresis loops of the second cycle.

The yield displacement (Δ_y) for this partially grouted wall was evaluated to be 1.83 mm. The test wall was defined as failing during the second push cycle to displacement ductility 4, giving it a ductility capacity μ_{av} of 2.0.

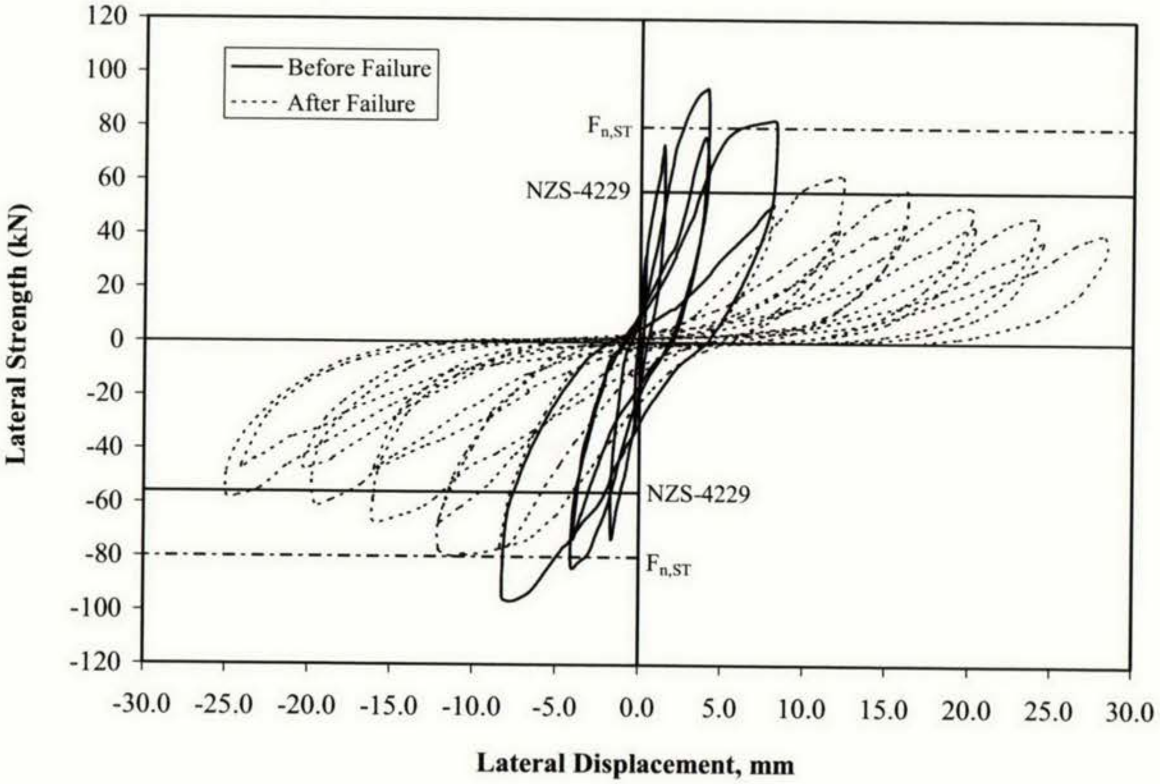

Figure A.6.6 Force-displacement behaviour of Wall 6.

A.6.4 Panel Displacement Components

The total horizontal displacement of the wall was decomposed into four displacement components according to the procedure outlined in section 4.7 with the results shown in Figure A.6.7. From the rocking, sliding, flexure and shear deformation components plotted in Figure A.6.7, it is shown that shear displacement was the single most dominant deformation mode. The influences of rocking, sliding and flexural component of deformations were negligible throughout the test.

It is noted that the summed up deformation (rocking + sliding + flexural + shear) approximately match the overall displacement measured at the loading beam. Ideally, the line representing the sum of components should coincide with the line representing the lateral displacement measured at the loading beam. Figure A.6.7 is useful in providing an indication of the relative size of each displacement component at various stages of the displacement envelope.

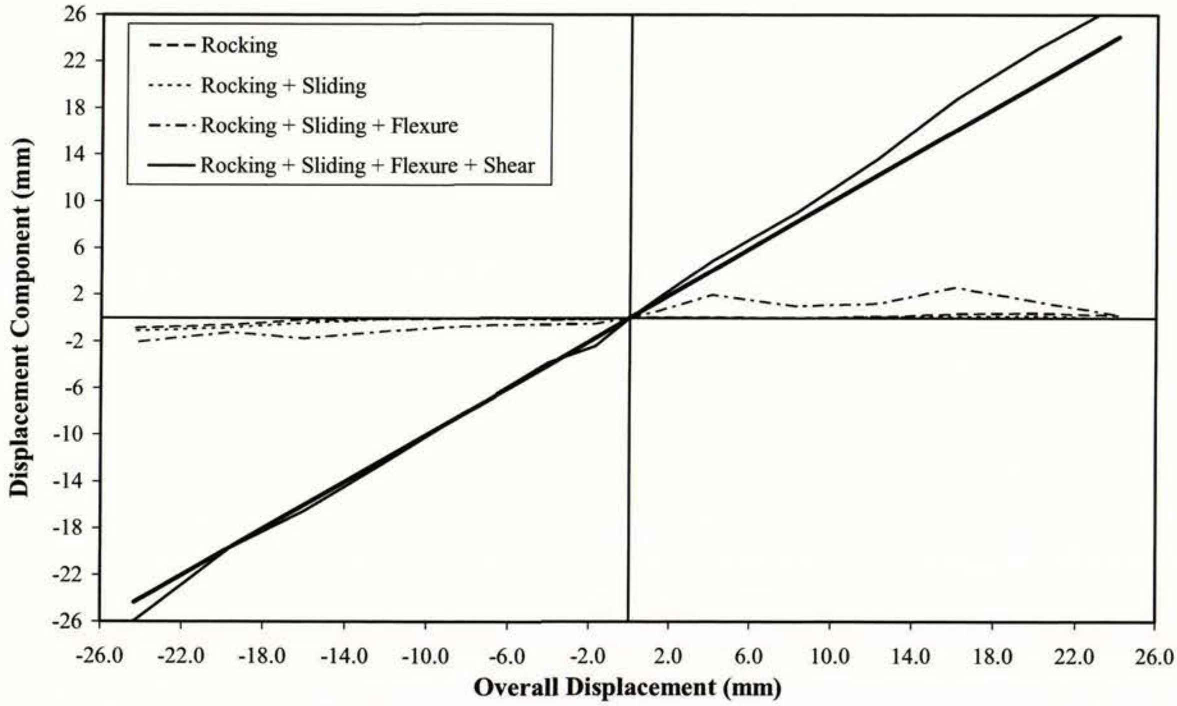

Figure A.6.7 Components of displacement.

A.7 Wall 7

This section describes the laboratory test of Wall 7. The wall geometry and reinforcement details are shown in Figure A.7.1. The wall nominal shear (V_n) was established to be 122.4 kN and the flexural (F_n) strengths calculated according to the improved strut-and-tie model described in section 4.1.3 were established to be 61.6 kN and 76.1 kN for the pushing and pulling directions respectively.

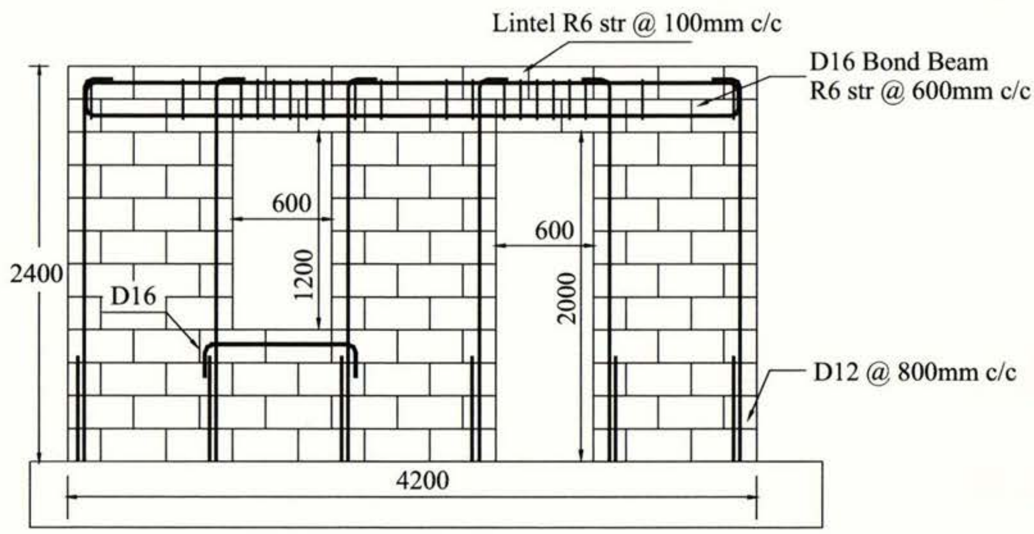

Figure A.7.1 Wall 7 geometry and reinforcing details.

A.7.1 Pre-test

The masonry wall was tested on the 34th days after construction. Instrumentation was attached to the wall according to section 3.5.1. Prior to wall testing the wall was inspected, with no cracks or structural defects being identified. Although the wall had different lateral strengths for the respective pushing and pulling directions, it was decided that (for convenience) the nominal lateral strength for this wall shall be taken as 76.1 kN for the two loading directions. This decision was taken because Davidson (1998) successfully showed that wall strength of over 80 kN was developed by concrete masonry wall of similar constructional geometries and reinforced with $\phi 12$ longitudinal steel bars of $f_y = 275$ MPa.

A.7.2 Testing

<u>$^3/_4 F_n$ push,</u>

An applied force of 61.0 kN was recorded when the wall was being pushed away (towards the right) from the strong wall. A corresponding displacement of 1.45 mm was recorded for this loading cycle. Diagonal cracks were identified throughout the wall (5 cracks on the left pier-of which 2 cracks extended beneath window, 4 cracks on the central pier and 3 cracks on the right pier). A maximum crack width of 0.2 mm was identified.

$^3/_4 F_n$ pull,

A maximum strength of -60.6 kN was recorded at the displacement of -1.56 mm. Hairlines diagonal cracks mirrored to those formed in the previous push cycle were identified.

According to the procedure outlined in section 4.5, the measured lateral forces for the two directions of loading resulted in an average yield displacement of:

$$\Delta_y = 0.5\left(\frac{76.1}{61.0}\times 1.45 + \frac{76.1}{60.6}\times 1.56\right) = 1.89 \text{ mm}$$

μ_2 push, 1st cycle

A maximum strength of 79.0 kN was recorded for this loading cycle. Extensions to existing diagonal cracks were identified. As shown in Figure A.7.2, diagonal cracks on the central pier elongated to reach the compression toe. It was clearly shown that diagonal cracks formed at this stage of testing correlated well with the strut-and-tie model (see section 4.1.2). A maximum crack width of about 2.0 mm was identified.

μ_2 pull, 1st cycle

A maximum strength of -82.2 kN was recorded. Three new diagonal cracks and elongations to existing cracks were identified. A maximum crack width of about 1.0 mm was identified.

μ_2 push, 2nd cycle

A maximum strength of 71.7 kN was recorded at the conclusion of this loading cycle. No new cracking or crack extensions were identified.

μ_2 pull, 2nd cycle

A maximum strength of -73.9 kN was recorded for this loading cycle. No new cracking was identified.

Figure A.7.2 Condition of test wall at end of first ductility 2 push cycle.

Figure A.7.3 Condition of test wall at end of first ductility 4 pull cycle.

μ_4 push, 1st cycle

A maximum strength of 82.8 kN was measured at the displacement of 7.89 mm. This strength was about 68% more than that prescribed by NZS 4229:1999. Elongation and widening of cracks formed in the previous push cycles were identified, with crack width (on central pier) up to 6.5 mm being identified. New diagonal cracks were only identified on the right pier. Grinding movement of masonry caused the commencement of mortar crushing along diagonal cracks.

μ_4 pull, 1st cycle

A "splitting" noise was heard when the wall was being pulled to a displacement of about -6.5 mm due to the widening of diagonal cracks formed in the previous pull cycles, but no strength loss was observed. The wall strength continued to increase to a maximum of –82.5 kN at the end this loading stage. Upon close observation, it was established that wall cracking patterns significantly mirrored to those observed in the previous push cycle. Also identified was the elongation of diagonal cracks to reach the upper right bond beam corner. Despite the presence of cracking on the bond beam, it was established that such damage was insignificant to affect the performance of the bond beam. A maximum crack width of about 7.5 mm was identified. The wall condition at this stage of testing is shown in Figure A.7.3.

μ_4 push, 2nd cycle

A maximum strength of 72.7 kN was measured. No new cracking or crack extensions were identified. Diagonal cracks were slightly widened to a maximum width of 8.5 mm.

μ_4 pull, 2nd cycle

A maximum strength of -66.4 kN was recorded at the displacement of -7.89 mm. No new cracking or crack extensions were identified.

μ_6 push, 1st cycle

A maximum strength of 74.8 kN was recorded at the target displacement. No new crack, but elongations and widening of existing diagonal cracks were identified, with crack width up to 11 mm being identified. The grinding movement of masonry had resulted in further crushing of mortar along diagonal cracks.

μ_6 pull, 1st cycle

The wall responded similar to observations made in the previous push cycle. A maximum strength of -59.7 kN was recorded at the target displacement. This strength corresponded to about 72% of the maximum strength achieved in the pull direction. Hence, the wall was defined as failing according to the test procedure outlined in section 4.5. No new crack was identified, but further elongations and widening of diagonal cracks were observed. The widening of cracks had resulted in further deterioration of masonry bond beam at the top right corner of the wall.

μ_6 push, 2nd cycle

A maximum strength of 61.1 kN was recorded at the displacement of 12.03 mm. No new crack was identified, but further widening of diagonal cracks were identified.

μ_6 pull, 2nd cycle

The wall responded similarly to observation made in the previous push cycle. A maximum strength of -47.4 kN was recorded for this load step.

μ_8 push, 1st cycle

A maximum strength of 67.0 kN was recorded at the displacement of 17.0 mm. No new cracking was identified. Further elongations and widening of diagonal cracks were observed to cause the spalling of masonry face shells.

μ_8 pull, 1st cycle

The wall responded similarly to observations made in the previous push cycle. A maximum strength of -53.6 kN was recorded at the target displacement.

μ_8 push, 2nd cycle

No new cracking or extensions of cracks were identified. A maximum strength of 51.3 kN was recorded at the target displacement. Upon stress released, a "hollow" sound was heard when hand tapping the face shells in the top right bond beam region, indicating the onset of face shell delamination. Consequently, the face shells were removed upon unloading to avoid damage to the measuring instruments that could be caused by fallen objects. The wall condition at this stage of testing is shown in Figure A.7.4.

μ_8 pull, 2nd cycle

A maximum strength of -46.4 kN was recorded at the corresponding displacement of -16.0 mm. No new cracking or extensions of cracks were identified.

μ_{10} push, 1st cycle

A maximum strength of 54.0 kN was recorded at the target displacement. No new cracking was identified. The wall response was dominated by the degradation and widening of existing diagonal cracks.

μ_{10} pull, 1st cycle

The wall response was similar to observations made in the previous push cycle. A maximum strength of -48.9 kN was measured at the displacement of -20.1 mm.

μ_{10} push, 2nd cycle

A maximum strength of 49.7 kN was measured in this pushing cycle. No new crack or extensions of cracks were identified. Further widening of diagonal cracks was observed.

μ_{10} pull, 2nd cycle

The wall response was similar to observations made in previous push cycle. A maximum strength of –39.3 kN was recorded at the completion of this loading stage.

μ_{12} push, 1st cycle

A maximum strength of 51.9 kN was recorded at the displacement of 24.1 mm. The grinding movement of masonry along diagonal cracks resulted in further spalling of face shells.

μ_{12} pull, 1st cycle

Similar to previous push cycle, the wall response was dominated by the further widening of existing diagonal cracks, with crack width up to 18 mm. A maximum strength of -47.8 kN was measured in this pulling cycle.

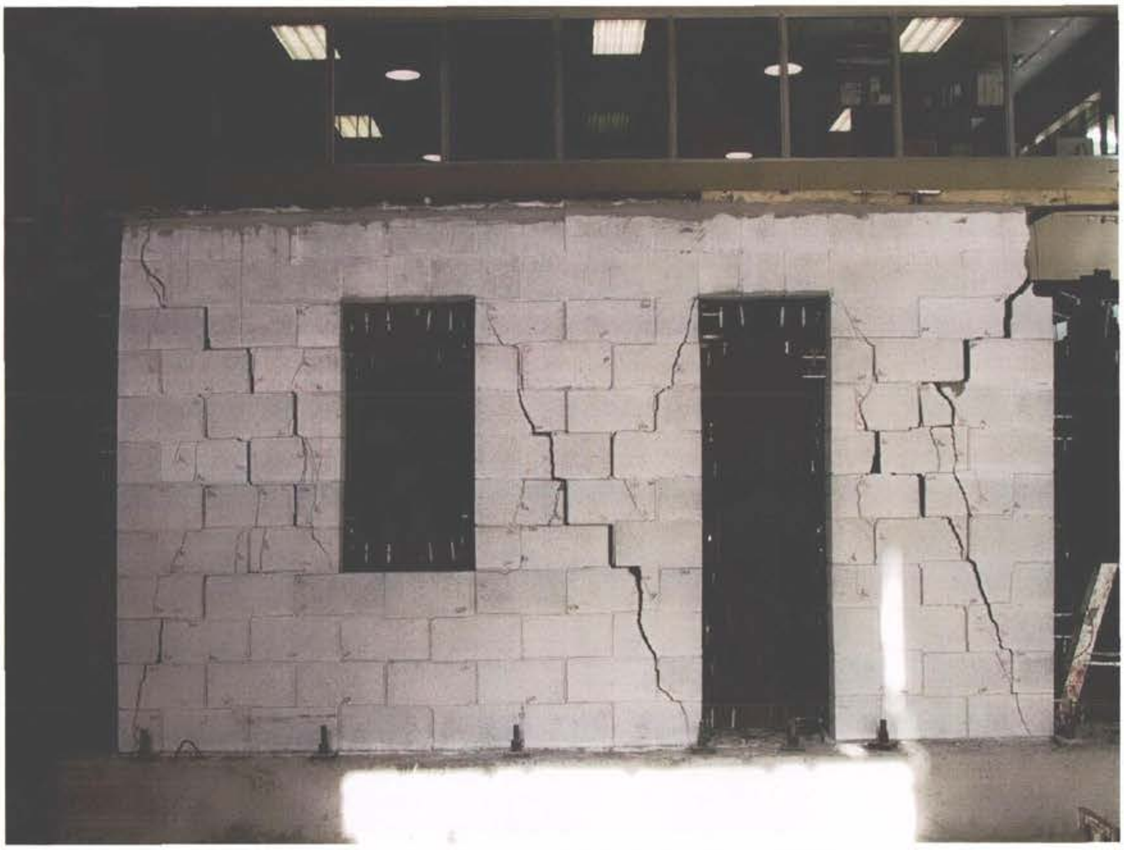

Figure A.7.4 Condition of test wall at end of second ductility 8 push cycle.

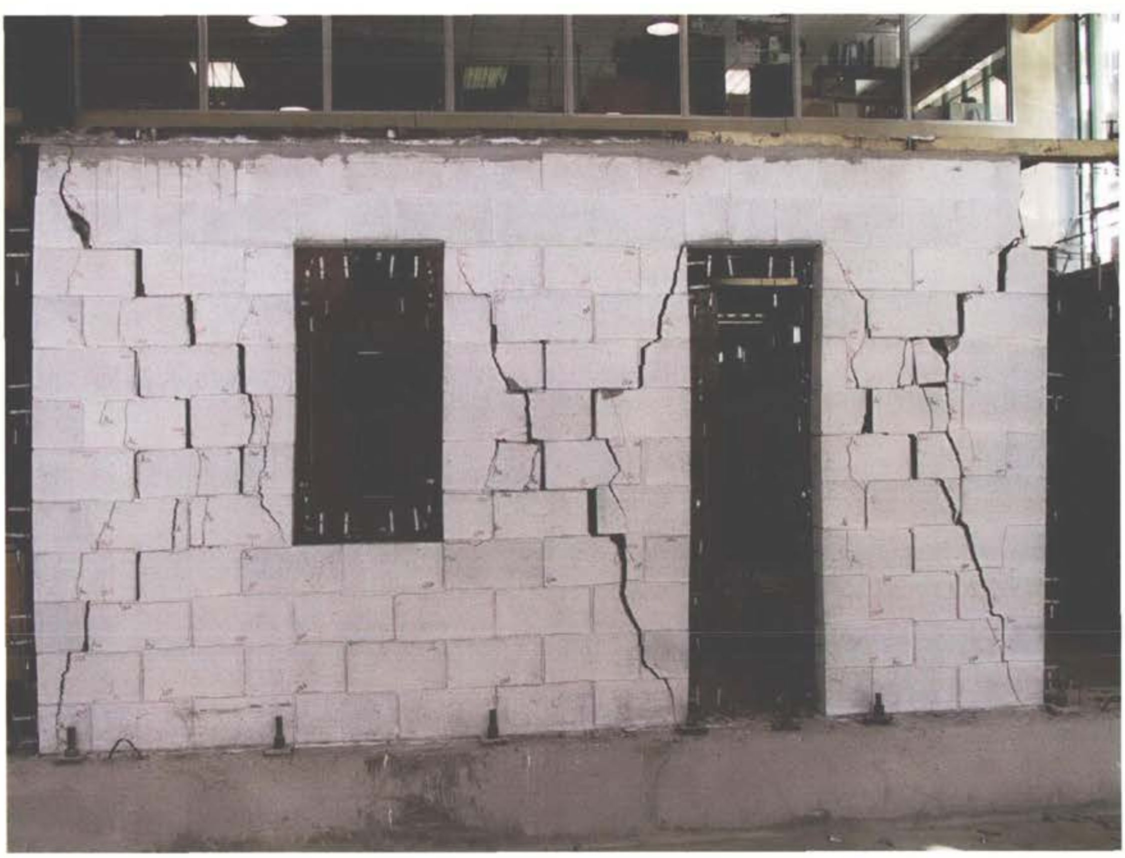

Figure A.7.5 Condition of test wall at end of first ductility 14 push cycle.

μ_{12} push, 2nd cycle

A maximum strength of 46.2 kN was measured at the target displacement of 24.0 mm.

μ_{12} pull, 2nd cycle

A maximum strength of -38.0 kN was measured for this loading cycle.

μ_{14} push, 1st cycle

The wall response was dominated by the widening of existing cracks, with maximum crack width of about 25 mm being identified. A maximum strength of 49.2 kN was recorded for this loading cycle. The wall condition at this stage of testing is shown in Figure A.7.5.

μ_{14} pull, 1st cycle

The wall responded similarly to observations made in the previous push cycle. A maximum strength of -43.8 kN was recorded.

μ_{14} push, 2nd cycle

No new crack or extensions of cracks were identified. A maximum strength of 41.2 kN was recorded at the displacement of 28.2 mm.

μ_{14} pull, 2nd cycle

No new crack or extensions of cracks were identified. A maximum strength of -31.0 kN was recorded at the displacement of -29.4 mm.

A.7.3 Summary Behaviour

The measured force-displacement curve for Wall 7 is presented in Figure A.7.6, depicting the lateral displacement at the top of the wall as a function of the applied lateral force. The maximum push and pull direction strengths of 82.8 kN and -82.5 kN were measured during the first cycle to displacement ductility 4. Despite the presence of widely open diagonal cracks, the wall exhibited a gradual and fairly symmetrical strength degradation of strength in both loading directions. Consequently, it was possible to classify Wall 7 as having a failure mode of diagonal tension. The desirable behaviour of this nominally reinforced partially grout-filled concrete masonry wall with openings was created by the solid filled bond beam at the top of the wall, which caused a frame-type action at latter stage of testing.

As shown in Figure A.7.6, it was established that the maximum strength achieved by Wall 7 was about 68% higher than the bracing capacity prescribed by NZS 4229:1999. Consequently, the experimental result of Wall 7 further suggests that an increased conservatism of NZS 4229:1999 may result when the length of a perforated masonry wall containing is increased. Experimental result of Figure A.7.6 illustrates that strength prediction using the improved strut-and-tie model under-predicted the wall strength by about 34% and 8% in the respective push and pull directions.

It was illustrated in Figures A.7.2 to A.7.5 that the diagonal cracking pattern of this wall aligned well with the load paths by which shear force was transferred to the foundation in the strut mechanism. This observation supports the use of strut-and-tie analysis as the tool to evaluate the strength of perforated walls with reinforcement details complying with specification of NZS 4229:1999. However, strength prediction using the simplified strut-and-tie analysis was about 65% less than the actual strength of this wall.

The average yield displacement (Δ_y) for this partially grouted wall was evaluated to be 1.89 mm. The test wall was defined as failing during the first pull cycle to displacement ductility 6, giving it a ductility capacity μ_{av} of 3.75.

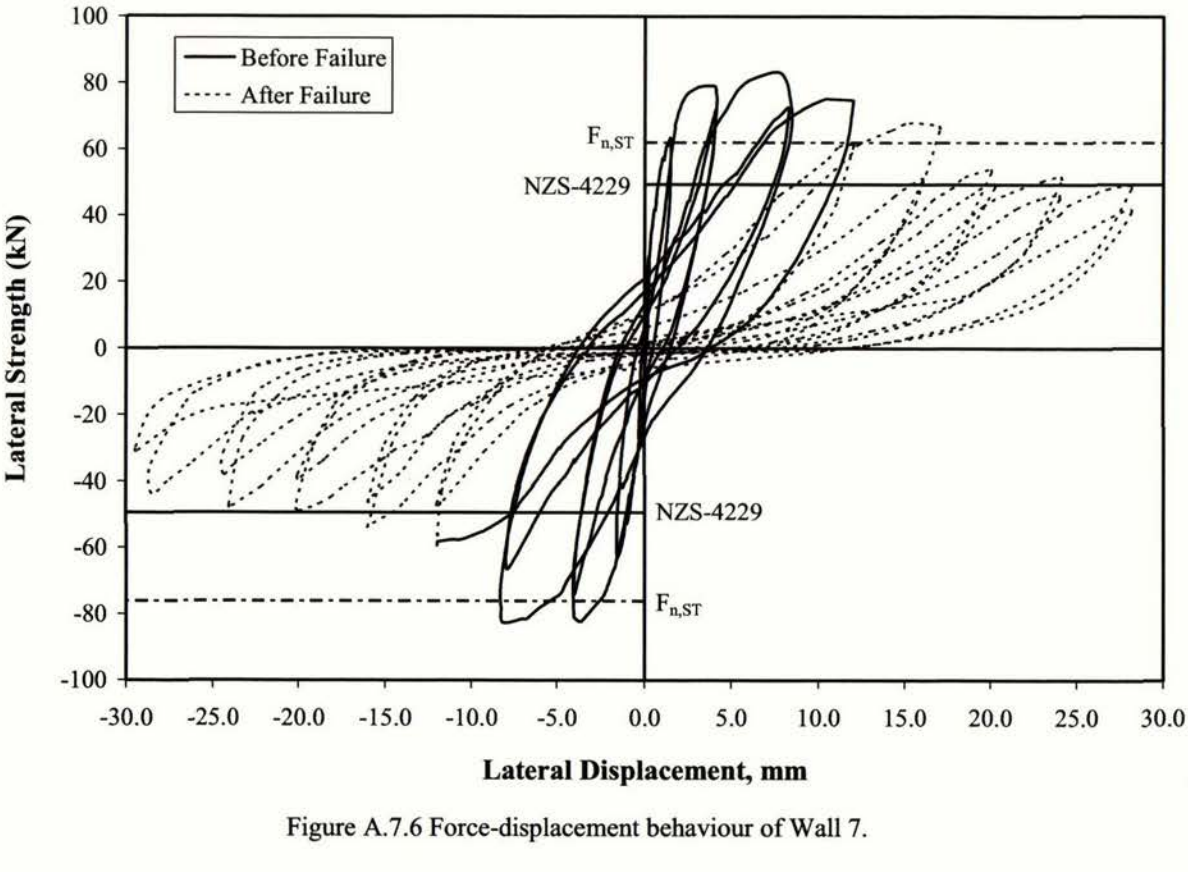

Figure A.7.6 Force-displacement behaviour of Wall 7.

A.7.4 Panel Displacement Components

The total horizontal displacement of the wall was decomposed into four components according to the procedure outlined in section 4.7 with the results as shown in Figure A.7.7. It is clearly demonstrated that shear displacement was the single most dominant deformation mode. The large shear deformation shown in Figure A.7.7 was consistent with the presence of large quantity of widely open diagonal cracks on the test wall. The influences of rocking, sliding and flexural component of deformations were negligible throughout the test.

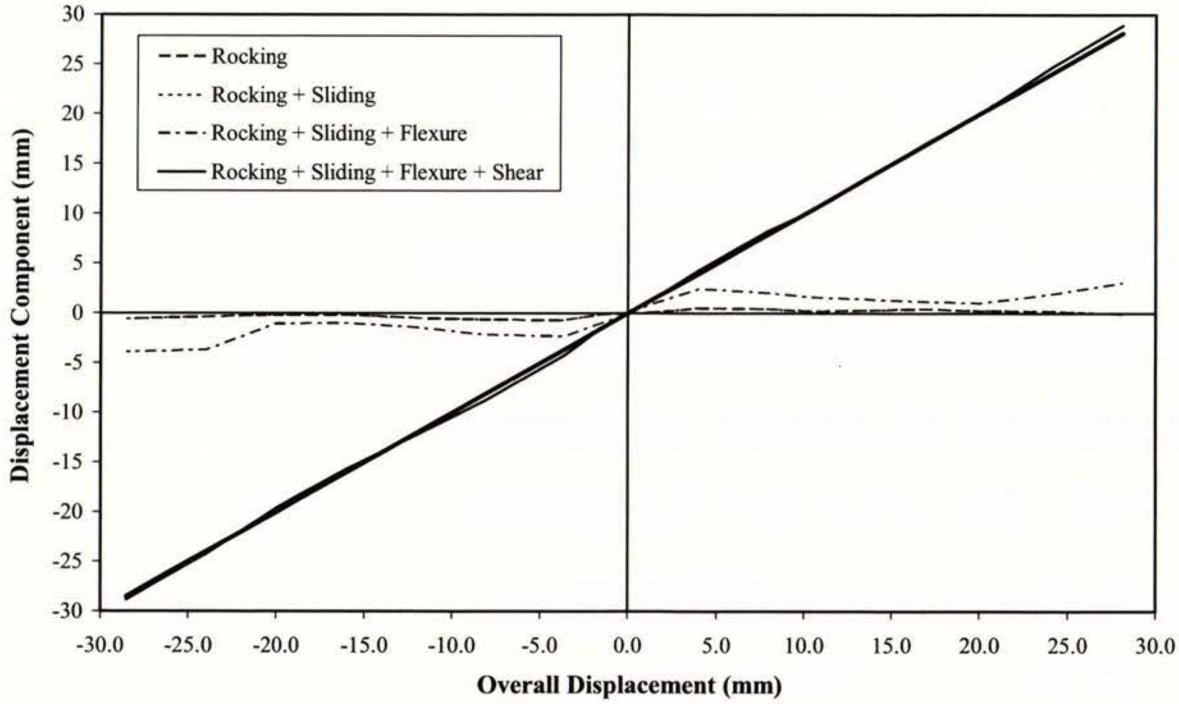

Figure A.7.7 Components of displacement.

A.8 Wall 8

This section describes the laboratory test of Wall 8. The wall geometry and reinforcement details are shown in Figure A.8.1. The wall nominal shear (V_n) was established to be 122.4 kN and the flexural (F_n) strengths calculated according to the improved strut-and-tie model described in section 4.1.3, were established to be 61.6 kN and 79.7 kN for the pushing and pulling directions respectively.

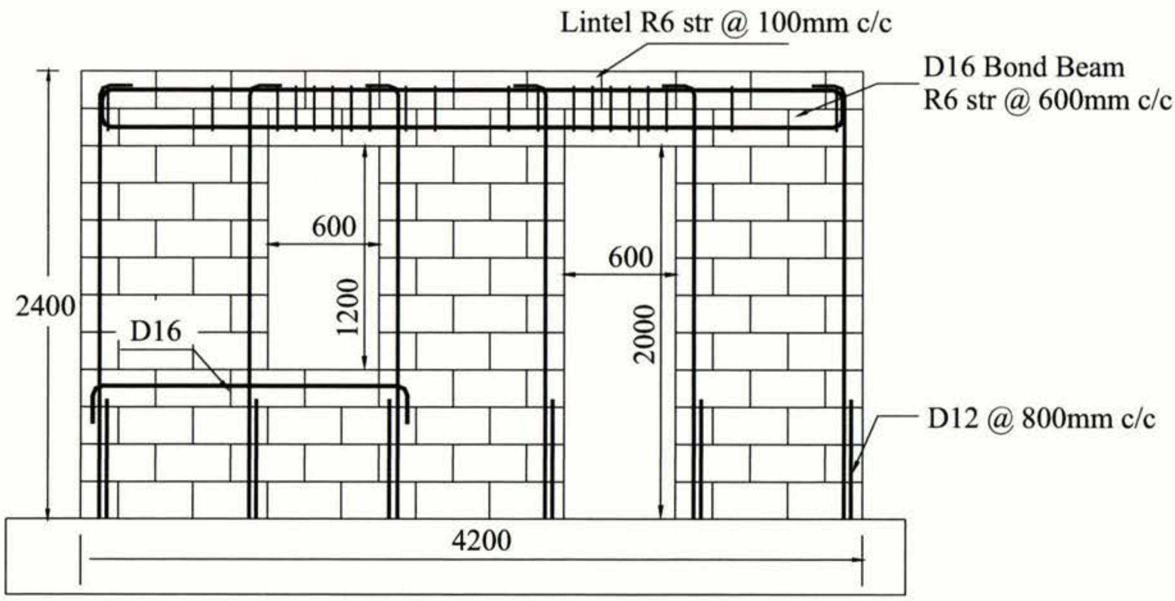

Figure A.8.1 Wall 8 geometry and reinforcing details.

A.8.1 Pre-test

The masonry wall was tested on the 45th days after construction. Instrumentation was attached to the wall according to section 3.5.1. Prior to wall testing the wall was inspected, with no cracks or structural defects being identified.

A.8.2 Testing

$^{3}/_{4}$ F_n push,

An applied force of 56.8 kN was recorded when the wall was pushed away from the strong wall. A corresponding displacement of 1.40 mm was recorded for this loading cycle. Hairline horizontal flexural cracks were identified along the mortar joints on the wall tension edge. These cracks were observed to close upon stress released.

Consequently, the measured lateral forces for this push direction of loading resulted in a yield displacement of:

$$\Delta_y = \frac{61.6}{56.8} \times 1.40 = 1.52 \text{ mm}$$

$^3/_4\, F_n$ pull,

An applied strength of -63.4 kN was recorded at the displacement of -1.33 mm. Hairlines horizontal cracks were identified on the wall tension edge. Similar to the previous push cycle, these horizontal cracks were observed to close upon load released.

Consequently, the measured lateral forces for the pull direction of loading resulted in a yield displacement of:

$$\Delta_y = \frac{79.7}{63.4} \times 1.33 = 1.67 \text{ mm}$$

Due to the difference of 0.15 mm for the yield displacements of the two loading directions, an average Δ_y of 1.60 mm was chosen as the yield displacement for both loading directions for convenience.

μ_2 push, 1st cycle

A maximum strength of 81.8 kN was recorded. Diagonal cracks were identified throughout the wall (3 diagonal cracks on the right pier-of which 1 crack extended beneath window, 5 diagonal cracks on the central pier and 4 diagonal cracks on the left pier). A maximum crack width of 1.6 mm was identified.

μ_2 pull, 1st cycle

A maximum strength of –85.0 kN was recorded. Diagonal cracks (significantly mirrored to those observed in the previous push cycle) consistent with the strut mechanism were identified on all three piers. A maximum crack width of about 1.3 mm was identified.

μ_2 push, 2nd cycle

A maximum strength of 72.8 kN was recorded at the conclusion of this loading cycle. No new cracking or extensions to previously formed cracks were identified.

μ_2 pull, 2nd cycle

A maximum strength of -80.4 kN was recorded for this loading cycle. No new cracking was identified.

μ_4 push, 1st cycle

A "splitting" noise was heard when the wall was pushed to a displacement of about 5.15 mm due to the sudden widening of diagonal cracks formed in the previous push cycles, but no strength loss was observed. The wall strength continued to increase to a maximum of 82.7 kN at the end of this loading stage. Upon close observation, it was identified that the wall response was mostly dominant by the elongations and widening of existing cracks. Diagonal cracks on the left and central piers were elongated to reach the compression toes. Elongations of diagonal cracks on the right pier caused minor spalling of masonry face shell at the window edge. Also identified was the elongation of diagonal cracks to reach the upper right bond beam corner. Despite the presence of cracking on the bond beam, it was established such damage was insignificant to affect the structural performance of the bond beam. Maximum crack width of 5.8 mm was identified. In addition to crack elongations, new hairline diagonal cracks were also identified on all three piers. The wall condition at this stage of testing is shown in Figure A.8.2.

μ_4 pull, 1st cycle

Maximum wall strength of -93.2 kN was recorded at the completion of this loading stage. Upon close observation, wall cracking patterns significantly similar to the strut mechanisms presented in section 4.1.2 were identified (see also Figure A.8.3). A vertical crack beneath the fully grouted trimming reinforcement (adjacent to the compression wall edge on the right pier) was identified at the completion of this loading stage. Also identified were the elongation and widening of existing diagonal cracks, with maximum crack width of about 7.5 mm being identified. In addition, elongations of diagonal cracks on the left pier were observed to reach upper left bond beam corner. However, the presence of such cracking on the bond beam was insignificant to affect the structural performance of the bond beam.

Figure A.8.2 Condition of test wall at end of first ductility 4 push cycle.

Figure A.8.3 Condition of test wall at end of first ductility 4 pull cycle.

μ_4 push, 2nd cycle

A maximum strength of 62.6 kN was measured for his loading cycle. This strength corresponded to about 76% of the maximum strength achieved in the push direction. Hence the wall was defined as failing according to the test procedure outlined in section 4.5. No new crack was identified, but further elongations and widening of diagonal cracks were observed. Diagonal cracks were slightly widened to a maximum width of 9.5 mm.

μ_4 pull, 2nd cycle

A maximum strength of -62.6 kN was recorded. No new cracking or extensions of cracks were identified.

μ_6 push, 1st cycle

A maximum strength of 72.5 kN was recorded for this loading cycle. No new crack, but elongations and widening of existing diagonal cracks were identified, with crack width up to 13 mm. Grinding movement of masonry along diagonal cracks resulted in minor crushing of mortar.

μ_6 pull, 1st cycle

A maximum strength of -65.6 kN was recorded for this loading cycle. Similar to previous push cycle, the wall response was dominant by the widening of existing cracks.

μ_6 push, 2nd cycle

A maximum strength of 60.1 kN was recorded for this loading cycle. No new crack was identified.

μ_6 pull, 2nd cycle

A maximum strength of -55.9 kN was recorded for this load step. No new cracking was identified.

μ_8 push, 1st cycle

A maximum strength of 69.1 kN was recorded at the displacement of 15.2 mm. No new cracking was identified. Further elongations and widening of diagonal cracks were observed.

μ_8 pull, 1st cycle

A maximum strength of -56.1 kN was recorded at the target displacement. Further widening of vertical crack (below the trimmer bar) caused further degradation of compression toe on the right pier.

μ_8 push, 2nd cycle

No new cracking or extensions of cracks were identified. A maximum strength of 64.9 was recorded at the target displacement. No new cracking was identified. The wall condition at this stage of testing is shown in Figure A.8.4.

μ_8 pull, 2nd cycle

A maximum strength of -46.0 kN was recorded at a corresponding displacement of -15.3 mm. No new cracking was identified. See Figure A.8.5 for wall condition at this stage of testing.

μ_{10} push, 1st cycle

A maximum strength of 64.1 kN was recorded for this loading cycle. No new cracking was identified. The wall response was dominated by the degradation and widening of existing diagonal cracks.

μ_{10} pull, 1st cycle

The wall response was dominant by the widening of existing cracks. A maximum strength of -51.5 kN was measured for this loading cycle.

μ_{10} push, 2nd cycle

A maximum strength of 59.1 kN was measured in this pushing cycle. No new crack was identified. Further widening of diagonal cracks was observed.

μ_{10} pull, 2nd cycle

A maximum strength of –43.1 kN was recorded at the completion of this loading stage.

Figure A.8.4 Condition of test wall at end of second ductility 8 push cycle.

Figure A.8.5 Condition of test wall at end of second ductility 8 pull cycle.

A.8.3 Summary Behaviour

The force-displacement history of Wall 8 is shown in Figure A.8.6. The maximum push and pull direction strengths of 82.7 kN and -93.2 were measured during the first cycle to displacement ductility 4. Despite the lack of distributed horizontal shear reinforcement and the fact that the wall was partially grout-filled, the wall exhibited gradual strength degradation in both loading directions. Consequently, it was possible to classify Wall 8 as having a failure mode of diagonal tension. This type of failure was characterised by the development of early horizontal flexural cracking, which was later exaggerated by diagonal cracking that extended throughout the wall panels. The desirable behaviour of this perforated masonry wall was created by the solid filled bond beam at the top of the wall, which caused a frame-type action at latter stage of testing. This notion was supported by the absence of significant structural damage in the bond beam. Furthermore, the force-displacement plot in Figure A.8.6 consistently illustrated a pinched shape. This was primarily due to the presence of significant shear deformation in this type of masonry construction (see section A.8.4). It was also observed that less hysteretic energy was expended during the second cycle to any displacement level, when compared with the first displacement cycle. This is illustrated by the more pinched hysteresis loops of the second cycle.

As shown in Figure A.8.6, the conservatism of NZS 4229:1999 was higher in the pulling direction than that in the pushing direction. A stronger strength in the pulling direction was resulted due to the presence of an extended trimmer reinforcement on the left pier. Consequently, the experimental result of Wall 8 successfully illustrates that an increased conservatism of NZS 4229:1999 may result when the length of trimmer reinforcement is extended below an opening.

It was illustrated in Figures A.8.2 to A.8.5 that the diagonal cracking patterns on this wall aligned well with the load paths by which shear force was transferred to the foundation in the strut mechanism (see also section 4.1.2). This observation supports the use of strut-and-tie analysis as the tool to evaluate the strength of walls with reinforcement details complying with specification of NZS 4229:1999. However, the wall actual strength was about 65% higher than that predicted using the simplified strut-and-tie model. Figure A.8.6, the strength developed by the wall was about 34% and 16% more than those predicted according to the improved strut-and-tie models in the respective push and pull directions.

Due to the non-symmetrical arrangement of trimming reinforcement, the yield displacements (Δ_y) for this partially grouted wall were evaluated to be 1.52 mm and 1.67 mm in the push and pull directions respectively. However, due to the slight difference of yield displacements for the two loading directions, an average Δ_y of 1.60 mm was chosen as the yield displacement for the two loading directions for convenience. The test wall was defined as failing during the second push cycle to displacement ductility 4, giving it a ductility capacity μ_{av} of 2.0.

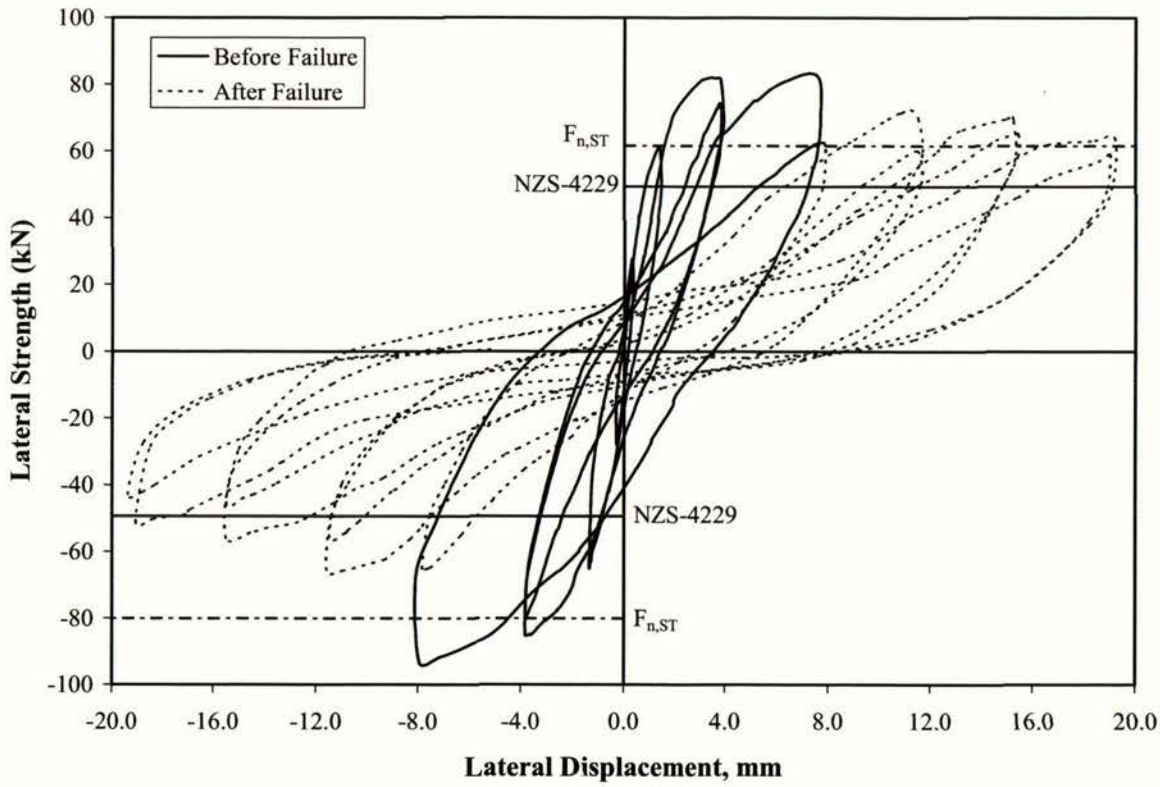

Figure A.8.6 Force-displacement behaviour for Wall 8.

A.8.4 Panel Displacement Components

The total horizontal displacement of the wall was decomposed into four components according to the procedure outlined in section 4.7 with the results as shown in Figure A.8.7. Similar to other test results presented earlier, it is seen that shear displacement was the single most dominant deformation mode. The rocking, sliding and flexural displacement components were insignificant throughout the test. Figure A.8.7 provides an indication of the relative size of each displacement component at various stages of the displacement envelope until displacement ductility ±8 (15.2 mm displacement).

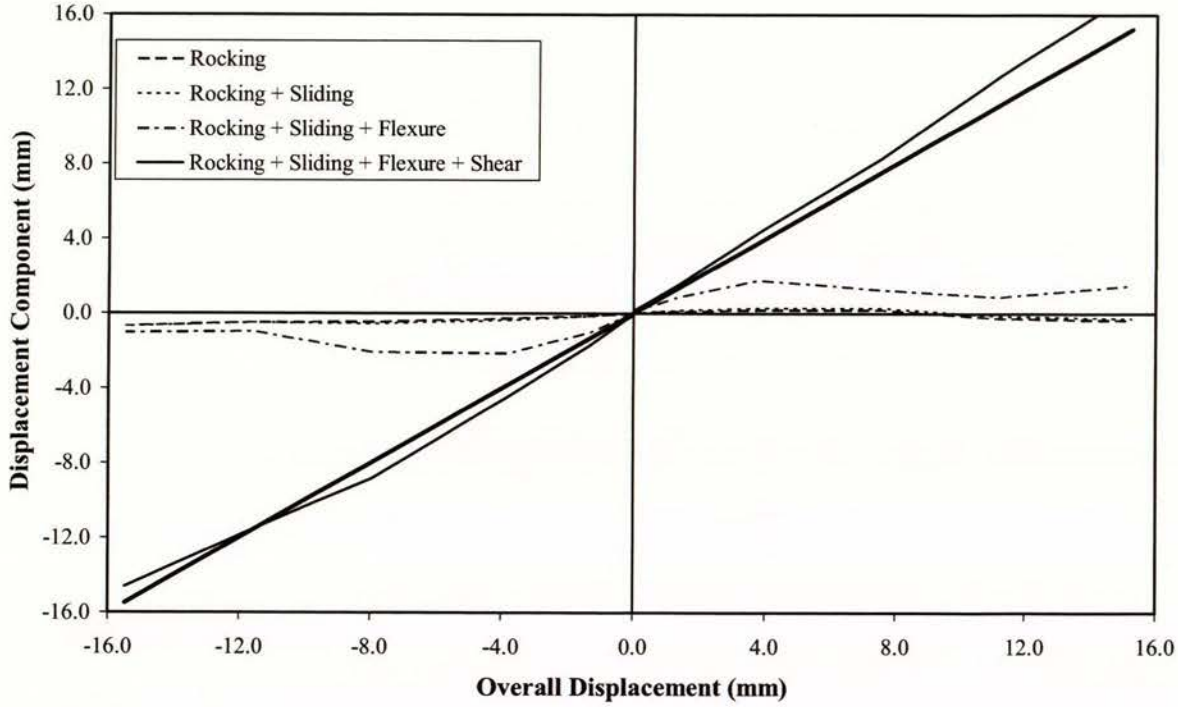

Figure A.8.7 Components of displacement.

Appendix B

Experimental Results – Series B "Walls with Control Joints"

Cracking due to shrinkage from drying or temperature drop is a major problem in concrete masonry walls. Masonry cracks when the shrinking tendency is restrained. In masonry walls, the restraint arises from several sources, such as the foundation line. If the masonry wall is allowed to contract freely, no stress is accumulated and therefore no cracking will occur.

Control joints are one method used to relieve horizontal tensile stresses due to shrinkage of the concrete masonry units, mortar, and when used, grout. They are essentially vertical separations built into the wall at locations where stress concentration may occur. Control joints are typically only required in exposed concrete masonry walls, where shrinkage cracking may detract from the appearance of the wall. Shrinkage cracks in concrete masonry walls are an aesthetic, rather than a structural problem. In many cases, strategically located control joints could eliminate random cracking, and prevent moisture penetration which might otherwise occur.

NZS 4229:1999 has prescribed a procedure to account for shrinkage control joints, but this detail has never been verified through structural testing. Consequently, two nominally reinforced partially grout-filled concrete masonry walls were tested under cyclic lateral loading at the University of Auckland in order to validate the structural adequacy of the shrinkage control joint detail published in NZS 4229:1999.

These two concrete masonry walls were constructed of 15 series CMUs, which resulted in an effective wall thickness of 60 mm for a partially grout-filled wall. These two walls were constructed to the same height and length of 2.4 m x 3.6 m but differed in the detailing of bond beam reinforcement at the control joint position.

The experimental results from these two concrete masonry walls are presented in Appendix B. These results played a significant role in formulating the conclusions of this report. For information about wall construction, test set-up, testing procedure and data reduction please refer to Chapters 3 and 4. The experimental results presented in this Appendix defines displacement in the push direction as positive while displacement in the pull direction as negative.

B.1 Wall 9

This section describes the laboratory test of Wall 9. The wall geometry and reinforcement details are shown in Figure B.1.1. The control joint of Wall 9 was constructed in accordance with the specifications of NZS 4229:1999 where the joint was terminated below the bond beam and the D16 longitudinal bond beam reinforcement was continuous through the joint. The wall nominal shear strength (V_n), calculated according to the shear expressions presented in section 4.3, was established to be 169.0 kN. The nominal flexural strength (F_n) of this wall was calculated as the combined strengths of two individual (1800 mm long) cantilever walls since it was expected that the presence of the 10 mm gap would prevent the proper transfer of shear force across the control joint. Consequently, the wall flexural strength was established to be 80.2 kN according to the $F_{n,st}$ presented in section 4.1.2.

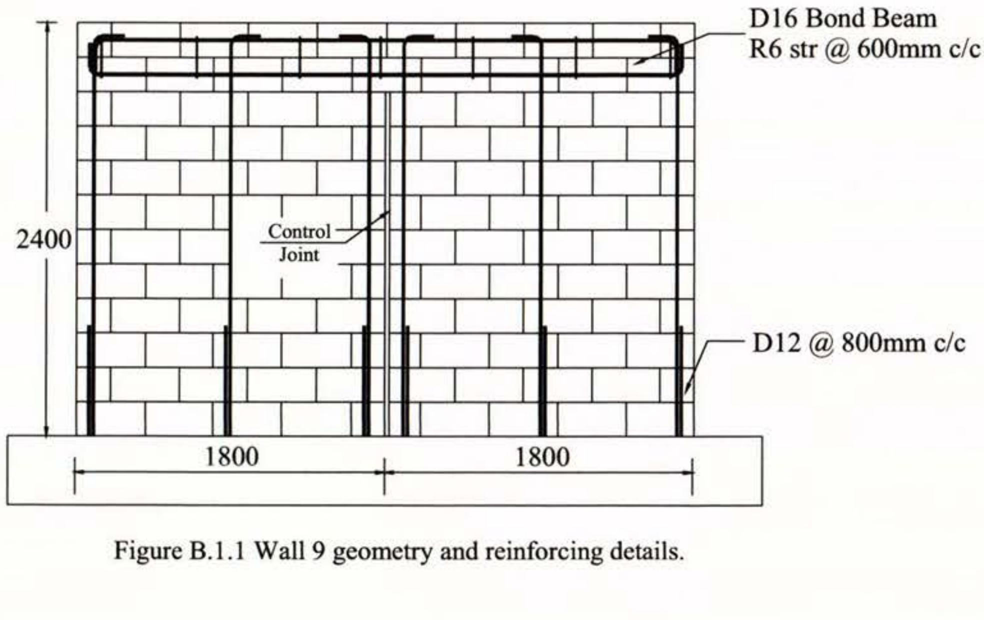

Figure B.1.1 Wall 9 geometry and reinforcing details.

B.1.1 Pre-test

The masonry wall was tested on the 60[th] days after construction. Instrumentation was attached to the wall according to section 3.5.1. Prior to wall testing the wall was inspected, with no cracks or structural defects being identified.

B.1.2 Testing

$^3/_4\,F_n$ push,

An applied force of 59.5 kN was recorded when the wall was being pushed away (towards the right) from the strong wall. A corresponding displacement of 0.77 mm was recorded for this loading cycle. No clear evidence of cracking.

$^3/_4\,F_n$ pull,

A maximum strength of -61.2 kN was recorded at the displacement of -0.83 mm. No cracking was identified.

According to the procedure outlined in section 4.5, the measured lateral forces for the two directions of loading resulted in an average yield displacement of:

$$\Delta_y = \frac{4}{3}\left(\frac{0.77+0.83}{2}\right) = 1.07 \text{ mm}$$

μ_2 push, 1st cycle

A maximum strength of 77.3 kN was recorded at the peak displacement of this load step. Hairline diagonal cracks were identified along mortar bed joints, initiating from the tension edges of each pier (5 diagonal cracks on the left pier and 3 diagonal cracks on the right pier). Maximum crack width of about 0.5 mm was identified.

μ_2 pull, 1st cycle

Cracking pattern mirrored to those observed in the previous push cycle was identified. 4 diagonal cracks were identified on the left pier accompanied by 6 diagonal cracks on the right pier. A maximum strength of -77.2 kN at the conclusion of this load cycle.

μ_2 push, 2nd cycle

A maximum strength of 65.0 kN was recorded. No new cracking was identified.

μ_2 pull, 2nd cycle

A maximum strength of -63.0 kN was recorded. No new cracking was identified.

μ_4 push, 1st cycle

The wall developed a maximum strength of 89.5 kN, exceeding the predicted $F_{n,st}$ of 80.2 kN. Extensions of previously formed diagonal cracks were noted on both piers, with a maximum crack width of about 1.3 mm, which was sufficient to allow daylight to pass through. Diagonal cracks were observed to elongate to reach the compression toes of both piers. Also observed was the elongation of diagonal crack towards the bond beam corner on top of the left pier. The width of control joint was measured to reduce by about 2 mm at the wall mid-height position.

μ_4 pull, 1st cycle

A maximum strength of -95.3 kN was recorded in this load cycle. Elongations of diagonal cracks mirrored to those observed in the previous push cycle were identified. Similar to the previous push cycle, the control joint was measured to close by about 2.2 mm at the wall mid height position.

μ_4 push, 2nd cycle

A maximum strength of 81.2 kN was measured. No new cracking or extensions of cracks were identified.

μ_4 pull, 2nd cycle

No new cracking or extensions of cracks were identified. A maximum strength of -89.6 kN was measured.

μ_6 push, 1st cycle

A maximum strength of 101.8 kN was recorded at the displacement of 6.55 mm. No new crack, but elongations and widening of existing diagonal cracks were identified, with crack width up to 4.0 mm. The face shells and mortar beds along the diagonal cracks showed sign of distress. Further closing of the control joint was identified. The control joint at the wall mid-height position was measured to remain about 4.3 mm in width.

μ_6 pull, 1st cycle

The wall responded similarly to observations made in the previous push cycle. A maximum strength of -99.4 kN was recorded at the displacement of -6.42 mm. No new crack, but widening of diagonal cracks was identified. The control joint at wall mid-height position was measured to remain about 3.4 mm in width. As shown in Figure B.1.2, the wall clearly showed mixed modes of deformation, with obvious shear deformation but also flexural cracking on wall tension edges. The figure also shows the significant closed similarity of wall cracking patterns on these two piers. The presence of a control joint below the fully grout-filled bond beam centre had resulted in two piers that performed (to a significant degree) independently of each other, as indicated by formation of diagonal cracks that significantly independent of each other (diagonal cracks initiated from the tension edges and ended at the compression toe of each pier). The fragmented crack pattern in the vicinities of the reinforcing bars indicated good bond between the reinforcement and the grouted cores. Overall, wall performance was satisfactory.

μ_6 push, 2^{nd} cycle

A maximum strength of 85.2 kN was recorded at the displacement of 6.25 mm. No new crack was identified.

μ_6 pull, 2^{nd} cycle

A maximum strength of -91.3 kN was recorded for this load step. No new crack was identified.

μ_8 push, 1^{st} cycle

In this cycle of loading, there was very little additional cracking. Wall deformation was predominately due to shear, signified by the widening of existing diagonal crack, with maximum crack width of about 5 mm. Also observed was the complete closing of control joint at the wall mid-height position, resulted in the partial transfer of shear force (through the points of contact) from the left pier to the right pier. A maximum strength of 109.2 kN was recorded at the displacement of 8.56 mm. This measured strength exceeded the predicted $F_{n,st}$ by 36%.

μ_8 pull, 1^{st} cycle

The wall responded similarly to observations made in the previous push cycle. Elongation and widening of previously formed diagonal cracks were identified. Similar to previous push cycle, the control joint (completely) closed at wall mid-height position, therefore resulted in the partial transfer of shear force through the contact points. A maximum strength of -110 kN was recorded for this loading step.

μ_8 push, 2nd cycle

The wall response was dominated by the elongation and widening of existing diagonal cracks. A maximum strength of 98.2 kN was recorded at the displacement of 8.58 mm.

μ_8 pull, 2nd cycle

The response was similar to those observed in the 1st cycle. A maximum strength of -98.9 kN was recorded at a corresponding displacement of -8.49 mm.

μ_{10} push, 1st cycle

A maximum strength of 117.8 kN was recorded at the target displacement. No new cracking was identified. The wall response was dominated by the widening of previously formed diagonal cracks, with maximum crack width of about 8 mm being identified. Fragmented cracks in the vicinities of the reinforcing bars were identified, therefore indicating good bond between the reinforcement and the grouted cores. Also, the control joint remained close at the wall mid-height position. Overall, wall performance was satisfactory.

μ_{10} pull, 1st cycle

The wall response was similar to observations made in the previous push cycle. A maximum strength of -109.2 kN was measured at the displacement of -10.8 mm. The wall condition at this stage of testing is shown in Figure B.1.3.

μ_{10} push, 2nd cycle

A maximum strength of 98.5 kN was measured in this loading step. No new crack or extensions of cracks were identified.

μ_{10} pull, 2nd cycle

The wall response was similar to observations made in the previous pull cycle. A maximum strength of -98.5 kN was recorded at the target displacement.

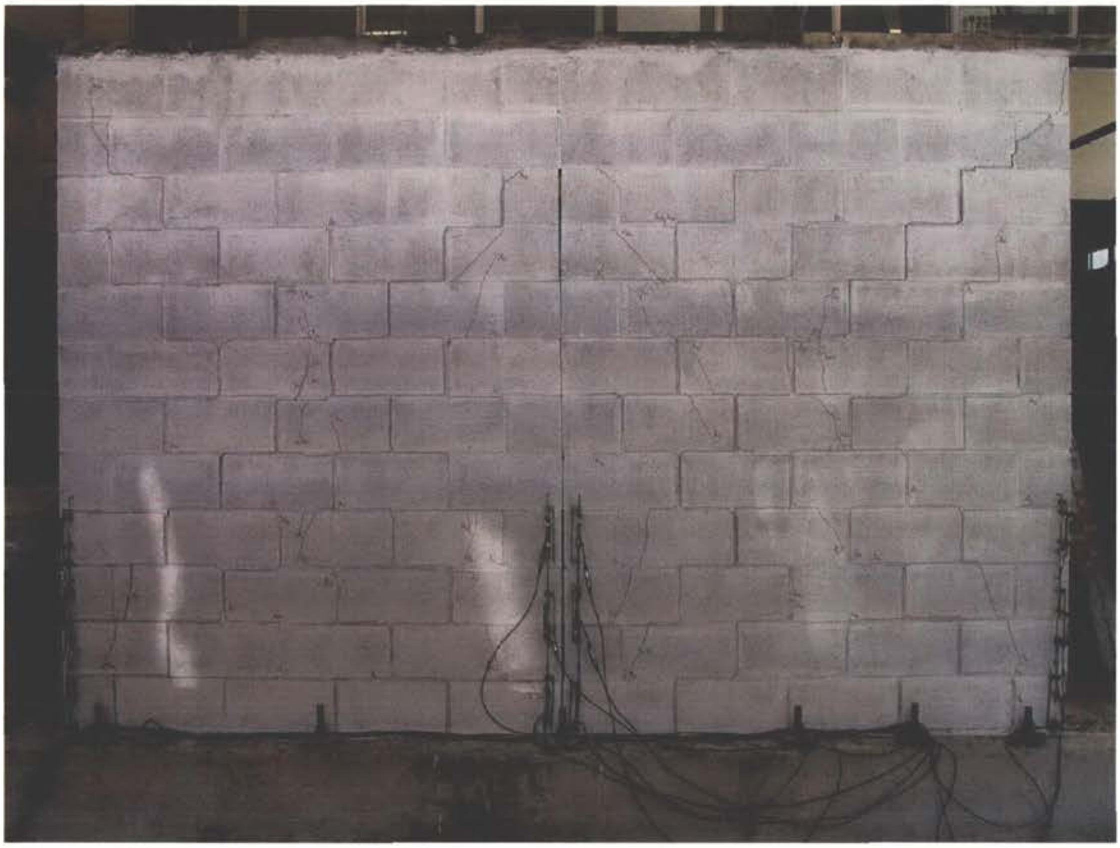

Figure B.1.2 Condition of test wall after first ductility 6 pull cycle.

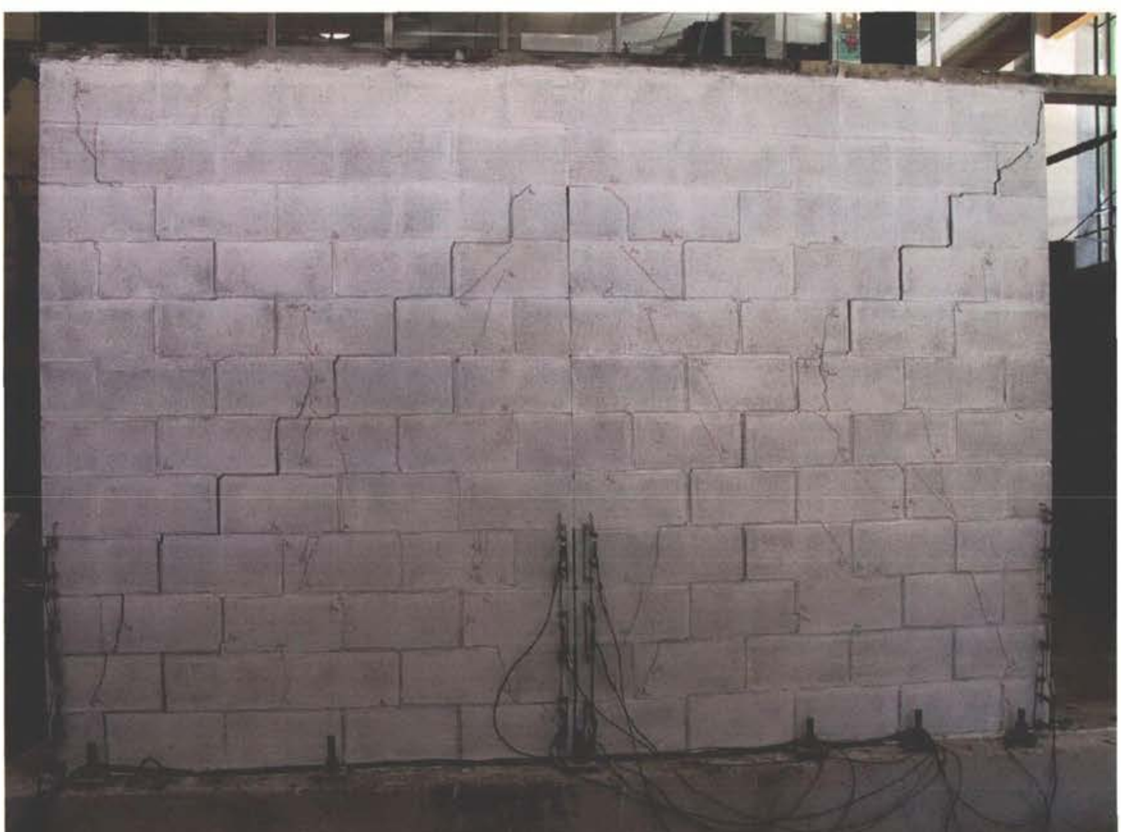

Figure B.1.3 Condition of test wall after first ductility 10 pull cycle.

μ_{14} push, 1st cycle

During this semi-cycle of loading, the wall developed a maximum strength of 125.3 kN at the lateral displacement of 13.85 mm. This was followed by a significant widening of diagonal crack at the lower halve section of the right pier, resulting in a sudden displacement increase (maximum crack width about 9.5 mm) and a corresponding loss in strength. A strength of 117.9 kN was recorded when the wall settled at the displacement of 15.08 mm. The grinding movement of masonry along diagonal cracks resulted in (first sign) mortar crushing. Also observed was the degradation of masonry face shells along the stress paths on both piers.

μ_{14} pull, 1st cycle

The wall response was dominated by further widening of diagonal cracks formed in previous cycles. A maximum strength of -114.6 kN was measured at the displacement of -14.97 mm.

μ_{14} push, 2nd cycle

No new crack or extensions of cracks were identified. A maximum strength of 86.0 kN was measured at the displacement of 15.43 mm. This strength corresponded 69% of the maximum strength recorded in the push direction. Therefore the wall was defined as failing according to the test procedure outlined in section 4.5.

μ_{14} pull, 2nd cycle

No new crack or extensions of cracks were identified. Further degradation of face shells along diagonal cracks was identified. A maximum strength of -92.44 kN was measured at the displacement of -15.03 mm.

μ_{18} push, 1st cycle

The wall strength (maximum of 117.9 kN) dropped suddenly when it was push to a displacement of 18.4 mm. The sudden loss in strength was accompanied by an instantaneous increment of wall lateral displacement to 19.6 mm. Inspection of the wall revealed elongation of cracks (on right pier) towards the compression toe and significant widening of existing diagonal cracks, with maximum crack width of about 16 mm. By hand tapping the face shells at compression toe region (right pier) upon unloading, it was established that the compression toe was still intact ("solid" sound when tapping face shell). Degradation of masonry along diagonal cracks resulted in minor spalling of masonry face shells.

μ_{18} pull, 1st cycle

The wall responded similarly to observations made in the previous push cycle. Of significant was the widening of existing diagonal cracks and extensions of cracks towards the compression region on the left pier. In addition, further degradation of mortar and masonry face shells along diagonal cracks were identified. A maximum strength of -101.1 kN was recorded for this loading step.

μ_{18} push, 2nd cycle

No new crack or extensions of cracks were identified. A maximum strength of 79.1 kN was recorded at 19.62 mm.

μ_{18} pull, 2nd cycle

No new crack or extensions of cracks were identified. A maximum strength of -82.7 kN was recorded at the displacement of -19.3 mm.

μ_{22} push, 1st cycle

The wall developed a maximum strength of 82.8 kN for this loading step. No new cracking was identified, but further widening of diagonal cracks were observed, with maximum crack width of about 21.5 mm being identified. Further degradation of masonry face shells along diagonal cracks was identified. The wall condition at this stage of testing is shown in Figure B.1.4.

μ_{22} pull, 1st cycle

The wall responded similarly to observations made in the previous push cycle. A maximum strength of -85.6 kN was recorded at the displacement of -22.8 mm.

μ_{22} push, 2nd cycle

Further widening of diagonal cracks was observed. A maximum strength of 69.2 kN was recorded for this loading cycle.

μ_{22} pull, 2nd cycle

A maximum strength of -69.2 kN was recorded. No new cracking was identified.

μ_{26} push, 1st cycle

The wall response was dominated by the widening of diagonal cracks. No new cracking was identified. A maximum strength of 78.5 kN was measured in this semi-cycle of loading.

μ_{26} pull, 1st cycle

The wall responded similarly to observations made in previous push cycle. A maximum strength of -88.2 kN was recorded at the displacement of -28.1 mm.

μ_{26} push, 2nd cycle

A maximum strength of 61.7 kN was recorded. No new cracking was identified.

μ_{26} pull, 2nd cycle

A maximum strength of -69.0 kN was recorded. No new cracking was identified.

μ_{30} push, 1st cycle

A maximum strength of 62.4 kN was measured. The wall response was dominated by the widening of diagonal cracks. No new cracking was identified. As shown in Figure B.1.5, further deterioration of masonry along diagonal cracks resulted in additional spalling of masonry face shells.

μ_{30} pull, 1st cycle

The wall responded similarly to observations made in the previous push cycle. A maximum strength of -69.8 kN was recorded at the displacement of -33.1 mm.

μ_{30} push, 2nd cycle

A maximum strength of 47.8 kN was recorded. No new cracking was identified.

μ_{30} pull, 2nd cycle

A maximum strength of -63.1 kN was recorded at the displacement of -34.3 mm. No new cracking was identified.

Figure B.1.4 Condition of test wall after first ductility 22 push cycle.

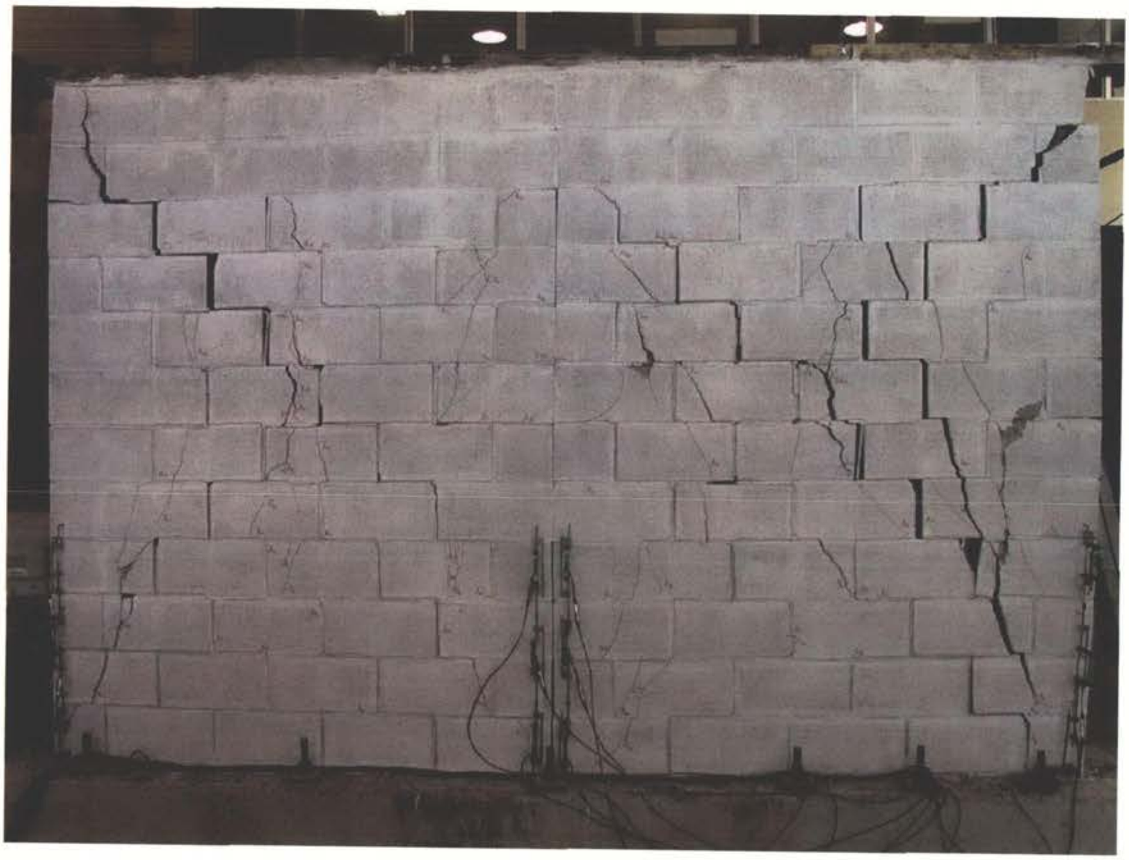

Figure B.1.5 Condition of test wall after first ductility 30 push cycle.

B.1.3 Summary Behaviour

The force-displacement history of Wall 9 is shown in Figure B.1.6, depicting the lateral displacement at the top of the wall as a function of the applied lateral force. The wall nominal strength F_n and the strength value derived from NZS 4229:1999 (denoted NZS-4229) are included in this plot. The flexural strength (F_n) of this wall was calculated as the sum of strengths of two individual (1.8 m long) cantilever walls since it was expected that the 10 mm gap (at the wall centre) would prevent the proper transfer of shear force across the control joint. Also shown in this plot is the theoretical failure point, corresponding to the cycle in which the peak strength failed to exceed 80% of the maximum previously attained strength.

The maximum push and pull direction strengths of 125.3 kN and -114.6 kN were measured during the first cycle to displacement ductility 14. The average yield displacement (Δ_y) for this partially grouted wall was evaluated to be 1.07 mm. The test wall was defined as failing during the second push cycle to displacement ductility 14, giving it a ductility capacity of $\mu_{av} > 6.0$. As shown in Figure B.1.6, the maximum strength achieved by Wall 9 was at least 43% higher than the $F_{n,st}$ predicted. This higher than expected experimental strength was due to the presence of a solid filled bond beam that had reinforcement that continued through the control joint. Consequently, the (un-debonded) continuous bond beam caused a frame-type action between the two piers, therefore allowing partial shear transfer. This notion was supported by the absence of significant structural damage in the bond beam. In addition, the closing of control joint at the wall mid-height position at latter stage of testing provided a mean for additional shear transfer between the two piers.

Despite the presence of widely open diagonal cracks, the wall exhibited a gradual and fairly symmetrical strength degradation of strength in both direction of loading. Consequently, it was possible to classify Wall 9 as having a failure mode of diagonal tension. This type of failure was characterised by the development of early horizontal flexural cracking on the pier tension edges, which was later exaggerated by diagonal cracking that extended throughout the wall panels. This desirable behaviour was created by the solid filled bond beam that was constructed continuously (un-debonded) above the control joint which caused a frame-type action at latter stage of testing.

Similar to the eight wall reported in Appendix A, the force-displacement plot in Figure B.1.6 consistently illustrated a pinched shape. This was primarily due to the presence of significant shear deformation in this type of masonry construction (see section B.1.4). It was also observed that less hysteretic energy was expended during the second cycle to any displacement level, when compared with the first displacement cycle. This is illustrated by the more pinched hysteresis loops of the second cycle.

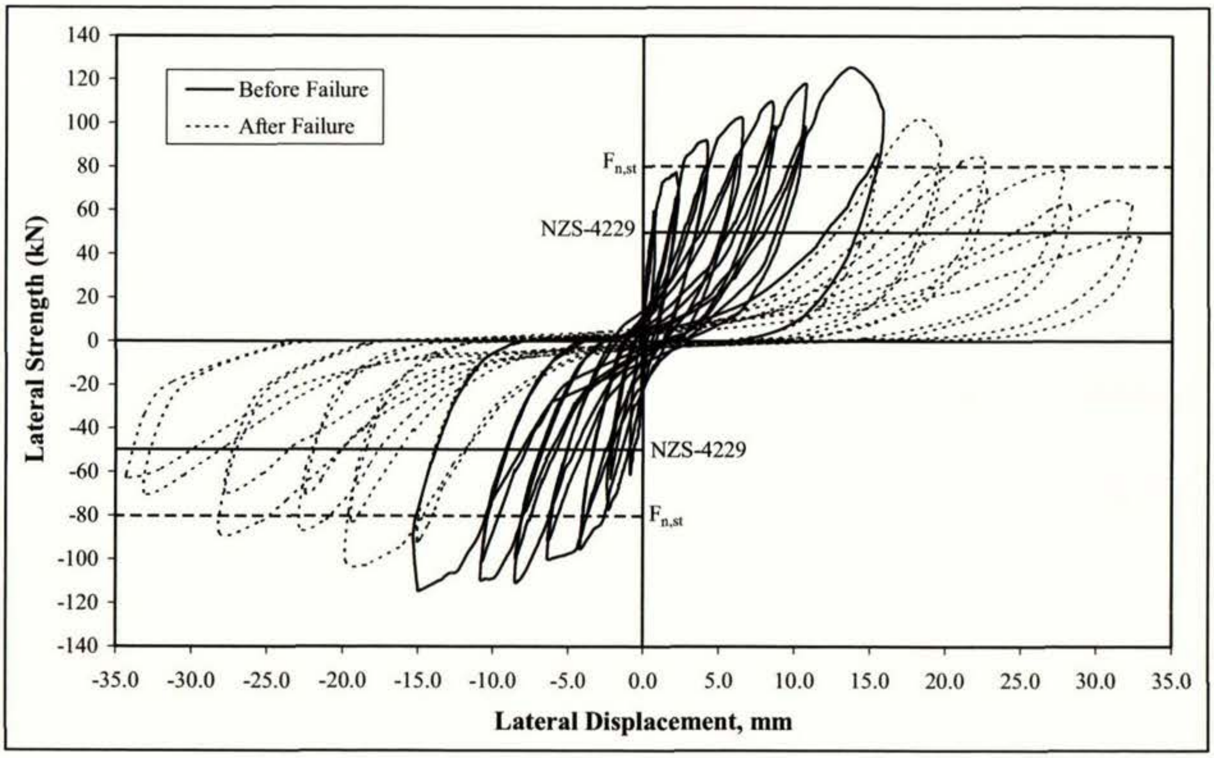

Figure B.1.6 Force-displacement behaviour for Wall 9.

B.1.4 Panel Displacement Components

The total horizontal displacement of the wall was decomposed into four displacement components according to the procedure outlined in section 4.7 with the results shown in Figure B.1.7. It is seen that shear displacement was the single most dominant deformation mode. The rocking, sliding and flexural displacement components were insignificant throughout the test. This is consistent with the development of significant diagonal cracking during the test. Figure B.1.7 provides an indication of the relative size of each displacement component at various stages of the displacement envelope.

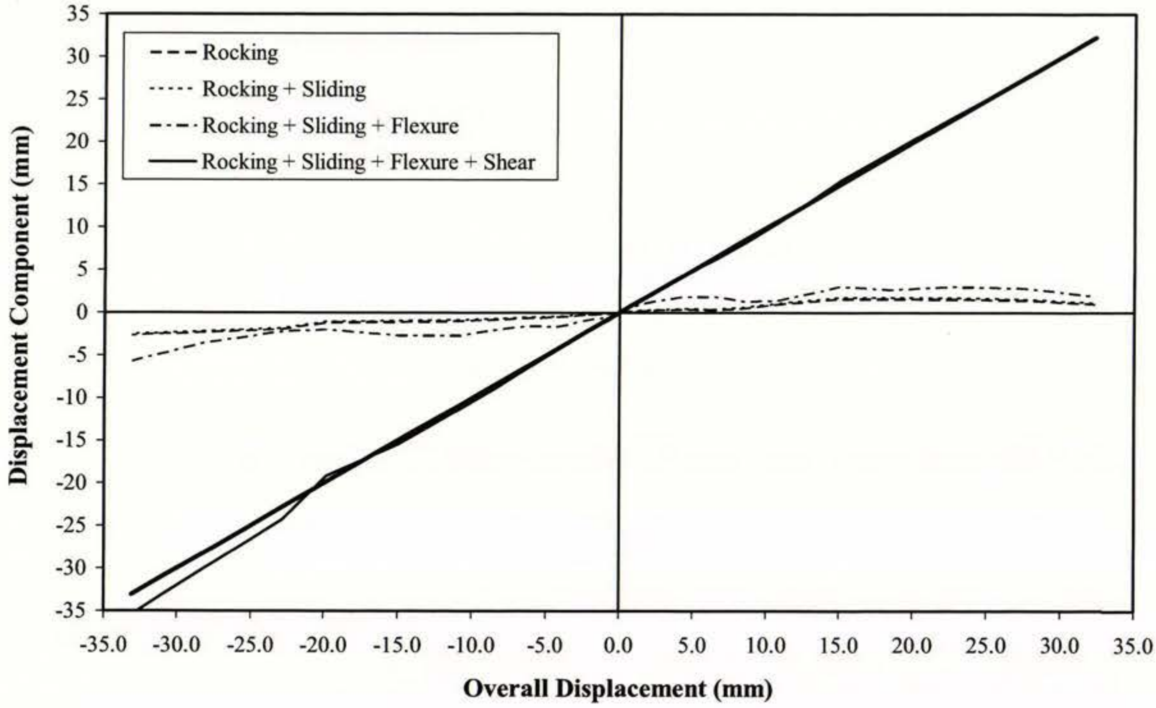

Figure B.1.7 Components of displacement.

B.2 Wall 10

This section describes the laboratory test of Wall 10. The wall geometry and reinforcement details are shown in Figure B.2.1. This wall shared similar construction detail as those of Wall 9, with only difference being the detailing of the D16 bond beam reinforcement at the control joint position. As shown in Figure B.2.1, the control joint was constructed up the full height of Wall 10. In order to prevent the flow of grout through the control joint at the bond beam layer, a thin polystyrene strip was inserted to form a gap between the two piers, and the D16 dowel bars were then punched through the polystyrene strip. Furthermore, in order to completely debond the dowel bars from the grout, the dowel bars were greased and sleeved with PVC pipe on one side. The wall nominal shear strength (V_n), calculated according to the shear expressions presented in section 4.3, was established to be 169.0 kN. The nominal flexural strength (F_n) of this wall, calculated as the sum of strengths of two 1.8 m long cantilever walls ($F_{n,st}$), was established to be 80.2 kN. Due to the presence of full height control joint, the horizontal cyclic load applied to the wall was achieved through the attachment of two jacks, one at each end of the wall. One jack was reacted off the strong wall, the other off a steel reaction frame. Both jacks were capable of pushing and pulling and were attached to the top of the wall by two separated pieces of 150 x 75 steel channels which was fastened to the bond beam by cast-in bolts. The decision to apply horizontal forces to the wall by two "point" loads added some difficulties to the test procedure but did not affect the results. The reason for using two "point" loads was taken so that the bond beams on either ends of the control joint were allowed to "flex", hence no additional strength was provided by the channel to the walls.

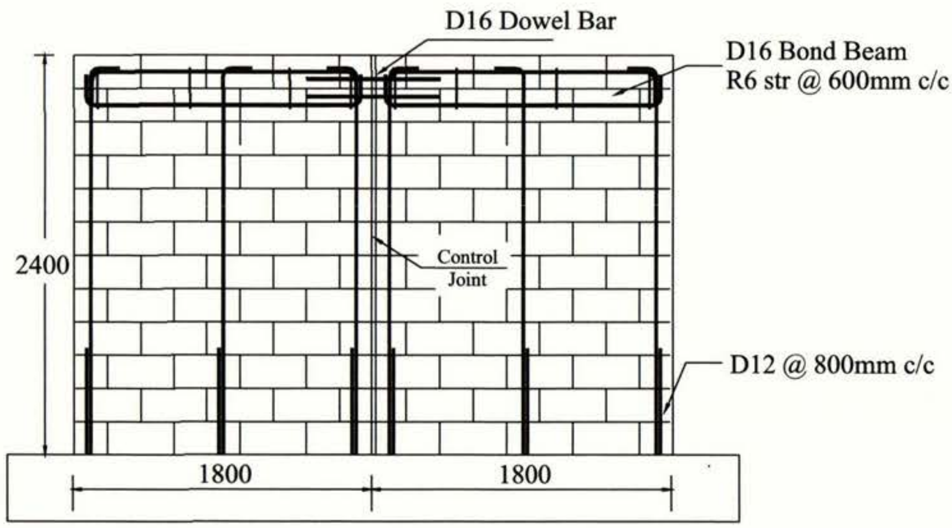

Figure B.2.1 Wall 10 geometry and reinforcing details.

B.2.1 Pre-test

The masonry wall was tested on the 67th days after construction. Instrumentation was attached to the wall according to section 3.5.1. Prior to wall testing the wall was inspected, with no cracks or structural defects being identified.

B.2.2 Testing

$^3/_4 F_n$ push,

An applied force of 65.5 kN was recorded when the wall was being pushed away from the strong wall. A corresponding displacement of 1.59 mm was recorded for this loading cycle. No clear evidence of cracking.

$^3/_4 F_n$ pull,

A maximum strength of -60.5 kN was recorded at the displacement of -1.70 mm. No cracking was identified.

According to the procedure outlined in section 4.5, the measured lateral forces for the two directions of loading resulted in an average yield displacement of:

$$\Delta_y = 0.5 \times \left(\frac{80.2}{65.5} \times 1.59 + \frac{80.2}{60.5} \times 1.70 \right) = 2.10 \text{ mm}$$

μ_2 push, 1st cycle

A maximum strength of 79.2 kN was recorded at the displacement of 4.30 mm. Diagonal cracks (5 cracks on the left pier and 3 cracks on the right pier), with maximum crack width of about 1.0 mm, were identified along mortar bed joints. These diagonal cracks inclined at an angle of approximately 50° to the horizontal, initiating from the tension edges of both piers.

μ_2 pull, 1st cycle

Cracking patterns mirrored to those formed in the previous push cycle were identified. 4 diagonal cracks were identified on the left pier accompanied by 3 diagonal cracks on the right pier. Maximum crack width of about 2.0 mm was identified. A maximum strength of -76.9 kN was recorded at the peak displacement of this load cycle.

μ_2 push, 2nd cycle

A maximum strength of 70.7 kN was recorded. No new cracking was identified.

μ_2 pull, 2nd cycle

A maximum strength of -66.3 kN was recorded. No new cracking was identified.

μ_4 push, 1st cycle

The wall developed a maximum strength of 89.0 kN at the target displacement. The maximum strength recorded in this load cycle exceeded the predicted flexural strength, $F_{n,st}$, by about 11%. Extensions of previously formed diagonal cracks were noted to take place on both piers, with diagonal cracks reaching the compression toe regions of both piers. Also observed was the elongation of diagonal crack towards the bond beam corner on top of the left pier. Cracks formed in the previous cycles were widened to a maximum crack width of about 4.5 mm. The width of control joint was measured to reduce by about 4 mm at the wall mid-height position. Fragmented crack pattern in the vicinity of the two centrally located vertical reinforcing bars indicated good bond between the reinforcement and the grouted core. Also, face shells at wall mid-height begun to dilate, indicating that the webs of the concrete masonry units had ruptures at some locations.

μ_4 pull, 1st cycle

A maximum strength of -84.6 kN was recorded at the target displacement of this load cycle. The wall responded similarly to observations made in the previous push cycle. Elongations of diagonal cracks mirrored to those observed in the previous push cycle were identified. Cracks formed in the previous cycles were widened to a maximum crack width of about 6.0 mm. Similar to the previous push cycle, the control joint was measured to close by about 4.0 mm at the wall mid-height position. As shown in Figure B.2.2, fragmented crack pattern in the vicinity of the two centrally located vertical reinforcing bars indicated good bond between the reinforcement and the grouted core. Face shells at the wall mid-height begun to dilate, indicating that the webs of the concrete masonry units had ruptures at some locations. As shown in the same figure, the wall clearly showed mixed modes of deformation, with obvious shear deformation but also flexural cracking on wall tension edges. The figure also shows the significant closed similarity of wall cracking patterns on these two piers. The presence of a full height control joint resulted in two piers that performed significantly independent of each other, as indicated by the diagonal cracks that initiated from the tension edges and ended at the compression toe of each pier, i.e. diagonal cracking on the piers formed independently of each other. Overall, wall performance was satisfactory.

μ_4 push, 2nd cycle

A maximum strength of 76.0kN was measured. No new cracking or extensions of cracks were identified.

μ_4 pull, 2nd cycle

No new cracking or extensions of cracks were identified. A maximum strength of -73.3 kN was measured.

μ_6 push, 1st cycle

A maximum strength of 81.9 kN was recorded at the displacement of 12.9 mm. No new crack, but elongations and widening of existing diagonal cracks were identified, with crack width up to 7 mm. Further closing of the control joint was identified. The width of control joint was measured to remain about 5.5 mm at the wall mid-height position.

μ_6 pull, 1st cycle

The wall responded similarly to observations made in the previous push cycle. A maximum strength of -80.2 kN was recorded at the displacement of -12.67 mm. No new crack, but further widening of diagonal cracks was identified. The width of control joint at wall mid-height position was measured to be about 3.9 mm.

μ_6 push, 2nd cycle

During this semi-cycle of loading, the wall developed a maximum strength of 60.1 kN at the lateral displacement of 12.26 mm. This was followed by a significant widening of diagonal crack on the left pier, resulting in a sudden displacement increase (maximum crack width about 12.5 mm) and a corresponding loss in strength. Wall strength of 40.9 kN was recorded when the wall settled the displacement of 12.87 mm. As shown in Figure B.2.3, the wall clearly showed significant shear modes of deformation. By hand tapping the face shells in the right pier compression toe region upon unloading, it was established that the compression toe was still intact. The fragmented crack pattern in the vicinities of the reinforcing bars indicated

Figure B.2.2 Condition of test wall after first ductility 4 pull cycle.

Figure B.2.3 Condition of test wall after second ductility 6 push cycle.

good bond between the reinforcement and the grouted cores. The control joint closed by about 6.7 mm at the wall mid-height position. The strength recorded in this load cycle corresponded to 68% of the maximum strength recorded in the push direction. Therefore the wall was defined as failing according to the test procedure outlined in section 4.5.

μ_6 pull, 2nd cycle

A maximum strength of -69.2 kN was recorded for this load step. No new crack was identified.

μ_8 push, 1st cycle

In this cycle of loading, there was very little additional cracking. Wall response was dominated by the significant widening of diagonal crack on the left pier, with maximum crack widths of about 16.3 mm. A maximum strength of 63.3 kN was recorded at the displacement of 17.0 mm. The wall condition at this stage of testing is shown in Figure B.2.4.

μ_8 pull, 1st cycle

Elongation and widening of previously formed diagonal cracks were identified. A maximum strength of -72.2 kN was recorded at the displacement of -17.0 mm.

μ_8 push, 2nd cycle

A maximum strength of 48.6 kN was recorded at the displacement of 17.5 mm. No new crack was identified.

μ_8 pull, 2nd cycle

The response was similar to those observed in the previous push cycle. A maximum strength of -62.4 kN was recorded at the corresponding displacement of -17.1 mm.

μ_{10} push, 1st cycle

A maximum strength of 58.8 kN was recorded at the target displacement. No new cracking was identified. The wall response was dominated by the widening of previously formed diagonal cracks, with maximum crack width of about 16.7 mm being identified on the left pier.

μ_{10} pull, 1st cycle

The wall response was similar to observations made in the previous push cycle. A maximum strength of -64.9kN was measured at the displacement of -21.6 mm.

μ_{10} push, 2nd cycle

A maximum strength of 50.6 kN was measured in this loading step. No new crack was identified.

μ_{10} pull, 2nd cycle

In this pull excursion towards the target displacement of -21 mm, significant widening of diagonal crack on the right pier (maximum crack width up to 12.2 mm) occurred at a displacement of approximately -20.7 mm resulting in slight loss of strength and a sudden increase in lateral displacement. The peak strength measured was -53.9 kN at the displacement of -20.7 mm. At the final displacement of -21.9 mm, the strength dropped to -48.9 kN. Figure B.2.5 clearly shows the shear mode of deformation exhibited by the test wall.

μ_{12} push, 1st cycle

The wall was accidentally pushed to a displacement of 31.3 mm. A maximum strength of 45.9 kN was measured at this displacement. The wall response was dominated by further widening of diagonal cracks formed in previous cycles.

μ_{12} pull, 1st cycle

A maximum strength of -58.9 kN was measured at the target displacement. No new cracking was identified. The wall response was dominated by further widening of existing diagonal cracks.

μ_{12} push, 2nd cycle

No new crack or extensions of cracks were identified. A maximum strength of 23.1 kN was measured at the displacement of 25.4 mm.

μ_{12} pull, 2nd cycle

A maximum strength of -45.3 kN was measured at the displacement of -25.8 mm. No new crack was identified.

Figure B.2.4 Condition of test wall after first ductility 8 push cycle.

Figure B.2.5 Condition of test wall after second ductility 10 push cycle.

B.2.3 Summary Behaviour

The force-displacement history of Wall 10 is shown in Figure B.2.6, depicting the lateral displacement at the top of the wall as a function of the applied lateral force. The nominal strength F_n and the strength value derived from NZS 4229:1999 (denoted NZS-4229) are included in this plot. Also shown in this plot is the theoretical failure point, corresponding to the cycle in which the peak strength failed to exceed 80% of the maximum previously attained strength.

The maximum push and pull direction strengths of 89.0 kN and -84.6 kN were measured during the first cycle to displacement ductility 4. The average yield displacement (Δ_y) for this partially grouted wall was evaluated to be 2.10 mm. The test wall was defined as failing during the second push cycle to displacement ductility 6, giving it a ductility capacity μ_{av} of 4.5. As shown in Figure B.2.6, the maximum strength achieved by Wall 10 was about 8% higher than the $F_{n,st}$ predicted.

Despite the presence of widely open diagonal cracks, the wall exhibited a gradual and fairly symmetrical strength degradation of strength in both direction of loading. Consequently, it was possible to classify Wall 10 as having a failure mode of diagonal tension. This type of failure was characterised by the development of early horizontal flexural cracking on the pier tension edges, which was later exaggerated by diagonal cracking that extended throughout the wall panels.

Similar to the other walls previously reported, the force-displacement plot in Figure B.2.6 consistently illustrated a pinched shape. This was primarily due to the presence of significant shear deformation in this type of masonry construction. It was also observed that less hysteretic energy was expended during the second cycle to any displacement level, when compared with the first displacement cycle. This is illustrated by the more pinched hysteresis loops of the second cycle.

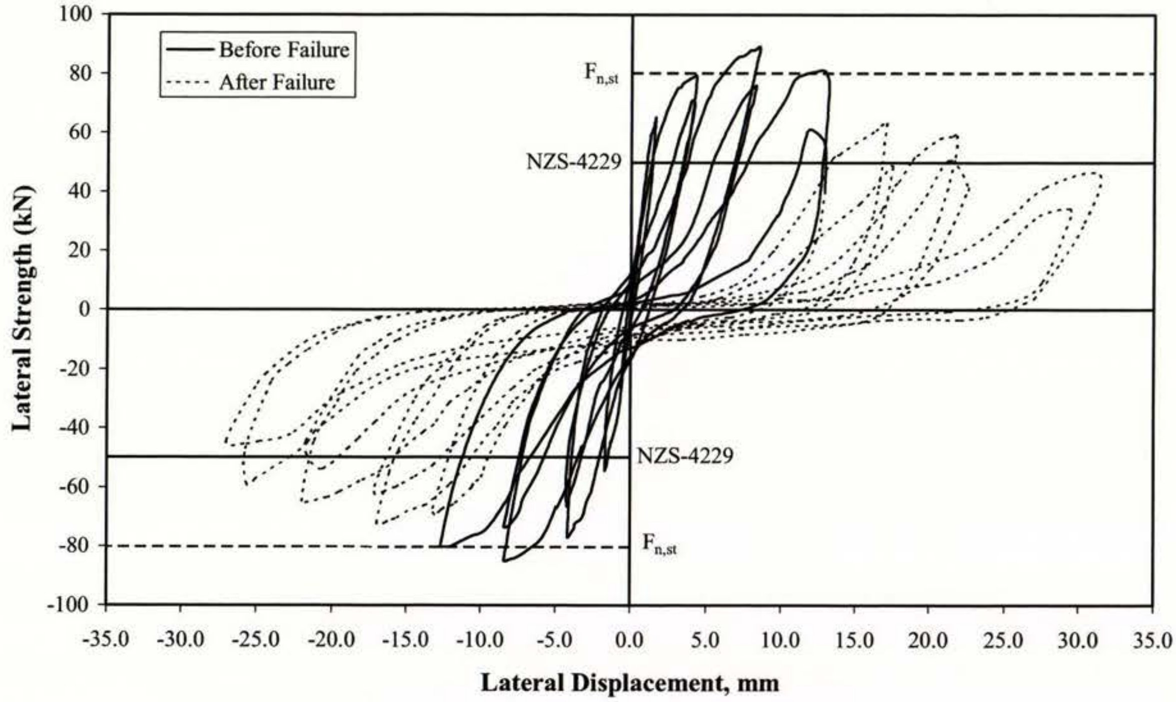

Figure B.2.6 Force-displacement behaviour for Wall 10.

B.2.4 Panel Displacement Components

The total horizontal displacement of the wall was decomposed into four components according to the procedure outlined in section 4.7 with the results as shown in Figure B.2.7. It is seen that shear displacement was the single most dominant deformation mode. The rocking and sliding displacement components were insignificant throughout the test. As shown in Figure B.2.7, the influence of flexural displacement component was more significant in the pushing direction than that in the pulling direction. The flexural mode of displacement accounted for about 26% of the total horizontal displacement when the wall was loaded to +30 mm displacement in the push direction.

It is noted that the summed up displacement (rocking + sliding + flexure + shear) approximately match the overall displacement measured at the top of the wall. Ideally, the line representing the sum of components should coincide with the line representing the lateral displacement measured at the loading beam. Figure B.2.7 provides an indication of the relative size of each displacement component at various stages of the displacement envelope.

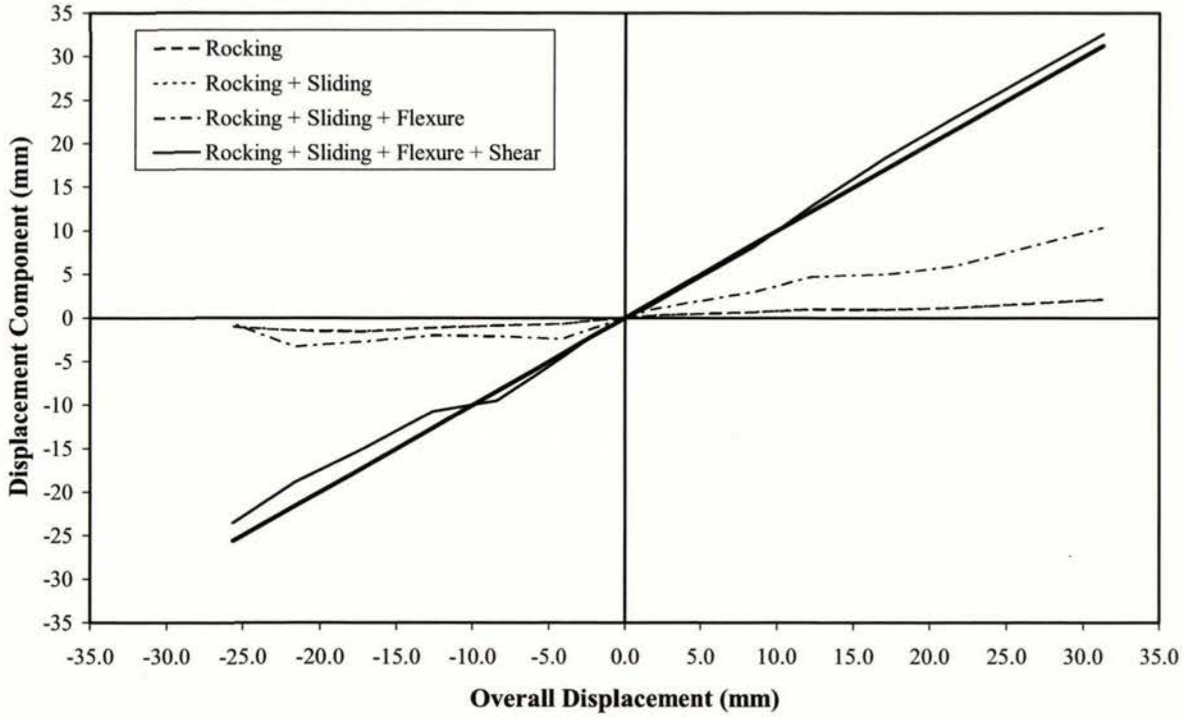

Figure B.2.7 Components of displacement.

Appendix C- Shear Displacement Component

The objective of decomposition of panel deformation is to calculate and identify the dominant displacement components. The components of displacement are calculated from the test data obtained during testing. This test data was attained from the measuring instrumentation attached to the wall face, and the typical arrangement of the instrumentation is shown in Figure 3.7. This appendix describes calculation of the shear displacement component.

Having measured the relative displacements between points of a panel section on the wall face denoted A, B, C and D, as shown in Figure C.1(a), it is possible to extract the shear displacement component from the deformation in the panel section. The total shear displacement of the wall can be evaluated by summation of shear deformation of each panel section. The method used in this report for the extraction of the shear displacement component is based on Hiraishi (1984) and Brammer (1995).

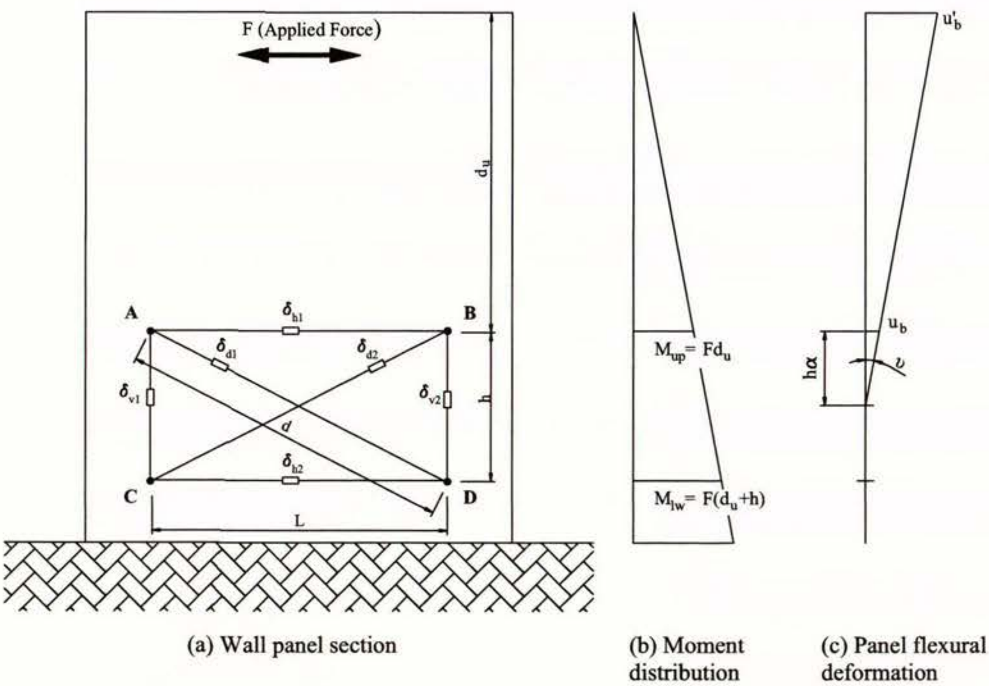

Figure C.1 Wall panel section.

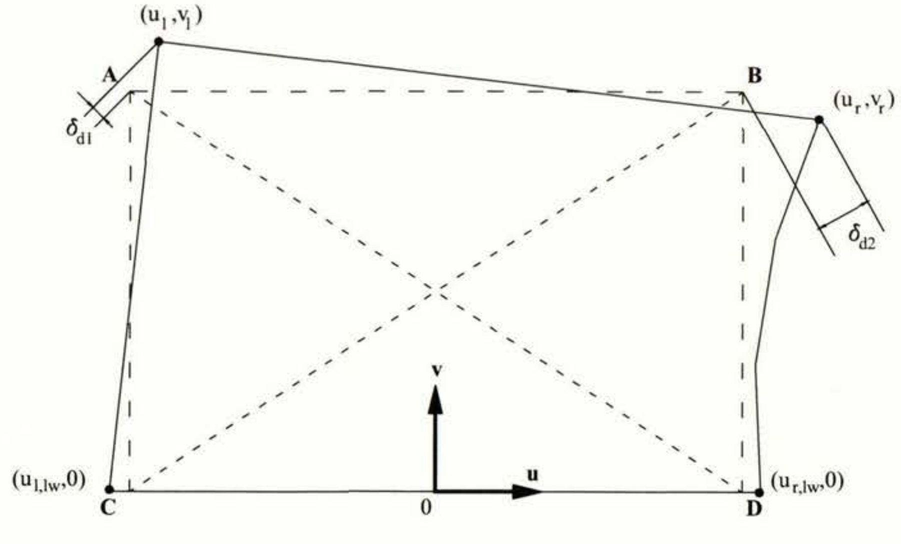

Figure C.2 Nodal displacement of a panel section.

The deformation of a panel section is illustrated in Figure C.2. It is assumed that the two upper points, A and B, may translate horizontally by u_l and u_r, and vertically by the amounts v_l and v_r. The lower points, C and D, are assumed to translate only horizontally by the amount $u_{l,lw}$ and $u_{r,lw}$. The subscripts 'l' and 'r' refer to the left and right hand sides respectively, while the subscript 'lw' refers to the lower points. The adopted sign convention is for positive displacements to be to the right and upwards. As shown in Figure C.1, δ_{d1} and δ_{d2} are the elongations of the respective diagonal, while elongations of the horizontal elements are termed δ_{h1} and δ_{h2}, and elongations of the vertical elements are termed δ_{v1} and δ_{v2}. The dimensions of the panel are defined by the length, L, the height, H, and the diagonal length, d. The termed d_u is used to defined the position of the panel bracing with respect to the top of the wall, see Figure C.1(a).

As shown in Figure C.3, the panel section deformation, represented by u_l, u_r, v_l, v_r, $u_{l,lw}$ and $u_{r,lw}$, is assumed to consist of the three components: shear, flexure and elongation. In this figure, the u and v represent the horizontal and vertical deformation components respectively. The subscripts 's', 'b' and 'e' represent the shear, flexural and elongation deformation components respectively.

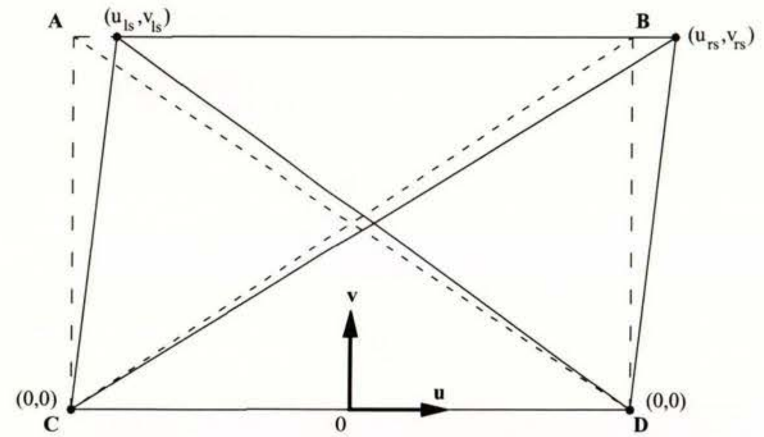

(a) Shear deformation

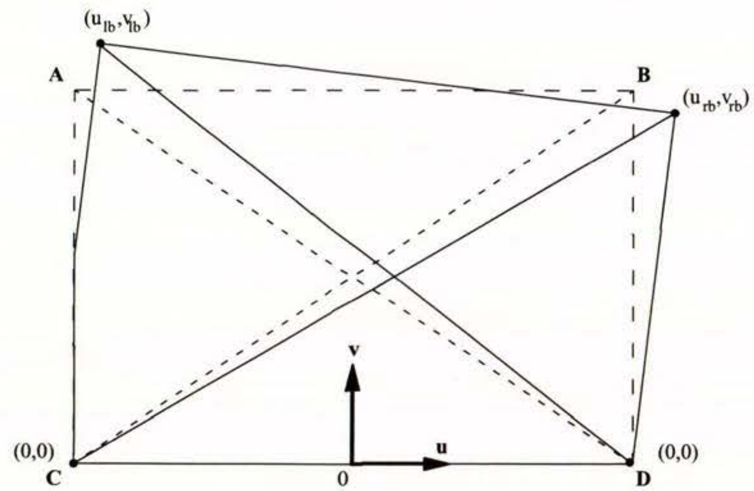

(b) Flexural deformation

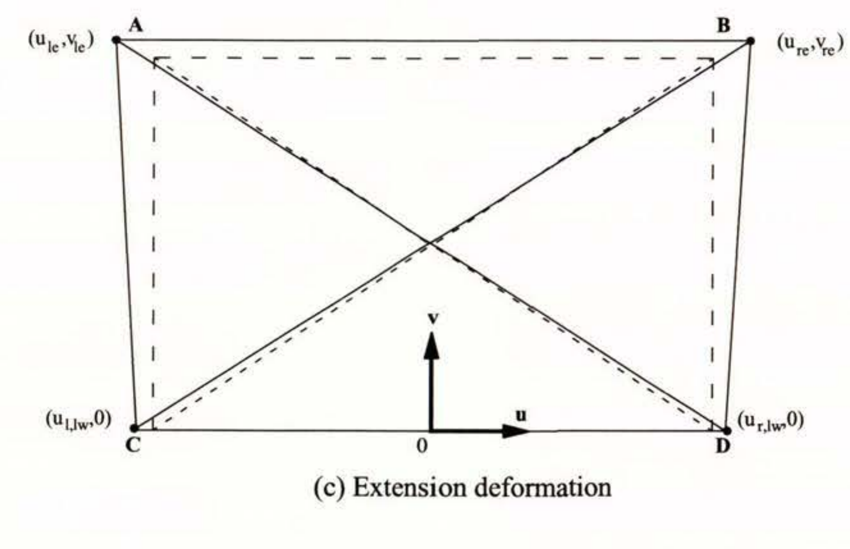

(c) Extension deformation

Figure C.3 Components of panel deformation.

The primarily purpose of the following derivation is to calculate the horizontal displacement at the top of the wall due to shear deformation, U_s, by relating the measured elongation (δ's) to individual displacement components: u's and v's. The following relations are assumed:

1. The left and right horizontal shear deformation components are equal.
2. The left and right horizontal flexural deformation components are equal.
3. The left and right horizontal extension components are equal but of opposite side.
4. The vertical shear deformation components are zero.
5. The upper left and right vertical extension deformation components are equal.

The above assumption can be represented as follow:

a) $u_{ls} = u_{rs} = u_s$

b) $u_{lb} = u_{rb} = u_b$

c) $u_{re} = -u_{le} = \frac{1}{2}u_e$ (C-1)

d) $u_{re,lw} = -u_{le,lw} = \frac{1}{2}u_{e,lw}$

e) $v_{le} = v_{re} = v_e$

The relationships between these displacements and those shown in Figure C.3 are as follows:

a) $u_l = u_s + u_b - \frac{1}{2}u_e$

b) $u_r = u_s + u_b + \frac{1}{2}u_e$

c) $u_{l,lw} = -\frac{1}{2}u_{e,lw}$ (C-2)

d) $u_{r,lw} = \frac{1}{2}u_{e,lw}$

e) $v_l = v_{lb} + v_e$

f) $v_r = v_{rb} + _{ve}$

The measured relative deformations can be expressed in terms of the global deformations by the following geometric relationships:

a) $\delta_{d1} = \frac{L}{d}\left(u_{r,lw} - u_l\right) + \frac{L}{h}v_l$

b) $\delta_{d2} = \frac{L}{d}\left(u_r - u_{l,lw}\right) + \frac{L}{h}v_r$ (C-3)

c) $\delta_{h1} = -u_l + u_r$

d) $\delta_{h2} = -u_{l,lw} + u_{r,lw}$

e) $\delta_{v1} = v_l$ (C-3)

f) $\delta_{v2} = v_r$

Substituting Equation C-2 into C-3:

a) $$\delta_{d1} = \frac{L}{d}\left(-u_s - u_b + \frac{1}{2}u_e + \frac{1}{2}u_{e,lw}\right) + \frac{L}{h}\left(v_{lb} + v_e\right)$$

b) $$\delta_{d2} = \frac{L}{d}\left(u_s + u_b + \frac{1}{2}u_e + \frac{1}{2}u_{e,lw}\right) + \frac{L}{h}\left(v_{rb} + v_e\right)$$

c) $\delta_{h1} = u_e$ (C-4)

d) $\delta_{h2} = u_{e,lw}$

e) $\delta_{v1} = v_{lb} + v_e$

f) $\delta_{v2} = v_{rb} + v_e$

From Equation C-4 it seems that the equation is under-determined since the equations are describing the relationship between 6 known measured relative displacements (δ's) and unknown panel deformation components (u's and v's). Inserting Equations C-4(c) and (d) into Equations C-4(e) and (f), and then subtracting C-4(e) from C-4(f) gives:

$$\delta_{d2} - \delta_{d1} = \frac{L}{d}\left(2u_s + 2u_b\right) + \frac{L}{h}\left(\delta_{v2} - \delta_{v1}\right) \tag{C-5}$$

Rearranging Equation C-5:

$$u_s = \frac{d}{2L}\left(\delta_{d2} - \delta_{d1}\right) + \frac{h}{2L}\left(\delta_{v1} - \delta_{v2}\right) - u_b \tag{C-6}$$

Equation C-6 can be solved by defining an equation relating the flexural deformation component to the measured relative displacement. This is displayed in Equation C-7:

$$u_b = \theta h \alpha \tag{C-7}$$

where:

$$\theta = \frac{\delta_{v1} - \delta_{v2}}{L}$$

Equation C-7 states that the flexural deformation is equal to the rotation at the top of the panel section multiplied by the panel section height and by α. When taking α as 2/3, the equation captures the exact flexural displacement of an elastic prismatic cantilever with a concentrated horizontal force applied at the top, with υ representing the rotation of the top of the wall. However, for reinforced concrete masonry and reinforced concrete walls, the parameter α is generally higher than 2/3 since the wall flexural cracking tends to concentrate rotation towards the bottom of the wall, therefore resulting in higher $h\alpha$ and higher u_b.

In this study, the flexural deflection u_b for a section of wall was calculated from the measured rotation that occurs within the section under study. This rotation is calculated from the bending moment diagram. The bending moment at the top (M_{up}) and the bottom (M_{lw}) of a panel section are known to vary linearly according to the vertical location as shown in Figure C-1(b).

The moment (M)-curvature (ω) relationship for an elastic section is given by:

$$M = \omega EI \qquad \text{(C-8)}$$

where E and I are the modulus of elasticity and inertia moment. As the curvature is a linear function of the moment, the total rotation of the panel section between d_u and d_u+h can be calculated from the average bending moment:

$$\theta = \frac{h\left(M_{up} + M_{lw}\right)}{2EI} \qquad \text{(C-9)}$$

The panel flexural deformation, u_b, is evaluated by integration of curvature along the height of the panel section with the following result:

$$u_b = \frac{h^2}{EI}\left(\frac{M_{lw}}{3} + \frac{M_{up}}{6}\right) = \theta h\left(\frac{d_u + \frac{2h}{3}}{2d_u + h}\right) \text{ where } \alpha = \frac{d_u + \frac{2h}{3}}{2d_u + h} \qquad \text{(C-10)}$$

The α given in Equation C-10 is defined with respect to the top of the investigated panel section.

u_b can be evaluated by incorporating Equation C-7:

$$u_b = \frac{h(\delta_{v1} - \delta_{v2})}{L}\left(\frac{d_u + \frac{2h}{3}}{2d_u + h}\right) \tag{C-11}$$

Subsequently, the shear deformation for the panel section can be evaluated by substituting Equation C-11 into Equation C-6:

$$u_s = \frac{d}{2L}(\delta_{d2} - \delta_{d1}) + \frac{h}{2L}(\delta_{v1} - \delta_{v2}) - \frac{h(\delta_{v1} - \delta_{v2})}{L}\left(\frac{d_u + \frac{2h}{3}}{2d_u + h}\right) \tag{C-12}$$

Rearranging Equation C-12 to give:

$$u_s = \frac{d}{2L}(\delta_{d2} - \delta_{d1}) - \frac{h^2}{6(2d_u + h)}\frac{(\delta_{v1} - \delta_{v2})}{L} \tag{C-13}$$

The total shear displacement, U_s, is given by the sum of the shear deformations from the individual panel sections:

$$U_s = \sum u_s \tag{C-14}$$

In addition, the total flexural displacement can be evaluated as follows. The flexural deformation of the investigated panel section (see Figure C.1(c)) with respect to the top of the wall, u'_b, is evaluated as:

$$u'_b = \theta(\alpha h + d_u) = \frac{(\delta_{v1} - \delta_{v2})}{L}\left(h\frac{d_u + \frac{2h}{3}}{2d_u + h} + d_u\right) \tag{C-15}$$

The total flexural displacement, U_b, is the summation of flexural deformation from individual panel section:

$$U_b = \sum u'_b \tag{C-16}$$

Appendix D – Bending Moment Capacity

This appendix presents the bending moment capacity calculations for the masonry pier and lintel of the perforated walls illustrated in Figure 3.4. The longitudinal reinforcement for the masonry pier and lintel are depicted in Figure D.1. For convenience, f'_m of 16 MPa was assumed and the self weight of masonry pier was not considered. Also, Brammer's (1995) recommendation of excluding the longitudinal steel adjacent to the neutral axis was adopted in the following strength calculations.

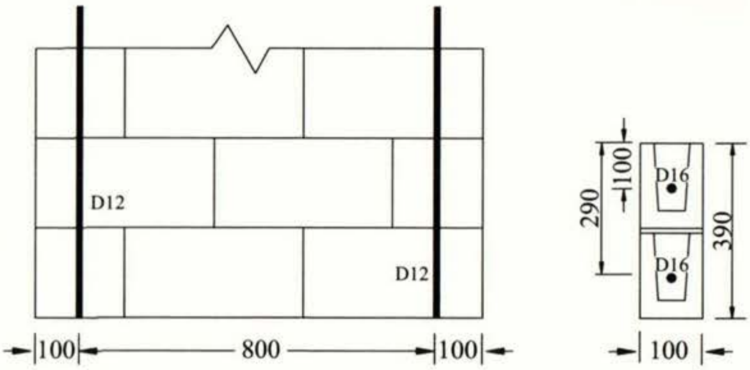

(a) Masonry Pier **(b) Masonry Lintel**

Figure D.1 Reinforcement details for concrete masonry pier and lintel.

a) Masonry Pier

Area of 1-D12 = $\pi \times \frac{12^2}{4}$ = 113.1 mm^2

Therefore tension force from longitudinal reinforcement:

$\Rightarrow$ T = 113.1 x 305 = 34.5 kN

Now consider force equilibrium:

$C_m = T$ where $C_m = 0.85f'_m ab$

$\Rightarrow$ $0.85f'_m ab = 34.5$ kN

$$a = \frac{34.5 \times 10^3}{0.85f'_m \times 140} = 18.1 \text{ mm}$$

Now taking moment about the neutral axis:

$$M_n = T \times jd$$
$$= Tx(900 - a/2)$$
$$= 30.7 \text{ kNm}$$

b) Masonry Lintel

Area of 1-D16 = $\pi \times \frac{16^2}{4} = 201.1 \text{ mm}^2$

Therefore tension force from longitudinal reinforcement:

$$\Rightarrow \quad T = 201.1 \text{ x } 305 = 61.3 \text{ kN}$$

Now consider force equilibrium:

$$C_m = T \qquad \text{where } C_m = 0.85f'_m ab$$
$$\Rightarrow \quad 0.85f'_m ab = 61.3 \text{ kN}$$
$$a = \frac{61.3 \times 10^3}{0.85f'_m \times 140} = 32.2 \text{ mm}$$

Now taking moment about the neutral axis:

$$M_n = T \times jd$$
$$= Tx(300 - a/2)$$
$$= 17.5 \text{ kNm}$$